RICE UNIVERSITY

Foam Rheology of Zwitterionic and Anionic Surfactant Blends in Porous Media
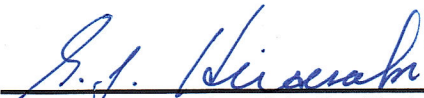
by

Aarthi Muthuswamy

A THESIS SUBMITTED
IN PARTIAL FULFILLMENT OF THE
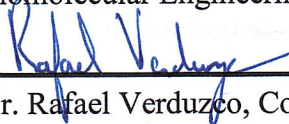REQUIREMENTS FOR THE DEGREE

Doctor of Philosophy

APPROVED, THESIS COMMITTEE

Dr. George J. Hirasaki, Co-Chair,
A. J. Hartsook Professor Emeritus of Chemical and
Biomolecular Engineering

Dr. Clarence A. Miller, Co-Chair,
Louis Calder Professor Emeritus of Chemical and
Biomolecular Engineering

Dr. Rafael Verduzco, Co-Chair,
Louis Owen Assistant Professor of Chemical and
Biomolecular Engineering

Dr. Sibani Lisa Biswal, Associate Professor of
Chemical and Biomolecular Engineering, Material
Science and NanoEngineering

Dr. Mason B. Tomson, Professor of Civil and
Environmental Engineering

HOUSTON, TEXAS
April, 2016

Abstract

Foam Rheology of Zwitterionic and Anionic Surfactant Blends in Porous Media

by

Aarthi Muthuswamy

Blending of certain types of surfactants is known to promote synergism as studied by bulk measurements. This study analyzes if such synergistic interactions are beneficial for foam rheology in porous media. Foam experiments were conducted systematically in porous media, at different ratios of zwitterionic and anionic surfactants, both in the presence and absence of crude oil. Interfacial studies were conducted to explain the behavior of surfactant mixtures with respect to foam rheology in porous media.

The zwitterionic surfactants used in this study were C_{12} straight chain betaine- Lauryl betaine (LB), C_{12} straight chain sultaine- Lauryl sultaine (LS), C_{18} tailed amido betaine (Rhodia A), C_{18-22} tailed amido sultaine (Rhodia B), C_{18-22} tailed amido betaine - with more C_{22} (Rhodia C) and C_{18-22} tailed amido betaine -with more C_{18} (Rhodia D). LB and LS surfactants had a viscosity close to that of water ~1 cP at room temperature. On the other hand 0.5 wt% of Rhodia A, Rhodia B, Rhodia C and Rhodia D were viscoelastic and shear thinning fluids due to the presence of wormlike micelles. Rheological studies which were conducted at room temperature revealed that salinity had a prominent effect on Rhodia A. On increasing salinity from ~ 4% (sea water) to 12% (formation brine), the relaxation time of Rhodia A increased by three orders of magnitude, thereby causing the weakly viscoelastic surfactant solution to change to a strongly viscoelastic solution. On the other hand salinity had a negligible effect on Rhodia B, Rhodia C and Rhodia D.

I

When 1 wt% surfactant solutions of Rhodia A, B, C or D(made in sea water) were mixed with ~ 35% synthetic crude oil (mass basis), all surfactant solutions lost viscosity and viscoelasticity except Rhodia C. Crude oil had an adverse effect on Rhodia A perhaps due to the conversion of wormlike micelles to spherical micelles. Rhodia B and D had lower elastic and viscous moduli most likely due to the shortening of the wormlike micelles. Additional tests were done to study the flow of these complex fluids in a 100 Darcy silica sand pack. Rhodia A, B and D showed no elongational effects during flow in porous media. Their shear thinning apparent viscosities in porous media were very close to the rheometric data in shear flow. Rhodia C exhibited yield stress behavior and hence could not be injected in a porous medium.

Zwitterionic surfactants Rhodia A/LB/LS were blended with anionic Alpha Olefin Sulfonate AOS $_{14-16}$ (AOS) surfactant (all made in sea water) at specific ratios - one with high and one with low bulk mass ratio of zwitterionic to anionic. Rhodia A which was weakly viscoelastic by itself, when blended with AOS in the ratio 9:1 respectively (by mass) produced a strongly viscoelastic solution. Nitrogen foam experiments were conducted in 100 Darcy silica sand at 25° C for Rhodia A and AOS blends and, in Bentheimer sandstone cores at 45° C, for LB/AOS blends and LS/AOS blends. Zwitterionic surfactants of this type have been reported to be "foam boosters" for bulk foams when added to anionic surfactant.

Rhodia A betaine was a weak foamer both in the presence and absence of oil. However when blended with AOS (9:1 ratio), its foam strength significantly improved in the absence of oil. In the presence of oil the viscoelastic surfactant helped generate strong foam in fewer pore volumes (PVs- a dimensional unit of time) but took a longer time than AOS to propagate through the sand pack.

In the case of LB/AOS and LS/AOS surfactant systems, the zwitterionic (LB, LS) foam by itself was weak, but AOS and the blends of zwitterionic and AOS had strong foam with comparable foam rheology. The regular solution theory approach of Rubingh combined with Rosen's application to water-air film interfaces and its adaption to oil-water interfaces was applied to understand this behavior, especially the high foam strength observed when the poor-foaming zwitterionics were added to the strong foamer AOS. It was found that the zwitterionic-anionic blends exhibited synergistic interactions. The Gibbs surface excess calculations suggested that the synergistic interactions promoted tighter packing at the interface thereby helping the poorly foaming zwitterionic surfactant to exhibit strong foam rheology in porous media. Interestingly, AOS surfactant by itself had tight packing at the interface. The trends observed in porous media were well explained by the Gibbs surface excess calculations. However, the synergism did not lead to improvement in foam performance in porous media beyond that seen for AOS alone.

Additionally foam strength in the presence of water flood residual oil was weak for the pure zwitterionic surfactants, but the blends with higher mole fraction of AOS and pure AOS had comparable foam performance. Again AOS by itself was able to achieve good mobility control in displacing residual oil. The addition of zwitterionic surfactant had apparently not boosted the foam performance of AOS in porous media in the presence of oil as well.

Interfacial shear rheology for the LB/AOS and LS/AOS systems were performed and it showed that none of the surfactants possessed interfacial shear viscosity. Qualitative film drainage studies were conducted and it was observed that a small addition of LB to AOS helped in creating very stable black film and substantially increased the longevity of the film more than

AOS itself. However all these thin film studies failed to offer any explanation to porous media foam studies but perhaps help develop an understanding on bulk foam studies.

In the case of Rhodia A:AOS 9:1 viscoelastic blend, an injection strategy can be proposed where in a small slug of A:AOS 9:1 blend can be injected which can aid in quicker foam generation followed by a large AOS slug which can help in faster propagation and hence more efficient oil recovery.

Anionic AOS $_{14\text{-}16}$ surfactant did not need a foam booster contrary to the opinion in literature that a betaine surfactant (coco amido propyl betaine) is needed to boost the foam strength of an anionic surfactant (AOS $_{16\text{-}18}$) in the presence and absence of crude oil in porous media.

Acknowledgements

I truly consider it as a privilege to complete my PhD dissertation under the guidance of Dr.George Hirasaki, Dr.Clarence Miller and Dr.Rafael Verduzco. Dr.Hirasaki has greatly inspired me to enjoy science and question the occurrence of every phenomenon, not just in enhanced oil recovery. I am deeply indebted to Dr.Miller for all the interesting discussions and for his immense patience in helping me shape up my thesis and guiding it to completion. I thank Dr.Verduzco for helping me stay focused on my work so I may finish it in a timely manner.

I thank Dr. Lisa Biswal and Dr. Mason Tomson for serving on my thesis committee and all the helpful discussions.

I owe my deepest gratitude to Maura Puerto who not only helped me design and build the experimental set up at Rice, but also has been a great friend and mentor to me.

This thesis would not have been possible without the valuable support of Dr.Rouhi Farajzadeh who invited me to TU Delft for an internship and also mentored me throughout my thesis. I sincerely thank Dr.Sebastien Vincent Bonnieu from Shell Rijswijk, for guiding me during my internship at TU Delft. I would also like to acknowledge Prof. Bill Rossen for very interesting discussions on foam. I am extremely grateful to Michel Slob who devoted much of his time helping me build the experimental set up and ensuring a smooth completion of my experiments. I thank Dr.Ali Akbar Efthekari for wonderful hospitability at TU Delft and also for guiding me during my project. Apart from this I would like to thank everyone who helped me in the lab and also for the great friends I met there.

I am thankful to all Hirasaki group lab mates for very useful discussion. I especially thank José Lopez Salinas, Neeraj Rohilla, Aparna Raju Sagi, Yongchao Zeng, Indrajyoti

Table of Contents

List of Figures

List of Tables

Chapter 1

Introduction

1.1 Enhanced oil recovery (EOR) scope of study:

The conventional methods for recovery of hydrocarbons (crude oil) are the primary and secondary methods. Primary method involves natural drive mechanisms like the gas cap drive, solution gas, and water influx or gravity drainage. This method recovers about 10% of the original oil in place (OOIP). Secondary method involves the use of pressure maintenance either by water or gas injection. This method recovers 20-40% of the OOIP[1]. When the conventional methods no longer recover oil at an economical rate, enhanced oil recovery plays an important role. EOR has prospects to recover 60% of the OOIP.

The main types of EOR are gas injection, thermal methods, chemical injection and miscible flood. In USA, thermal (steam) injection accounts for about 40% of the EOR-produced oil, much of it in California. Gas injection accounts for 60% and chemical injection for only 1% of EOR-produced oil. The lower degree use of chemical injection is due to the cost of the chemicals used in the process. In 1961 Kern River Oil Field in California produced 19,000 barrels per day. In 1964 steam flooding was introduced. In 1985 it produced 141,000 barrels a day which was at its peak[2]. The life of the field was greatly expanded. This shows how effective EOR techniques can be. It is important to note that the efficiency of EOR projects depend on reservoir characteristics, nature of the displacing fluids and the fluids being displaced and arrangement of the production and injection wells[3].

A comprehensive literature review on where we stand in terms of the EOR projects in the United States is provided by Alvarado and Manrique[4]. Figure 1.1 shows an evolution chart of the various EOR projects. The figure informs that maximum EOR projects were applied in the field of thermal recovery. However there has been continuous progress in chemical injection and gas injection. EOR projects are mostly based on litology[4] and especially applied in sandstone reservoir due to the success of the pilot and commercial tests.

Figure 1.1: Evolution of the application of EOR techniques in United States[4].
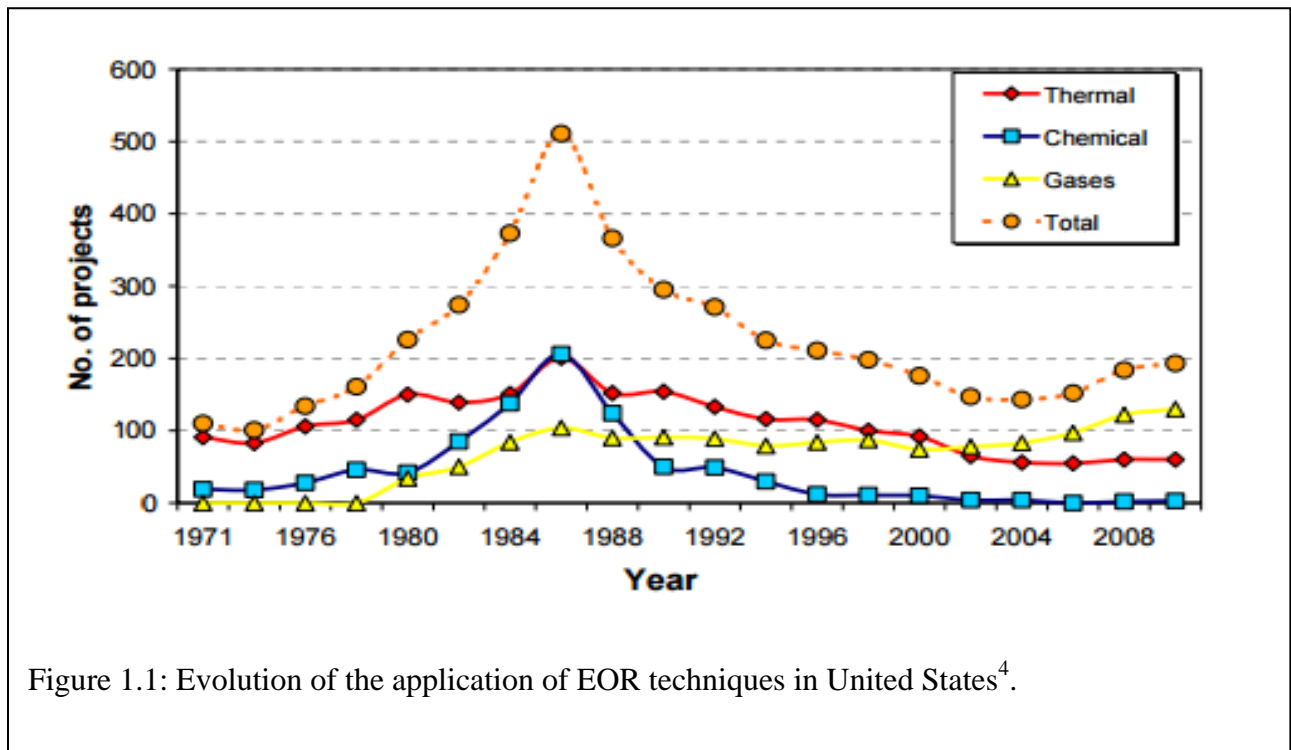
1.2 Chemical injection methods

A number of chemical injection methods are put in to practice like alkaline flooding [5–7], polymer flooding[8–11] which is considered one of the most mature technology, alkaline surfactant (AS)[12,13], Alkaline polymer flooding (AP)[14], Surfactant Polymer flooding (SP)[15,16], Alkaline Surfactant Polymer flooding (ASP)[17–20], Surfactant Foam injection[21–27]. For an ASP process Daqing field in China has been one of the widely studied fields[28].

2

It has been known for long that surfactants which are surface active materials can lower the interfacial tension (IFT) to ultra-low values when tailored for the particular reservoir environment. Hence in the chemical injection method, not only surfactants alone, but surfactants in combination with alkali can lower the IFT to ultra-low values. Alkali reacts with the naphthenic acid in the crude oil and generates soap. However it is important to optimize the soap- to- surfactant ratio for an efficient recovery process[29].Advantage of an ASP over SP is the reduction in adsorption, hence less surfactant is required. But most of the oil is not recovered just by injecting surfactant. It is also important to have good sweep efficiency in the reservoir to improve oil recovery. Hence polymer is used to improve mobility control.

1.3 Foam enhanced oil recovery:

Due to the high cost of polymers and their degradation at high temperature, high salinity and in the presence of divalent ions it has been proposed to use foam as a method to enhance sweep efficiency in the reservoir. Foam is a dispersion of a gas in a continuous liquid phase[30]. Foam has high apparent viscosity and can displace oil efficiently. This has been shown by a number of researchers[21,31–34]. Surfactant foam has an advantage of withstanding shear and high temperature based on the surfactant formulation used.

Following the foam studies using betaines[31,32,34], it was envisioned that betaines help as foam boosters[35] when blended with anionic surfactants and help to produce very strong and more stable foam in the presence of oil. The current study is about zwitterionic and anionic blended surfactants which have the potential to form very strong foam in porous media. Some of the surfactant systems which are used in this study are viscoelastic and are thought to be a potential candidate for mobility control. Surfactant blends of zwitterionic and anionic surfactants studied, showed strong foam rheology in porous media. Their performance was mainly characterized by

3

the synergistic interaction between the surfactants. This study systematically evaluates if synergistic interactions are beneficial for foam boosting in porous media.

1.4 Thesis organization

Thesis is organized as follows

Chapter 2- Gives an introduction to the basic aspects of porous media flow. It briefly discusses the different surfactants used and the schemes followed in different chemical and thermal injection techniques and their advantages and disadvantages. It gives some background information on how foams are generated, what causes foam to collapse and what governs their stability against crude oil.

Chapter 3- Gives a brief literature of rheology of complex fluid (viscoelastic solutions) and basics aspects of a rheology experiments. It discusses the various parameters that affect viscoelasticity and viscosity of solution like salinity, effect of crude oil, blend ratio, alkyl chain length of surfactant. It also compares the behavior of viscoelastic fluid flow with polymer flow in porous media and highlights the important advantages.

Chapter 4- This chapter describes all the experimental protocols on choosing a suitable surfactant candidate and procedure followed to conduct foam studies in porous media. It also describes the foam stability in the presence of crude oil. These porous media observations provide the key information to developing a deeper understanding on what surfactant formulation can benefit an operator for foam EOR.

Chapter 5- This chapter highlights all the interfacial and film drainage studies which help develop a fundamental understanding that can explain the observations of foam studies in porous media. Fundamental aspects like surfactant synergism, monolayer composition and surface

excess adsorption (adsorption at air-water and oleic-water interfaces) is described. It helps to

develop an insight on the relationship between rheological behavior of foam in porous media

and the interfacial aspects of surfactants, and if they have any beneficial effects on foam

boosting.

Chapter 6- This chapter highlights the conclusions of the study and provides recommendation

for future work.

References:

(1)   Lake, L. W. Enhanced Oil Recovery**,** 1st edition, Prentice Hall, **1989**.
(2)   Will Enhanced Oil Recovery Be An Oil Supply Savior? - Scitizen
        http://scitizen.com/future-energies/will-enhanced-oil-recovery-be-an-oil-supply-savior-_a-
        14-3424.html (accessed Oct 6, 2015).
(3)   Latil, Marcel. *Enhanced Oil Recovery*; Editions TECHNIP, **1980**.
(4)   Alvarado, V.; Manrique, E. Enhanced Oil Recovery: An Update Review. *Energies* **2010**,
        3, 1529–1575.
(5)   Gittler, W. E. Alkaline Flooding for Enhanced Oil Recovery. *Drill.-DCW U. S.* **1983**,
        44:12.
(6)   Taber, J. J.; Martin, F. D.; Seright, R. S. EOR Screening Criteria Revisited - Part 1:
        Introduction to Screening Criteria and Enhanced Recovery Field Projects. *SPE Reserv.
        Eng.* **1997**, *12*, 189–198.
(7)   Mayer, E. H.; Berg, R. L.; Carmichael, J. D.; Weinbrandt, R. M. Alkaline Injection for
        Enhanced Oil Recovery - A Status Report. *J. Pet. Technol.* **1983**, *35*, 209–221.
(8)   Wassmuth, F. R.; Green, K.; Arnold, W.; Cameron, N. Polymer Flood Application to
        Improve Heavy Oil Recovery at East Bodo. *J. Can. Pet. Technol.* **2009**, *48*, 55–61.
(9)   Seright, R. S.; Seheult, J. M.; Talashek, T. **2008,** Injectivity Characteristics of EOR
        Polymers.Society of Petroleum Engineers, SPE Annual Technical Conference and
        Exhibition, 21-24 September, Denver, Colorado, SPE -115142-MS.
(10)   Bauer, R. G.; Klemmensen, D. F. **1982,** A New Polymer for Enhanced Oil Recovery.
        Society of Petroleum Engineers, SPE Enhanced Oil Recovery Symposium, 4-7 April,
        Tulsa, Oklahoma, SPE- 10711.
(11)   Han, M.; Xiang, W.; Zhang, J.; Jiang, W.; Sun, F. **2006,** Application of EOR Technology
        by Means of Polymer Flooding in Bohai Oilfields. Society of Petroleum Engineers,
        International Oil & Gas Conference and Exhibition in China, 5-7 December, Beijing, SPE-
        104432-MS**.**
(12)   Liu, Q.; Dong, M.; Ma, S.; Tu, Y. Surfactant Enhanced Alkaline Flooding for Western
        Canadian Heavy Oil Recovery. *Colloids Surf. Physicochem. Eng. Asp.* **2007**, *293*, 63–71.
(13)   Liu, Q.; Dong, M.; Ma, S. **2006,** Alkaline/Surfactant Flood Potential in Western Canadian
        Heavy Oil Reservoirs. Society of Petroleum Engineers, SPE/DOE Symposium on
        Improved Oil Recovery, 22-26 April, Tulsa, Oklahoma, SPE-99791-MS.

(14) Shuler, P. J.; Kuehne, D. L.; Lerner, R. M. Improving Chemical Flood Efficiency With Micellar/Alkaline/Polymer Processes. *J. Pet. Technol.* **1989**, *41*, 80–88.

(15) Hongyan, W.; Xulong, C.; Jichao, Z.; Aimei, Z. Development and Application of Dilute Surfactant–polymer Flooding System for Shengli Oilfield. *J. Pet. Sci. Eng.* **2009**, *65*, 45–50.

(16) Shah, D. O.;Schechter,R.S. *Improved Oil Recovery by Surfactant and Polymer Flooding*; Elsevier, **2012**.

(17) Chang, H. L.; Zhang, Z. Q.; Wang, Q. M.; Xu, Z. S.; Guo, Z. D.; Sun, H. Q.; Cao, X. L.; Qiao, Q. Advances in Polymer Flooding and Alkaline/Surfactant/Polymer Processes as Developed and Applied in the People's Republic of China. *J. Pet. Technol.* **2006**, *58*, 84–89.

(18) Clark, S. R.; Pitts, M. J.; Smith, S. M. Design and Application of an Alkaline-Surfactant-Polymer Recovery System to the West Kiehl Field. *SPE Adv. Technol. Ser.* **1993**, *1*, 172–179.

(19) Liu, S.; Zhang, D.; Yan, W.; Puerto, M.; Hirasaki, G. J.; Miller, C. A. Favorable Attributes of Alkaline-Surfactant-Polymer Flooding. *SPE J.* **2008**, *13*, 5–16.

(20) Demin, W.; Zhenhua, Z.; Jiecheng, C.; Jingchun, Y.; Shutang, G.; Li, L. Pilot Test of Alkaline Surfactant Polymer Flooding in Daqing Oil Field. *SPE Reserv. Eng.* **1997**, *12*, 229–233.

(21) Simjoo, M.; Dong, Y.; Andrianov, A.; Talanana, M.; Zitha, P. L. J. **2012**, A CT Scan Study of Immiscible Foam Flow in Porous Media for EOR. Society of Petroleum Engineers, SPE EOR Conference at Oil and Gas West Asia, 16-18 April Muscat, PE-155633-MS.

(22) Lawson, J. B.; Reisberg, J. **1980**, Alternate Slugs Of Gas And Dilute Surfactant For Mobility Control During Chemical Flooding. Society of Petroleum Engineers, SPE/DOE Enhanced Oil Recovery Symposium, 20-23 April Tulsa, Oklahoma, SPE-8839-MS.

(23) Turta, A. T.; Singhal, A. K. Field Foam Applications in Enhanced Oil Recovery Projects: Screening and Design Aspects. *J. Can. Pet. Technol.* **2002**, *41*.

(24) Farajzadeh, R.; Andrianov, A.; Zitha, P. L. J. Investigation of Immiscible and Miscible Foam for Enhancing Oil Recovery. *Ind. Eng. Chem. Res.* **2010**, *49*, 1910–1919.

(25) Zhang, Y.; Yue, X.; Dong, J.; Yu, L. **2000**, New and Effective Foam Flooding To Recover Oil in Heterogeneous Reservoir. Society of Petroleum Engineers, SPE/DOE Improved Oil Recovery Symposium, 3-5 April Tulsa, Oklahoma, SPE- 59367.

(26) Patzek, T. W. Field Applications of Steam Foam for Mobility Improvement and Profile Control. *SPE Reserv. Eng.* **1996**, *11*, 79–86.

(27) Blaker, T.; Aarra, M. G.; Skauge, A.; Rasmussen, L.; Celius, H. K.; Martinsen, H. A.; Vassenden, F. Foam for Gas Mobility Control in the Snorre Field: The FAWAG Project. *SPE Reserv. Eval. Eng.* **2002**, *5*, 317–323.

(28) Demin, W.; Jiecheng, C.; Junzheng, W.; Zhenyu, Y.; Yuming, Y. **1999**, Summary of ASP Pilots in Daqing Oil Field. Society of Petroleum Engineers, SPE Asia Pacific Improved Oil Recovery Conference, 25-26 October Kuala Lumpur, SPE-57288-MS.

(29) Liu, S. Alkaline Surfactant Polymer Enhanced Oil Recovery Process; Rice University, PhD Dissertation,**2008**.

(30) Laurier L. Schramm; Fred Wassmuth. Foams: Basic Principles. In *Foams: Fundamentals and Applications in the Petroleum Industry*; Advances in Chemistry; American Chemical Society, **1994**; Vol. 242, pp. 3–45.

(31) Li, R. F. Study of Foam Mobility Control in Surfactant Enhanced Oil Recovery Processes in One-Dimensional, Heterogeneous Two-Dimensional, and Micro Model Systems; Rice University, PhD Dissertation **2011**.

(32) Lopez-Salinas, J. L. Transport of Components and Phases in a Surfactant/Foam EOR Process for a Giant Carbonate Reservoir; Rice University, PhD Dissertation **2012**.

(33) Farajzadeh, R.; Andrianov, A.; Bruining, H.; Zitha, P. L. J. Comparative Study of CO2 and N2 Foams in Porous Media at Low and High Pressure−Temperatures. *Ind. Eng. Chem. Res.* **2009**, *48*, 4542–4552.

(34) Cui, L. Application of Foam for Mobility Control in Enhanced Oil Recovery (EOR) Process; Rice University, PhD Dissertation **2014**.

(35) Basheva, E. S.; Ganchev, D.; Denkov, N. D.; Kasuga, K.; Satoh, N.; Tsujii, K. Role of Betaine as Foam Booster in the Presence of Silicone Oil Drops. *Langmuir* **2000**, *16*, 1000–1013.

Chapter 2

Technical Background on EOR processes

2.1 Fundamentals of flow through porous media-Darcy's law

Flow in porous media is famously described by Darcy's law[1]. It is given as

$$q = \frac{k\,A\,dP}{\mu\,dx}$$ Equation 2.1

Where q is the flow rate, k is the permeability, A is the cross sectional area, *dP/dx* is the dynamic pressure gradient and μ is the viscosity of the flowing fluid. The ratio of the permeability of the medium *k* and the viscosity μ of the fluid can be described as λ the mobility.

$$\lambda = \frac{k}{\mu}$$ Equation 2.2

2.2 Capillary pressure

In a reservoir when one fluid displaces another fluid, capillary forces play a dominant role. The effect of capillary force results from the combined forces existing between the rock and fluids and also between the fluids. Typically in reservoir engineering immiscible fluids are injected. When two immiscible fluids contact each other, it leads to a discontinuous pressure at the interface due to its curvature. This curved surface tends to attain the smallest possible area per unit volume. This discontinuous pressure due to the curvature of the interface is called capillary pressure[2]. Capillary pressure occurs between any immiscible fluids like oil-water, oil-gas, and water-gas.

A relation between the interfacial tension σ and the capillary pressure P_c is given by the Young-Laplace equation as

$$P_c = \frac{2\sigma \cos\theta}{R} \qquad \text{Equation 2.3}$$

P_c is the minimum pressure required to displace the wetting phase from out of the largest pore of radius R, by the non-wetting phase. *Cos θ* term arises due to the effect of wettability.

2.3 Interfacial tension and capillary number

Interfacial tension is the force exerted when two immiscible fluids come together and form a curved interface. Surface tension is when one of the phases is gas or vapor. The relative importance of the viscous forces and the capillary forces is given by a dimensionless number called the capillary number N_{CA}. It is expressed as

$$N_{CA} = \frac{v\mu}{\sigma} \qquad \text{Equation 2.4}$$

Where v is the velocity, μ is the viscosity of the fluid and σ the interfacial tension.
If the driving force is gravity instead of viscous force the corresponding dimensionless group is known as the Bond number N_B.

$$N_B = \frac{\Delta\rho \, L^2 g}{\sigma} \qquad \text{Equation 2.5}$$

Where Δρ is the density difference between the phases, L is the characteristic length scale of the flow path, g is acceleration due to gravity and σ is the interfacial tension.

At the end of water flood the capillary number is in the range[3] of 10^{-6} to 10^{-7}. As the capillary number increases the oil displacement efficiency also increases. Increasing capillary number by 4 orders of magnitude can increase oil recovery to a large extent. The capillary number can be increased by increasing the flowrate of the displacing medium or by increasing

the viscosity of the displacing medium. Typically in the case of oil recovery the displacing medium is an aqueous phase. Generally the viscosity of the aqueous phase remains constant and so is the flow rate that is inside the reservoir. Additionally if $v\mu$ is increased greatly the injection pressure will increase enormously leading to fracture of the medium. When a fracture is present the fluids easily bypass through it without entering into the matrix. Hence reducing the interfacial tension (IFT) to a large extent will increase the capillary number by orders of magnitude than that of waterflood values. This can be done with the help of surfactants.

2.4 Surfactants

Surfactants are amphiphilic moieties which have a hydrophilic head group and a hydrophobic tail. When the concentration is low, surfactants form monomers in solution. When the concentration increases micelles start to form. The concentration at which micelles start to form is known as the critical micelle concentration. Surfactants tend to adsorb at the interface between two liquids and hence reduce the IFT. In some cases they reduce IFT to ultra-low values of 10^{-3} mN/m, but this requires the formation of microemulsions between the oleic and aqueous phase.

Since the hydrophobic tails try to keep away from water, they aggregate and form micelles in which the hydrophobic tails face towards the center and the hydrophilic heads face towards the water. The driving force for the micellization process is the hydrophobic effect as mentioned above. The different shapes of the micelles are formed due to various geometric considerations. The packing of the micelles depends on the optimal area of the head group a_0, the critical chain length l_c of the hydrocarbon tail, and volume v of the hydrocarbon chain. The maximum effective tail length l_c and the tail volume v are given by a relation as [4]

$$l_c \approx (1.54 + 1.265\, n_c)\ \text{Å} \quad \text{Equation 2.6}$$

$$v \approx 27.4 + 26.9 n_c \text{Å}^3 \qquad \text{Equation 2.7}$$

where n_c is the number of carbon atoms. The estimation of a_0 is hard as it depends on the solvent

environment. If the ionic strength is low, there is more repulsion between head groups for ionic

surfactants leading to a larger effective area. As the ionic strength increases the repulsions are

screened leading to smaller effective head group areas. A term called the critical packing

parameter (CPP) a dimensionless number $\frac{v}{a_0 l_c}$ determines the shape a molecule can adopt. For the

micelles to pack in to a spherical configuration the CPP must be <1/3. Cylindrical micelles are

formed when 1/3<CPP<1/2. When CPP is between ½ - 1, flexible bilayers or vesicles can form.

When CPP=1, lamellar structures are formed. When CPP>1 inverse hexagonal, inverse micellar

structures are formed.

Surfactants are classified as

- Anionics
- Cationics
- Non -Ionics
- Zwitterionics

Anionic surfactants have a negatively charged headgroup. Cationic surfactants have a

positively charged headgroup. Non-Ionic surfactants have no charge on the head group.

Zwitterionic surfactants have both the positive and negative charge on the head group. Table 2.1

gives a classification of surfactants used.
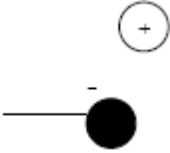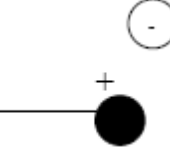
Class	Examples	Structures
Anionic: negatively charged head group	Sulfonates Sulfates Carboxylates Phosphates	
Cationic: positively charged head group	Quaternary ammonium organics, amines, pyridinium, imidazolinium, piperidinium, sulfonium compounds	
Non-ionic: No charge on the head group	Alkyl-,aryl-,acyl-,acylamindo-,acyl-aminepolyglycol polyol ethers Alkanolamides	
Zwitterionic: Both positive and negative charge on the head group	Aminocarboxylic acids, Betaine surfactants, Sulfo betaines	

Table 2.1: Classification of surfactants used for enhanced oil recovery[4]

The main role of surfactant is to lower the interfacial tension between oil (displaced phase) and aqueous phase (displacing phase).

Figure 2.1 shows the capillary desaturation curve for sandstone cores[5]. The figure shows that when the capillary number is increased to the order of 10^{-2}, residual oil saturation comes close to 0. This is the aim of a low IFT surfactant flood.
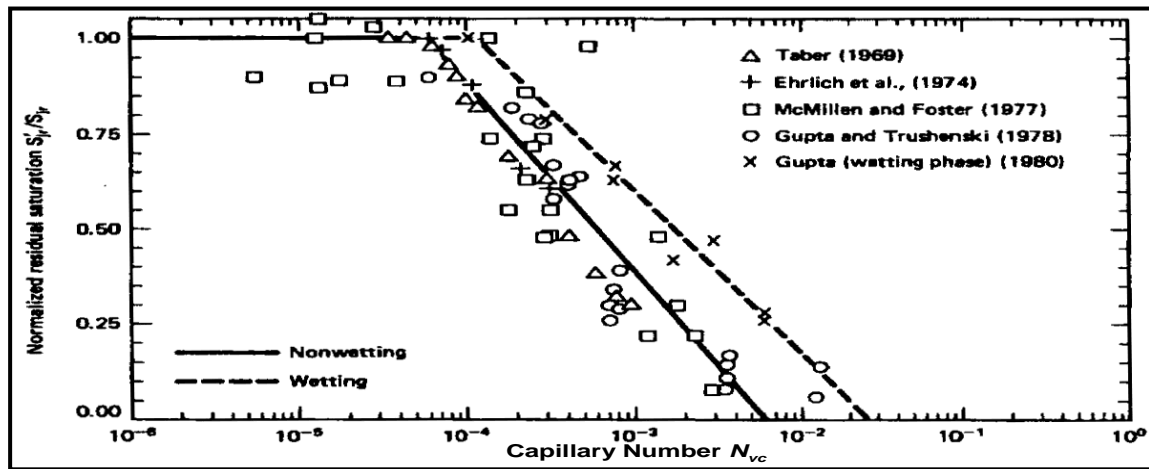
Figure 2.1: Capillary desaturation curves in sandstone cores [5].

2.5 Fundamentals of foam flow in porous media:

Foam is used to reduce the mobility of gases such as steam, CO_2, nitrogen and natural gas. Foam was used as an alternative to polymer in surfactant flood. Polymer in use for EOR processes was susceptible to degradation in the presence of excess divalent ions and high salinity brine and high temperature as well. Typically for EOR process foam is generated by contacting an aqueous surfactant solution with a gas phase, and hence the foam which contains the surfactant has the potential to reduce tension to low values with properly chosen formulation and at the same time improve volumetric sweep efficiencies to a large extent.

Figure 2.2 shows a schematic of a foam system in two-dimensional view (bulk foam). A lamella consists of a thin liquid film and is bounded by gas on either side. The three neighboring lamellae meet at angle of $120°$. This junction is known as the Gibbs -Plateau border[6].

13
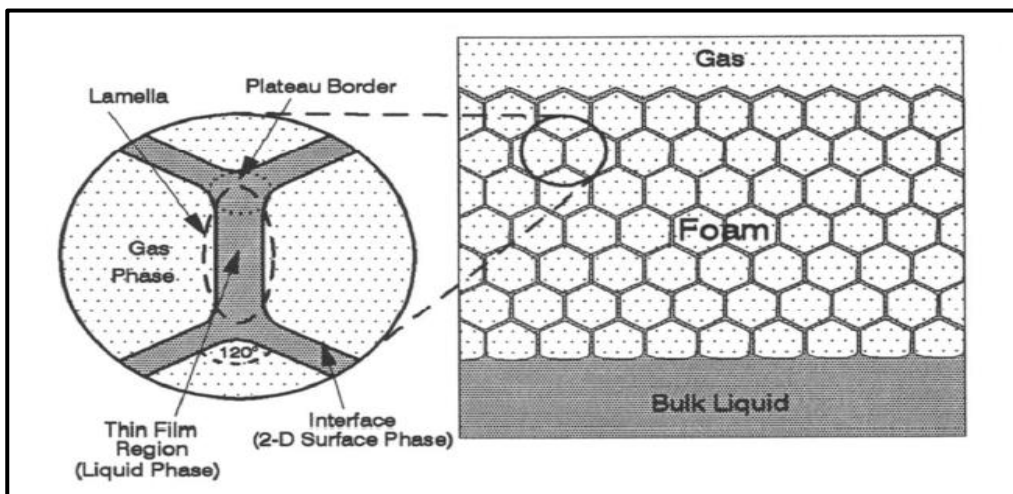
Figure 2.2: A generalized two dimensional foam system- schematic representation[6]

Hirasaki defined foam as "*Dispersion of a gas in a liquid such that the liquid phase is continuous (i.e. connected), and at least some part of the gas is made discontinuous by thin liquid films called lamella*"[7]. There are three important things about foam flow in porous media[8]. One is that porous media consists of a distribution of pore sizes. Pore body is connected to another pore body through a pore throat. The aspect ratio, which is the size ratio of the body and throat, governs the generation of foam in porous media by capillary snap off. Secondly the pores are not cylindrical in shape, rather they have corners. The wetting phase (typically the aqueous phase in case of water wet media) fills the small pores and also the thin liquid film remains continuous by wetting the walls through the corners. The non wetting phase (mostly the gas) occupies the large pore spaces. Thirdly when two-phase flow occurs, the non wetting phase flows through the large pore spaces which are interconnected and the wetting phase flow through the smaller interconnected pores and also as thin films in the non wetting phase occupied pores due to the pressure gradients in the liquid phase.

Foam is an effective mobility control agent because the resistance to foam flow is higher than that of either the gas or the liquid phase. The reduced mobility ($\lambda = k/\mu$) arises due to the reduced gas relative permeability and the increase in its apparent viscosity. The reduced gas relative permeability arises due to the trapped gas saturation in the porous media. The viscosity increase results from not only the viscous shear stresses in the films, but also due to the force created in pushing the lamellae through pore constrictions[9]. The main factor that affects the apparent viscosity of foam in porous media is the bubble texture (bubble volume) [10]. It has been found that foam is non-Newtonian and shear thinning[10,11]. The shear thinning apparent viscosity scales with the exponent of -1/3 to -2/3 with velocity of flow. The contribution to foam apparent viscosity during flow through a cylindrical capillary tube is explained by Hirasaki and Lawson[11] as a sum of three important contributions due to a) the liquid slugs in between bubbles, b) the viscous resistance between the wall and the bubble during flow that deforms the interface and c) surface tension gradients on the foam films. It has been found that porous media contain significant amounts of trapped gas[12] which affects foam flow. When the gas phase is continuous, weak foam in generated. When the gas phase is discontinuous, strong foam is generated (Figure 2.3).

Figure 2.3: Schematic representation of discontinuous and continuous gas flow and trapped gas.(Reference for figure is from PhD thesis of Jose Lopez Salinas which is an adaptation of the work of Radke and Gillis.)[12,14]
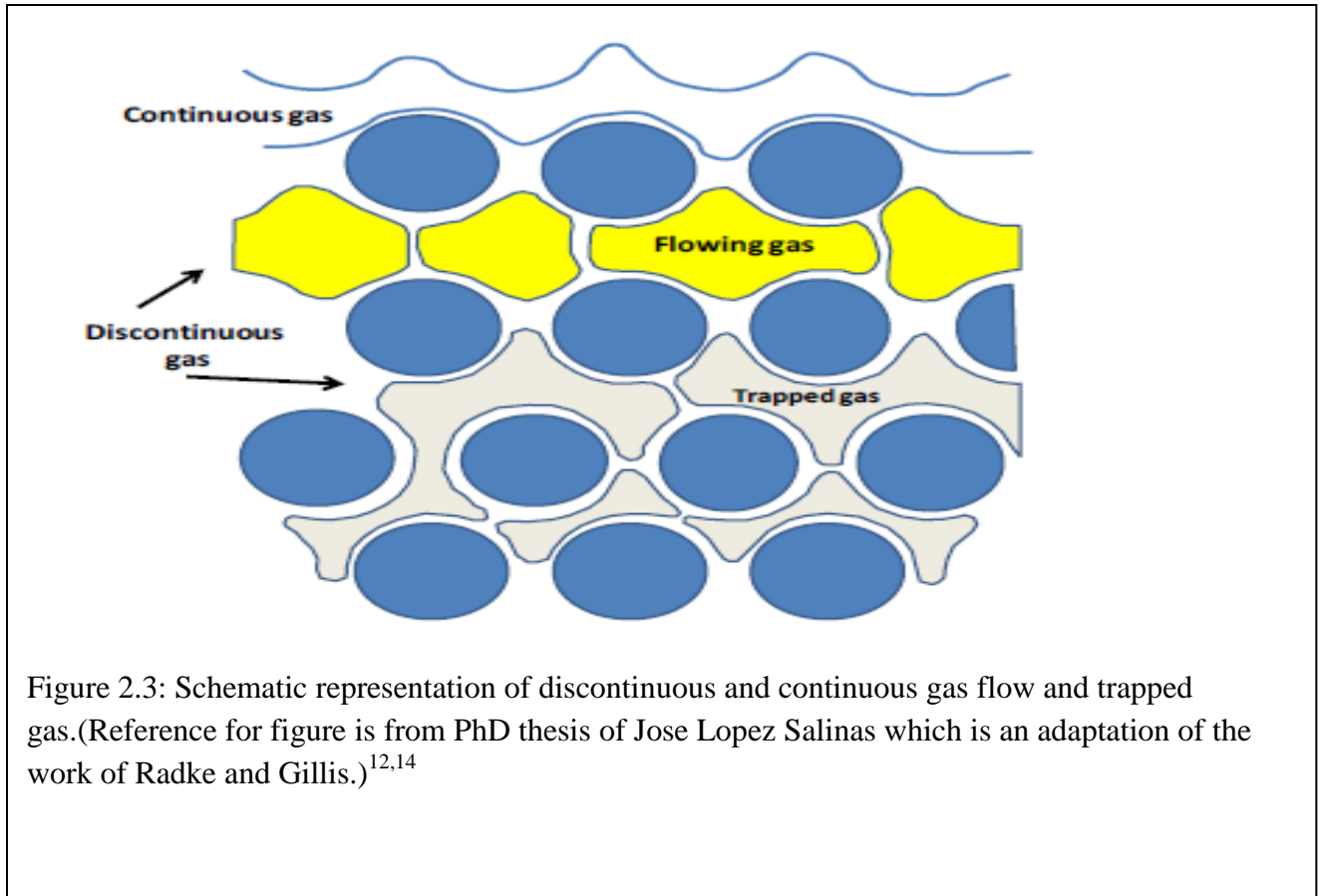
2.6 Mechanisms of foam generation in porous media:

The three most prevalent mechanisms for pore level foam generation[10,13] have been a) snap off, b) lamella division and c) leave behind

Snap off: Figure 2.4 shows a schematic representation of the snap off mechanism. This was first studied by Roof[14] who actually explained how snap off of an oil droplet in a water filled media occur. A gas bubble enters a pore constriction and passes through the constriction. As it moves out, it expands, causing an increase in the bubble diameter which in turn, causes the capillary pressure to decrease. As a result, the liquid phase experiences a pressure gradient causing the liquid from the surroundings to flow in to the neck constriction. The incoming liquid accumulates as a collar in the neck of the constriction. When the capillary pressure drops below a

16

critical value the liquid will snap off, forming a new gas bubble. Capillary pressure plays a central role in snap off mechanism. The pressure must drop to below a critical capillary pressure $P_c^{sn} \approx \sim 0.4\ P_c^{e}$ the capillary entry pressure , for snap off to occur[10]. Snap off generates separate gas bubbles and hence it creates a discontinuous flow of the gas phase. This creates strong foam. The most dominant mechanism of foam generation in porous media is lamella divison when gas and surfactant are co-injected. Snap off generally occurs in multiphase flow even in the absence of surfactant. However, if surfactant is absent the bubbles that are formed will coalesce rapidly which will result in continuous gas flow.
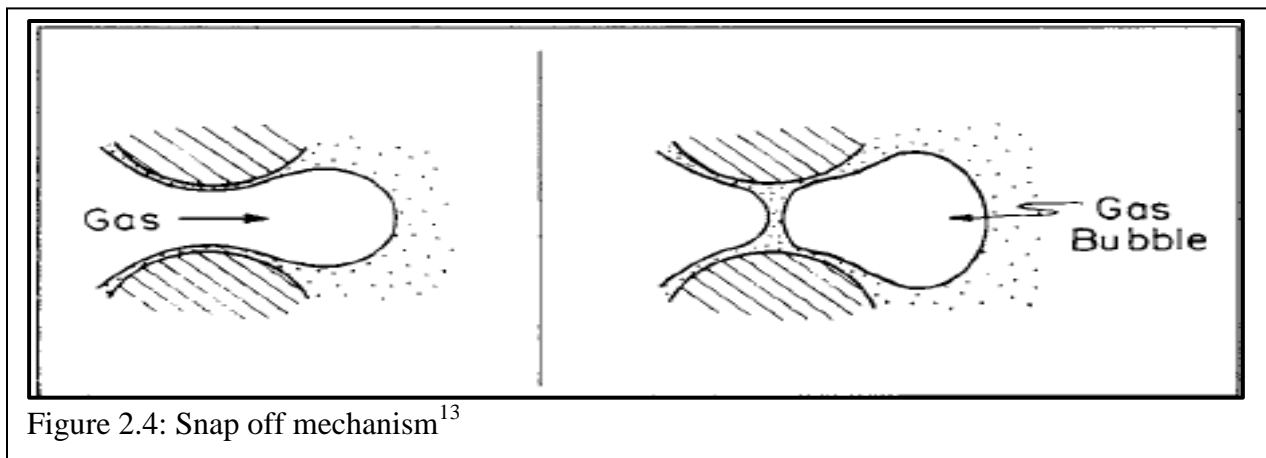
Figure 2.4: Snap off mechanism[13]

Lamella Division: For lamella division to occur the pre-existence of a moving lamella is necessary. Figure 2.5 shows a schematic representation of a lamella division mechanism for foam generation. When a lamella approaches a branch point in the porous medium as shown in the figure, the bubble tends to split into two and flow in the two channels (branches). If there is only a single train of bubbles the lamella flows into only one of the channels, in which case there is no alteration in the lamella. Whether or not the lamella divides depends on the bubble size, pore geometry and pressure gradient. If the size of the bubble is smaller than the pore body space then it will flow into only one of the channels unaltered. If the bubble size is larger than the pore

17

body space, the interface will span across the grain and cause a split into two lamellae. This mechanism depends on the pressure gradient. This mechanism is similar to snap off in that it generates a discontinuous gas flow when the division of the lamella occurs. This mechanism generates strong foam too.
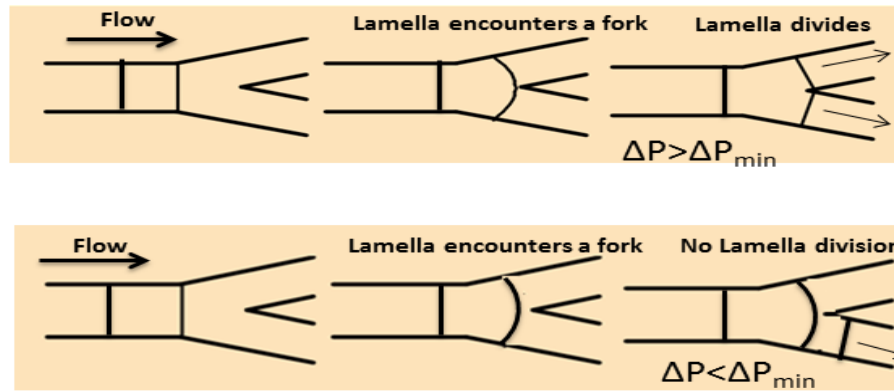
Figure 2.5: Lamella Division mechanism(Adapted from Prof. Bill Rossen's lecture notes)

Leave behind mechanism: When gas invades a liquid-saturated region, two gas fronts can

 approach the same region from different direction. The times at which the gas fronts approach

the region can happen at different times. But when the gas fronts reach the region they squeeze

the liquid in between them to form a lamella. In the presence of sufficient surfactant this lamella

remains stable. In this mechanism no separate gas bubble is generated and hence the gas phase

 remains as a continuous phase. A lamella once ruptured in this pore space, cannot be recreated

unless the liquid invades the pore space again. But the lamella that is created by this way is a

potential source for moving lamella. The type of foam generated is generally weak (Figure 2.6).

Figure 2.6: Leave Behind mechanism[8]
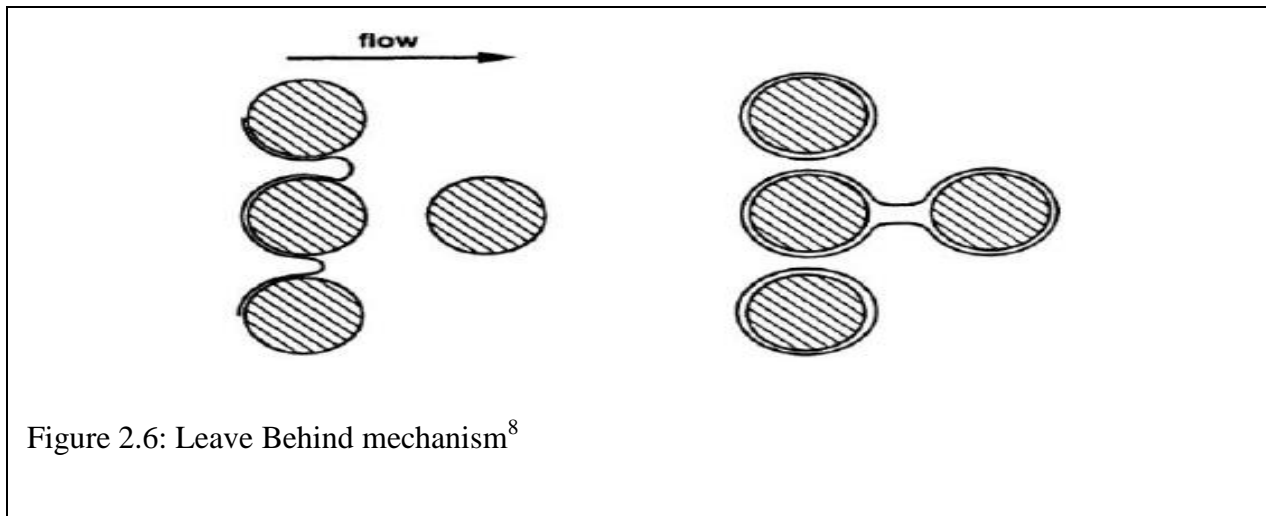
2.7 Mechanism of foam destruction

The three main mechanisms for foam destruction are a) capillary suction coalescence, b) gas diffusion (Oswald ripening) due to bubbles of different sizes c) liquid film drainage due to gravity.

When bulk foam is formed, the liquid in the thin film between the gas bubbles has the tendency to keep draining downwards as a result of the forces due to gravity. At this point the gas bubble moves from a spherical shape to a polyhedral shape. The capillary forces start competing with the gravity forces. As the thin liquid film starts to thin, the interface becomes flat. But at the Gibbs-Plateau border the interface is still curved. At this curved the pressure is lower than at the flat interface. At the flat interface pressure is equal to gas phase pressure. Hence the liquid starts to move from the lamellae to the Gibbs-Plateau border. If this thinning continues, then eventually the foam will rupture or "destabilize". This destabilizing effect is known as capillary suction coalescence. Van der Waals attractive forces cause the lamella to thin down too. However there exist restoring forces that help in increasing the stability of the liquid

19

lamella. This restoring effect is known as the Gibbs Marangoni effect which acts in addition to the repulsive component of the disjoining pressure.

Foam film must possess certain amount of elasticity to be able to withstand deformation during flow through porous media. When a surfactant-stabilized liquid film undergoes a sudden expansion, the expanded region has a lesser number of surfactant molecules per unit area due to increased area. The expanded portion has an increased local surface tension that increases the resistance to further expansion. The remaining portion has low surface tension. The surface gradient helps in pulling liquid from the unexpanded region into the expanded region. This flow of liquid resists film thinning. The flow of liquid due to surface tension gradient is known as the Marangoni effect. This resisting force exists until the adsorbed surfactant molecules minimize the free energy. The surface tension gradient as a result of stretching and thinning a portion of the film induces interfacial flow that drags water to the stretched region. This gives the film elasticity and helps reduce thinning. When an ionic surfactant is used to stabilize the films, the electric double layers of the interfaces on either side of the film will repel each other. Hence this resists the film from thinning.

When a lamella is bound by two interfaces, the interacting electric double layers exert a pressure which keeps the interfaces apart (prevents foam thinning). Disjoining pressure is the pressure per unit area which if repulsive, can balance the capillary pressure which tends to drain the water from the film. It is a function of the thickness of the liquid film and is comprised of the electrical, van der Waals and steric interactions. The disjoining pressure Π is expressed as a function of film thickness

$$\Pi(h) = -\frac{dV}{dh}$$ Equation 2.8

V is the interaction potential which is the sum of the attractive and the repulsive energies as predicted by the DLVO theory.

The other influence on film stability is the gas diffusion between bubbles, which occurs when there is a distribution of bubble sizes. In this case pressure gradients will exist across films bounded by bubbles of different sizes which cause the gas to diffuse through the liquid lamella. This effect is also called coarsening.

2.8 Stability of foam in presence of oil

Pseudoemulsion film is a water film which is bounded by air on one side and oil on the other side. Several researchers have shown the destabilizing effect of oil on foam flow in porous media[15–20].They have found the destabilizing effect to be surfactant specific. Further research done on the stability of foam in the presence of oil, has found that the stability of the pseudoemulsion film[19,21–25] is a controlling factor for foam flow in porous media. Figure 2.7 shows the process of pseudoemulsion film rupture[26] due to the presence of oil. The initial configuration shows an emulsified oil droplet. As the oil droplet interacts with the gas-water interface, there is a deformation of the oil droplet which is separated from the gas by a pseudoemulsion film. When the pseudoemulsion film ruptures, the oil forms a lens on the solution surface which eventually spreads. This is one of the most important mechanisms for foam destabilization by crude oil[26]. Pseudoemulsion film stability depends on the surfactant structure, ionic environment, temperature, external disturbances and also on the oil type.

Other mechanisms for the effect of crude oil on foam films have been described in literature by three coefficients which thermodynamically describe the foam stability using

interfacial tensions[27]. They are entry coefficient (E), Spreading coefficient (S) and Bridging coefficient (B)

$$E = \gamma_{AW} + \gamma_{OW} - \gamma_{AO}$$

$$S = \gamma_{AW} - \gamma_{OW} - \gamma_{AO}$$

$$B = \gamma_{AW}^2 + \gamma_{OW}^2 - \gamma_{AO}^2$$

Where A represents air, W- water, O- oil and γ is the surface tension.

When oil spreads over the aqueous gas interface, some amount of aqueous oil- interface is created and some oil-gas interface is created. There is a decrease in the aqueous-gas interface. This causes the film to thin. Spreading is said to be favorable when S is positive and can eventually damage the foam film. When a droplet of oil enters the aqueous-gas interface, it is known as entry. Positive values of E specify easy entry of oil drop into the foam lamella and cause to rupture it. Positive values of B lead to the rupture of foam lamellae. When a bridge is formed between the aqueous-oil-gas phases, the bridge is stretched due to the effects of capillary pressure and can eventually rupture.

Figure 2.7: Process of oil droplet spreading on a gas-water interface thereby causing the rupture of the interface. The sequence shows a) the initial configuration of an oil droplet, b) oil droplet is hindered from entering the gas water interface by a pseudoemulsion film, c) a lens of oil is formed as the oil enters the surface and d) the oil spreads on the surface thereby causing rupture. (Picture is reproduced from the work of Wasan et.al[27])

When foam films move through porous media, there is stretching and contraction taking place. This action can cause the film to thin. In addition to that the presence of oil can change the tension at the interfaces. Some reasons for thinning of film in the presence of oil are a) depletion of surfactant at the air-water interface due to surfactant partitioning in to the oil phase, b) oil can get solubilized in to the core of the micelle or even adsorbed on the air-water interface.

Schramm and Novosad[28] have proposed a lamella number which is the ratio of suction force in the Plateau border and the resisting force due to the oil's tendency to minimize interfacial tension. They suggest that if Lamella number >1 the oil droplets will enter the Plateau border. For foam to be stable the Lamella number should be very small and the entering

coefficient should be negative. However irrespective of the Lamella number pseudoemulsion film will be stable for E<0.

Basheva et.al have found that when oil has a large barrier to enter the gas water interface, the surfactant can create stable foam in the presence of oil[29]. In this scenario the entering, spreading, bridging coefficients are not adequate to describe the effect of oil on foam film because disjoining pressure creates an additional barrier for the oil drop entry into the gas-water interface. Schramm and Novosad have shown that light oil tends to destabilize foam more than heavy oil[30,31].A comprehensive literature has already been recorded and can be found in reference[27,32].

2.9 Disjoining pressure, limiting capillary pressure and foam stability

Foams are metastable objects. The longevity of the foam film is determined by the longevity of the single film. The single film at molecular scale is governed by the disjoining pressure. Disjoining pressure is the change in energy per unit area when two interfaces are brought together to a finite thickness h[33]. The disjoining pressure isotherm is comprised of the van der Waals component which is attractive and takes effect when films become extremely thin (few nm), and the electrostatic repulsive forces, which cause the repulsion of the two interfaces when ionic surfactants are adsorbed there. The electrostatic repulsive component can cause metastable or stable films, depending on the thickness of the film (See Figure 2.8). Such films are usually referred to as common black films, which have a positive disjoining pressure. Additionally Newton black films, which are very thin with the two monolayers almost in contact, can be formed as well.

The disjoining pressure as mentioned earlier is governed by the electrolyte concentration and surfactant structure. Hence in order to get stable foam the right choice of surfactant formulation is desired. Figure 2.8 is a disjoining pressure isotherm showing regions where stable, metastable and unstable films are formed. At equilibrium disjoining pressure of a flat film is equal to the capillary pressure

$$\Pi = \Pi_{elec} + \Pi_{vdw} + \Pi_{steric} = P_c \qquad \text{Equation 2.9}$$

At a critical capillary pressure P_c^{crit} the lamellae may rupture due to the high capillary suction which is higher than the maximum disjoining pressure.

Figure 2.8: Disjoining pressure isotherms, 1 – stable state, 2- metastable state, 3- unstable state[32].
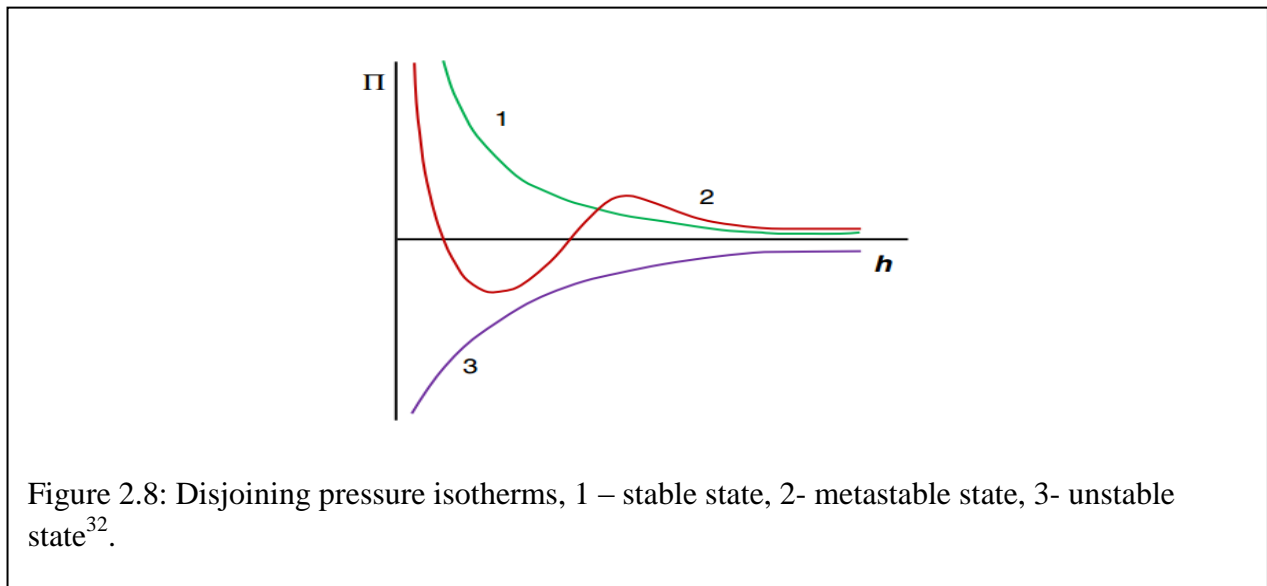
Foam flow in porous media is a complex combination of the petrophysical properties of the rock and also the thin film dynamics, the latter, in turn depends on the surfactant structure. Khatib et.al [34] observed that whenever the gas fraction of flowing foam in porous media was increased beyond a certain value for a given system, foam coalescence was observed. This limiting capillary pressure depended on surfactant structure and the salinity, permeability of the

25

media and the gas flow rates. Figure 2.9 shows the region of the limiting capillary pressure and the corresponding water saturation. At the limiting capillary pressure, usually at very high gas fraction, the foam becomes very unstable. Aronson et.al[35] studied foam flow in porous media and also measured the disjoining pressures of the corresponding surfactant films and established a relation between the limiting capillary pressure and the rupture pressure of the film. He found that when the surfactant SDS at a certain electrolyte concentration showed high pressure drop during foam flow in porous media, its thin films remained stable at high disjoining pressures. The foams that were weak in porous media showed a lower magnitude of disjoining pressure required for film rupture.

Figure 2.9: Capillary pressure curve for gas/water system. Pc* is the limiting capillary pressure below which foam is stable. Sw* is the water saturation corresponding to Pc*[32].
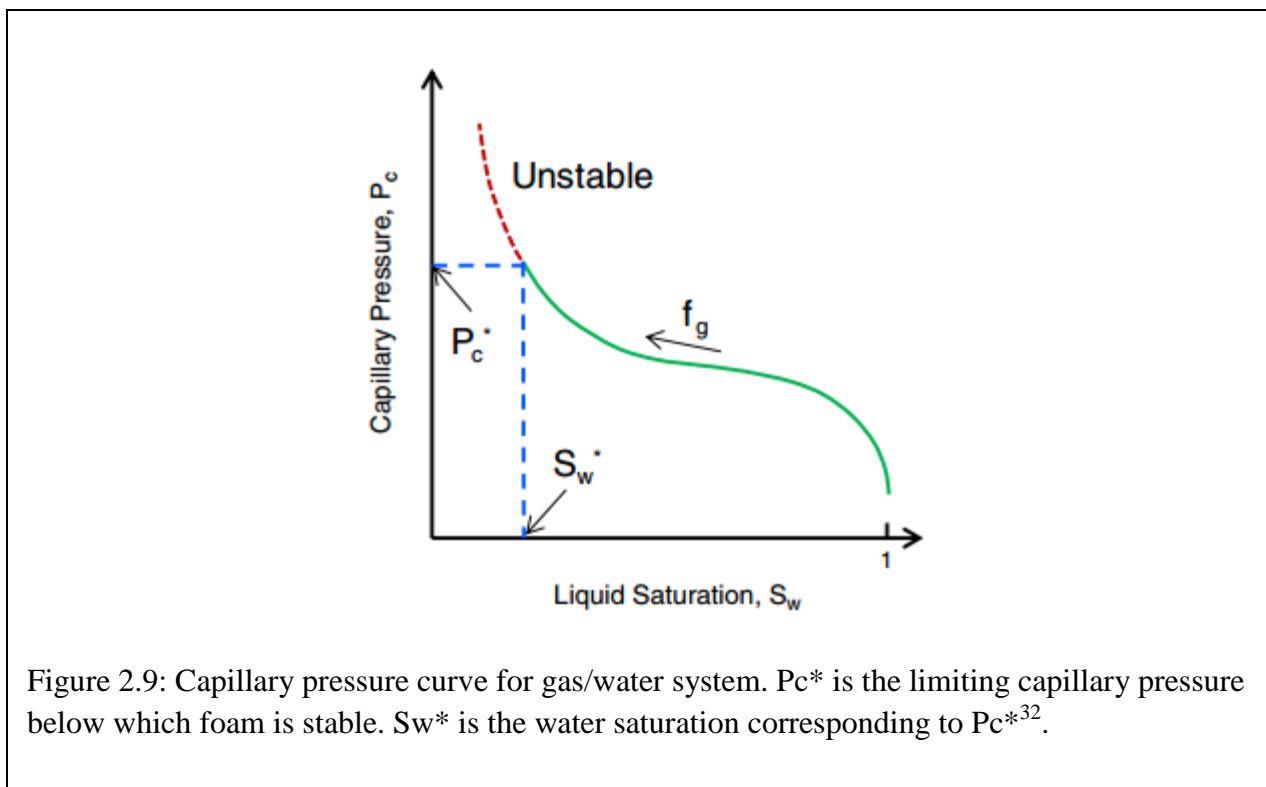
Hence for the application of foam flow for enhanced oil recovery, suitable surfactant formulations are needed for creating strong and stable foam films. Formulation selection is an

interrelated area in which massive amount of research has been done, but it is beyond the scope of this chapter.

2.10 Recovery efficiency of EOR process

Based on the material balance the overall recovery efficiency E_R can be expressed as[5]

$$E_R = \frac{N_p}{N} \quad \text{Equation 2.10}$$

where N is the original oil in place

N_p is the cumulative oil recovered after a process.

The overall efficiency is given as the

$$E_R = E_V E_D \quad \text{Equation 2.11}$$

where E_V is the macroscopic volumetric sweep efficiency

E_D is the microscopic displacement efficiency.

$$E_V = \frac{Volume\ of\ oil\ contacted\ by\ displacing\ agent}{Volume\ of\ oil\ originally\ in\ place} \quad \text{Equation 2.12}$$

$$E_D = \frac{Amount\ of\ oil\ displaced}{Amount\ of\ oil\ displacing\ agent\ contacts} \quad \text{Equation 2.13}$$

Volumetric sweep efficiency depends on the injection pattern, location of the wells, heterogeneity, reservoir thickness, mobility ratio, fractures in the reservoir, flow rate and density difference between the displacing fluid and the displaced fluid. The volumetric sweep efficiency E_V can be further decomposed into the product of areal sweep efficiency and the vertical sweep efficiency. Figure 2.10 shows the difference between areal and vertical sweep efficiency. Areal sweep is the fraction of formation area swept the by displacing fluids. Vertical sweep is the

27

volume of the formation swept in the vertical direction. Poor volumetric sweep efficiency

significantly reduces oil recovery.

The displacement efficiency E_D can be described in terms of the saturation where

$$E_D = 1 - \frac{S_{or}}{S_{in}}$$ Equation 2.14

S_{or} is the residual oil saturation

S_{in} is the initial oil saturation.

Microscopic displacement efficiency E_D depends on relative permeabilities and capillary

number.
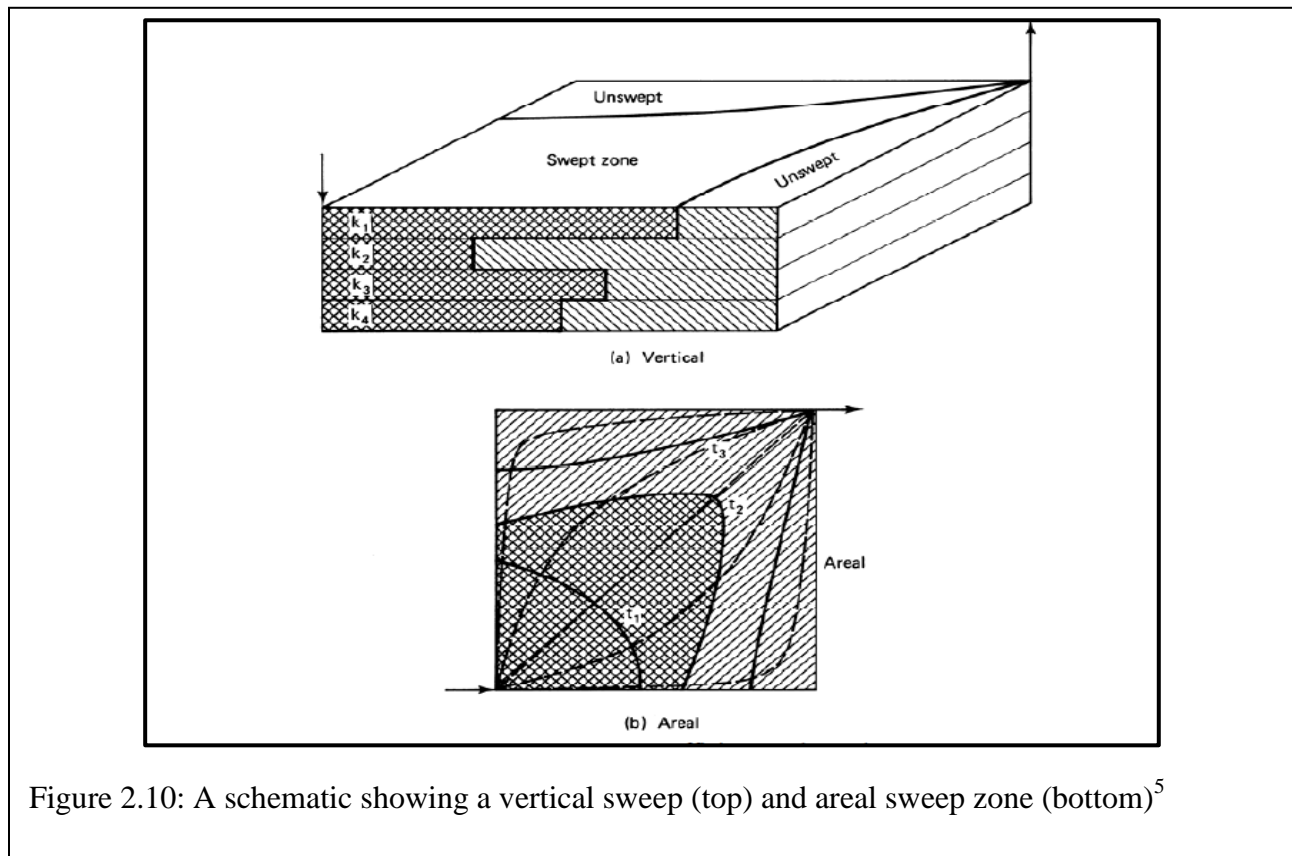
Figure 2.10: A schematic showing a vertical sweep (top) and areal sweep zone (bottom)[5]

In a typical oil recovery process the reduction of IFT by reducing the capillary forces is responsible for the microscopic displacement efficiency. Polymers, foam or other means are responsible for reducing the mobility of the injected fluids which promotes good volumetric sweep efficiency.

References:

(1)   Bear, J. *Dynamics of Fluids in Porous Media*; Courier Corporation, **2013**.
(2)   Tarek Ahmed.. *Reservoir Engineering Handbook*; Gulf Professional Publishing, 2006.
(3)   Donaldson, E. C.; Chilingarian, G. V.; Yen, T. F. *Enhanced Oil Recovery, II: Processes and Operations*; Elsevier, **1989**.
(4)   Israelachvili, J. N. *Intermolecular and Surface Forces: Revised Third Edition*; Academic Press, **2011**.
(5)   Lake, L. W. Enhanced Oil Recovery**,** 1ˢᵗ edition, Prentice Hall, **1989**.
(6)   Laurier L. Schramm; Fred Wassmuth. Foams: Basic Principles. In *Foams: Fundamentals and Applications in the Petroleum Industry*; Advances in Chemistry; American Chemical Society, **1994**; Vol. 242, pp. 3–45.
(7)   Hirasaki, G. J. Supplement to SPE 19505, The Steam-Foam Process--Review of Steam-Foam Process Mechanisms. **1989**.
(8)   Kovscek, A. R.; Radke, C. J. *Fundamentals of Foam Transport in Porous Media*; DOE/BC--93000174; Lawrence Berkeley Lab., CA (United States), **1993**.
(9)   Falls, A. H.; Musters, J. J.; Ratulowski, J. The Apparent Viscosity of Foams in Homogeneous Bead Packs. *SPE Reserv. Eng.* **1989**, *4*, 155–164.
(10)   Falls, A. H.; Hirasaki, G. J.; Patzek, T. W.; Gauglitz, D. A.; Miller, D. D.; Ratulowski, T. Development of a Mechanistic Foam Simulator: The Population Balance and Generation by Snap-Off. *SPE Reserv. Eng.* **1988**, *3*, 884–892.
(11)   Hirasaki, G. J.; Lawson, J. B. Mechanisms of Foam Flow in Porous Media: Apparent Viscosity in Smooth Capillaries. *Soc. Pet. Eng. J.* **1985**, *25*, 176–190.
(12)   Radke, C. J.; Gillis, J. V. A Dual Gas Tracer Technique for Determining Trapped Gas Saturation During Steady Foam Flow in Porous Media. **1990**, Society of Petroleum Engineers, SPE Annual Technical Conference and Exhibition, 23-26 September New Orleans, Louisiana, SPE-20519.
(13)   Ransohoff, T. C.; Radke, C. J. Mechanisms of Foam Generation in Glass-Bead Packs. *SPE Reserv. Eng.* **1988**, *3*, 573–585.
(14)   Roof, J. G. Snap-Off of Oil Droplets in Water-Wet Pores. *Soc. Pet. Eng. J.* **1970**, *10*, 85–90.
(15)   Suffridge, F. E.; Raterman, K. T.; Russell, G. C.; et.al. **1989**, Foam Performance under Reservoir Conditions. Society of Petroleum Engineers, SPE Annual Technical Conference and Exhibition, 8-11 October San Antonio, Texas, SPE-19691.
(16)   Vikingstad, A. K.; Aarra, M. G. Comparing the Static and Dynamic Foam Properties of a Fluorinated and an Alpha Olefin Sulfonate Surfactant. *J. Pet. Sci. Eng.* **2009**, *65*, 105–111.
(17)   Bernard, G. G.; Holm, L. W. Effect of Foam on Permeability of Porous Media to Gas. *Soc. Pet. Eng. J.* **1964**, *4*, 267–274.

(18) Schramm, L. L.; Turta, A. T.; Novosad, J. J. Microvisual and Coreflood Studies of Foam Interactions With a Light Crude Oil. *SPE Reserv. Eng.* **1993**, *8*, 201–206.

(19) Nikolov, A. D.; Wasan, D. T.; Huang, D. W.; Edwards, D. A. **1986,** The Effect of Oil on Foam Stability: Mechanisms and Implications for Oil Displacement by Foam in Porous Media. Society of Petroleum Engineers, SPE Annual Technical Conference and Exhibition, 5-8 October, New Orleans, Louisiana, SPE-15443-MS.

(20) Jensen, J. A.; Friedmann, F. **1987,** Physical and Chemical Effects of an Oil Phase on the Propagation of Foam in Porous Media. Society of Petroleum Engineers, SPE California Regional Meeting, 8-10 April, Ventura, California,MS-16375.

(21) Hanssen, J. E.; Dalland, M. **1990,** Foams for Effective Gas Blockage in the Presence of Crude Oil. Society of Petroleum Engineers, SPE/DOE Enhanced Oil Recovery Symposium, 22-25 April, Tulsa, Oklahoma, SPE-20193.

(22) Manlowe, D. J.; Radke, C. J. A Pore-Level Investigation of Foam/Oil Interactions in Porous Media. *SPE Reserv. Eng.* **1990**, *5*, 495–502.

(23) Lobo, L.; Wasan, D. T. Mechanisms of Aqueous Foam Stability in the Presence of Emulsified Non-Aqueous-Phase Liquids: Structure and Stability of the Pseudoemulsion Film. *Langmuir* **1993**, *9*, 1668–1677.

(24) Nikolov, A. D.; Wasan, D. T. Ordered Micelle Structuring in Thin Films Formed from Anionic Surfactant Solutions. *J. Colloid Interface Sci.* **1989**, *133*, 1–12.

(25) Bergeron, V.; Fagan, M. E.; Radke, C. J. Generalized Entering Coefficients: A Criterion for Foam Stability against Oil in Porous Media. *Langmuir* **1993**, *9*, 1704–1713.

(26) D. T. Wasan; K. Koczo; A. D. Nikolov. Mechanisms of Aqueous Foam Stability and Antifoaming Action with and without Oil. In *Foams: Fundamentals and Applications in the Petroleum Industry*; Advances in Chemistry; American Chemical Society, **1994**; Vol. 242, pp. 47–114.

(27) Laurier L. Schramm. Foam Sensitivity to Crude Oil in Porous Media. In *Foams: Fundamentals and Applications in the Petroleum Industry*; Advances in Chemistry; American Chemical Society, **1994**; Vol. 242, pp. 165–197.

(28) Schramm, L. L.; Novosad, J. J. Micro-Visualization of Foam Interactions with a Crude Oil. *Colloids Surf.* **1990**, *46*, 21–43.

(29) Basheva, E. S.; Ganchev, D.; Denkov, N. D.; Kasuga, K.; Satoh, N.; Tsujii, K. Role of Betaine as Foam Booster in the Presence of Silicone Oil Drops. *Langmuir* **2000**, *16*, 1000–1013.

(30) Schramm, L. L.; Novosad, J. J. The Destabilization of Foams for Improved Oil Recovery by Crude Oils: Effect of the Nature of the Oil. *J. Pet. Sci. Eng.* **1992**, *7*, 77–90.

(31) Simjoo, M.; Rezaei, T.; Andrianov, A.; Zitha, P. L. J. Foam Stability in the Presence of Oil: Effect of Surfactant Concentration and Oil Type. *Colloids Surf. Physicochem. Eng. Asp.* **2013**, *438*, 148–158.

(32) Farajzadeh, R.; Andrianov, A.; Krastev, R.; Hirasaki, G. J.; Rossen, W. R. Foam–oil Interaction in Porous Media: Implications for Foam Assisted Enhanced Oil Recovery. *Adv. Colloid Interface Sci.* **2012**, *183–184*, 1–13.

(33) Hirasaki, G. J. Wettability: Fundamentals and Surface Forces. *SPE Form. Eval.* **1991**, *6*, 217–226.

(34) Khatib, Z. I.; Hirasaki, G. J.; Falls, A. H. Effects of Capillary Pressure on Coalescence and Phase Mobilities in Foams Flowing Through Porous Media. *SPE Reserv. Eng.* **1988**, *3*, 919–926.

(35) Aronson, A. S.; Bergeron, V.; Fagan, M. E.; Radke, C. J. The Influence of Disjoining Pressure on Foam Stability and Flow in Porous Media. *Colloids Surf. Physicochem. Eng. Asp.* **1994**, *83*, 109–120.

Chapter 3

Rheology of Viscoelastic Surfactants

Introduction

Surfactant molecules self-assemble into specific structures called micelles at a certain

concentration known as the critical micelle concentration. These structures are generally

spherical in shape in dilute solutions, which have a viscosity near that of water. However certain

surfactant micelles in dilute solutions tend to assemble as rods due to the effect of a counter ion

or hydrotrope, surfactant hydrophobe tail, ionic environment, concentration etc. When

concentration is increased, rod like micelles elongate, become flexible and start to entangle just

like dilute polymer solutions. It is the effect of entanglement that leads to viscoelasticity which

can be quantified using a rheometer. Viscoelasticity is the time dependent response of a complex

structure when a constant strain is applied[1]. When a purely viscous fluid is subjected to a step

strain, the stress would relax almost instantaneously after the strain is constant. When a purely

elastic solid is subjected to a step strain, it would show no relaxation. On the other hand stress of

a viscoelastic liquid would relax to zero over a finite amount of time on the application of

constant strain. The time taken for the fluid elements to relax after a deformation is called

relaxation time.

Viscoelastic surfactants (VES) have found wide application in oil industry in the

application of well stimulation [2–5]and as fracturing fluids[6–8]. During production of hydrocarbons,

a large fraction of water is produced along with it. Viscoelastic surfactants in combination with

polymers have been used to prevent the flow of aqueous phase along with the hydrocarbon phase

thereby reducing the water production in the production well[9]. Recently the application of a

proprietary zwitterionic surfactant (supplier is Rhodia now Solvay) forming wormlike micelles

in NaCl brine has been shown to be efficient in displacing mineral oil in a high permeability medium. The total recovery was much higher than for HPAM polymer injection alone. There is some ambiguity in data due to plugging of medium[10]. Another study used a proprietary viscoelastic surfactant to displace residual mineral oil and found an incremental oil recovery of ~29%[11]. Use of viscoelastic surfactant in combination with low tension formulations has shown better mobility control leading to 15% additional oil recovery than the alkaline surfactant flooding process. However the singular viscoelastic surfactant prevented the solubilization of oil, hence the lower cmc was not effective for a low IFT process[12] by itself. From the above studies there seemed a potential for the application of VES in the field of EOR in terms of mobility control.

In this present study VES were evaluated as surfactants for foam injection in tertiary recovery of crude oil, as discussed in Chapter 4 of the thesis. This chapter discusses the interesting rheological properties of these complex structures and compares their flow behavior in porous media with polymer flow (from literature). It is also intended to take advantage of their beneficial properties for injection in porous media.

3.1 Features of wormlike micelles

Figure 3.1 show a schematic of formation of wormlike micelles[13]. Rod like micelles start to form when the packing parameter is between 1/2 and 1/3[14]. The packing parameter is given as p= V/la where V is the volume of the hydrophobic tail, a is the effective area of the head group and l is the length of the hydrophobic tail. Wormlike micelles were observed to have dynamics similar to entangled polymer solutions with one exception: they can relax stress by means of breaking and reforming in addition to polymeric stress relaxation by reptation (movement like a snake). Reptation is diffusion controlled and the break reform mechanism is kinetically

controlled. Rheological measurements show that most viscoelastic surfactants can be characterized by a single relaxation time τ. A very good review on the theoretical and dynamical properties of wormlike solutions can be found in literature[13,15].
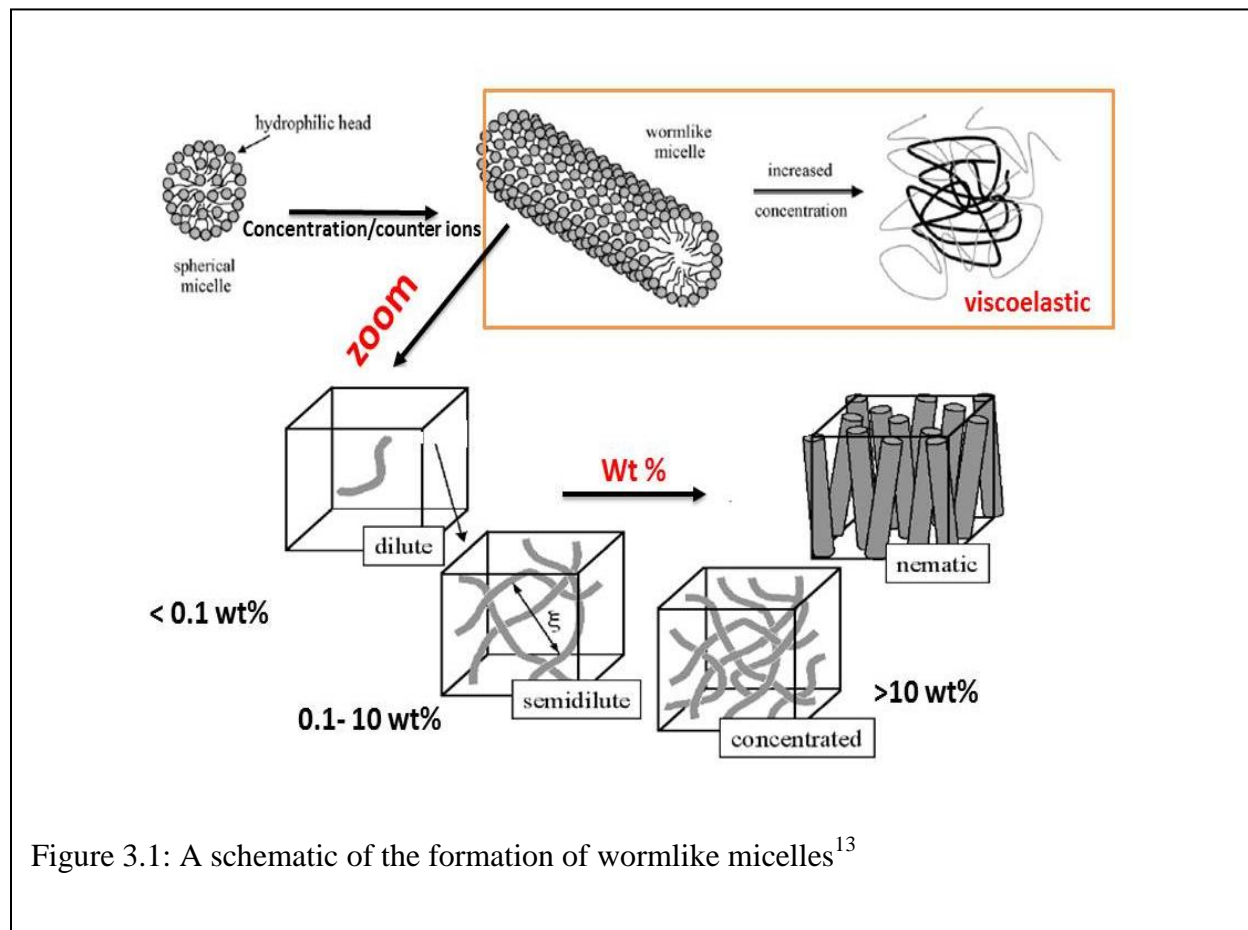
Figure 3.1: A schematic of the formation of wormlike micelles[13]

3.2 Surfactant systems forming viscoelastic solutions

Some of the early works have studied wormlike micelle formation in cationic surfactants like cetyl trimethyl ammonium bromide (CTAB), cetyl trimethyl ammonium chloride(CTAC), cetyl pyridinium bromide (CPyBr), cetylpyridinium salicylate (CPySal) in the presence of organic/ inorganic salts [16–25]. Figure 3.2 shows the zero shear viscosity behavior (viscosity of a sample at extremely low shear rates) of cationic surfactant in the presence of salt[26,27]. One observes that on increasing the salt concentration there is a marked increase in zero shear

viscosity until it reaches a maximum. This is because the salt screens the electrostatic repulsion between the head groups, thereby facilitating closer packing of the surfactant molecules and leading to the formation of rod like micelles. When these micelles grow in length and become flexible they entangle and behave like dilute polymer solutions. At the viscosity maximum point they form a very strong entangled network. However on additional increase in the salt concentration there is a decrease in the zero shear viscosity. This is attributed to the fact that these micellar structures start forming branched networks[28] and hence the stress relaxation takes place through these branched structures during shear flow.

Another interesting study on the surfactant system CPySal with sodium salicylate (NaSal) shows an interesting phenomenon in zero shear viscosity versus NaSal concentration where in there is successive maximum followed by a minima , followed by another maximum of lower viscosity magitude[25]. The first maximum obeys Maxwellian behavior. The minimum that follows it is due to the network or branched structure formation. Following this it is suggested that further increase in salt concentration can change the dynamics of the micelle leading to nematic phase formation [29]. At very high concentration ratio of $C_{salt}/C_{surf,}$ rod like micelles get shortened due to micelle inversion and hence cause a decrease in viscosity.

Anionic surfactants like sodium dodecyl sulfate (SDS) also exhibited viscoelastic nature in the presence of monovalent salt[30] and also a hydrotrope[31]. Sodium dodecyl trioxyethylene sulfate (SDES) is observed to form viscoelastic systems in the presence of bivalent[32] and trivalent salts[33]. They were observed to exhibit non-linear viscoelastic behavior.

Non-ionic surfactants have also exhibited viscoelastic phenomena [34,35] which are temperature sensitive. Zwitterionic surfactants dimers from acid betaine have shown pronounced

viscoelastic effects[36] which do not follow a mono exponential decay like many other viscoelastic surfactants. Some zwitterionic surfactants show viscoelastic behavior based on the degree of protanantion[37] whereas some others show formation of rod like micelles based on the

a)

b)

Entangled linear micelles

Branched networks

Figure 3.2: Effect of salt: above mentioned cationic surfactants have concentration of ~ 0.3M. With increase in salt content C_S, there is a maximum in the zero shear viscosity due to formation of long flexible entangled worm like micelles. On additional increase in salt concentration the zero shear viscosity drops due to micellar branching. Picture references a) [26] b) [27]

number of methylene groups between the positive and negative part of the zwitterionic molecule[38]. A long tailed C_{22} betaine has shown gel like behavior at room temperature in the absence of any salt. This particular betaine is supplied by Rhodia. It is found that the hydrophobicity of aromatic salt such as sodium salicylate and sodium hydroxynaphthalene has some influence on its viscoelastic properties but inorganic salts have no effect on its viscoelastic properties[39]. Zwitterionic surfactants are capable of forming wormlike micelles even in the absence of salt[40].

Mixtures of anionic and cationic surfactants have strong synergistic interactions which lead to the formation of wormlike micelles[41,42]. Even mixtures of zwitterionic and anionic surfactants have been found to exhibit this phenomenon[43–47], including some systems that will be discussed later in the current chapter.

Surfactants used in this study:

- *C_{18} amido N,N dimethyl betaine -Rhodia A (unsaturation in carbon chain).*

- *C_{18-22} amido N,N dimethyl sultaine-Rhodia B(unsaturation in carbon chain).*

- *C_{18-22} amido N,N dimethyl betaine- Rhodia C(unsaturation in carbon chain).*

- *C_{18-22} amido N,N dimethyl betaine LE) -Rhodia D(unsaturation in carbon chain).*

- *Mixtures of Rhodia A and Alpha Olefin Sulfonate AOS$_{14-16}$*

3.3 Models describing viscoelastic behavior

Most viscoelastic fluids obey a simple Maxwell model. A Maxwell model is represented by a spring and dashpot connected in series. The spring corresponds to an elastic element with shear modulus G and the dashpot corresponds to a viscous element having viscosity μ. This model is characterized by the single dominant relaxation time τ_r, which is the longest relaxation time. Relaxation time can be thought of as the "measure of the time for which the fluid

37

remembers the flow history"[48]. The simple Maxwell model has the following expressions for the elastic component G' and the viscous component G"[15]

$$G'(\omega) = \frac{G_0 \omega^2 \tau_r^2}{1+\omega^2 \tau_r^2} \qquad \textbf{Equation 3.1}$$

$$G"(\omega) = \frac{G_0 \omega \tau_r}{1+\omega^2 \tau_r^2} \qquad \textbf{Equation 3.2}$$

Where ω is the angular frequency and G_0 is the plateau modulus.

Another model used for viscoelastic systems is Kelvin- Voigt model which depicts a more solid like response. It is analogous to a spring and dashpot in parallel. A Burgers model is a combination of the Kelvin-Voigt model and Maxwell's model in series, which predicts the entire fluid behavior, whereas the complex fluid can be considered to form structures as depicted by Kelvin –Voigt model. References can be found in literature[49]. The schematics for various models are shown in Figure 3.3. For all the work described in this chapter a Maxwell model is used to predict the relaxation time.

3.4 Rheology experiments

Rheology is the study of flow and deformation of materials, in terms of their elasticity and viscosity. This is done by applying a precisely measured strain to deform the sample and accurately measuring the stress produced. The stress is expressed by Hooke's law and Newton's law. The ARES rheometer was used to make all rheological measurements in the current study.

ARES(Advanced Rheometric Expansion System) Rheometer:

The ARES (Figure 3.4) uses a 1K FRTNI transducer (the mechanism of working of the transducer is not discussed). The transducer measures the torque generated by the sample during its deformation by the motor. The lowest value it can measure is 0.02 g.cm. The motor in the

ARES can be operated in two modes. 1. Dynamic mode (Sinusoidal). 2. Steady mode (steady rotational rate). The frequency and the amplitude of the strain can be input by the user.

Figure 3.3: Schematic for a) Simple Maxwell model b) Kelvin-Voigt model c) Burgers model d) Generalized Kelvin-Voigt model e) Generalized Maxwell model [49]
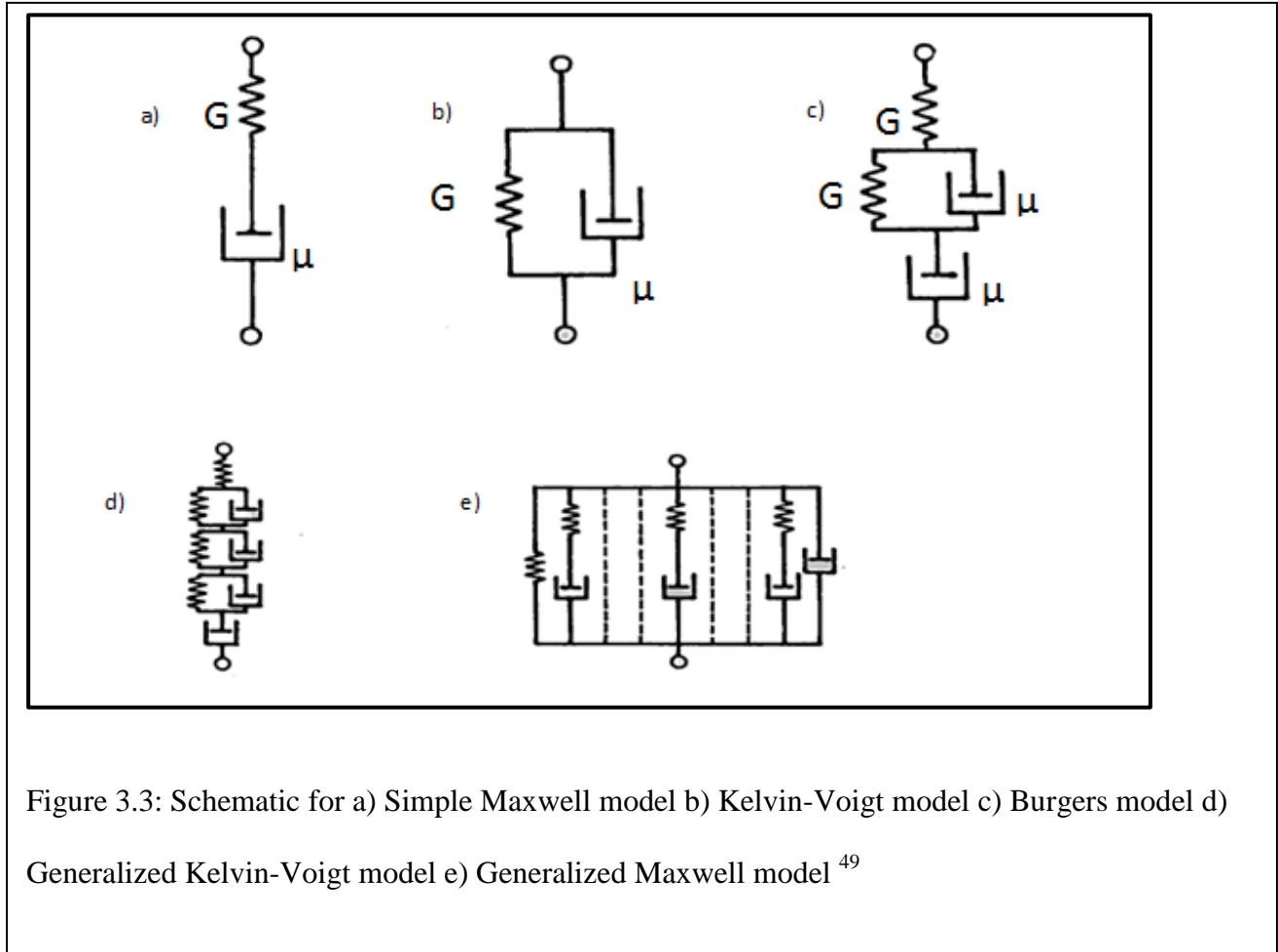
In small amplitude oscillatory dynamic measurements the phase angle between the stress and strain vectors is measured by the ARES. A small amplitude oscillatory measurement means the amplitude of strain is very low ($\ll 1$) to remain in the linear viscoelastic region. At this strain value the fluid structures are not greatly disturbed. The linear viscoelastic region is found by keeping a constant frequency and measuring the moduli as a function of increasing strain. Up to a certain value of strain the elastic modulus G' and viscous modulus G" remain constant.

However above a critical strain value γ_{crit} G' will decrease and G'' will increase. Above the critical value the deformation made on the fluid disturbs the structure of the fluid greatly.

Transducer

Motor
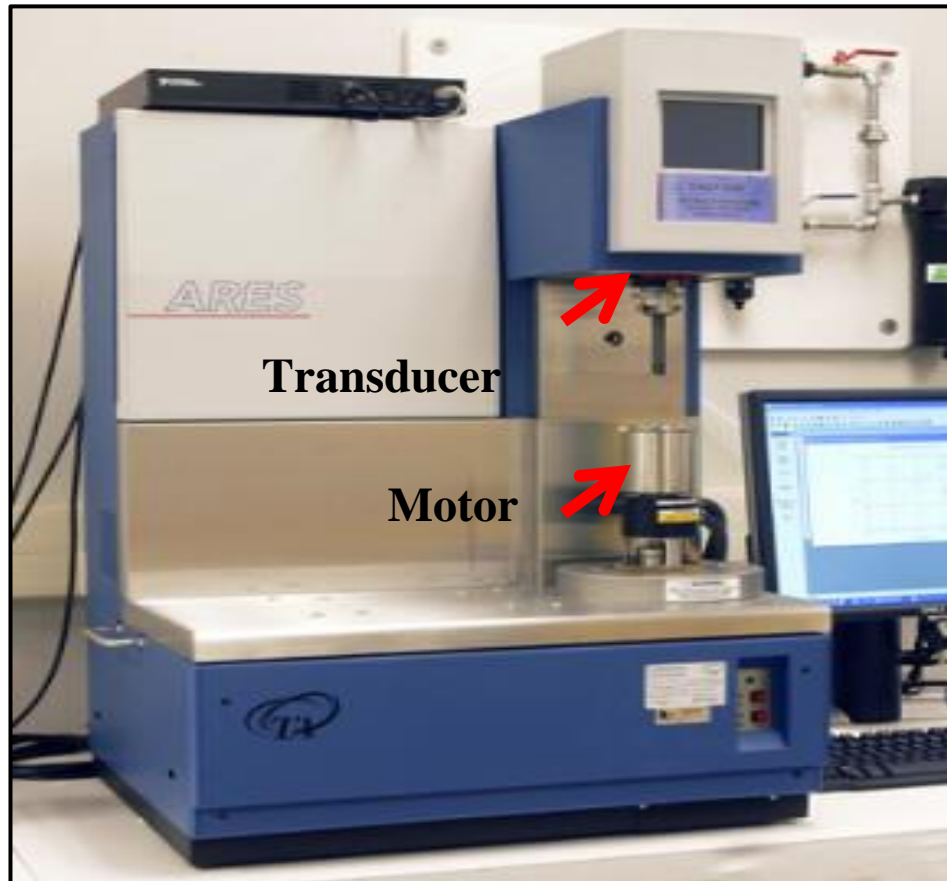
Figure 3.4: ARES rheometer

Hence it is important to work within the linear region to avoid appreciable perturbation of the sample. When the phase angle between the stress and strain vector is 0° the material is purely elastic. If the phase angle is 90°, the material is purely viscous. But when the phase angle is between 0° and 90° the material is viscoelastic[50]. This is represented schematically in Figure 3.5.
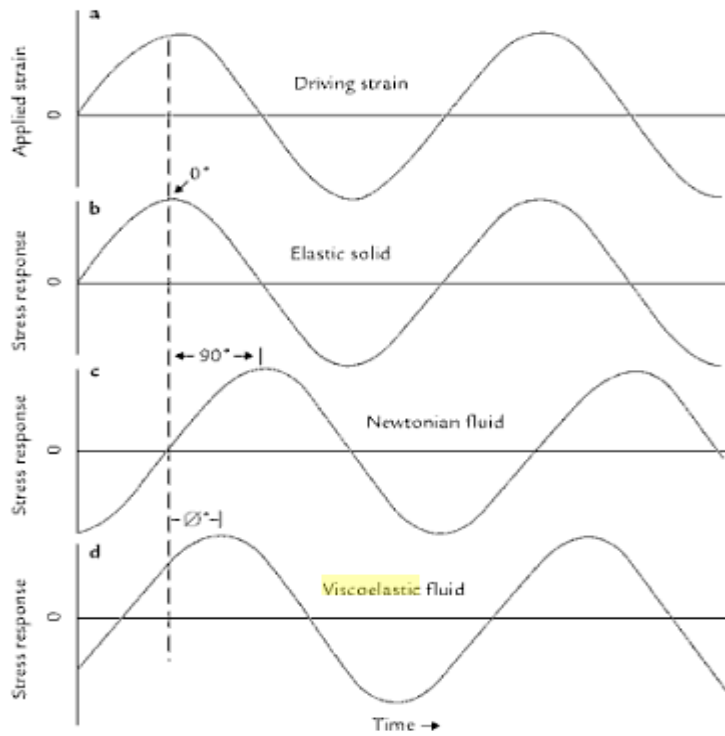
Figure 3.5: Phase angle between applied strain and stress for different fluids[51].

Figure 3.5 shows the stress response for elastic, viscous and viscoelastic fluids[51]. A purely elastic material will regain its original form on the removal of stress. A purely viscous fluid gets deformed on the application of stress. A viscoelastic fluid regains a part of the original shape, as governed by the elastic modulus but the viscous component is dissipated.
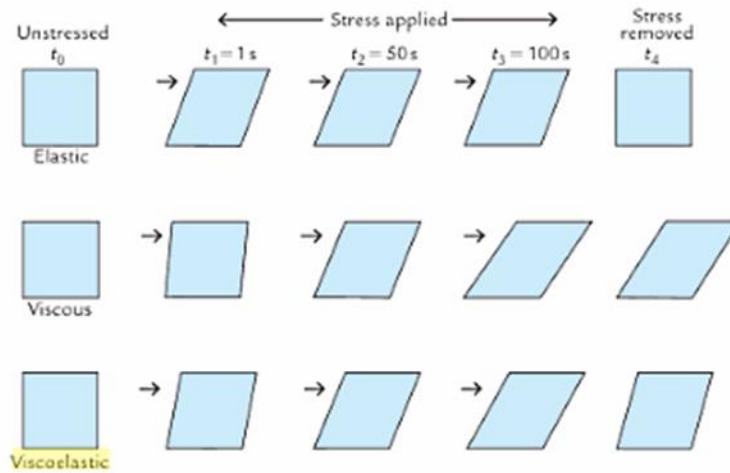
Figure 3.6: Schematic representation of elastic, viscous and viscoelastic substances [51].

3.4.1 Rheological behavior - Effect of salt

All the samples were tested on single walled couette (cup and bob) geometry. This geometry was chosen since having a larger surface area gives more torque which makes it easier to perform measurements at very low frequencies/shear rates. It was required to remove all air bubbles from the sample before loading it into the couette. The bob was slowly submerged into the sample to prevent formation of air bubbles. A solvent trap was used over the couette to prevent evaporation. All experiments were conducted at 25° C.

All the surfactants labelled Rhodia were supplied by Rhodia now part of Solvay. Two brines which were of interest for injection for an EOR foam process were used. One was sea water (SW) and the other was formation brine (FB). The compositions can be found in Table 3.1. The ionic strength of formation brine was ~2.8 times that of sea water. Both oscillatory and steady shear measurements were performed. Figure 3.7 shows the dynamic frequency response of Rhodia A and B. Rhodia A as described is a C_{18} amido betaine, and B is a C_{18-22} amido

sultaine. From the rheograms we see that Rhodia A made in sea water has a short relaxation time of 0.026 seconds, where as the sample in formation brine has a longer relaxation time of ~ 20 seconds. The relaxation time for a Maxwell fluid is calculated by taking the inverse of frequency ω where G' and G" cross over. Also one can observe that Rhodia A behaves like a typical Maxwell fluid. The rheogram of Rhodia B suggest that relaxation times of the solution in sea water and formation brine are 0.1 s and 0.3 s respectively. This means the salt content almost has no effect on the long chain sultaine surfactant. Figure 3.8 shows the dynamic frequency response of Rhodia C and D. Rhodia D in FB shows a slightly increased elastic modulus G' over that in sea water at the frequency 0.02-1 rad/s. But on the whole the rheograms seem to be only slightly affected by an increased salt content. It seems like the long chain C_{18-22} betaines/sultaine are unaffected by the presence of salt. This has been observed in literature[39] where a C_{22} chain amido betaine was unaffected by the presence of inorganic salt. However aromatic salts seemed to affect the viscoelasticity. The rheograms of Rhodia C and D have no cross over point as observed in the experimentally studied range. This shows that they have a long relaxation time approximately >30-50 s (the inverse of the lowest frequency up to which the experiment was possible). The rheometer is limited by torque in the low frequency region and by the inertia of the geometry in the high frequency (60-100 rad/s).

Salts	Sea water (g/L)	Formation brine (g/L)
NaCl	26.95	106.043
$MgCl_2.6H_2O$	11.15	1.229
$CaCl_2. 2H_2O$	1.76	14.080
Na_2SO_4	4.80	0.746
Ionic Strength	0.71M	2.13 M

Table 3.1: Composition of sea water and formation brine

Figure 3.9 shows the comparison of the Rhodia zwitterionic surfactants made in sea water at a concentration of 0.5wt%. It shows that the C_{18} betaine Rhodia A has the lowest viscosity owing to the shorter chain length when compared to the rest. The C_{18-22} betaines Rhodia C and D have viscosities up to 10,000 cP at shear rates of ~0.01 s^{-1}. Interestingly Rhodia C shows an infinite viscosity behavior at shear rates below 0.1 s^{-1}. This signifies that it has a yield stress and an infinite relaxation time. The solutions of Rhodia C at 0.5wt% in sea water and formation brine, looked like gels. The rheograms of Rhodia C and D suggest that the samples have an entangled network of wormlike micelles that creates this interesting rheological behavior. Whereas the rheograms of Rhodia A and B show the formation of wormlike micelles, but with slight overlap of the micelles. Hence they have a lower relaxation time.
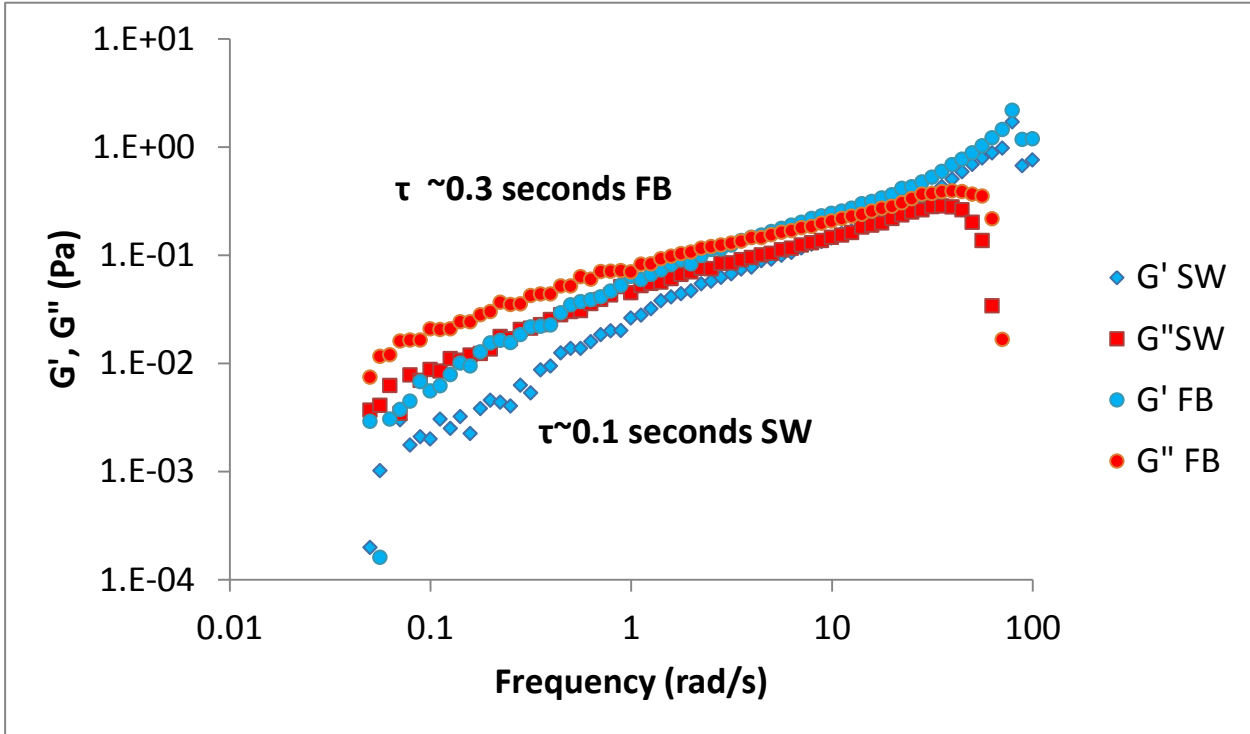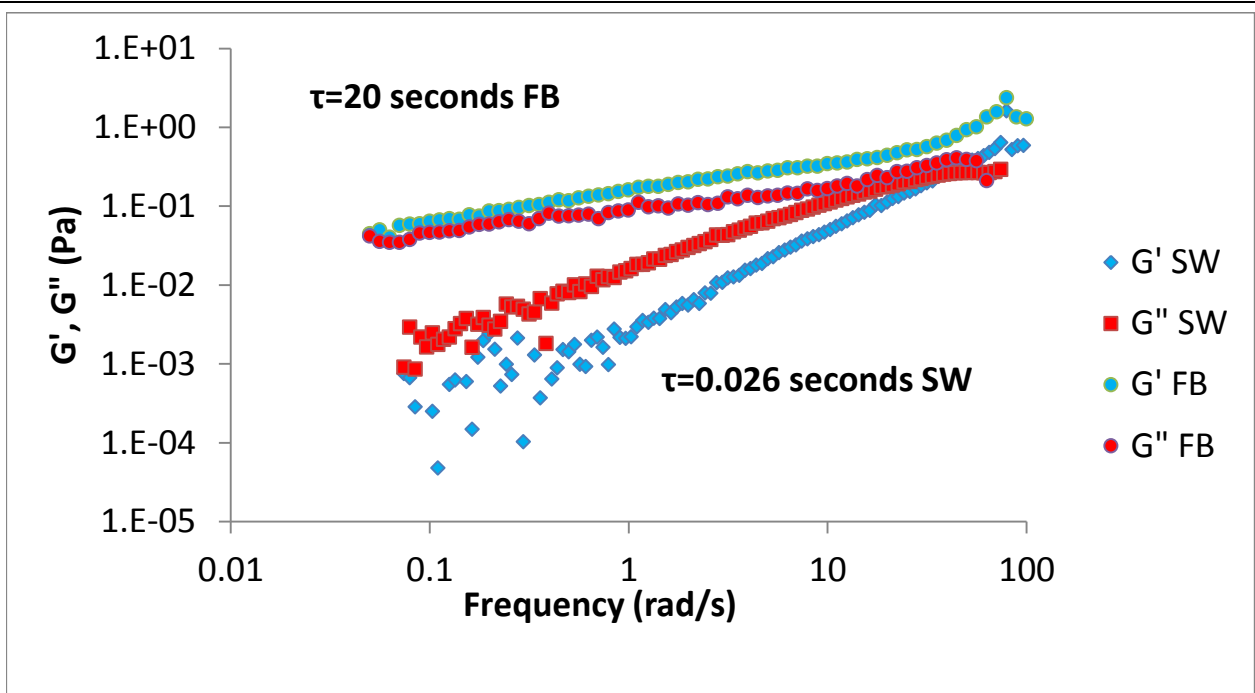
Figure 3.7: Dynamic frequency response rheograms showing the effect of salt (sea water SW and Formation brine FB) on Rhodia A (top) and Rhodia B (bottom). Concentrations are 0.5wt%.
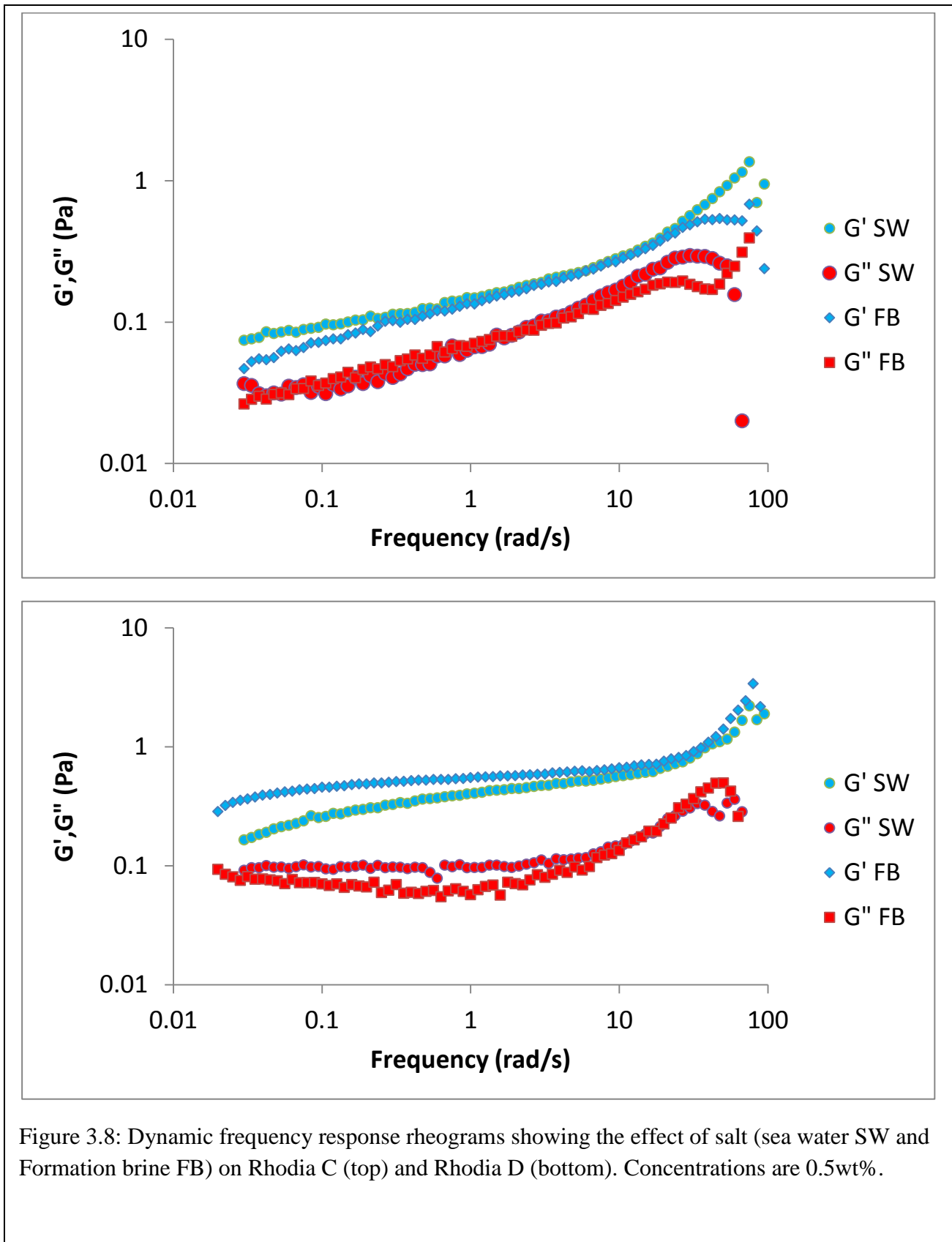
Figure 3.8: Dynamic frequency response rheograms showing the effect of salt (sea water SW and Formation brine FB) on Rhodia C (top) and Rhodia D (bottom). Concentrations are 0.5wt%.
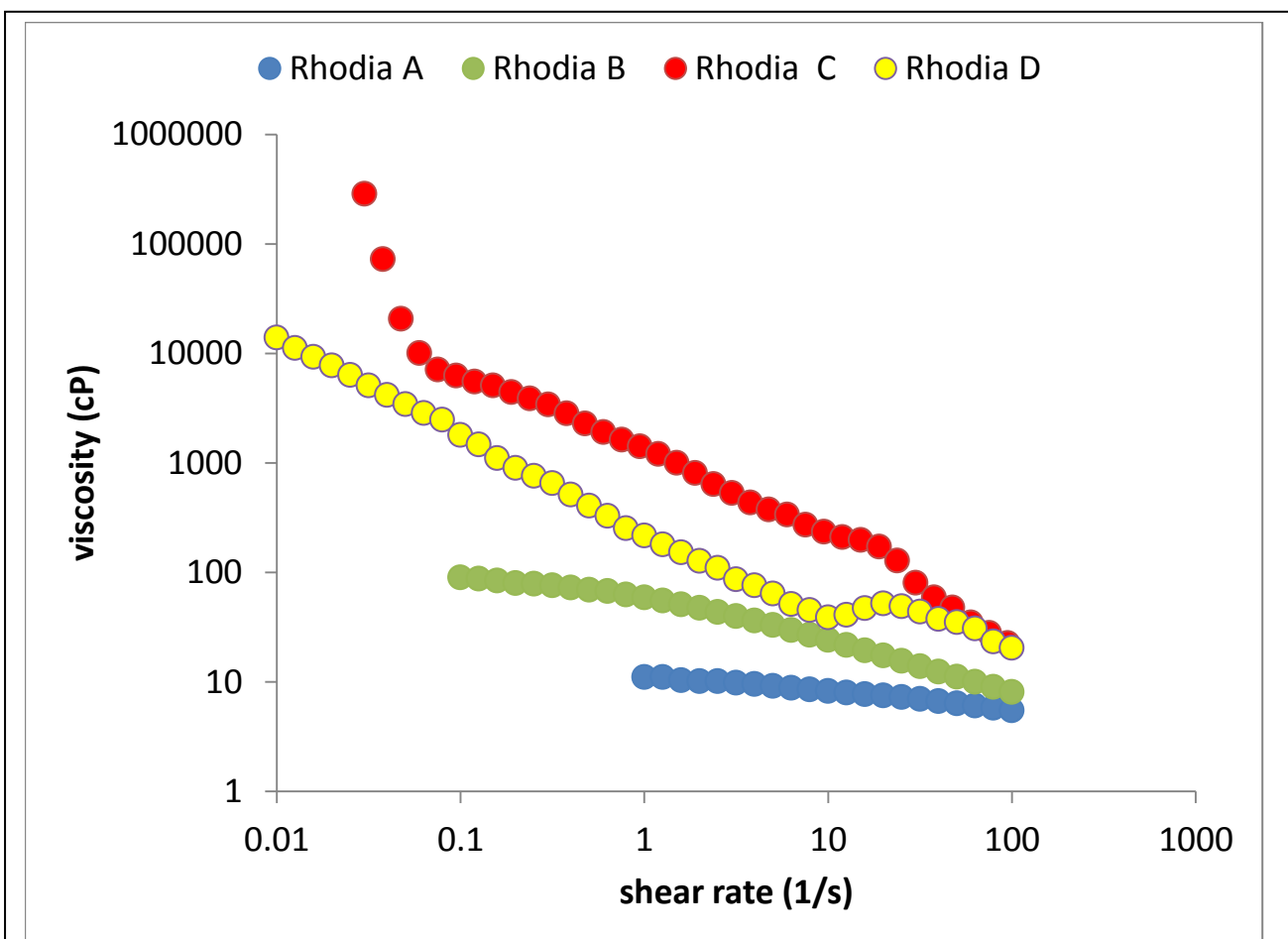
Figure 3.9: Comparison of viscosities of all Rhodia zwitterionic surfactants made in sea water at a concentration of 0.5 wt%.

Due to the lower viscosity of samples Rhodia A and B, they are of interest for flow in porous media. This will be discussed in the subsequent sections. Figure 3.10 shows the comparison of Rhodia A betaine and Rhodia B sultaine made at 0.3 wt% in different aqueous media. Rhodia A shows a pronounced increase in viscosity when the salinity is increased. However Rhodia B has the same viscosity magnitude in all the aqueous media.
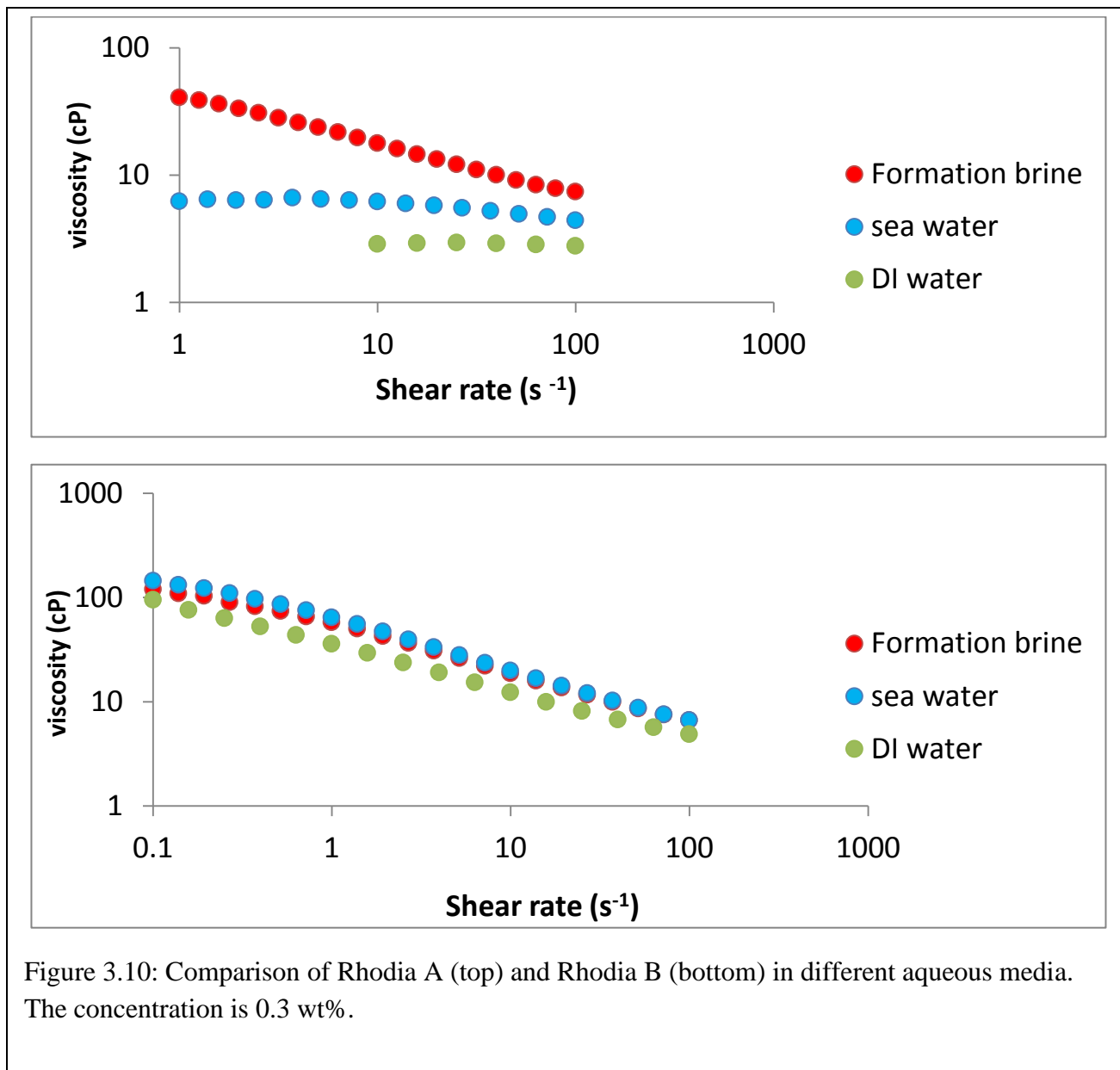
Figure 3.10: Comparison of Rhodia A (top) and Rhodia B (bottom) in different aqueous media. The concentration is 0.3 wt%.

From the above studies on the rheological properties the main observation is, the presence of certain amount of C_{22} chain makes the surfactant insensitive to salt i.e. they show similar rheological behavior with increasing salinity. This holds an important advantage for our studies since reservoirs usually have harsh environment in terms of salinity, and a surfactant that can withstand this environment is desired. One important thing to note about Rhodia B 0.3 wt% in DI water was it appeared cloudy after 7 days. When assessed under a cross polarizer

48

microscope (Figure 3.11) - it was found to be birefringent. However on the addition of salt the solutions became clear.

Figure 3.11: Birefringence in sample of Rhodia B (0.3 wt%) in DI water on a 7 day old sample. Image obtained under a cross polarized microscope.

3.4.2 Flow of viscoelastic surfactants in porous media

The surfactants were injected into a sandpack containing US silica 20/40 mesh sand. Prior to surfactant injection several pore volume of sea water was injected to measure the absolute permeability of the sand pack and was measured to be ~100 Darcy. The porosity was ~ 0.36. Several pore volumes of surfactant solution were injected, and pressure drop was

monitored. The shear rheological viscosity values were compared with porous media data. The

apparent viscosity in porous media was calculated using the Darcy's law

$$\mu_{app} = -\frac{k}{u}\nabla p \quad \textbf{Equation 3.3}$$

where k is the medium absolute permeability

μ_{app} - apparent viscosity

u- total flux

∇p - pressure gradient

And the shear rate was calculated using

$$\dot{\gamma} = \frac{1.38\,u}{\sqrt{\phi k}} \quad \text{Equation 3.4}$$

where u is the superifical velocity, k – permeability, ϕ -porosity

Figure 3.12 , Figure 3.13 , Figure 3.14 show the porous media data. Viscoelastic polymer

solutions exhibit dilational or extensional viscosity at high flow rate. However no such behavior

is observed for these systems. More will be discussed in the next section on comparison of

polymer flow and wormlike micelle flow in porous media. For the case of Rhodia B the shear

thinning slope is very close for the rheometer and the porous media studies.

Figure 3.15 shows the rheograms of Rhodia C made in sea water at different

concentrations. There is strong evidence of yield stress behavior. When a complex fluid like this

was studied in porous media, it plugged the porous medium and gave rise to high pressure drop

(see Figure 3.16).
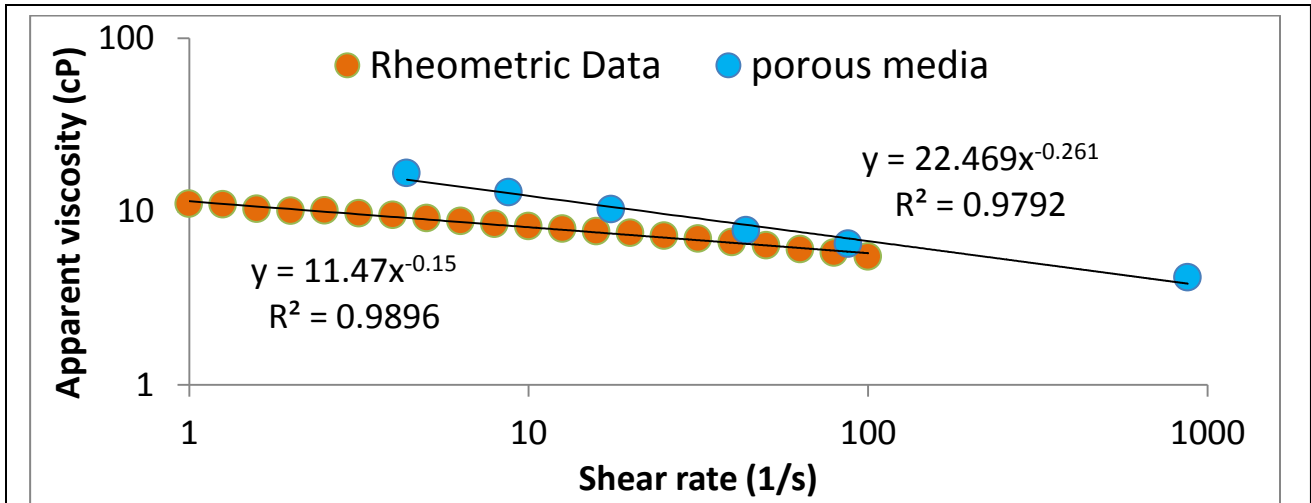
Figure 3.12: Shear rheology of Rhodia A (0.5 wt% made in sea water) and its comparison with flow in porous media
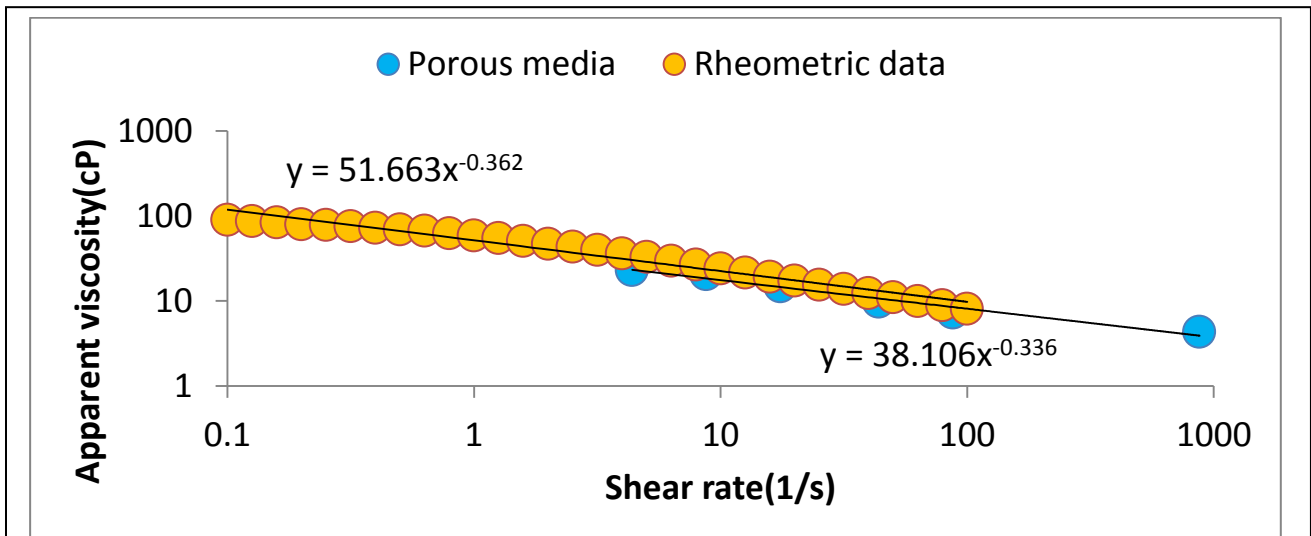
Figure 3.13: Shear rheology of Rhodia B (0.5 wt% made in sea water) and its comparison with flow in porous media
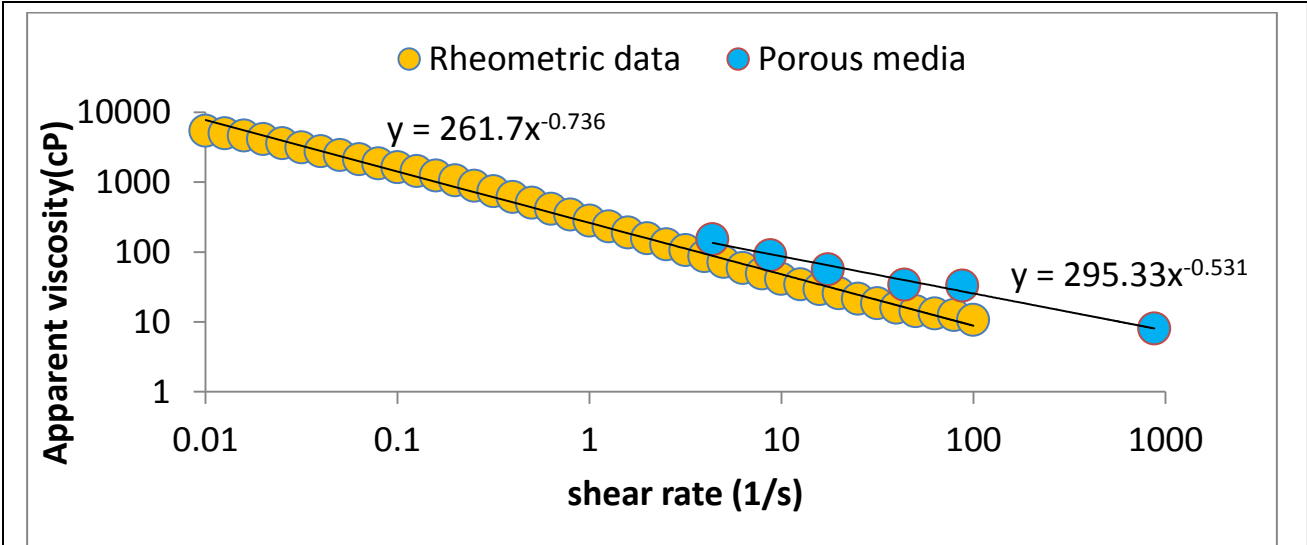
Figure 3.14: Shear rheology of Rhodia D (0.5 wt% made in sea water) and its comparison with flow in porous media
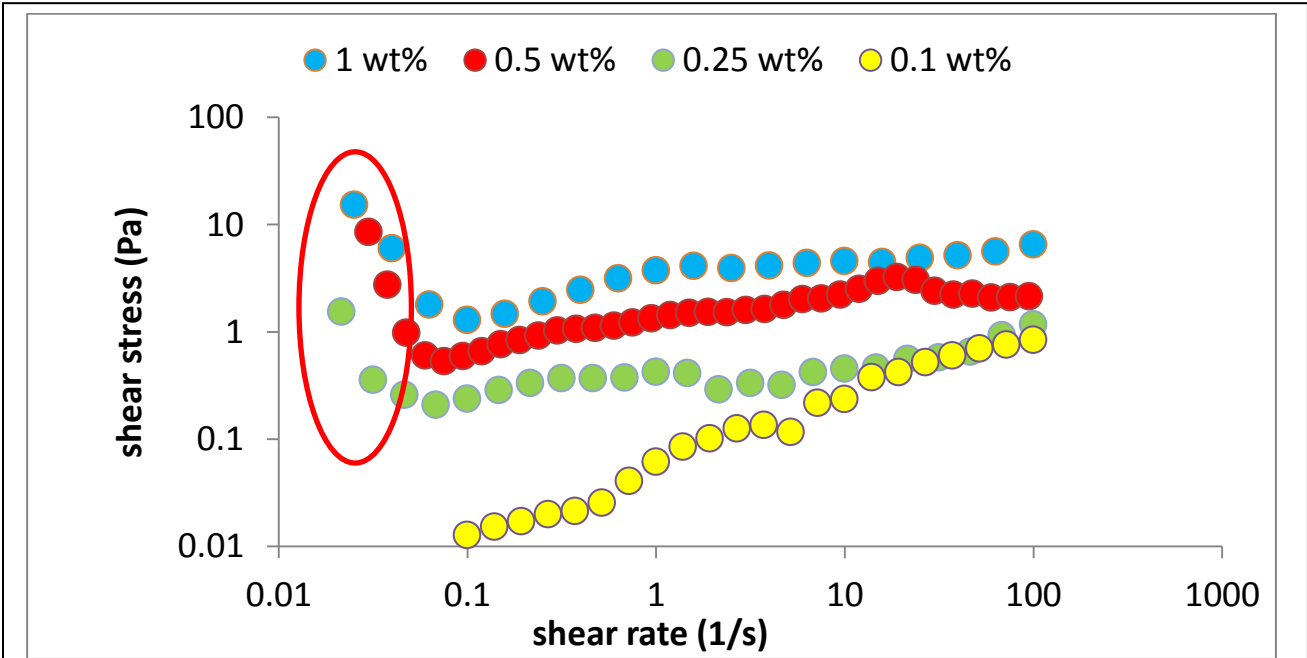
Figure 3.15: Yield stress behavior exhibited by Rhodia C at various concentrations. The brine used was sea water.
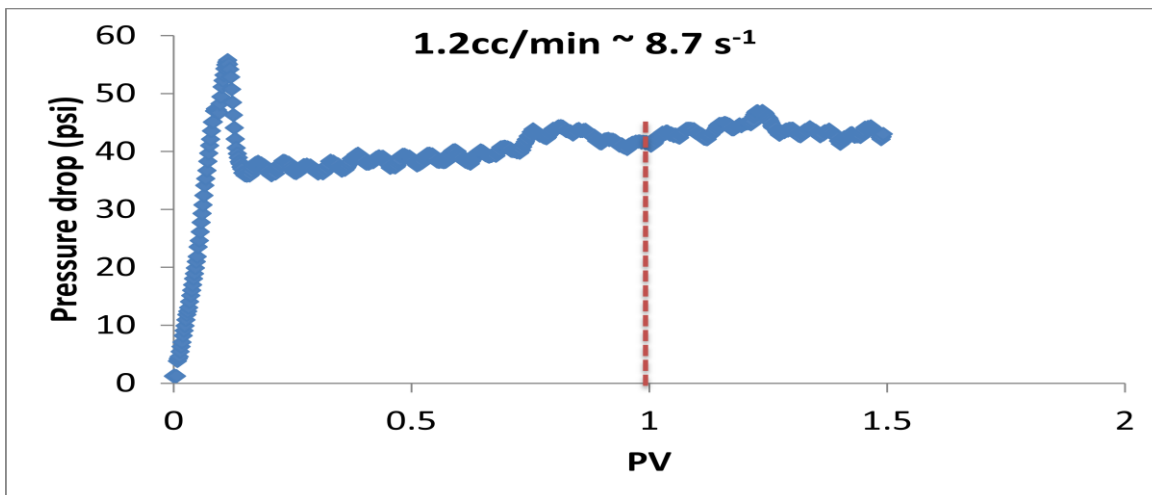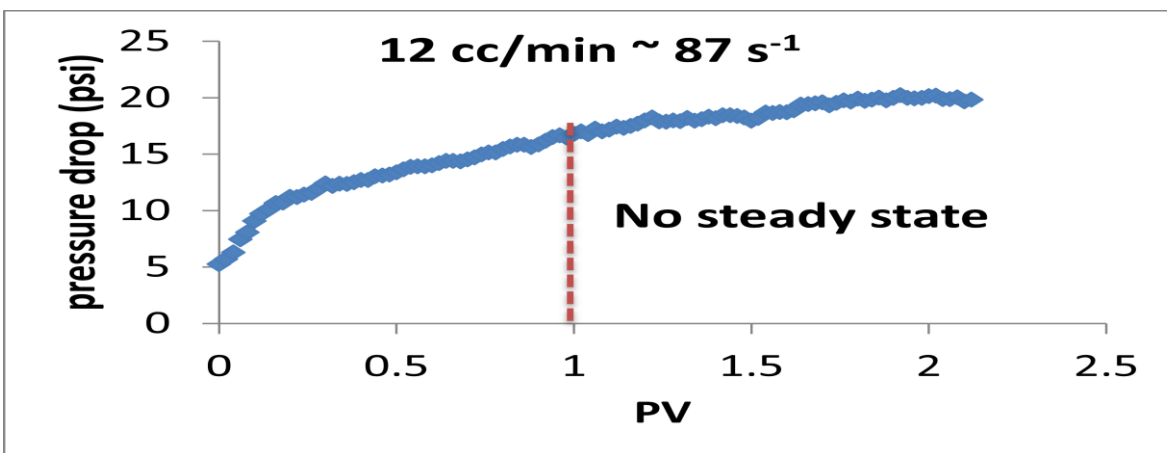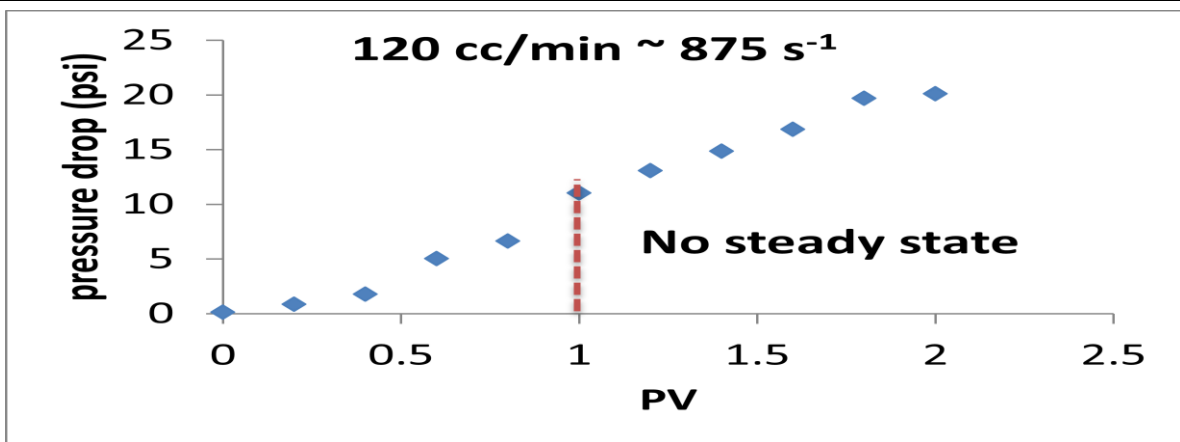
Figure 3.16: Pressure drop at different flow rates for Rhodia C (0.5wt% in sea water). There seems no steady state pressure drop after 1 PV. At 1.2cc/min the pressure drop is higher than at higher flow rates indication of plugging.

In Figure 3.16 the flow rate was varied from 120 cc/min to 1.2 cc/min. It is observed that the pressure drop does not reach steady state in 1 PV. Part of the reason could be due to the adsorption of the surfactant on silica sand but the other reason could be the effects of plugging. The flow rate was dropped to 12cc/min and the pressure drop still failed to reach steady after more than 1PV. The flow rate was dropped further to 1.2 cc/min and it was seen that the pressure drop value was much higher than that obtained at higher flow rates. This strongly suggested that there was plugging at the inlet. Also when the effluent was observed at the outlet it seemed more like water flowing out rather than a viscoelastic fluid. This was suggestive that the medium was filtering the surfactant and sending most of the water to the outlet and hence the high pressure drop behavior.

3.4.3 Comparison of viscoelastic surfactants flow with polymers in porous media

Hirasaki and Pope have shown that certain polymers show a marked increase in apparent viscosity in porous media after a Deborah number of 1[52]. Deborah number is a dimensionless number which is defined as the ratio of relaxation time of the viscoelastic fluid and the elongation strain rate.

$$N_{Deb} = \frac{\theta_f V}{D_P} \qquad \textbf{Equation 3.5}$$

Where θ_f is the relaxation time of the fluid

D_p is particle diameter

V is the interstitial velocity

The polymers show an elongational hardening effect at $N_{Deb} >= 1$ for a Maxwell fluid (Figure 3.17).
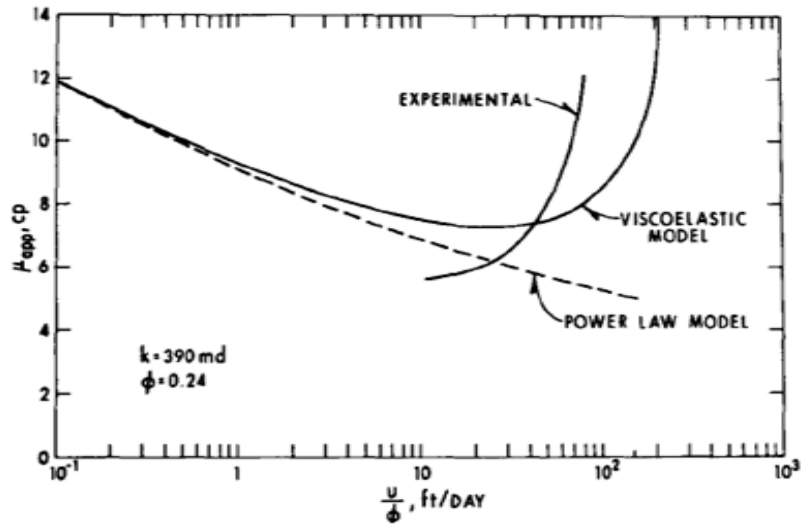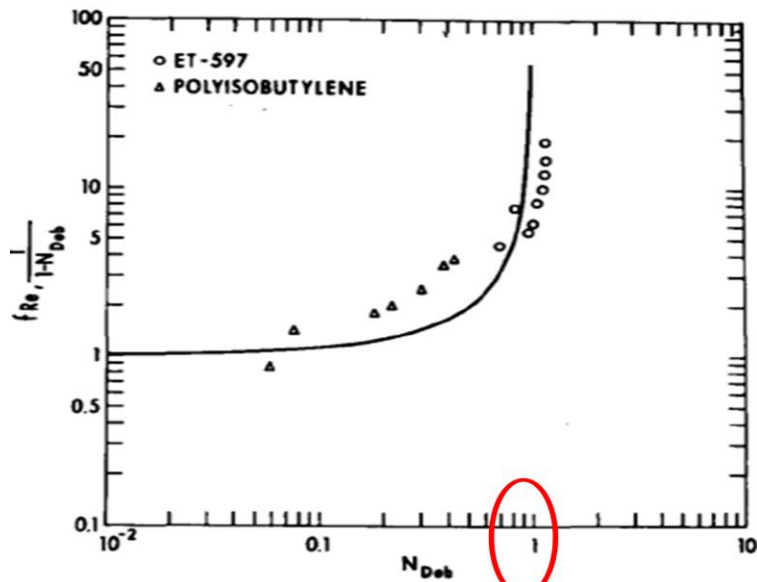
Figure 3.17: Polymer behavior in porous media. Above Deborah number 1 , polymer exhibits elongational effects[52].

This approach was tried for the viscoelastic surfactants Rhodia A, B,D(Figure 3.18). No elongational hardening is observed for the Rhodia VES surfactants. This might be due to the mechanism of breaking and reforming, the result being that wormlike micelles don't show an elongational effect during flow. They are well represented by power law behavior and are shear thinning fluids.

Figure 3.18: No elongational hardening observed with Rhodia A,B,D.
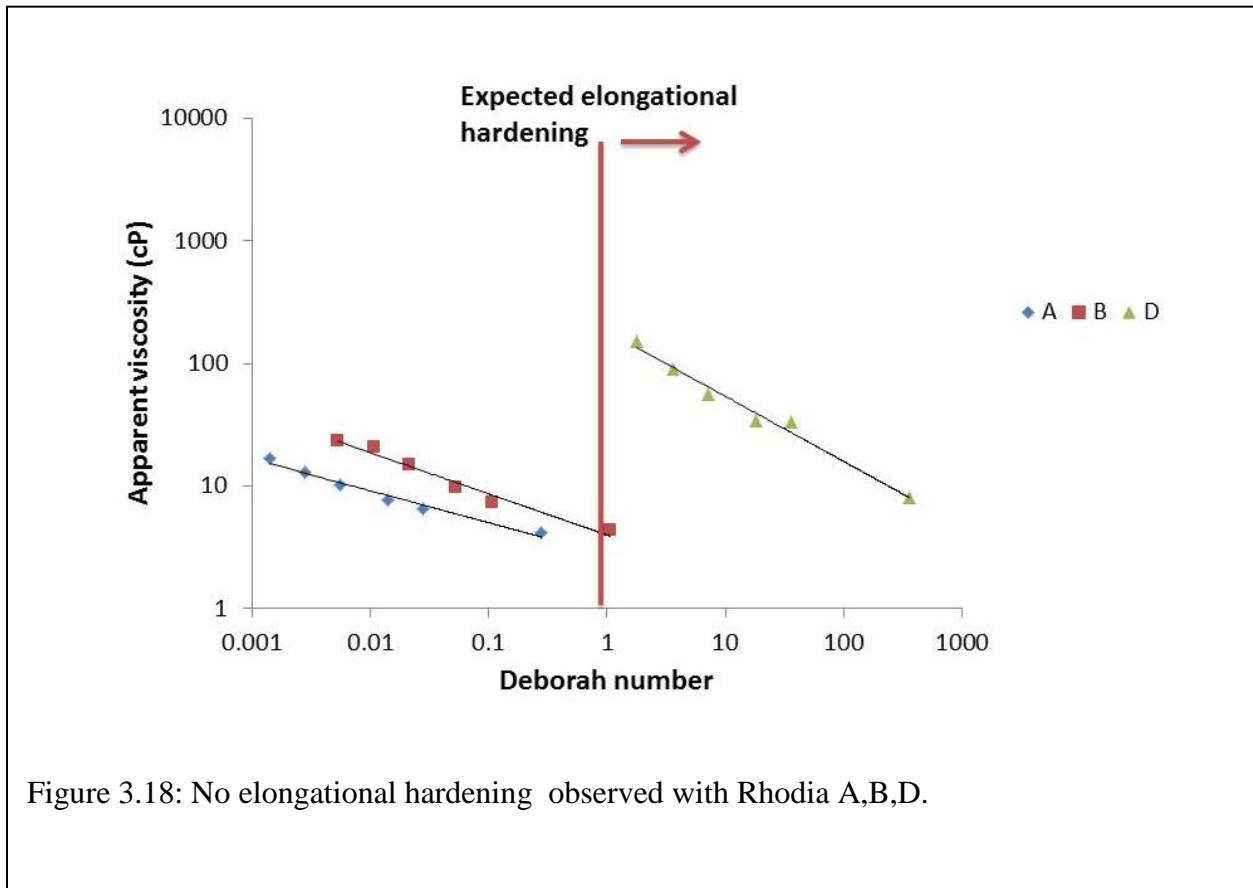
3.4.4 Effect of crude oil on wormlike micelles

Initially a 1wt% (based on active material) of surfactant solution was prepared in sea water (total mass = 22 g). To this 0.22 g of synthetic crude oil was added (Pemex crude oil details in Chapter 4). Hence based on the mass percentage of the surfactant amount and the oil

amount, the solution contains ~ 25% oil in it. This is a good representation of residual oil left in a reservoir after a waterflood.

Figure 3.19 show the effect of crude oil on Rhodia A and B. From the rheograms of Rhodia A, it can be concluded that over the entire frequency range of study, the viscous modulus G" is dominant and no cross over of G' over G" is seen. This indicates that the C_{18} amido betaine lost its viscoelasticity to a considerable amount. A possible reason could be the shortening of the rods or conversion to spherical micelles. Such an effect has been observed in a mixture of sugar surfactant and non-ionic surfactant which forms long wormlike micelles in aqueous media. However in the presence of decane the micelles were converted to short micelles due to the solubilization of decane inside the core. With m-xylene the viscoelasticity was maintained as the xylene was solubilized in the palisade layer[53,54] which led to the growth of wormlike micelles. Other work has shown that the increase in oil content above a certain fraction led to a decrease in the length of wormlike micelles[55]. A similar effect might be seen in Rhodia A. There might be shortening of the rod like micelles and hence the viscoelasticity is not pronounced in the range studied.

Rhodia B shows a significant drop in the elastic modulus in the low frequency range too. In this case the solution still remains viscoelastic, possibly due to the existence of some of the wormlike micelles. As pointed out earlier Rhodia B has C_{18-22} chain surfactant molecules. There might be shortening in the length of the wormlike micelles but not so much to make the solution lose its viscoelasticity.

Figure 3.20 show the effect of oil on Rhodia C and D. It is remarkable to notice that the oil has had no effect on Rhodia C. There is a slight decrease in the magnitude of G' in the

presence of oil however the long relaxation time still exists in the system. This exhibits a behavior of the mixture of the sugar surfactant and non ionic surfactant in the presence of an aromatic hydrocarbon[56]. The possible explanation for this is due to the extremely entangled network of the C_{18-22} surfactant molecules, the oil molecules would have entered the palisade layer without disrupting much of the micellar structure. Another possibility is that the molecules would have packed tightly, that the oil molecules are not solubilized to any significant extent.

Rhodia D on the other hand has shown significant decrease in the modulus value and a loss of viscoelasticity. The rheogram shows that it is viscoelastic but with a low modulus value thereby indicating the reduction in the length of the wormlike micelles.

Figure 3.21 and Figure 3.22 show the complex viscosity plot (plot of viscosity in an oscillatory mode experiment) of the surfactant solutions in the presence of oil. By Cox-Merz rule the complex viscosity must be close to the value of a steady shear viscosity[50]. All of the solutions show shear thinning behavior, indicating the presence of some amount of rod like micelles. Rhodia A shows a decrease in complex viscosity by an order of magnitude in the presence of crude oil. Rhodia B shows a slight decrease in complex viscosity. Rhodia C is almost unaffected by the crude oil. Rhodia D has a drop in complex viscosity especially in the lower frequency region.

One possible application of this type of wormlike micellar solution for oil recovery is when oil is displaced by surfactants like Rhodia B, D, they still retain their viscoelastic nature. There is some loss in viscosity on the surfactant oil bank, however the incoming surfactant solution, still not in contact with oil, can aid in pushing the oil bank by controlling the mobility.
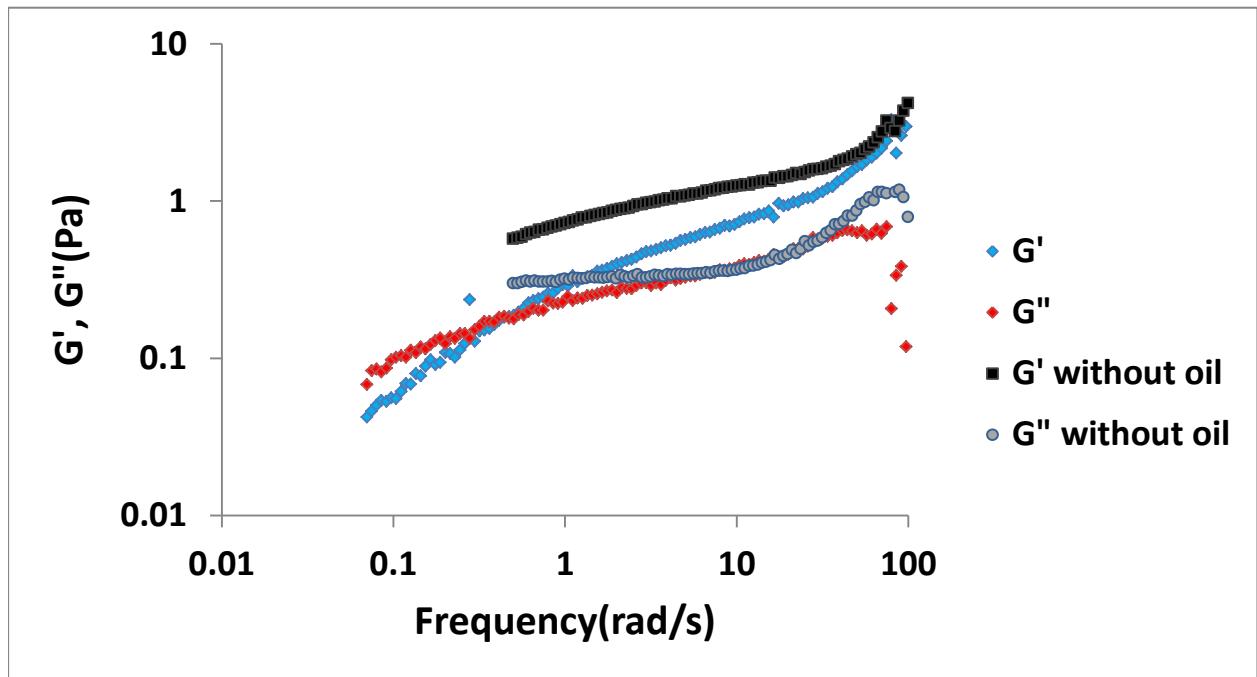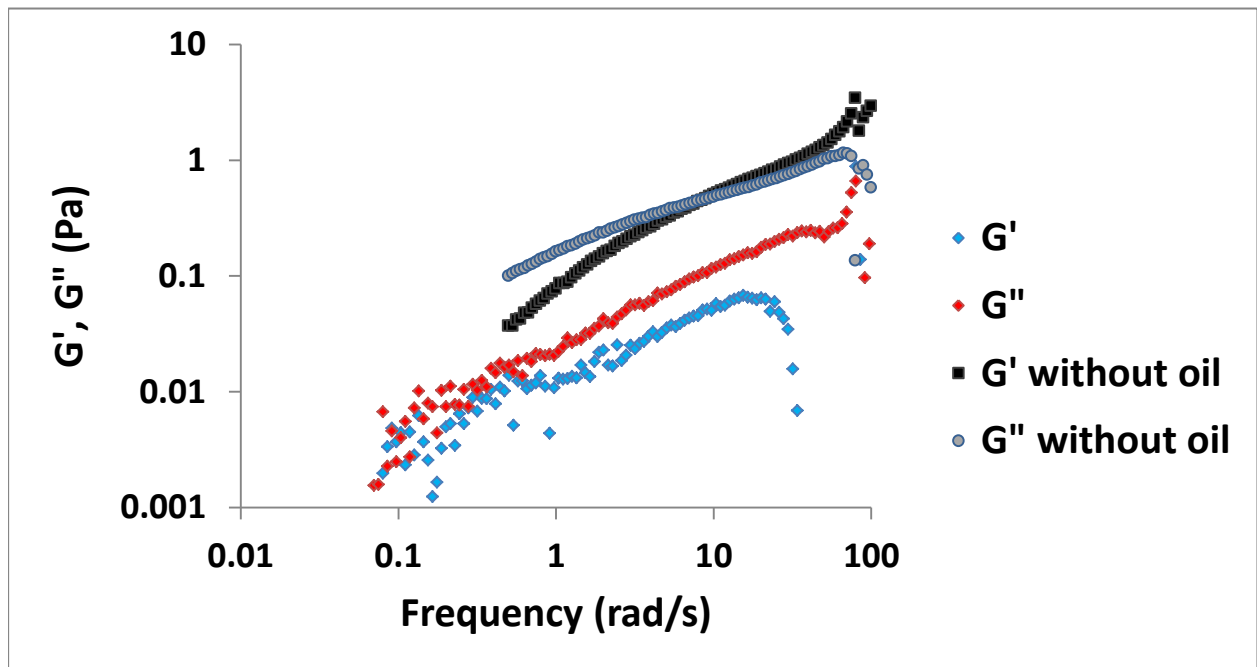
Figure 3.19: Effect of crude oil on 1wt%- Rhodia A(top) and Rhodia B (bottom). Solution was prepared in sea water.
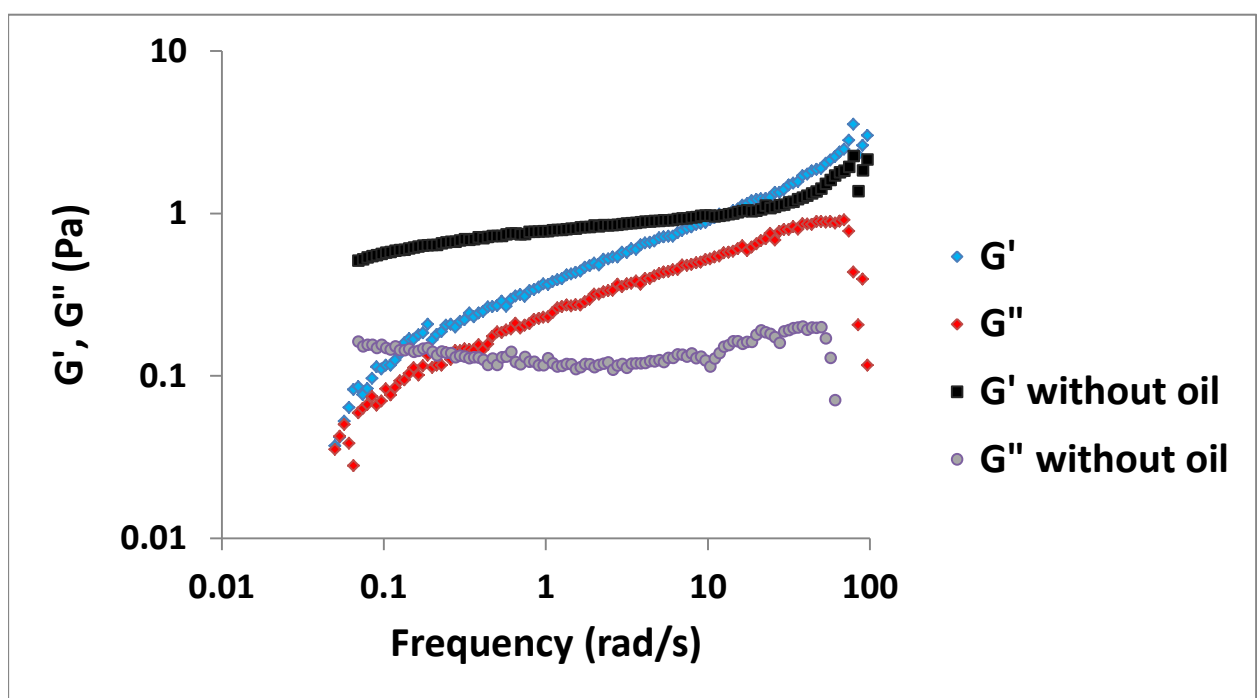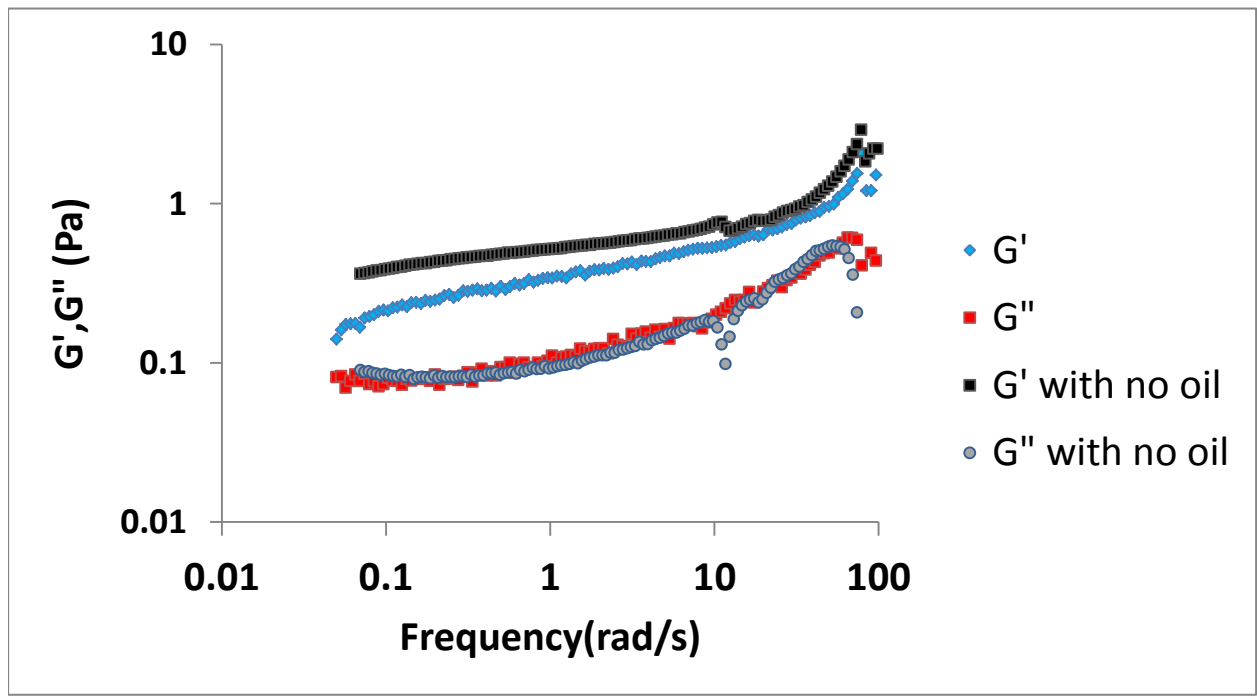
Figure 3.20: Effect of crude oil on 1wt%- Rhodia C(top) and Rhodia D (bottom). Solution was prepared in sea water.
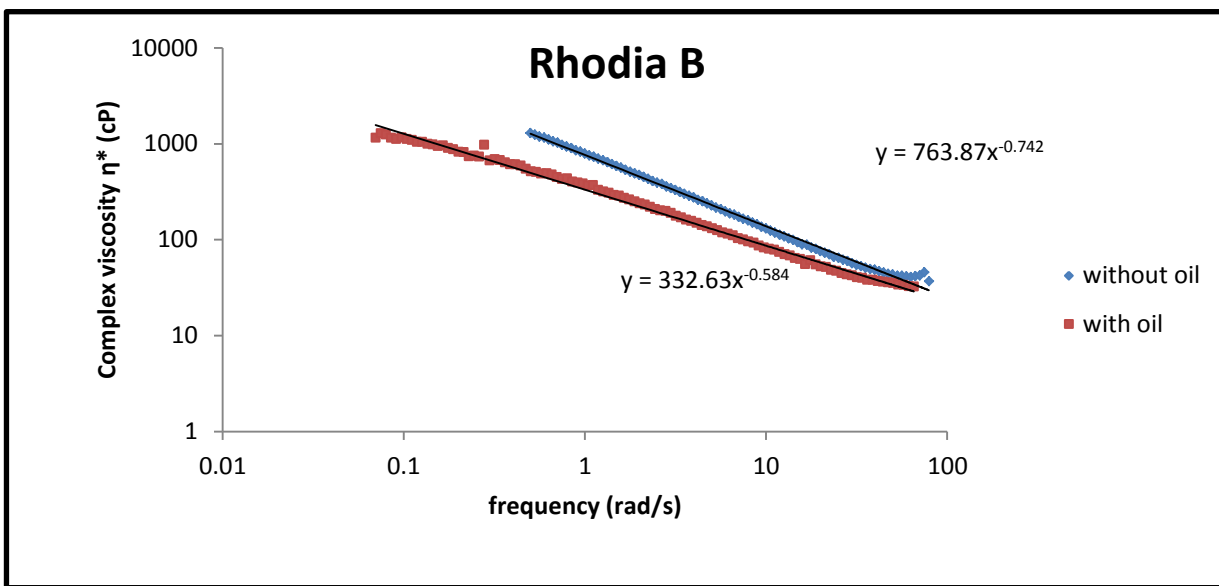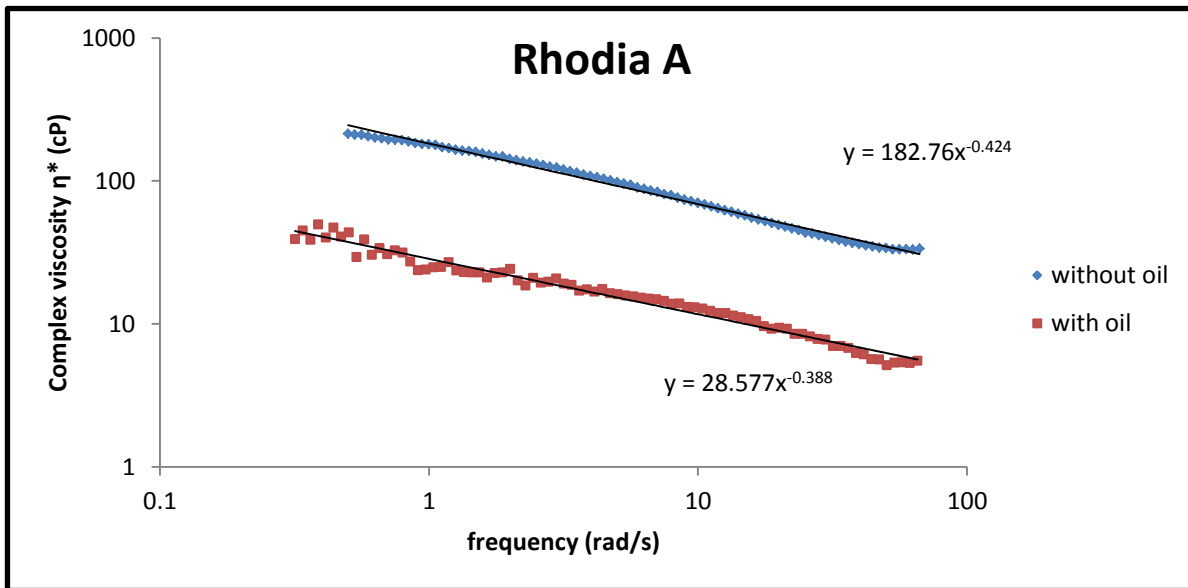
Figure 3.21: Complex viscosity of Rhodia A (top) and Rhodia B in the presence of crude oil (bottom)
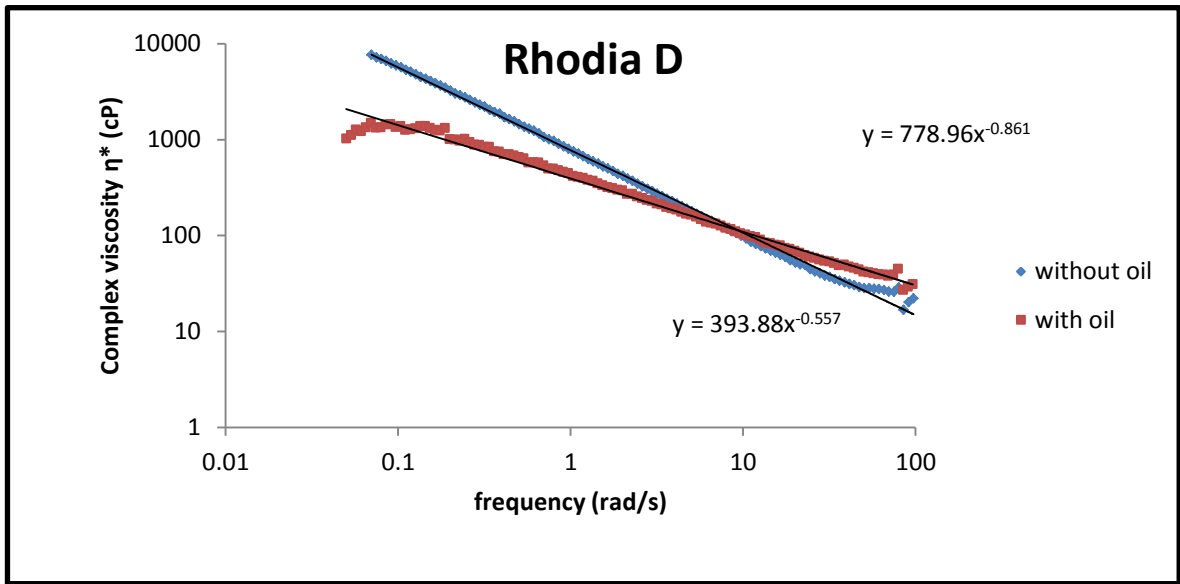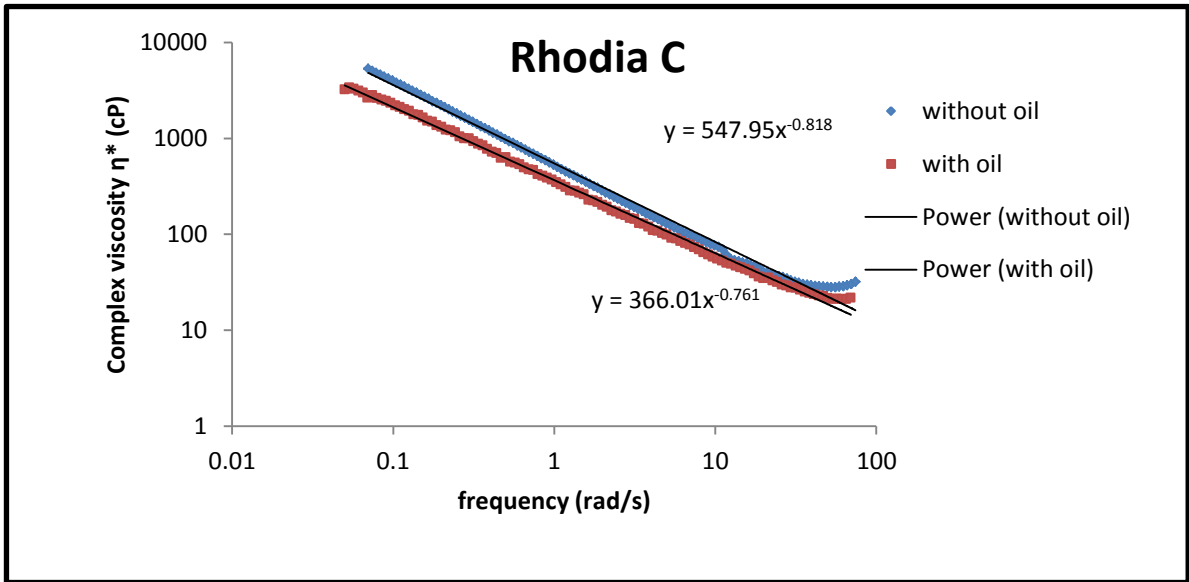
Figure 3.22: Complex viscosity of Rhodia C (top) and Rhodia D in the presence of crude oil (bottom)

3.4.5 Effect of blend ratio

Figure 3.23 is a plot showing the effect of AOS $_{14-16}$ (Newtonian fluid) on Rhodia A (mildly viscoelastic). All the solutions were prepared in NaCl brine having the same ionic strength as sea water. The total concentration for all surfactants was 0.5 wt%. All the fluids for which the relaxation time is plotted exhibit a Maxwell fluid behavior which is characterized by a single relaxation time. The relaxation time seem to be the longest at ratios close to 60% and 20% of AOS mass fraction in the system. The possible reason could be a synergistic interaction between the betaine and the anionic AOS at those particular ratios. When the mole fraction of AOS is above 75% the solution is no longer viscoelastic. The viscosity is just about the viscosity of water. It is interesting to see the effect of the AOS molecules which aid the zwitterionic betaine to form longer wormlike micelles due to the tighter packing at the micelle surface, thereby increasing the critical packing parameter towards 1/2. It is quite possible that the negative anion interacts with the positive quaternary ammonium thereby causing tighter packing.

Figure 3.24 shows the viscosity plot for the different ratios. Some ambiguity is seen in that the viscosity of the A:AOS 4:6 blend is ~ 3times higher than the 8:2 blend. However by looking at the respective relaxation times the 8:2 blend is more viscoelastic and is expected to be more viscous as well. There is no explanation for these effects yet but perhaps it might be within experimental error.

Figure 3.23: Blend ratio of Rhodia A and AOS_{14-16}. Total concentration is 0.5wt% and solution is made in NaCl brine (ionic strength equal to sea water).
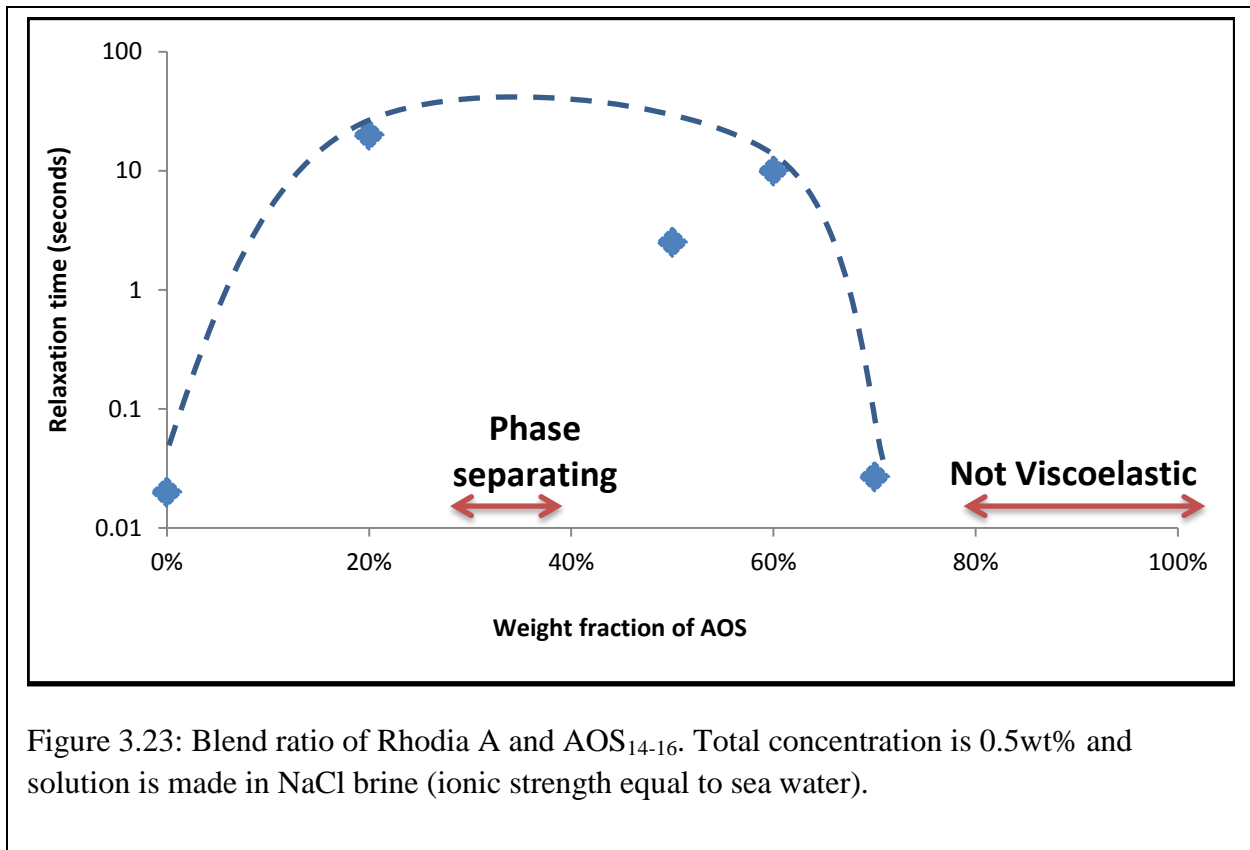
Figure 3.25 shows an interesting blend made of the weakly viscoelastic solution Rhodia A and AOS at volumetric ratio of A:AOS 9:1. When 9 parts of the weakly viscoelastic Rhodia A is blended with 1 part of AOS_{14-16} the solution shows a remarkable viscoelastic effect. This blend was studied in porous media for foam injection and showed some interesting foam rheology (discussed in Chapter 4). There might be a synergistic interaction between Rhodia A and AOS causing a tight packing of the micelles. Addition of 1 part of AOS promoted the formation of very long wormlike micelles, causing them to entangle and give rise to viscoelastic solutions. There was no injection issue of this blend in a 100 Darcy sand pack.
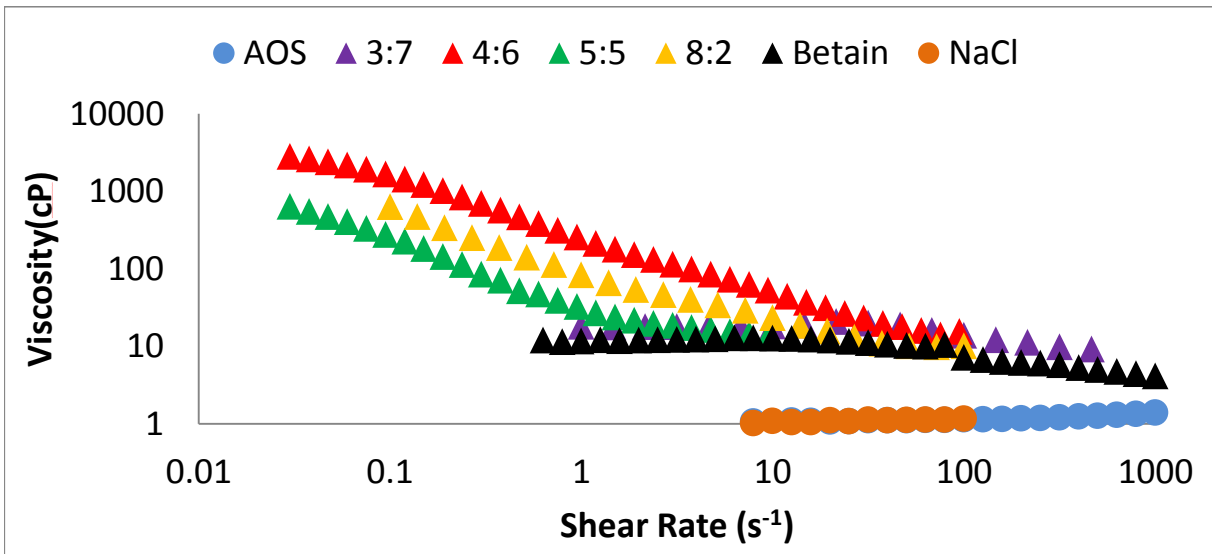
Figure 3.24: Viscosity of the different surfactant blends. Solutions were made in NaCl brine having same ionic strength as sea water. The ratio mentioned in the legend is A:AOS. Total concentration for all blends is 0.5 wt%.
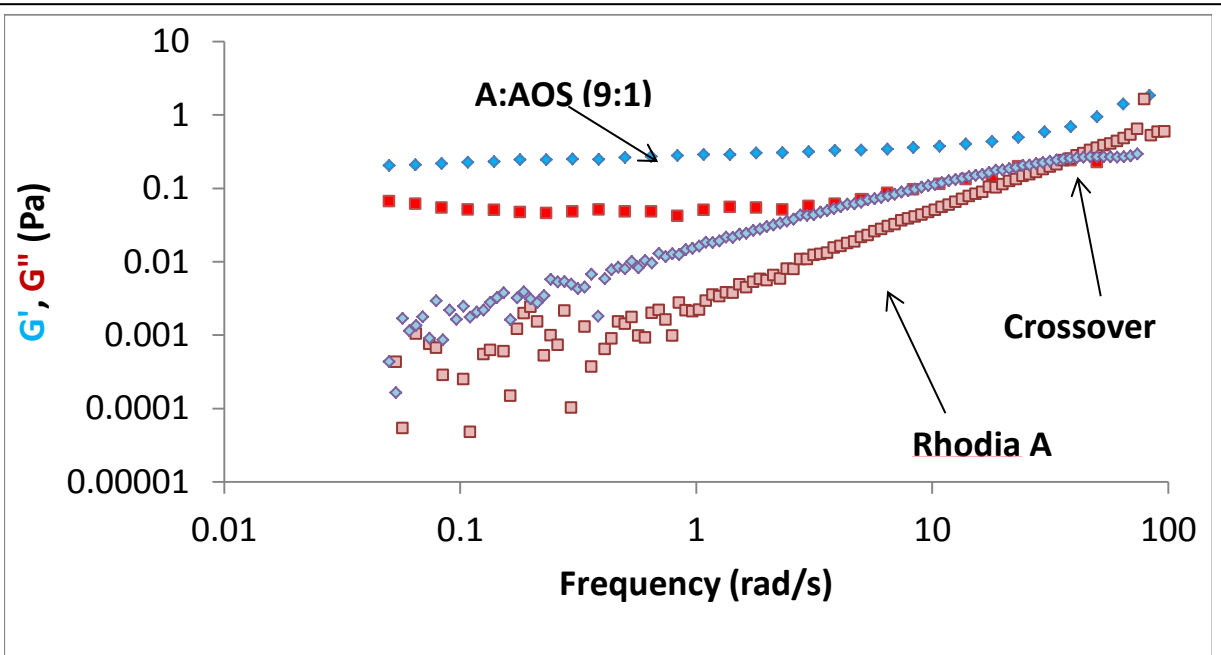
Figure 3.25: Rhodia A:AOS 9:1 blend made in sea water. Total concentration is 0.5wt%.

Observations and conclusions:

- Rhodia zwitterionic surfactants with C_{18-22} chains were able to withstand the effect of salinity. Rhodia A which had a C_{18} chain showed increase in viscosity and viscoelasticity with increase in salinity. Zwitterionic surfactants are generally used due to their insensitivity to salinity.

- Rhodia C had yield stress behavior and plugged the porous medium. Hence, this surfactant may not be suitable for porous media application.

- The effect of crude oil on most of these surfactants was a decrease in viscoelasticity, possibly due to solubilization of oil in the micellar cores, casuing the wormlike micelles to get shorter. In contrast, Rhodia C was unaffected by the presence of oil.

- Unlike polymers, the Rhodia viscoelastic surfactants did not show elongational effects in porous media probably due to their ability to break and reform micelles. This is a major advantage in porous media application.

- When 1 part of AOS $_{14-16}$ was added to 9 parts of weakly viscoelastic Rhodia A, the resulting solution was very viscoelastic. This could be possibly due to synergistic interactions between the zwitterionic and anionic surfactant.

References:

(1) Wiley: Rheology: Principles, Measurements, and Applications - Christopher W. Macosko http://www.wiley.com/WileyCDA/WileyTitle/productCd-0471185752.html (accessed Oct 3, 2015).
(2) Chang, F.; Qu, Q.; Frenier, W. A Novel Self-Diverting-Acid Developed for Matrix Stimulation of Carbonate Reservoirs. **2001,** Society of Petroleum Engineers, SPE International Symposium on Oilfield Chemistry, 13-16 February, Houston, Texas, SPE-65033.
(3) Nasr-El-Din, H. A.; Samuel, E.; Samuel, M. **2003,** Application of a New Class of Surfactants in Stimulation Treatments. Society of Petroleum Engineers, SPE International Improved Oil Recovery Conference in Asia Pacific, 20-21 October, Kuala Lumpur, SPE-84898.

(4)   Lungwitz, B.; Fredd, C.; Brady, M.; Miller, M.; Ali, S. **2004,** Hughes, K. Diversion and Cleanup Studies of Viscoelastic Surfactant-Based Self-Diverting Acid. Society of Petroleum Engineers, SPE International Symposium and Exhibition on Formation Damage Control, 18-20 February, Lafayette, Louisiana, SPE- 86504.

(5)   Taylor, D.; Kumar, P. S.; Fu, D.; Jemmali, M.; Helou, H.; Chang, F.; Davies, S.; Al-Mutawa, M. **2003,** Viscoelastic Surfactant Based Self-Diverting Acid for Enhanced Stimulation in Carbonate Reservoirs. Society of Petroleum Engineers, SPE European Formation Damage Conference, 13-14 May, The Hague, Netherlands, SPE- 82263.

(6)   Chase, B.; Chmilowski, W.; Marcinew, R.; Mitchell, C.; Dang, Y.; Krauss, K.; Nelson, E.; Lantz, T.; Parham, C.; Plummer, J. Clear Fracturing Fluids for Increased Well Productivity. *Oilfield Rev.* **1997**, *9*, 20–33.

(7)   Samuel, M.; Polson, D.; Graham, D.; Kordziel, W.; Waite, T.; Waters, G.; Vinod, P. S.; Fu, D.; Downey, R. **2000,** Viscoelastic Surfactant Fracturing Fluids: Applications in Low Permeability Reservoirs. Society of Petroleum Engineers, SPE Rocky Mountain Regional/Low-Permeability Reservoirs Symposium and Exhibition, 12-15 March, Denver, Colorado, SPE-60322-MS,.

(8)   Dahayanake, M. S.; Yang, J.; Niu, J. H. Y.; Derian, P.-J.; Li, R.; Dino, D. Viscoelastic Surfactant Fluids and Related Methods of Use. US 6258859 B1, July 10, **2001**.

(9)   Jones, T. G. J.; Tustin, G. J. Gelling Composition for Wellbore Service Fluids. US6194356 B1, February 27, **2001**.

(10)   Bertin, H.; Tognisso, E.; Morvan, M.; Colin, A. **2013,** Wormlike Micelles for Mobility Control - A Comparison with Different EOR Techniques. 17th European Symposium on Improved Oil Recovery Poster Session.

(11)   Morvan, M.; Moreau, P.; Degre, G.; Leng, J.; Masselon, C.; Bouillot, J.; Zaitoun, A. **2009,** New Viscoelastic Fluid for Chemical EOR. Society of Petroleum Engineers, SPE International Symposium on Oilfield Chemistry, 20-22 April, The Woodlands. Texas, SPE- 121675-MS.

(12)   Lakatos, I. J.; Toth, J.; Bodi, T.; Lakatos-Szabo, J.; Berger, P. D.; Lee, C. H. **2007,** Application of Viscoelastic Surfactants as Mobility-Control Agents in Low-Tension Surfactant Floods. Society of Petroleum Engineers, International Symposium on Oilfield Chemistry, 28 February-2 March, Houston, Texas, SPE- 106005.

(13)   Berret, J.-F. Rheology of Wormlike Micelles: Equilibrium Properties and Shear Banding Transitions. In *Molecular Gels*; Weiss, R. G.; Terech, P., Eds.; Springer Netherlands, **2006**; pp. 667–720.

(14)   Israelachvili, J. N. *Intermolecular and Surface Forces: Revised Third Edition*; Academic Press, **2011**.

(15)   Cates, M. E.; Candau, S. J. Statics and Dynamics of Worm-like Surfactant Micelles. *J. Phys. Condens. Matter* **1990**, *2*, 6869.

(16)   Porte, G.; Appell, J.; Poggi, Y. Experimental Investigations on the Flexibility of Elongated Cetylpyridinium Bromide Micelles. *J. Phys. Chem.* **1980**, *84*, 3105–3110.

(17)   Imae, T.; Kamiya, R.; Ikeda, S. Formation of Spherical and Rod-like Micelles of Cetyltrimethylammonium Bromide in Aqueous NaBr Solutions. *J. Colloid Interface Sci.* **1985**, *108*, 215–225.

(18)   Couillet, I.; Hughes, T.; Maitland, G.; Candau, F.; Candau, S. J. Growth and Scission Energy of Wormlike Micelles Formed by A Cationic Surfactant with Long Unsaturated Tails. *Langmuir* **2004**, *20*, 9541–9550.

(19) Porte, G.; Appell, J. Growth and Size Distributions of Cetylpyridinium Bromide Micelles in High Ionic Strength Aqueous Solutions. *J. Phys. Chem.* **1981**, *85*, 2511–2519.

(20) Candau, S. J.; Hirsch, E.; Zana, R. Light Scattering Investigations of the Behavior of Semidilute Aqueous Micellar Solutions of Cetyltrimethylammonium Bromide: Analogy with Semidilute Polymer Solutions. *J. Colloid Interface Sci.* **1985**, *105*, 521–528.

(21) Shikata, T.; Hirata, H.; Kotaka, T. Micelle Formation of Detergent Molecules in Aqueous Media. 2. Role of Free Salicylate Ions on Viscoelastic Properties of Aqueous Cetyltrimethylammonium Bromide-Sodium Salicylate Solutions. *Langmuir* **1988**, *4*, 354–359.

(22) Shikata, T.; Hirata, H.; Kotaka, T. Micelle Formation of Detergent Molecules in Aqueous Media. 2. Role of Free Salicylate Ions on Viscoelastic Properties of Aqueous Cetyltrimethylammonium Bromide-Sodium Salicylate Solutions. *Langmuir* **1988**, *4*, 354–359.

(23) Ikeda, S.; Ozeki, S.; Tsunoda, M.-A. Micelle Molecular Weight of Dodecyldimethylammonium Chloride in Aqueous Solutions, and the Transition of Micelle Shape in Concentrated NaCl Solutions. *J. Colloid Interface Sci.* **1980**, *73*, 27–37.

(24) Candau, S. J.; Hirsch, E.; Zana, R. New Aspects of the Behaviour of Alkyltrimethylammonium Bromide Micelles : Light Scattering and Viscosimetric Studies. *J. Phys.* **1984**, *45*, 1263–1270.

(25) Rehage, H.; Hoffmann, H. Rheological Properties of Viscoelastic Surfactant Systems. *J. Phys. Chem.* **1988**, *92*, 4712–4719.

(26) Zana, R.; Kaler, E. W. *Giant Micelles: Properties and Applications*; CRC Press, **2007**.

(27) Khatory, A.; Lequeux, F.; Kern, F.; Candau, S. J. Linear and Nonlinear Viscoelasticity of Semidilute Solutions of Wormlike Micelles at High Salt Content. *Langmuir* **1993**, *9*, 1456–1464.

(28) Appell, J.; Porte, G.; Khatory, A.; Kern, F.; Candau, S. J. Static and Dynamic Properties of a Network of Wormlike Surfactant Micelles (cetylpyridinium Chlorate in Sodium Chlorate Brine). *J. Phys. II* **1992**, *2*, 8.

(29) Göbel, S.; Hiltrop, K. Influence of Organic Counterions on the Structure of Lyotropic Mesophases. In *Trends in Colloid and Interface Science V*; Corti, M.; Mallamace, F., Eds.; Progress in Colloid & Polymer Science; Steinkopff, **1991**; pp. 241–242.

(30) Arleth, L.; Bergström, M.; Pedersen, J. S. Small-Angle Neutron Scattering Study of the Growth Behavior, Flexibility, and Intermicellar Interactions of Wormlike SDS Micelles in NaBr Aqueous Solutions. *Langmuir* **2002**, *18*, 5343–5353.

(31) Hassan, P. A.; Raghavan, S. R.; Kaler, E. W. Microstructural Changes in SDS Micelles Induced by Hydrotropic Salt. *Langmuir* **2002**, *18*, 2543–2548.

(32) Mu, J.-H.; Li, G.-Z. The Formation of Wormlike Micelles in Anionic Surfactant Aqueous Solutions in the Presence of Bivalent Counterion. *Chem. Phys. Lett.* **2001**, *345*, 100–104.

(33) Mu, J.-H.; Li, G.-Z. Rheology of Viscoelastic Anionic Micellar Solutions in the Presence of a Multivalent Counterions. *Colloid Polym. Sci.* **2001**, *279*, 872–878.

(34) Lin, Z.; Scriven, L. E.; Davis, H. T. Cryogenic Electron Microscopy of Rodlike or Wormlike Micelles in Aqueous Solutions of Nonionic Surfactant Hexaethylene Glycol Monohexadecyl Ether. *Langmuir* **1992**, *8*, 2200–2205.

(35) Bernheim-Groswasser, A.; Wachtel, E.; Talmon, Y. Micellar Growth, Network Formation, and Criticality in Aqueous Solutions of the Nonionic Surfactant C12E5. *Langmuir* **2000**, *16*, 4131–4140.

(36) Fischer, P.; Rehage, H.; Grüning, B. Rheological Properties of Dimer Acid Betaine Solutions. *Tenside Surfactants Deterg.* **1994**, *31*, 99–108.

(37) Maeda, H.; Yamamoto, A.; Souda, M.; Kawasaki, H.; Hossain, K. S.; Nemoto, N.; Almgren, M. Effects of Protonation on the Viscoelastic Properties of Tetradecyldimethylamine Oxide Micelles. *J. Phys. Chem. B* **2001**, *105*, 5411–5418.

(38) Weers, J. G.; Rathman, J. F.; Axe, F. U.; Crichlow, C. A.; Foland, L. D.; Scheuing, D. R.; Wiersema, R. J.; Zielske, A. G. Effect of the Intramolecular Charge Separation Distance on the Solution Properties of Betaines and Sulfobetaines. *Langmuir* **1991**, *7*, 854–867.

(39) Kumar, R.; Kalur, G. C.; Ziserman, L.; Danino, D.; Raghavan, S. R. Wormlike Micelles of a C22-Tailed Zwitterionic Betaine Surfactant: From Viscoelastic Solutions to Elastic Gels. *Langmuir* **2007**, *23*, 12849–12856.

(40) Shikata, T.; Itatani, S. Viscoelastic Behavior of Aqueous Threadlike Micellar Solutions of Oleyldimethylamineoxide. *Colloid Polym. Sci.* **2003**, *281*, 447–454.

(41) Koehler, R. D.; Raghavan, S. R.; Kaler, E. W. Microstructure and Dynamics of Wormlike Micellar Solutions Formed by Mixing Cationic and Anionic Surfactants. *J. Phys. Chem. B* **2000**, *104*, 11035–11044.

(42) Raghavan, S. R.; Fritz, G.; Kaler, E. W. Wormlike Micelles Formed by Synergistic Self-Assembly in Mixtures of Anionic and Cationic Surfactants. *Langmuir* **2002**, *18*, 3797–3803.

(43) Christov, N. C.; Denkov, N. D.; Kralchevsky, P. A.; Ananthapadmanabhan, K. P.; Lips, A. Synergistic Sphere-to-Rod Micelle Transition in Mixed Solutions of Sodium Dodecyl Sulfate and Cocoamidopropyl Betaine. *Langmuir* **2004**, *20*, 565–571.

(44) Ghosh, S.; Khatua, D.; Dey, J. Interaction Between Zwitterionic and Anionic Surfactants: Spontaneous Formation of Zwitanionic Vesicles. *Langmuir* **2011**, *27*, 5184–5192.

(45) Hoffmann, H.; Rauscher, A.; Gradzielski, M.; Schulz, S. F. Influence of Ionic Surfactants on the Viscoelastic Properties of Zwitterionic Surfactant Solutions. *Langmuir* **1992**, *8*, 2140–2146.

(46) Hoffmann, H.; Hofmann, S.; Illner, J. C. Phase Behavior and Properties of Micellar Solutions of Mixed Zwitterionic and Ionic Surfactants. In *Trends in Colloid and Interface Science VIII*; Ottewill, R. H.; Rennie, A. R., Eds.; Progress in Colloid & Polymer Science; Steinkopff, **1994**; pp. 103–109.

(47) Saul, D.; Tiddy, G. J. T.; Wheeler, B. A.; Wheeler, P. A.; Willis, E. Phase Structure and Rheological Properties of a Mixed Zwitterionic/anionic Surfactant System. *J. Chem. Soc. Faraday Trans. 1 Phys. Chem. Condens. Phases* **1974**, *70*, 163.

(48) Renardy, M. *Mathematical Analysis of Viscoelastic Flows*; SIAM, **2000**.

(49) Briant, J.; Denis, J.; Parc, G. *Rheological Properties of Lubricants*; Editions TECHNIP, **1989**.

(50) Larson, R. G. *The Structure and Rheology of Complex Fluids*; Oxford University Press, USA, **1999**.

(51) *Food Texture and Viscosity: Concept and Measurement*; Academic Press, **2012**.

(52) Hirasaki, G. J.; Pope, G. A. Analysis of Factors Influencing Mobility and Adsorption in the Flow of Polymer Solution Through Porous Media. *Soc. Pet. Eng. J.* **1974**, *14*, 337–346.

(53) Sato, T.; Acharya, D. P.; Kaneko, M.; Aramaki, K.; Singh, Y.; Ishitobi, M.; Kunieda, H. Oil-Induced Structural Change of Wormlike Micelles in Sugar Surfactant Systems. *J. Dispers. Sci. Technol.* **2006**, *27*, 611–616.

(54)   Rodriguez-Abreu, C.; Aramaki, K.; Tanaka, Y.; Lopez-Quintela, M. A.; Ishitobi, M.; Kunieda, H. Wormlike Micelles and Microemulsions in Aqueous Mixtures of Sucrose Esters and Nonionic Cosurfactants. *J. Colloid Interface Sci.* **2005**, *291*, 560–569.

(55)   Menge, U.; Lang, P.; Findenegg, G. H. From Oil-Swollen Wormlike Micelles to Microemulsion Droplets: A Static Light Scattering Study of the L1 Phase of the System Water + C12E5 + Decane. *J. Phys. Chem. B* **1999**, *103*, 5768–5774.

(56)   Sato, T.; Acharya, D. P.; Kaneko, M.; Aramaki, K.; Singh, Y.; Ishitobi, M.; Kunieda, H. Oil-Induced Structural Change of Wormlike Micelles in Sugar Surfactant Systems. *J. Dispers. Sci. Technol.* **2006**, *27*, 611–616.

Chapter 4

Foam for Zwitterionic and Anionic blended Surfactants

Introduction:

Foam injection has been widely studied as an enhanced oil recovery process on a laboratory scale [1–7] as well as field scale[8–11]. However the major concern using foam is the detrimental effect of crude oil on foam films [12,13] and hence finding a suitable surfactant formulation is essential. Betaine is an amphoteric surfactant which has both the positive and negative charge on its head group. It has been used widely in shampoos along with another anionic/non ionic surfactant mainly due to its ability to boost foam and increase foam stability[14,15]. A wide application of betaine/sulfobetaine type surfactants in personal care products as well as industrial application has been elaborated in literature[16].

Foam boosting ability of betaine in an anionic-betaine blended surfactant was studied against silicone oil and it was observed that the presence of betaine caused an increase in the stability of the pseudo emulsion film[17,18]. Laboratory studies have shown that betaine-anionic blended surfactants have been better foam performers in the presence and absence of crude oil than the anionic surfactants itself[19,20]. An anionic surfactant which could not remain in solution in the presence of hardness, produced a clear solution, upon addition of a betaine surfactant and the blend proved to be a super foamer in the presence of crude oil[2]. Still there is no clear understanding on the role of betaine at an interfacial level. Conjectures[21] have been proposed that the betaine might aide the anionic surfactants pack at the interface more rigidly and possibly giving rise to interfacial viscosity.

Studies have shown when dodecanol is added to anionic sodium dodecyl sulphate (SDS) there is an increased interfacial viscosity, which in turn slows down film thinning process [22]. Danov et.al have developed a model to fit surface tension isotherms and have predicted that adding a betaine to SDS remarkably increases surface elasticity and think this might be a possible explanation to foam film stability[23].

Experimental studies on mixtures of zwitterionic (betaine and sulfobetaine also known as sultaine) and anionic surfactants demonstrate synergistic interaction as measured by the single molecular β parameter, developed from the simple yet widely used regular solution theory[24–31]. The regular solution theory however has limitations in its applications and several molecular theoretical have hence been developed[32–40]. The work of Blankschtein and co –workers, extensively developed a theory for zwitterionic and anionic mixtures and predict significant interactions between them[36]. Following these studies there was interest in developing a deeper understanding on the foam rheology of zwitterionic-anionic blended surfactants in porous media for the purpose of enhanced oil recovery.

This chapter elaborates on the experimental procedure followed in studying foam rheology in porous media. Prior to doing this an aqueous solubility test was performed to identify clear solutions which were chosen as suitable candidates for porous media studies. Solutions that remained unclear/cloudy and contained precipitates were avoided since plugging in porous media has been observed with such solutions. The main objective of this study is to answer

- *If a blend of zwitterionic surfactant and anionic AOS$_{14-16}$ (AOS), at any particular ratio can enhance the foam strength to a better value than the individual surfactants (pure AOS or pure zwitterionic) in the absence of oil.*

- *If addition of a zwitterionic surfactant (betaine or sultaine) to anionic AOS_{14-16} (AOS) is beneficial for foam- assisted oil recovery process of water flood residual oil.*

- *If use of viscoelastic surfactant solutions help to generate stronger and more stable foam than Newtonian surfactant solutions and if it helps in faster recovery of waterflood residual oil.*

4.1 Aqueous solubility test

The following zwitterionic surfactants and their blends with anionic AOS have been studied in porous media.

Surfactant	Molecular Weight(g/mol)
Rhodia A (C_{18} N,N dimethyl amido betaine)	384
Rhodia B (C_{18-22} N,N dimethyl amido sultaine)	461
Alpha Olefin Sulfonate AOS_{14-16} (AOS)	316
Lauryl Betaine (LB)	281.5
Lauryl Sultaine (LS)	351

Salts	NaCl brine (g/L)	Sea water(g/L)
NaCl	44.43	26.95
$MgCl_2.6H_2O$		11.15
$CaCl_2. 2H_2O$		1.76
Na_2SO_4		4.80
Ionic Strength	0.75 M	0.71M

Table 4.1: Composition of sea water. All salts were added to deionized water.

For the purpose of foam studies in porous media all the surfactant solutions were made in sea water(see Table 4.1 for composition). This sea water composition was chosen for a particular giant carbonate reservoir in Gulf of Mexico.

4.1.1 Rhodia A: AOS blends

Solutions made in sea water

Figure 4.1 shows a blend scan of zwitterionic Rhodia A with anionic AOS at room temperature and solutions made in sea water. It can be observed that the A:AOS blends in the ratios of 9:1, 2:8, 1:9 remain clear at this studied temperature. In addition to that A:AOS 9:1 and 2:8 blends are also viscoelastic solutions as observed visually and tested in a rheometer (Chapter 3). The ratio A:AOS 1:9, which is predominantly composed of AOS, is a Newtonian solution.

Solutions made in NaCl brine

When the same blends were made in NaCl brine (see Table 4.1), which had the same ionic strength as sea water, all ratios but A:AOS 7:3, 6:4 gave clear solutions (picture is not shown but rheological measurements for the blends can be found in Chapter 3). Most of the obtained clear solutions were viscoelastic except A:AOS 2:8, 1:9, which were Newtonian (See Chapter 3 for rheological measurements).

The blend scan studies suggest that there is an effect of divalent salts both on the solubility and also on viscoelastic properties of the blends. For the C_{18} amido betaine, in the presence of divalent salts , very few ratios produced a clear solution as compared to when NaCl brine is used at room temperature. The blend scan was not studied for this particluar surfactant mixture at elevated temperatures.

74

For the purpose of foam studies Rhodia A, AOS, A:AOS 9:1 and A:AOS 1:9 were chosen for study in porous media. These particular ratios were chosen based on their aqueous solutions producing single clear phases, keeping in mind that one blend had higher zwitterionic content and the other had lower content.

Figure 4.1: Aqueous solubility tests for Rhodia A(A) and AOS_{14-16} (AOS) surfactant blends ratios (based on mass ratio) showing the region where clear solutions are obtained at room temperature (~23 °C). The brine used was sea water.
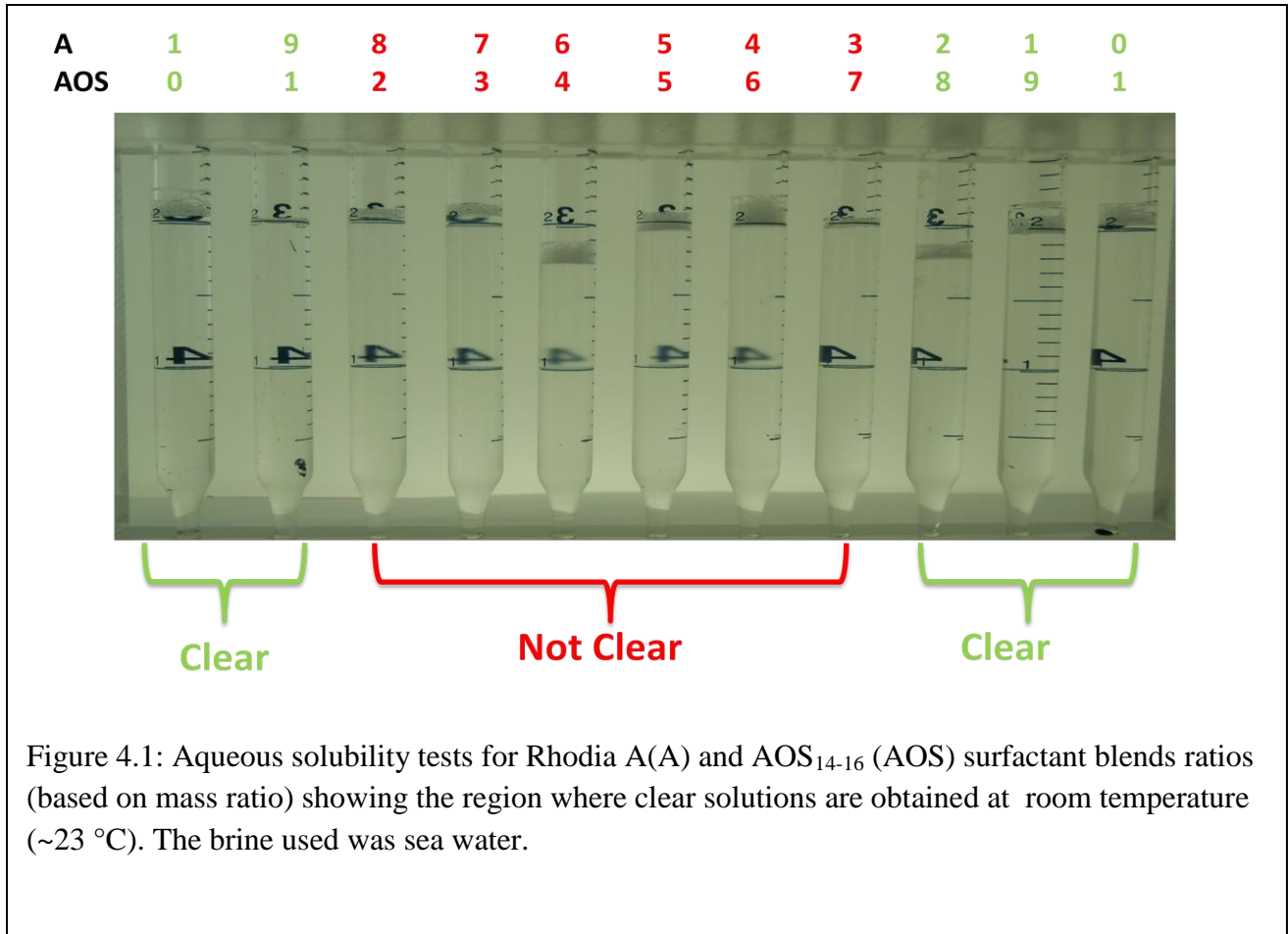
4.1.2 LB: AOS blends

Solutions made in sea water

Initially all experiments were planned at room temperature. However LB:AOS (7:3) blend made in sea water would get cloudy at room temperature, but would stay a clear solution at an elevated temperature of 45 °C. To prevent plugging of the core it was decided to conduct

the foam experiment at 45°C. In order to be systematic all foam experiments were performed at 45°C for the LB: AOS blends. Pure LB and pure AOS solutions by themselves remain clear at room temperature and at 45 °C to 90°C. The blends LB:AOS (9:1, 8:2, 7:3) remain clear at an elevated temperature of ca. 45 °C and above as seen in Figure 4.2, Figure 4.3b. They exhibit Krafft point like phenomenon where when the solution cools to room temperature it turns cloudy again after ~ 2 hours. This Krafft point phenomenon could be occurring due to the presence of divalent in sea water which might be lowering the solubility of the surfactants at room temperature[41]. Literature shows a Krafft point value of ~ 36° C for these types of surfactant mixtures. The LB: AOS (1:9) blend remains clear both at room temperature and elevated temperatures.

Solutions made in NaCl brine:

For the LB:AOS blends made in NaCl brine all the blends remain clear from room temperature upto a studied temperature of 90° C (Figure 4.4). This implies that the hardness of the brine (divalent salts) has an effect on the solubility of the surfactant mixtures.

Compounds of betaine type in combination with sulfonate/sulfate group anionic surfactants have shown to exhibit Krafft point phenomenon due to the formation of an additional intermolecular complex especially near 50:50 molar fraction[42] made in DI water. This is attributed to the strong interactions between the quaternary cationic nitrogen group and the negative anionic group. In the case of LB: AOS system, the solutions of all compositions remain clear in NaCl brine at temperature ranges from ~ 22-90 ° C. However certain compositions in sea water form permanent precipitates even at elevated temperatures (studied up to 90° C). This is occurring mostly due to the hardness content in the brine. Table 4.2 shows the pH of the

solutions when they were prepared. Most solutions are in pH ~6 range. Though the pH of the other blends was not measured it can be thought perhaps they are in the same range as well. In this pH range the zwitterionic LB is mostly deprotonated (remains zwitterionic).

In solution, micelles and monomers are in dynamic equilibrium. Some of the anionic sulfonate monomers may be binding with the cations Mg^{2+} and Ca^{2+} forming calcium olefin sulfonates causing them to precipitate or it is also possible that the carboxylate group of the LB might be forming higher chain calcium carboxylates like compounds (commonly called soap scum) or both forms of precipitates could co-exist. It has been studied with anionic sodium dodecyl sulfate (SDS) that precipitates of $Ca(DS)_2$ have been formed in the presence of calcium cations. Nonionic surfactant was added to shield the repulsions between DS^- head groups and helped increase calcium tolerance[41]. If we go by a similar logic, the zwitterionic LB which has a net charge equal to zero is also expected to screen repulsions between the AOS^- head groups. Zwitterionic LB being a dipole, along with negative anionic surfactant, causes a negative surface charge density on the micelle surface. Due to complex interactions among the surfactant molecules and the divalent salts, there is possibly a reduced tendency to form micelles, and thus causing a larger amount of free monomers in solutions to bind with the divalent cations causing them to precipitate. Of course this depends on the composition of the micelles (how much LB and AOS the micelle consists of). Further interpretations are beyond the scope of this thesis. These aqueous solubility tests are studied to pick a suitable candidate for foam injection in porous media.

(LB)	1	9	8	7	6	5	4	3	2	1	0
(AOS)	0	1	2	3	4	5	6	7	8	9	1
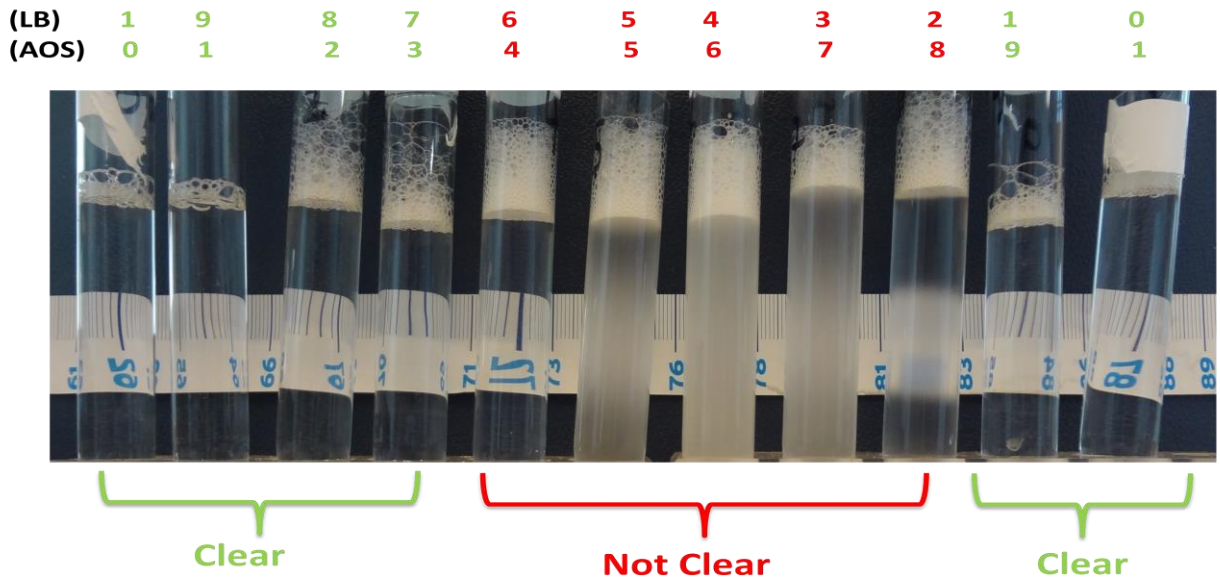
Figure 4.2 :Aqueous stability tests for Lauryl Betaine (LB) and AOS_{14-16} (AOS) surfactant blends ratios(based on mass ratio) showing the region where clear solutions are obtained at temperature 45 °C. Total concentration is 0.5 wt%. Trend remains the same at 65, 75, 85, 90 °C. Brine is sea water.
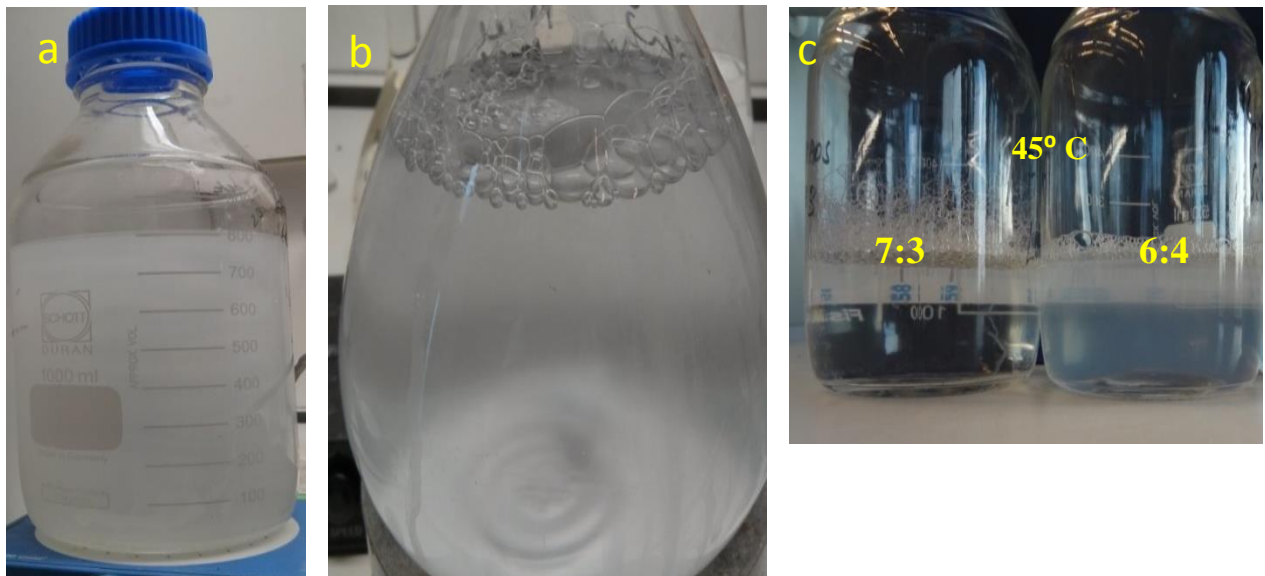
Figure 4.3: a)From above figure 4.2 though LB:AOS 6:4 appears clear, when made in bulk it is cloudy. This picture is taken at room temperature 21 °C.   b) LB:AOS 7:3 blend at 21°C when made in bulk gets cloudy with time. The same trend remains for 9:1, 8:2 blends at 21°C.   c) LB:AOS 7:3 blends becomes a clear solution at 45° C. But 6:4 blend remains cloudy at 45° C. The total concentrations for all the above pictures are 0.5 wt%.

Figure 4.4: Aqueous stability tests for LB and AOS surfactant blends ratios (based on mass ratio) in NaCl brine having same ionic strength as sea water, showing the region where clear solutions are obtained at 45°C. The trend remains the same at room temperature, 65, 75, 85 and 90 °C.
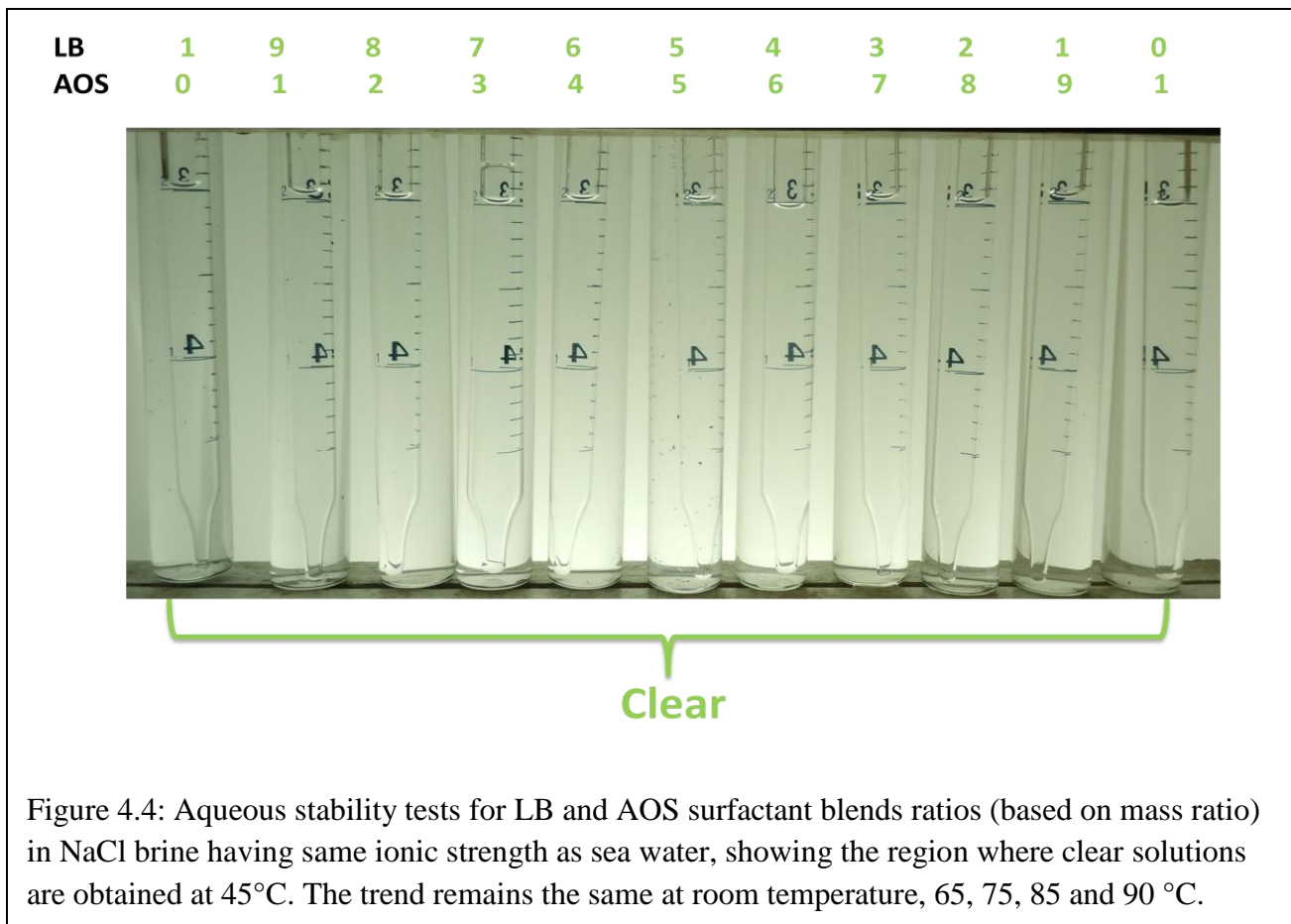
Surfactant solution	pH for a 0.5wt% concentration
LB	6.5
LB:AOS 7:3	6
LB:AOS 1:9	6
AOS $_{14\text{-}16}$	6
LS	7.5
LS:AOS 8:2	6.5
LS:AOS 1:9	6

Table 4.2: Values of pH for surfactant blends for a 0.5wt% total concentration made in seawater. All solution pH was measured using a pH paper.

4.1.3 LS: AOS blends

Solutions made in sea water

Figure 4.5 shows the blend scan of LS and AOS at different compositions. At room temperature ~ 20° C the composition LS:AOS 7:3, 3:7 appears cloudy, however at an elevated temperature of 45° C it becomes clear. Increasing the temperature seems to increase the solubility. The solution was not cooled back to see if it became cloudy on cooling. This blend was studied only at room temperature and 45° C. At both these temperatures the compositions LS:AOS 6:4, 5:5, 4:6 appear cloudy. It could be that these blends have a higher Krafft point or these blends could be forming complexes with the divalent cations. Further studies on aqueous behavior is beyond the scope of this thesis.

All the surfactant solutions mentioned in Table 4.2 were studied for foam flow in porous media . The ratios were chosen based on the clarity of the aqueous solutions produced when mixed, and also for studying the effect of blend ratio on foam rheology in porous media.
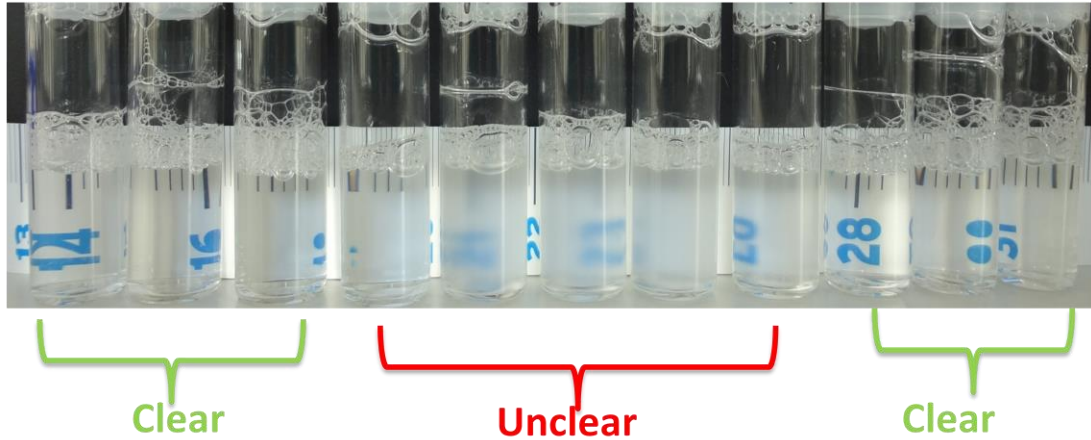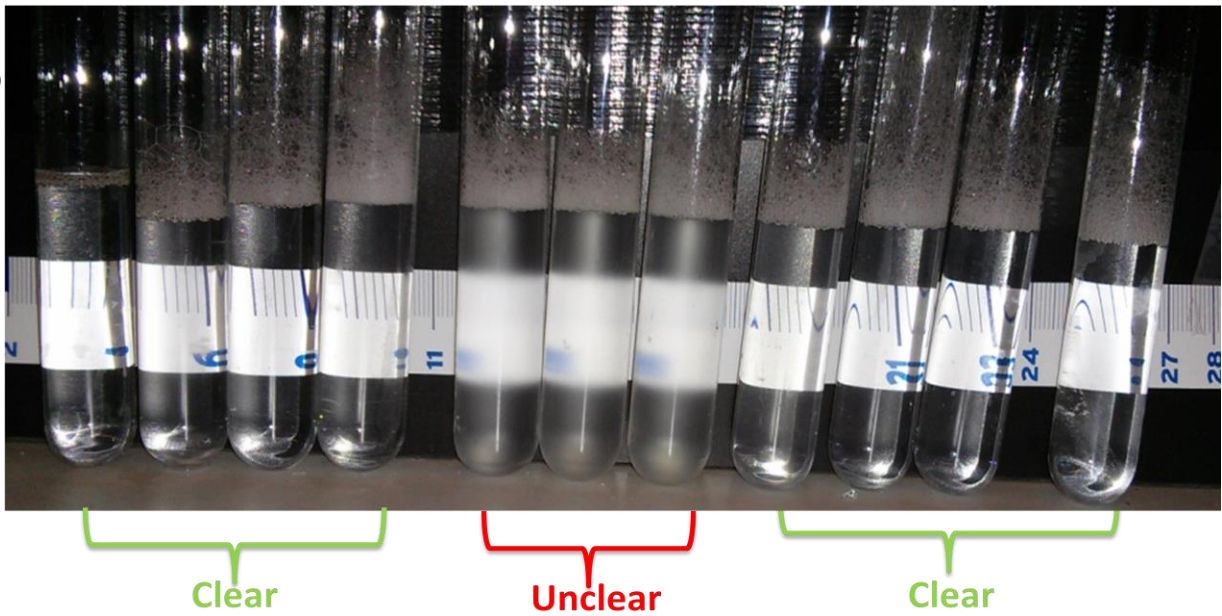
Figure 4.5: Aqueous stability tests for Lauryl Sultaine (LS) and AOS$_{14-16}$ (AOS) surfactant blends ratios(based on mass ratio) showing the region where clear solutions are obtained at temperature a) 20° C b) 45 °C. Total concentration is 0.5 wt%. Brine is sea water.

4.2 Foam experimental set up

Two foam experimental set ups were used to study the surfactant mixtures.

4.2.1 Foam experimental set up I (Rice University)

Figure 4.6 a) is a schematic representation of the experimental set up used. This set up was built at Rice University. It consists of a stainless steel sand pack which is 2 ft long and 1 inch diameter. The sand pack includes three internal taps. The first internal tap is located 6 inches away from the inlet. The second internal tap is at a distance of 6 inches from the first tap and the third tap is at a distance of 6 inches from the second tap. A schematic representation of the position of internal taps is found in Figure 4.6 b). The differential pressure was measured across the first and second taps (referred to as section 1 in the remainder of the text) and also across second and third taps (section 2). The porous medium used was U.S.Silica sieved using 20/40 mesh. The sand pack was placed horizontally. The internal taps were connected to differential transducers (Validyne) having a diaphragm limit of 50 psi. Additionally pressure drop across the inlet and outlet was measured using a differential transducer (Validyne) having a diaphragm limit of 200 psi. The raw data obtained was pressure drop values which were monitored throughout the experiment and recorded using Validyne data acquisition software.

Liquid was injected through Quizzix pump (QX series) and gas was injected through a mass flow controller (Matheson for nitrogen gas). Check valves (1psi) downstream of the liquid injection and gas injection was installed to prevent the backflow of injected phases.

The outlet of the sand pack was connected to a relief valve (Swagelok RL3 50-130 psi rating) which served as a back pressure regulator system(BPR). An auxiliary syringe pump was

used to inject water at a low flow rate to keep the diaphragm of the relief valve open always.

This arrangement prevented fluctuations in the back pressure readings.
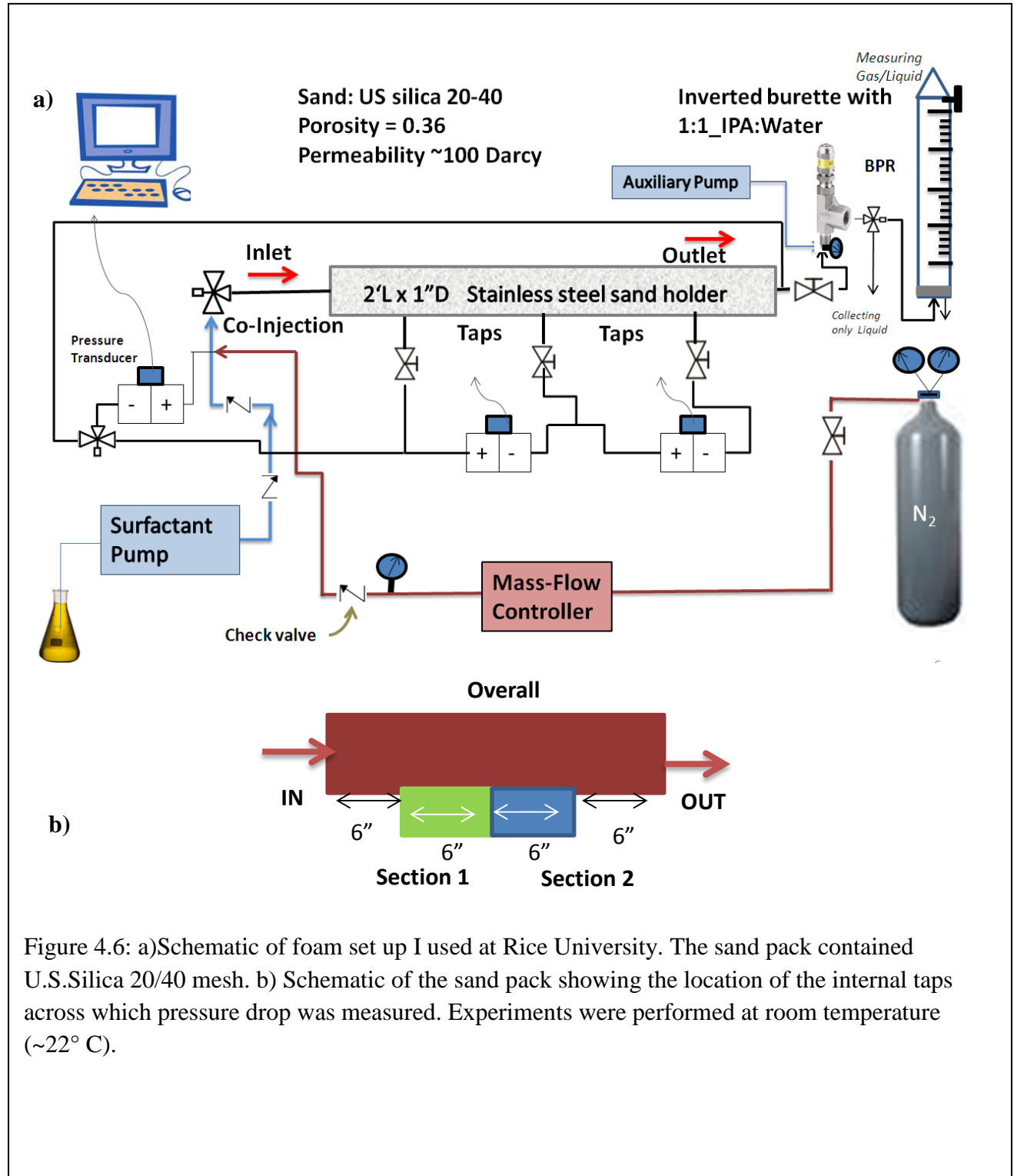
Figure 4.6: a)Schematic of foam set up I used at Rice University. The sand pack contained U.S.Silica 20/40 mesh. b) Schematic of the sand pack showing the location of the internal taps across which pressure drop was measured. Experiments were performed at room temperature (~22° C).

Ocassionaly the gas/liquid ratio was measured using an inverted burette set up. The inverted burette was filled with IPA/water (1:1) mixture. The volume of liquid displaced at a given time is calculated to get the gas liquid ratio.

The sand pack was filled with sand by gently tapping the holder with a weight placed on top, to be able to pack uniformly. Tapping was continued till the weight moved no further. Rubber stoppers were inserted at the inlet and outlet of the sand pack to keep the sand tight and immovable. Additonally fine mesh screens were placed between the rubber cork and packed sand to prevent sand particle from entering into the tubings which may potentially plug them. Swagelok fittings were used to seal them well. The sand pack was kept under vaccum -29 in Hg for minimum of 8 hours to remove any moisture from the system. When the vaccum was held by the pack it was considered as a sign that there was no leak anywhere. Following this brine (sea water) was injected into the sand pack and the pore volume (PV) was measured. Several PVs of brine were injected at various flow rates and the pressure drop was measured. It was done to calculate the permeability of the sand pack. Permeability was always ~ 100 Darcy. Following this several PVs of surfactant solution were injected to saturate the sand pack with surfactant to satisfy adsorption. It was also done because the surfactants used in this set up were viscoelastic and exhibited shear thinning behavior as observed in rheological measurements (Chapter 3). The intent was to compare and quantify this behavior in the porous medium. All prepared surfactant solutions had a total concentration of 0.5 wt% and this concentration can be assumed throughout this chapter unless otherwise specified.

Gas and surfactant solution were co-injected to study the foam rheology in porous media. Pressure history was used to monitor the foam propogation through the sand pack. The presence of internal taps was very helpful to guage this propoagation better. The rheology of foam flow

84

was quantified using the Darcy's law for apparent viscosity. It was calculated using **Equation 4.1**.

$$\mu_{app} = -\frac{k}{u_{total}}\nabla p \qquad \textbf{Equation 4.1}$$

Where k is the medium absolute permeability

μ_{app} - apparent viscosity

u_{total} - total flux (gas+liquid)

∇p - pressure gradient

The *gas fraction* or also known as the *foam quality* is given as

$$\Gamma = \frac{q_g}{q_g + q_l} \qquad \textbf{Equation 4.2}$$

q_g – gas flow rate q_l- liquid flow rate Γ – Foam quality

Crude oil experiments

The sand pack which was used for a particular surfactant foam flood was cleaned with several PVs (10-12) of IPA/water (1:1) mixture to kill all the foam and to clean the system of surfactant solution. It was then cleaned with several PVs of brine (8-10 PVs sea water) to remove any IPA in the system. When the effluent would no longer smell of IPA it was assumed that all the alcohol was removed from the system. Following this additional 3-4 PVs of brine were injected just to ensure the system was clean. The permeability was measured again and always the measured values were close to ~95-100 Darcy. This showed that all the trapped gas was removed from the system. Crude oil was injected using an ISCO pump. Crude oil displaced the brine inside the system and when the first drop of crude oil was seen in the effluent injection was stopped. Connate water and crude oil saturations were calculated from amount of oil injected and

amount produced. The oil saturated pack was water flooded (sea water) to recover as much oil as possible. The oil produced was used to estimate the remaining oil inside the sand pack. Following this surfactant solution and N_2 gas were co-injected as foam and the pressure drop was monitored. Since foam stability studies were primarily of interest, the oil cuts were not measured for the experiments. After the crude oil studies were conducted for a particular surfactant solution the sand pack was dismantled cleaned thoroughly with toluene, acetone, tap water and scrubbed with detergent till no oil drops could be seen inside the pack under visual inspection. Then new and clean sand was packed for studies using another surfactant formulation.

Note: Back pressure value of ~ 50 psi was maintained at the outlet of sand pack for all experiments where gas was injected to minimize gas compressibility effects. However for the sequence of experiments using surfactant solution Rhodia A, back pressure was not used. When foam was injected, gas flow rate was calculated by taking into account the average value of injection and back pressure.

Crude oil properties

The dead crude oil was supplied to us by PEMEX. Synthetic crude oil (84% dead crude +16% cyclohexane) was used to match the live oil viscosity. The viscosity at 25°C as measured by the Brookfield viscometer was ~50 cP. The crude oil had 10-20% asphaltene content. The specific gravity of the synthetic crude oil is 0.9. More details of this can be found in Salinas's thesis[2].

4.2.2 Foam experimental set up II (TU Delft)

The second experimental set up was built at TU Delft (Figure 4.7). Bentheimer sandstone was used as the porous medium for the foam experiments. The length of the core was 17cm and diameter 3.8cm. The core had a 2mm layer of Araldite resin which helped prevent

Figure 4.7: Foam experimental set up II at TU Delft. Bentheimer sandstone core (17 cm = 6.6 inch) is used. All experiments performed at 45° C.
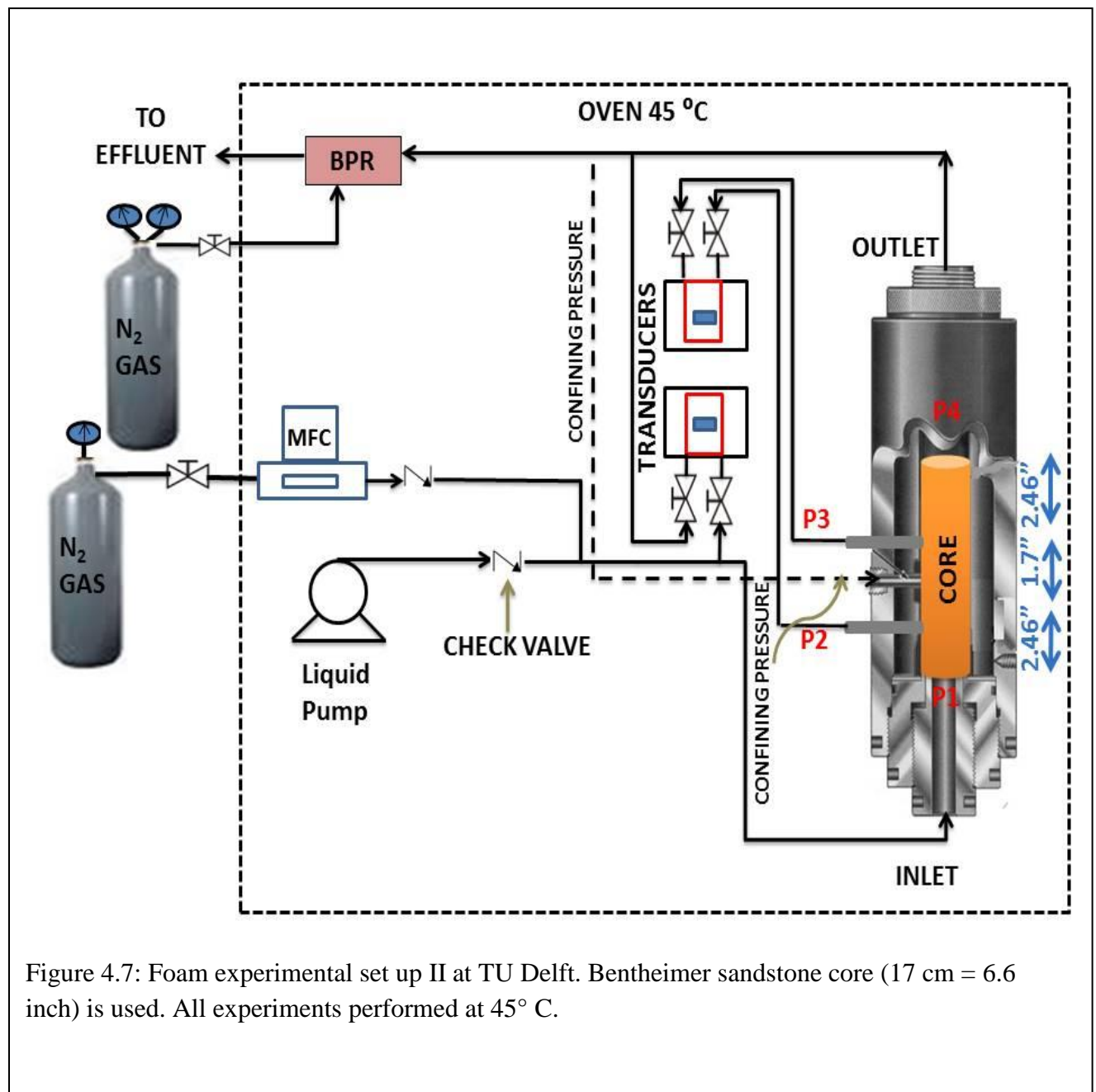
fluid bypassing. Core was placed inside a PEEK (polyether ether ketone) core holder. The core holder was placed vertically. The system was flushed with helium and a leak test was performed using a helium leak detector to ensure the system waswell sealed. Following this CO_2 was injected to displace the helium gas. Then brine was injected by setting the value of back pressure to ~25 bar to dissolve all the CO_2 , till no more bubbles were observed at the effluent. All the cores had a porosity of 21-22%. The permeability was measured with respect to sea water (single phase flow) first and then surfactant solution (single phase flow). They both gave close permeability values. The cores were flooded with several pore volumes (6-8 PV) of surfactant (single phase flow) in each case to satisfy adsorption. For foam experiments nitrogen was used as the gas phase. For each surfactant solution system a new Bentheimer core was used. Details of the experiments are given in Table 4.3. Cores for experiment 1, 4,5,6,7 were obtained from the same Bentheimer block. Cores for experiment 2, 3 were obtained from a different block which seemed to have iron content when observed visually. The cores of this block also had a lower permeability than the rest.

Experiment number	Surfactant solution	Bentheimer core permeability (Darcy)	Core permeability after cleaning (Darcy)	Temperature (°C)
1	LB	2.5	N/A	45
2	LB:AOS 7:3	0.65	1.2	45
3	LB:AOS 1:9	0.9	0.7	45
4	AOS $_{14-16}$	2.6	2.4	45
5	LS	3.0	2.7	45
6	LS:AOS 8:2	2.4	2.1	45
7	LS:AOS 1:9	2.7	2.4	45

Table 4.3: Permeabilities of Bentheimer cores with respect to sea water and temperature at which foam studies were conducted for different surfactant solutions.

The core holder consisted of two internal taps enclosing a distance of 4.3cm (1.7 inches). It was located equidistant from both the inlet and outlet. A differential transducer connected across the internal taps (P2-P3) was used to measure the pressure difference across it. The outlet of the core was connected to a back pressure regulator (Eigen merk CTS MB420) which was maintained at a back pressure value of ~5 bar (~73.5 psi) for experiment 2,3 and at ~25 bar (~367.5 psi) for experiment 1,4,5,6,7. Back pressure regulator is used to minimize the gas compressibility effects. The absolute pressure at the injection (P1) is measured using a transducer. Nitrogen gas was delivered through a mass flow controller (Bronkhorst N_2 502) and surfactant solution was delivered through a Quizix Pump (Vindum QX6000 HC-0-0-C-L-0). All data were collected through a data acquisition system. The set up was placed inside an oven at

45°C. For foam experiments gas and surfactant solution were co-injected and the pressure drop was monitored continuously. The foam apparent viscosity was calculated using Equation 4.1 and the gas fraction using Equation 4.2. All foam experiments mentioned were done at 45° C except the foam flow in presence of crude oil for LB which was done at 20°C. Initially all experiments were planned at room temperature but due to the krafft point phenomena of certain surfactant blends (see *4.1 Aqueous solubility test*, it was decided to conduct the experiment at 45° C for all surfactant solutions in order to be systematic). Since LB (Lauryl betaine solution) remained clear at room temperature and it was the first to be studied, the entire foam sequence of experiments were done both in the absence and presence of crude oil at ~ 20°C. The next time LB sequence was repeated at 45°C but the crude oil experiments were not repeated.

Crude oil experiments

After the foam flood, the core was cleaned with 8-9 PVs of IPA/water (50:50) mixture till no more bubbles was observed at the outlet. At this time the back pressure was released and outlet maintained at atmospheric pressure. Following this 8-9 PVs of brine (sea water) was injected to remove all the IPA from the system. The entire system was dried by blowing CO_2 into the system to remove the water as much as possible. Then the entire system was left under vacuum overnight.

The system was saturated with brine once again to measure the permeability. The permeabilities of all the cores after cleaning procedure were very close to the original absolute permeability measured when the new core was installed. However for the experiment 2 (LB:AOS 7:3), the permeability had increased to 1.2 Darcy from 0.65 Darcy on cleaning. One of the hypotheses might be that the cleaning might have caused some content to dissolve from the

90

core causing the permeability to increase. But nothing was visually seen in the effluent during the cleaning process. However it was decided to proceed with saturating the core with crude oil.

Oil was flooded from top to bottom for ~ 2PV to get a good saturation. Connate water and oil saturation were estimated. Following this CO_2 gas was injected from top to bottom and bottom to top for 5 minutes each from the gas network at a pressure of ~6-7 bar. Following this water flood was done this time setting a back pressure of ~ 25 bar. This was done to dissolve any trapped CO_2. It was continued till no more oil was seen in the effluent. After this ~ 2 PV of surfactant was injected and very little oil production was observed as none of the surfactants were low IFT formulations. The purpose of following this procedure was to remove as much oil out as possible and study only the foam stability against immovable crude oil. Then foam was injected at various flow rates and total oil production was estimated. However foam had ended up removing some amount of oil. The pressure was constantly monitored throughout the experiments.

Crude oil properties

The crude oil was from a Norwegian company. The specific gravity of crude oil at room temperature (20°C) was 0.94.The crude had API gravity of 19.03° at 20°C. The oil was heavy crude and viscous as well. The viscosity as measured by the rheometer was 230 cP at shear rates 1-10 s $^{-1}$ and temperature 25° C. At 50° C and shear rates 1-10 s^{-1}, the viscosity was 58 cP.

4.3 Foam rheology in sandpack for Rhodia A, Rhodia B and A-AOS [14-16] blends

4.3.1 Single Phase flow

The sand pack was saturated with several PVs of surfactant to satisfy adsorption. During that process the surfactant rheology was studied.

Figure 4.8 is the experimental result of the shear thinning nature of the viscoelastic surfactants Rhodia A, the blend A:AOS 9:1 and Rhodia B. Similar behavior was observed in bulk rheological measurements (refer to Chapter 3 for further discussion). In order to scale behavior in porous media, pseudo shear rate was calculated as per a model proposed by Carreau for polymeric fluids. Since the viscoelastic surfactants are "living polymers" their behavior can be defined by a pseudo shear rate[2,43] as

$$\dot{\gamma} = \frac{1.38 \, u}{\sqrt{\phi k}} \qquad \textbf{Equation 4.3}$$

1.38 is a constant that includes tortuosity, and a constant for spherical particle shape[2]

u is superficial velocity, ϕ is porosity and k is absolute permeability.

For AOS surfactant solution, only high flow rates (shear rates) were measured since there were a lot of fluctuations in the transducer reading for low flow rates due to very low pressure drops. The viscosity in the rheometer was measured to be around 1cP which is close to the value obtained in sand pack. AOS exhibited Newtonian flow behavior in sand pack.

Viscoelastic surfactants have found wide application in oil recovery in the application of well stimulation [44–47] and as fracturing fluids[48–50]. Rhodia A surfactant solution is shear thinning with negative slope of 0.136 and weakly viscoelastic. However on blending 9 parts of the weakly

viscoelastic A and 1 part of Newtonian AOS by mass ratio, the solution produced is highly viscoelastic and ~ 2 orders of magnitude higher viscosity than Rhodia A. This is probably due to screening of the head group repulsions by the monovalent and divalent salts present in solution and also synergistic interactions between the anionic and zwitterionic surfactants enhancing the formation of the wormlike micelles. This has been observed in literature as well[51–53]. A:AOS 9:1 solution shear thins with a negative slope of 0.681 as fitted by the power law model. There were no injection issues or plugging during the flow of A:AOS 9:1 or Rhodia B. Rhodia B is viscoelastic and shows a shear thinning slope of negative 0.936.

Viscoelastic solutions like polymers show extensional rheology at higher shear rates[54,55]. However these wormlike micelle solutions do not exhibit shear hardening at high shear rates, at least in the case of Rhodia B. A:AOS 9:1 was not studied at very high shear rates due to the limitations of the pump and transducers. This is because wormlike micelles are known to break and recombine at high shear rates and hence known as "living polymers". Surfactants of this type have an advantage over polymers, since their molecular backbone structure is not destroyed under high shear rates unlike polymers.

4.3.2 Foam rheology

Figure 4.9 is an example of a typical foam transient experiment of AOS $_{14-16}$. The figure clearly shows the pressure build up, and the presence of internal pressure taps aids in understanding how the foam propagates through the sand pack. Gas flow rate is calculated by taking the average of the injection pressure and the back pressure. We see how foam propagates from inlet to outlet as indicated by the pressure rise which reaches a steady value a little over a PV in first internal section. It then crosses the second internal section in less than the 2nd PV. The overall pressure drop rises from 0psig to a steady state value at 2.6 PV. Since there is some gas compressibility

effect due to a low value of BPR it can be observed that the foam quality varies from ~ 60% at the start of the experiment to ~ 40% at the steady state. Also we note that this is just the start of the foam experiment following the single phase flow. Hence the foam might be expected to fill the sand pack in about 1 PV. However foam takes about 2.6 PV to cross the entire sand pack as indicated by the overall pressure drop. The occurrence of gas break through was not noted visually in any of the experiments and only pressure drop was observed for the purpose of calculating the foam strength. The reader should note that steady state value is the value at which no more changes in pressure drop occur and gas breakthrough is the first time at which gas bubbles are observed at the effluent. It is possible to have an early gas breakthrough and yet not reach a steady state pressure drop.
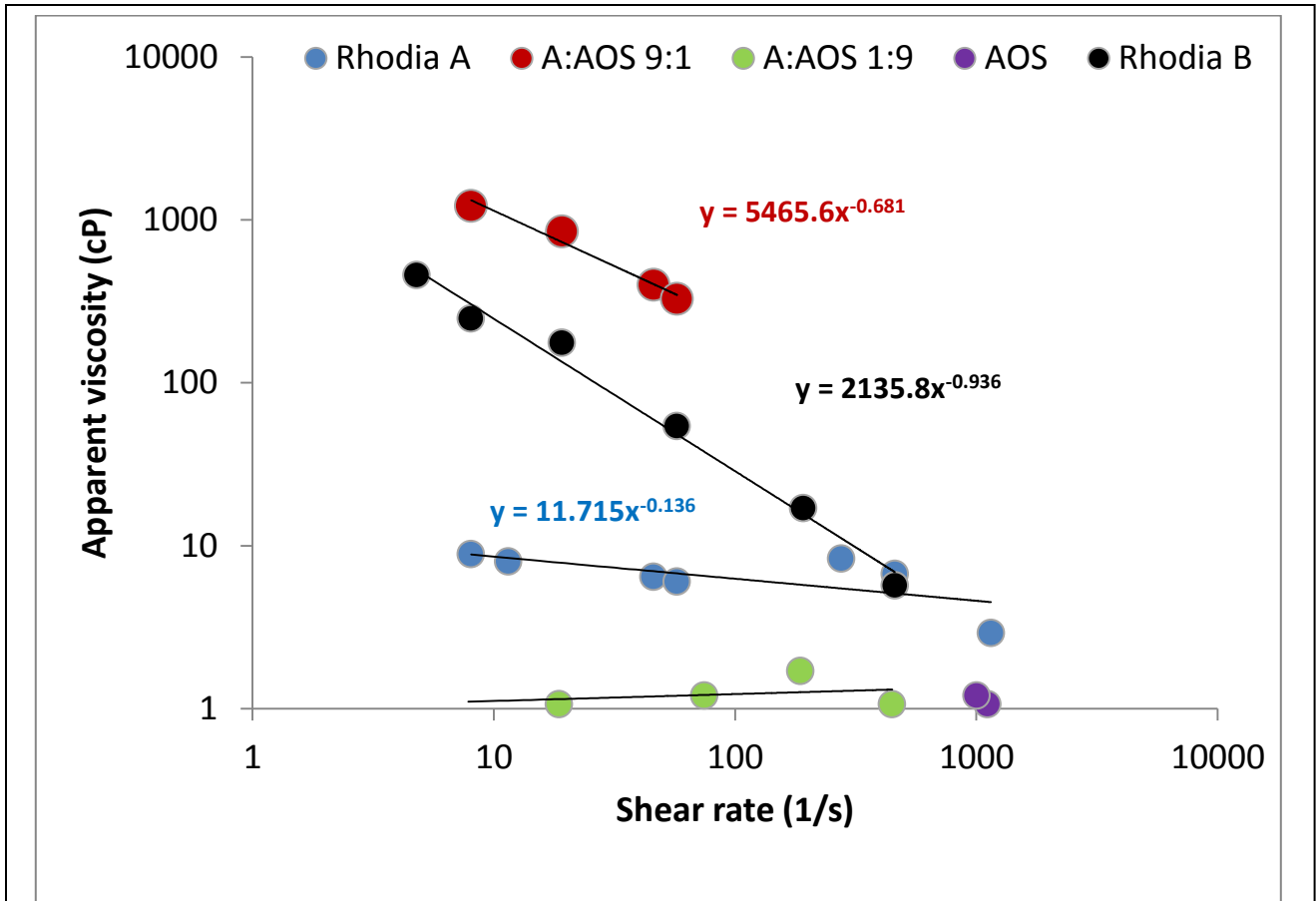
Figure 4.8: Single phase flow rheology in 100 Darcy U.S.silica 20/40 mesh sand pack (only surfactant solutions). Several PVs (5-6 PV) were injected to saturate the sand pack prior to foam injection. Shear thinning behavior of viscoelastic surfactants is observed for Rhodia A, Rhodia B, A: AOS 9:1. The blend A: AOS 1:9 shows Newtonian behavior (~1 cp). Pure AOS shows Newtonian behavior with viscosity ~ 1 cP. Only high shear rate values are plotted.
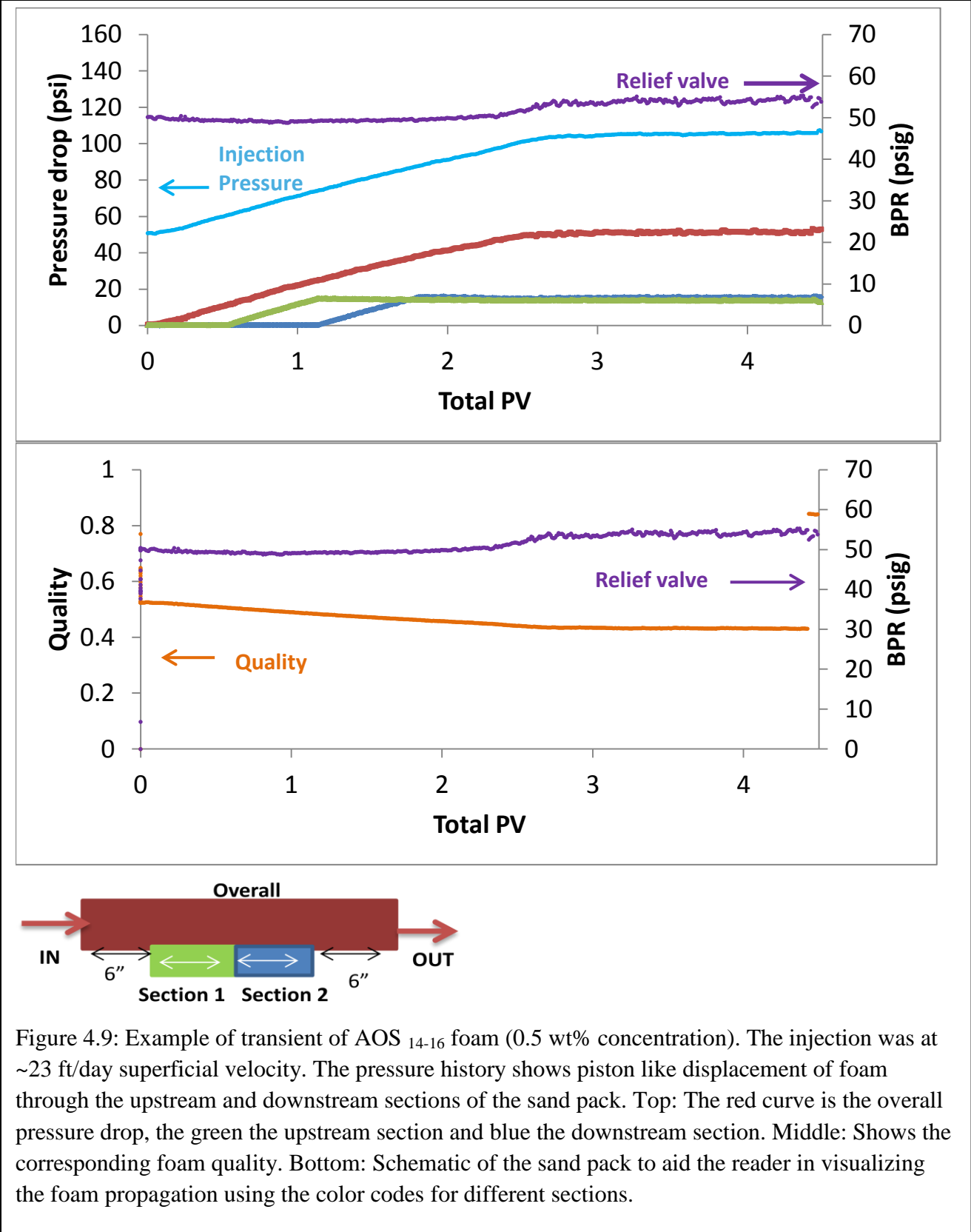
Figure 4.9: Example of transient of AOS $_{14-16}$ foam (0.5 wt% concentration). The injection was at ~23 ft/day superficial velocity. The pressure history shows piston like displacement of foam through the upstream and downstream sections of the sand pack. Top: The red curve is the overall pressure drop, the green the upstream section and blue the downstream section. Middle: Shows the corresponding foam quality. Bottom: Schematic of the sand pack to aid the reader in visualizing the foam propagation using the color codes for different sections.

It has been observed in a SAG(Surfactant Alternating Gas) scheme N_2 foam injection for AOS $_{14-16}$ using CT imaging that foam breakthrough occured at ~1.3-1.7 PV (only gas flow rate taken for calculation). However the pressure drop took several PVs to come to steady state[56]. Another case of AOS $_{14-16}$ and N_2 foam injection in Bentheimer sandstone showed foam breakthrough at ~0.76 PV, however a secondary desaturation front developed due to the liquid hold up near outlet caused by capillary end effects, which caused foam to move backward towards inlet. However the foam took 40 PV to reach a steady state value [57].

In our AOS $_{14-16}$ case there might not be a secondary desaturation front developing, if not we should be able to track the pressure growth from the second internal section. The foam reaches the first tap at ~0.5 PV and fills the first section in ~1.09 PV. The foam reaches the second tap only at 1.09 PV and fills the second section at ~1.77 PV. One reason for the delayed propagation might be due to the entrance effect as observed and defined in literature[58] where the foam has been observed to require a length of ~ 6 inches to start getting stronger . This is perhaps why the foam in our system takes 0.5 PV to even reach the first internal section instead of the roughly estimated 0.25 PV(roughly 1st tap is located at 0.25 PV, 2nd tap at 0.5 PV and 3rd tap at 0.75 PV as each section is at a distance of 6 inches. Please note tap is different from section (section is a region enclosed between two taps.). Additionally the foam quality also decreased from 48.6% in section 1 to 46.4% in section 2 and 43% at the outlet of the pack. For AOS$_{14-16}$ foam the foam quality is strongest at 92 % at room temperature as seen in Figure 4.10. Similar to the above experiment gas and liquid flow rates were varied as required for the experimental studies and the steady state pressure drop value was noted to calculate the apparent viscosity of foam.

Two kinds of experiments were performed: one was the foam quality scan (Figure 4.10) and the other shear thinning behavior (Figure 4.12). In foam quality scan the flow rate was fixed for all the surfactants at ~ 21-25 ft/day superficial velocity and gas fraction was varied. In shear thinning behavior, gas fraction was fixed at the transition foam quality and flow rates (superficial velocities) were varied. Foam has two regimes known as the high quality regime and the low quality regime[59,60].The high quality regime is governed by the limiting capillary pressure which causes the bubbles to coalesce[61] and the low quality regime which has finer textured bubbles, is governed by bubble trapping and mobilization mechanisms[59,62]. The quality at which the transition from low to high takes place is called the transition foam quality.

Figure 4.11 is a picture taken to demonstrate the effluent foam for a transition foam quality and foam at high quality regime. The foam at the transition quality has a higher density of finely textured bubbles, whereas foam at the high quality is coarser due to bubble coalescence.

Figure 4.10 shows the quality scan of the surfactants Rhodia A, AOS and their blends and Rhodia B. As mentioned earlier all the surfactant solutions except AOS and the blend A:AOS 1:9 were viscoelastic to some measure i.e. they contained rod like micelles. One can observe that the Rhodia A betaine foam is weak in the foam quality region of 80-90%, whereas all the other surfactants foam are strong at the 80-90% quality. AOS foam has a transition foam quality at ~92% at room temperature which is close to that observed in literature in sandstone [63,64]. In this plot the transition foam quality for Rhodia A is chosen as ~ 60% and the rest of the surfactants ~ 85-90%.
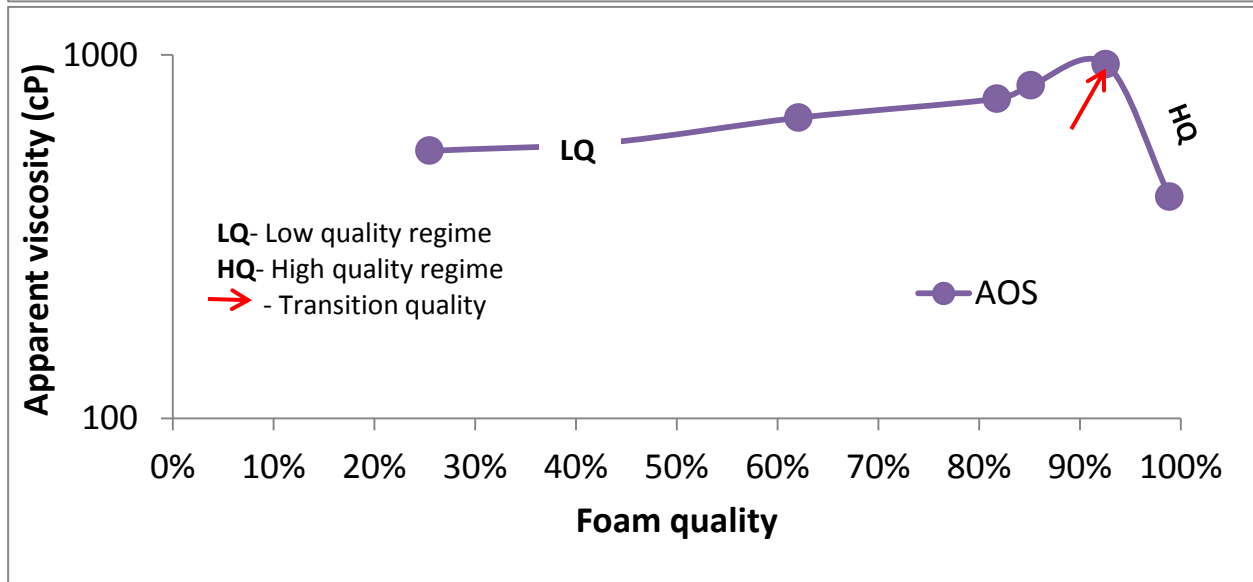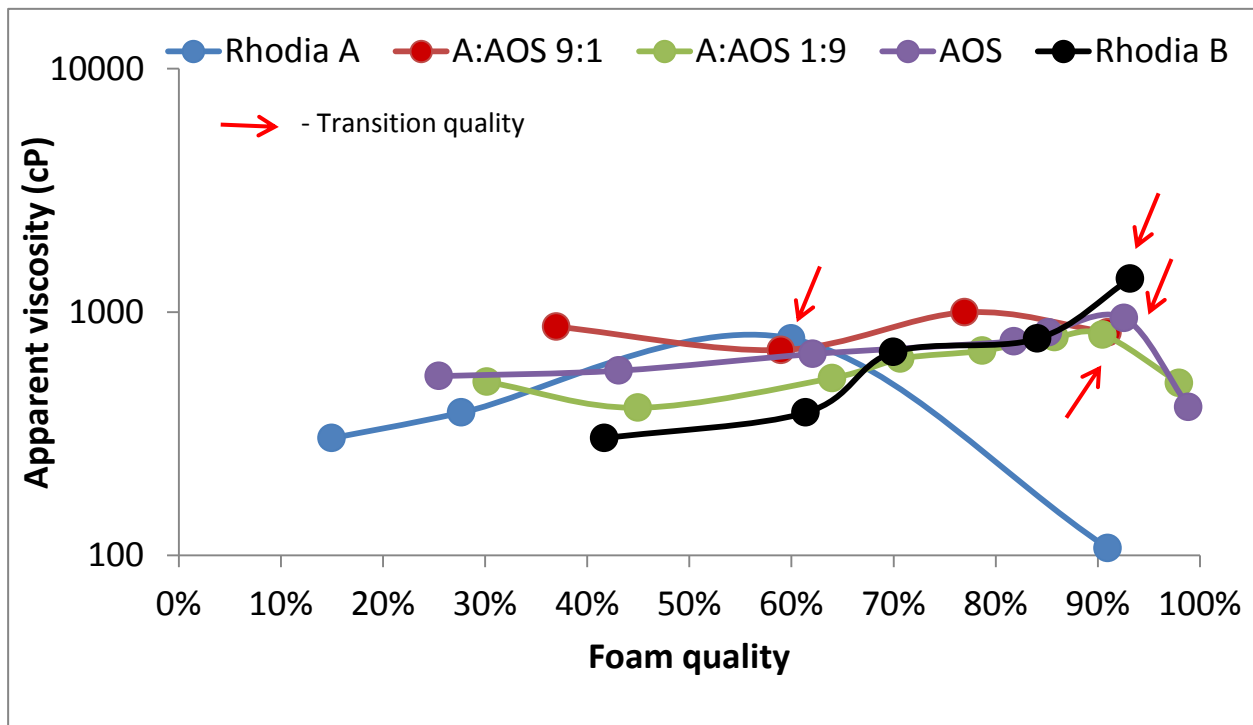
Figure 4.10: (Top) Foam quality scan of Rhodia A, AOS, blends A:AOS 9:1, A:AOS 1:9 and Rhodia B at ~21-25 ft/day. The red arrow mark indicates the foam transition quality. The region to the left of transition quality is low quality regime where the foam is wetter and the region to the right of transition quality the foam is coarser due to the limiting capillary pressure. Rhodia A is observed to have a transition quality at ~ 60% gas fraction whereas the other surfactant foam has a transition quality at ~80-90% gas fraction. (Bottom) An example of AOS foam distinctly showing the high and low quality regimes of foam.

Figure 4.11: Picture of foam at effluent. Left: Transition foam quality(~ 60%) Right: Foam at the high quality regime (~75%-90%). Picture was taken for Rhodia A foam.

The thought behind using a viscoelastic betaine surfactant is that higher elasticity of the thin film might help in improving the foam film stability. The foam film stability is mainly governed by the individual lamella stability in a flowing foam system. Aronson et al. [65] have measured the disjoining pressure of SDS as function of salinity and concentration and have shown that the foam steady state pressure drop is high for those solutions that have the largest repulsive disjoining pressure which in turns offers highest resistance in porous media . Their work also supports the idea of limiting capillary pressure regime which is also the high quality regime in the quality scan studies. It shows that the rupture pressure values of the individual films are on the same order of the limiting capillary pressure in porous media. Foam flow in porous media is a phenomenon that is a combination of disjoining pressure, which is function of the surfactant properties, and imposed capillary pressure which is a function of the petrophysical properties (rock properties). A very good literature review on factors governing foam stability in porous media can be found in literature [21]. It is in the interest of enhanced oil recovery purposes to inject foam at high qualities to have an economic value for the surfactant usage. Here Rhodia A, even though being weakly viscoelastic in the bulk solution, does not perform better than the

AOS surfactant in the high quality regime. The surfactant structure might be a possible limiting cause since all other parameters like concentration, salinity, permeability, flow rate, gas type etc. are fixed.

They key observations are 1. Rhodia A by itself reaches a limiting capillary pressure at lesser gas fraction than AOS, the blended surfactants or Rhodia B. 2. When a small proportion of AOS is added to Rhodia A (A:AOS 9:1) there is significant enhancement in foam strength especially at higher gas fractions. 3. A:AOS 1:9 blend has a foam rheology very similar to AOS. 4. Rhodia B, a zwitterionic surfactant, seems to have very high foam apparent viscosities at high gas fractions. The plausible explanation for the above observations will be discussed in the subsequent paragraphs.

Since these surfactants are proprietary and we don't have the exact structure, it is possible that the lager head group area perhaps owing to the number of methylene groups between the COO^- and N^+ might lead to more gas diffusion in between the monomers on the gas liquid interface as studied in the work of Weers et al. [66]. Their work also shows that there is no intramolecular ion pairing between the positive and negative group on the betaine molecule. AOS has smaller head group area and the sodium counter ions in the liquid lamella help in shielding the electrostatic repulsion between the AOS interfaces creating a stronger film to withstand the higher limiting capillary pressure.

A blend of A:AOS 9:1 which is a very viscoelastic solution, seems to have foam strength quite independent of the quality. One of the reasons might be the synergistic interactions between the anionic sulfonate group and the betaine head group which not only helps to enhance

viscoelasticity in the bulk solution but also perhaps gives enough elasticity in lamellae. Even the single phase flow at about the same velocity gives an apparent viscosity of ~ 850 cP.

Figure 4.8 is plotted in terms of shear rate and apparent viscosity. The plot can also be interpreted as superficial velocities (ft/day) vs apparent viscosity i.e. $1 \text{ s}^{-1} \cong 1.02$ ft/day. The interfacial viscosity was not measured for this surfactant blend but literature shows that SDS in the presence of dodecanol has some interfacial viscosity which prevents the film from draining faster[22].

Rhodia B a sulfobetaine has a longer carbon chain C_{18-22} and one reason for the observed strong foam could be the stronger steric and hydrophobic tail interaction aiding in tighter packing. Also the surfactant is much more viscoelastic than Rhodia A, thereby giving rise to the possibility of having a more elastic interface capable of withstanding higher pressures before film rupture can occur.

Figure 4.12 shows the shear thinning behavior of foam. All surfactants show a good shear thinning behavior which can be fitted by power law model as indicated in the figure. However Rhodia A shows a minimum velocity effect, whereby the foam gets weaker below ~ 10 ft/day, above ~10 ft/day it appears stronger. This effect has been observed and studied in literature[2,67–69]. More data points are required at lower velocities to clearly understand this behavior but this experimental studies were limited by the mass flow controller flow rates. The minimum velocity effect was reproducible even when the flow rates were switched from very high flow rate to low flow rate. Velocity and pressure gradient are related and hence several research work show that

either minimum pressure gradient or minimum velocity is required for the mobilization of the lamellae[67–73]. This observation points out that Rhodia A may not be a good foamer at low

Figure 4.12: Shear thinning behavior of foam. All surfactant foam have negative shear thinning slopes between ~ 0.6-0.9. The orange circled points indicate that Rhodia A betaine exhibit some minimum velocity phenomena where below ~ 10ft/day the foam gets weaker. This observation is reproducible. The foam quality was fixed at Rhodia A = ~60%, AOS= ~88%, A:AOS 9:1 = ~ 80% , A:AOS 1:9= ~ 85%, Rhodia B= ~ ~ 85%.

velocities like ~ 1ft/day which is characteristic of reservoir flow rates. Whereas all other surfactants can foam below 10 ft/day superficial velocity. With all these observations about Rhodia A betaine not being a suitable candidate for EOR applications one reason is the structure of the surfactant that plays an important role in foam generation and propogation in porous media.

4.3.3 Effect of crude oil on foam for Rhodia A, Rhodia B, AOS and A-AOS blends in sandpack

Foam injection was first proposed by Boud et al [74]. AOS_{14-16} surfactant was studied at various concentrations in the presence of waterflood residual oil(model oil) and foam flooding caused 5-12% incremental oil recovery of the OOIP (at 3 PV injection) and is definitely an effective agent for mobility control[75]. Experimental works that are available in literature show oil is detrimental to foam [76–82]mainly due to the stability of pseudoemulsion film. However some of the work suggest that the proper choice of surfactant can be beneficial to foam propagation in the presence of crude oil[2,3,19,20,83–85]. The stability of pseudoemulsion film can depend on a number of factors like the electrolyte environment, type and concentration of the surfactant, type of oil. Here in this work we use viscoelastic surfactants with the hypothesis that they may give rise to an viscoelastic interface[86–88] which can better withstand the effect of oil on the pseudoemulsion film. AOS_{14-16} which is a well-known foamer and has been studied previously is also tested with our crude oil systems and a comparison between the surfactants is made and discussed in the following section.

The experimental protocol to saturate a sand pack with crude oil is discussed in section 4.3.1. Figure 4.13 gives the pressure versus the PVs of crude oil injected. It can be observed that a piston- like displacement takes place.

Figure 4.13: Typical oil flood (drainage experiment). Initial water = 83 cc, Connate water after oil flood = 8.4cc, Oil content = 74.6 cc, Oil saturation = 89.8 %, Connate water= 10.2 %
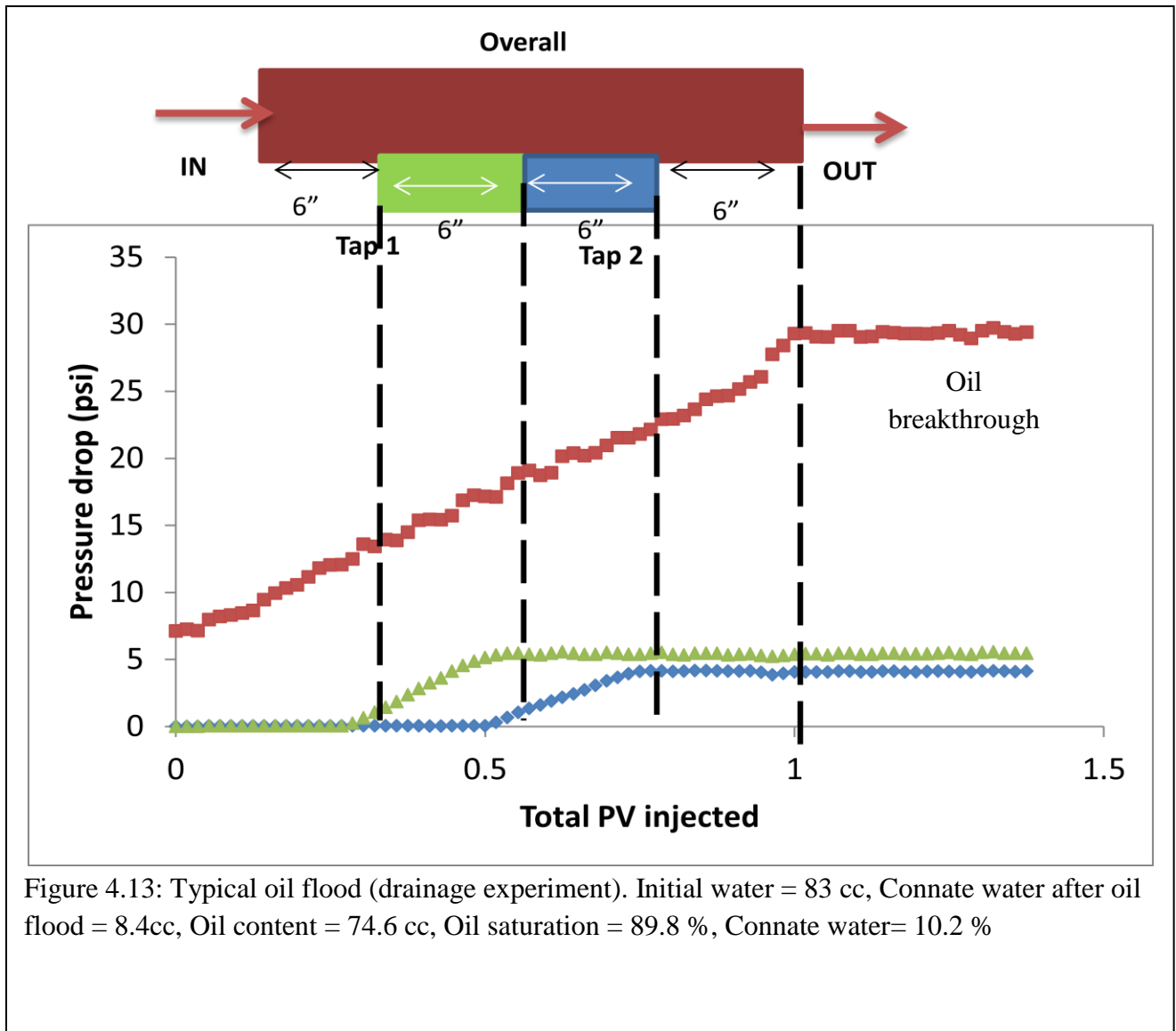
Rhodia A-For Rhodia A surfactant alone, after the drainage experiment, the oil was

removed using 1 PV surfactant solution instead of water (waterflood) as was done for all the

other experiments. This was the first experiment to be done and the goal was to get as much oil

out as possible to assess foam stability in presence of residual oil. The amount of remaining oil

was ~ 15.5 %. There could be some error in the estimation of the remaining oil since an emulsion

was observed in the effluent. Given the complete dark color of the crude oil and not enough

separation in the time observed (~ 1 week), the oil content inside the sand pack could be

somewhere between ~15.5-26%. The upper number 26% is more a rough estimate on the volumes that might be collected, but it was hard to read the volume.

Figure 4.14 is the foam pressure drop behavior during the surfactant flood to displace oil. We see that the foam pressure drop is low because the foam is destabilised by the oil. In the effluent some oil droplets were observed (nothing to be measured). However, when foam bubbles came out of the effluent it would break soon. The amount of oil produced was not measured for any of the experiments since initially it was planned only to study the foam stability. However, even in the case of Rhodia A some oil droplets were found and this may be due to the gas injection. After close to 11 PV injection there was no improvement in the foam strength. The apparent viscosity of the foam which was calculated using the absolute permeability obtained after the cleaning procedure (before oil injection), showed foam to have a strength of ~ 5cP in the internal sections. The overall apparent viscosity ~ 20cP may be due to the end effects or due to the transducer's inaccuracy in reading very low values.We do notice from the pressure drop curve that foam has indeed propagated from the inlet to the outlet and there seems no backward foam flow. Figure 4.15 shows results of foam injection for an additional ~ 10PV. The foam does not recover from the effect of oil. The experiment ran for a total of ~ 20PV, and Rhodia A betaine foam remained weak. Note that there was no back pressure used in this experiment. But because the pressure drops were very low, there was negligible gas compressibility. We may argue that the betaine foam was weak to begin with at 80% gas fraction in the absence of oil and hence it was not going to perform in the presence of oil. Since it was not tried at a lower quality to see if the foam recovers its strength in this experiement, it was decided to try that in another experiment with lauryl betaine foam which will

be discussed later in this chapter.

Figure 4.14: Rhodia A foam performance at ~80% gas fraction, ~40 ft/day superficial velocity. The remaining oil was ~15.5-26% (Read text for information)
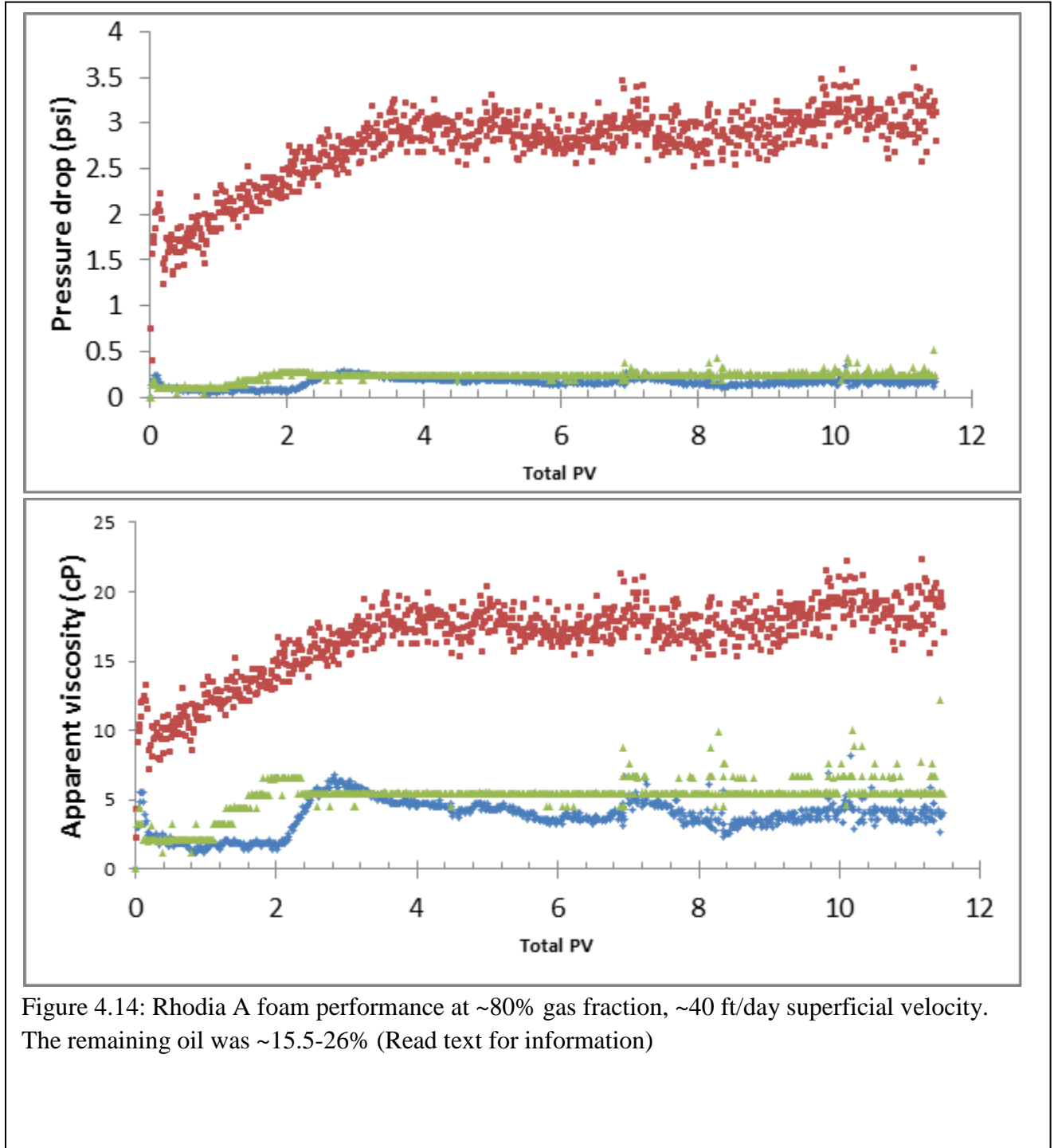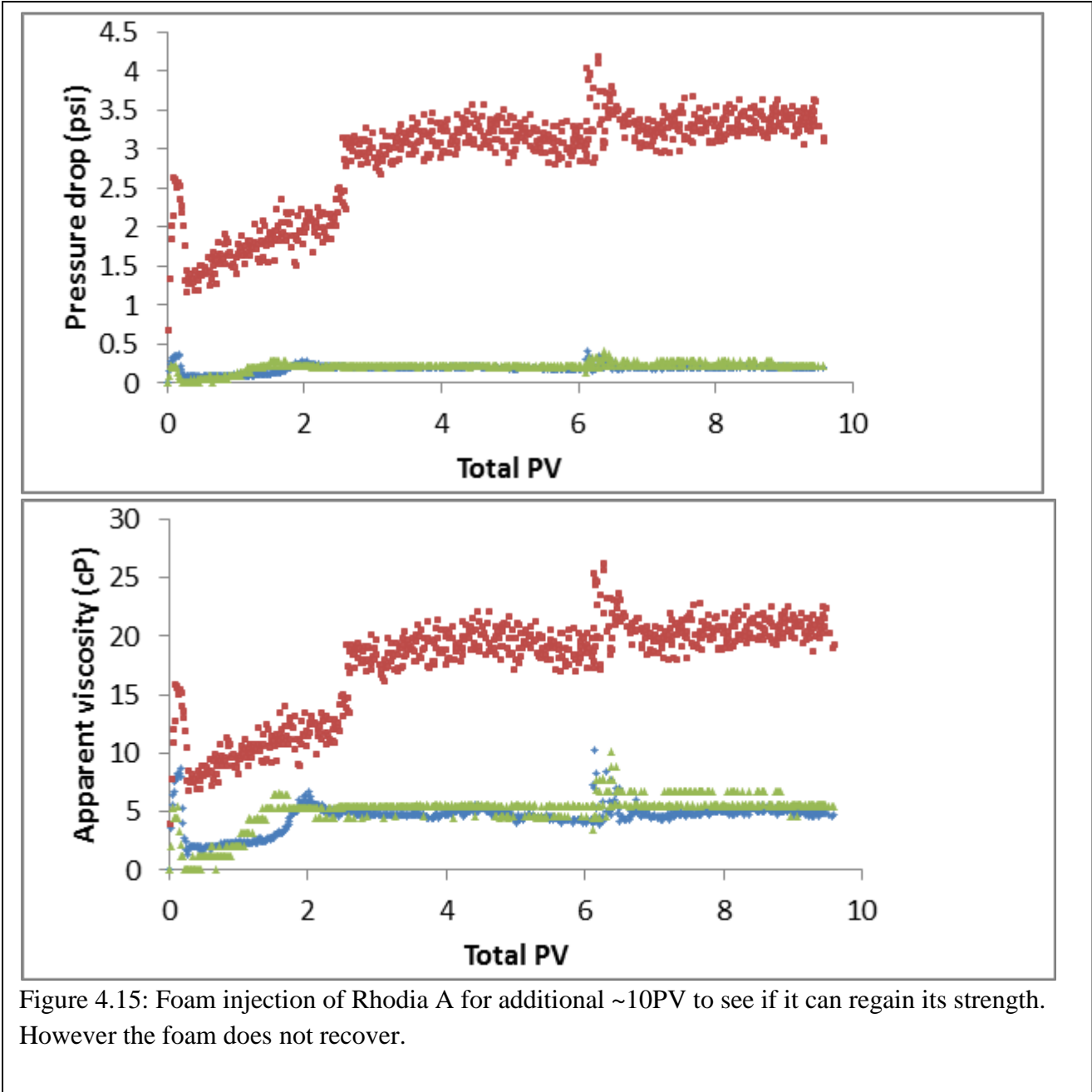
Figure 4.15: Foam injection of Rhodia A for additional ~10PV to see if it can regain its strength. However the foam does not recover.

A:AOS 9:1- Foam pressure history for A:AOS 9:1 is shown in Figure 4.16. We see that foam reaches the first internal section after a little over 5PV injected, and from then on it gets stronger. It takes an additional 10 PV to reach the second internal section and then the foam gets stronger in the downstream section. There is a steady rise in the overall pressure drop as well

from ~ 5th PV to 35th PV. At steady state the apparent viscosity for both the internal taps and overall sandpack have the same value. The pressure history has been more like a piston like displacement. There are two possibilities for the above mentioned observation – a) since the Pemex synthetic crude oil and viscoelastic A:AOS 9:1 contact each other, they might have formed an emulsion giving rise to a piston like displacement, b) another possibility is that the surfactant foam must be indeed a strong foamer owing to an elastic lamellae. It seems like strong foam has been generated in about 5 PV, however the entire propogation of strong foam has taken 30 PV (5 PV- 35 PV)

A:AOS 1:9 -Figure 4.17 shows the pressure history of *A:AOS 1:9* foam in the presence of 56% remaining oil and at 30 f/day , approximately 90% gas fraction. It takes about 24 PV for strong foam to start generating as can be observed from the pressure drop rise in the internal section 1. At close to 29th PV, the pressure rise can be observed in the second internal section. The overall pressure drop reaches a steady state value at ~ 39th PV. The foam apparent viscosity is the same as the foam at these conditions of injection in the absence of oil (since this is actually a 3 phase flow of gas, oil and aqueous phase, there is a relative permeability for the phases and using an absolute permeability for foam calculations might not be accurate. However since we are relatively comparing all surfactant formulations at more or less same water flood conditions it can qualitatively provide reasonable information). Following this the flow velocity was decreased to ~ 4ft/day. Foam had only one tenth of its viscosity as would be the case in the absence of oil.
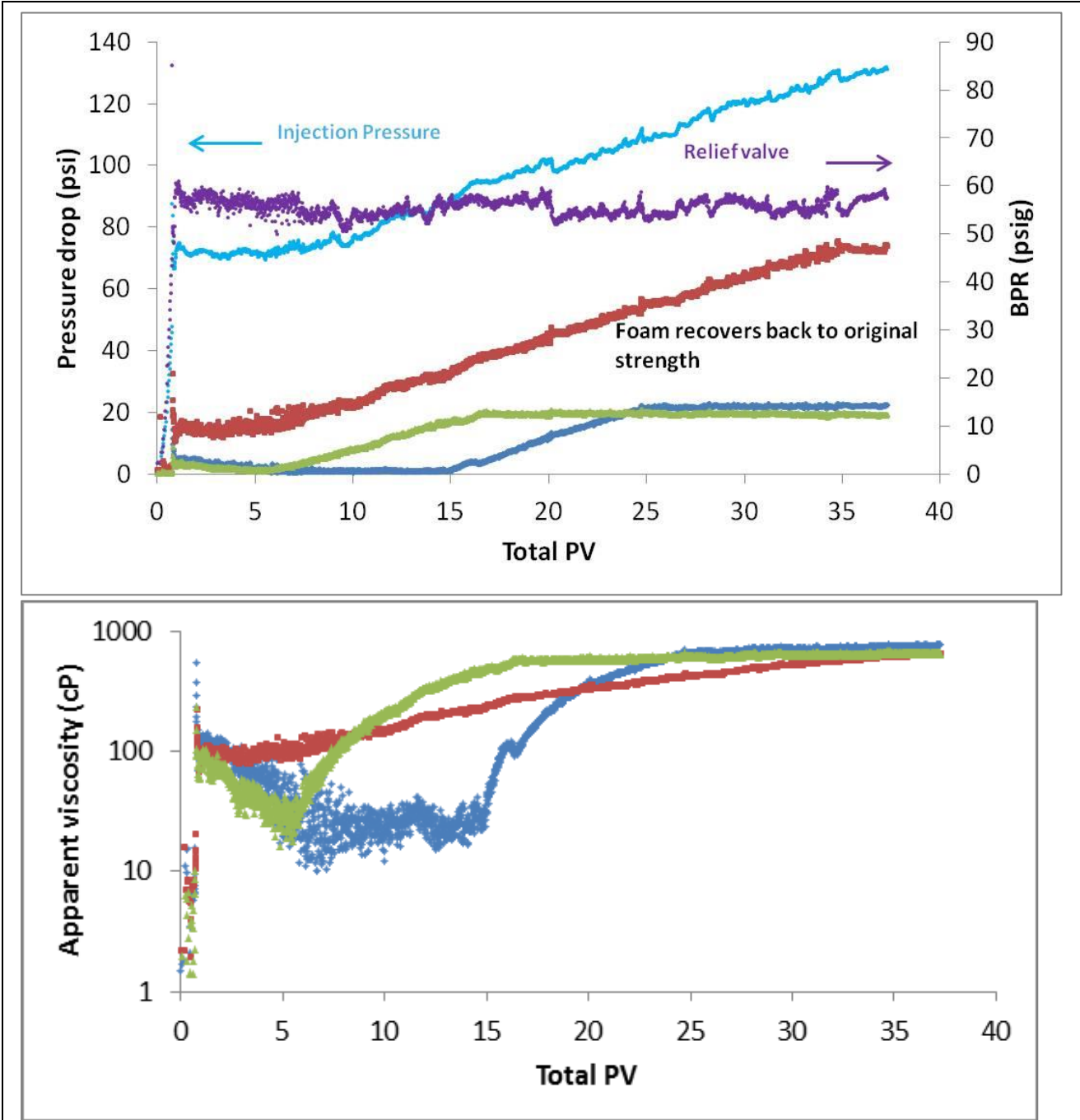
Figure 4.16: A:AOS 9:1 foam performance in the presence of 63% remaining oil, ~30ft/day at ~80-85% gas fraction.
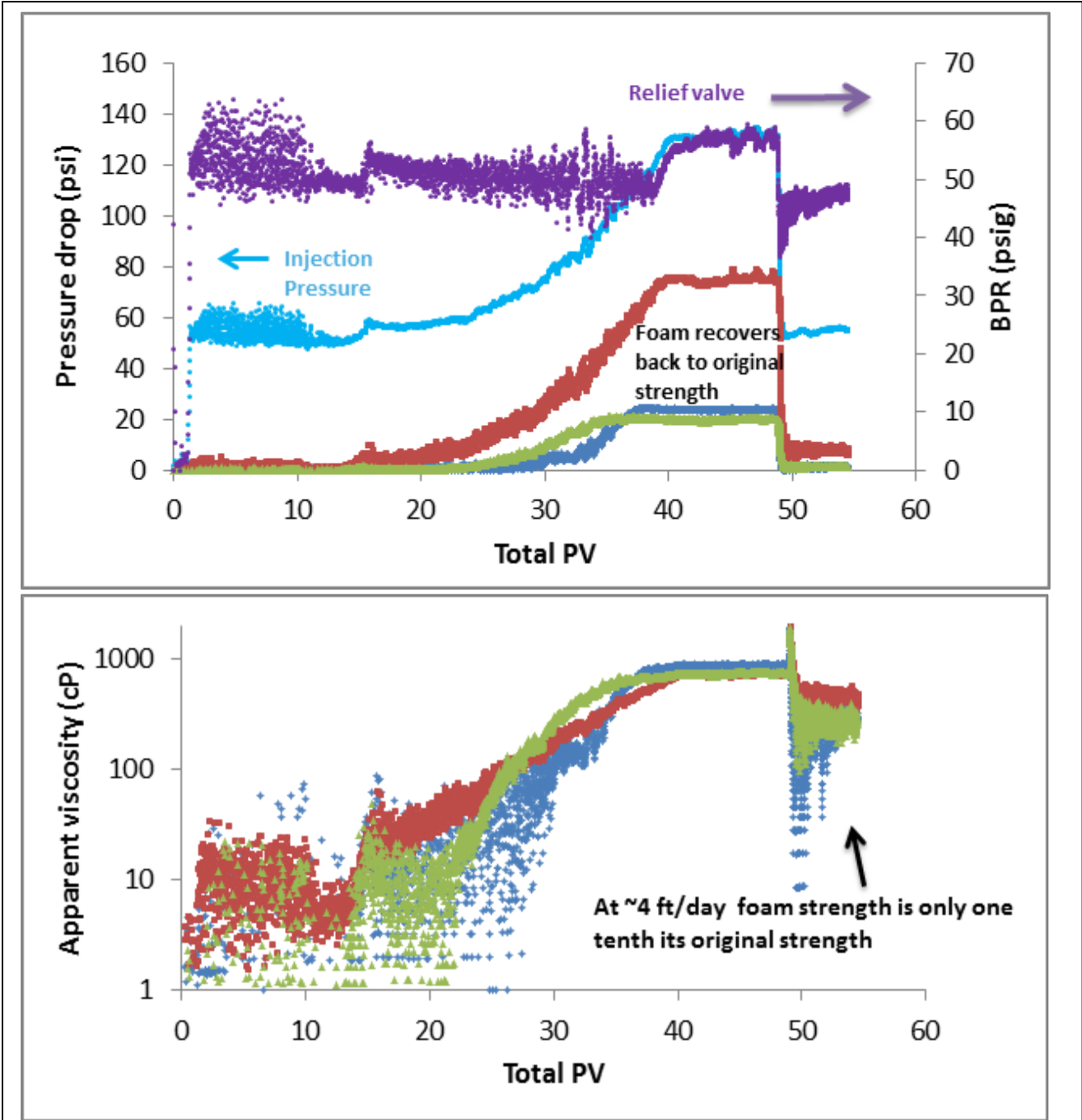
Figure 4.17: A:AOS 1:9 foam performance in the presence of 56% remaining oil, ~30ft/day at ~90% gas fraction.

AOS- Figure 4.18 shows the pressure drop versus PV of injected foam for AOS surfactant solution. At about ~13th PV foam starts getting stronger as seen in the overall pressure drop. By 15th PV strong foam is found to enter internal section 1.Between the 16th -17th PV foam

111

enters the second section. By 25th PV the foam reaches a steady state. Even though it took about 13 PV for foam to get stronger but in about the subsequent 12 PVs foam reaches steady state. This is based on the assessment of pressure drop from the overall section. In fact once strong foam is generated and proceeds to the first internal section, in about a PV it propogates to the second internal section as seen by the pressure rise in the 17th PV. AOS foam does take a longer time than a viscoelastic blend i.e. A:AOS 9:1 to generate strong foam. However when strong foam is generated it propogates fairly sooner than the other surfactants. We see a lot of oscillations in the pressure value. Once the experiment was over and the sand pack was dismantled it was found the swagelok back ferrule near the inlet had moved slightly towards the edge of the sand pack. This may have caused something with the seal, but not necessarily a leak, as there was no foam bubbles at the sand pack inlet. But even with this issue, AOS_{14-16} was the best foamer compared to other surfactants in the presence of oil.

Rhodia B- Figure 4.19 is Rhodia B foam performance in presence of crude oil. It takes 37PV for the overall pressure drop to rise. The internal sections show that the downstream section has stronger foam in the pack than the upstream. Suddenly in the 43rd PV foam gets weak in section 1. The section 2 foam continues to be strong till the end of the experiment.

Figure 4.20 gives a qualitative idea of how the sand appeared at the end of the foam flood experiment. AOS which had the best overall foam performance seems to have left some amount of oil behind. Rhodia A, which had the worst performance had the poorest sweep in the sandpack. The sultaine Rhodia B had clean swept the sand pack even though it had taken maximum number of PVs to generate strong foam . Table 4.4 summarizes all the foam crude oil

results and shows that AOS had the best performance in terms of foam strength and the PVs

taken for the foam to reach steady state.
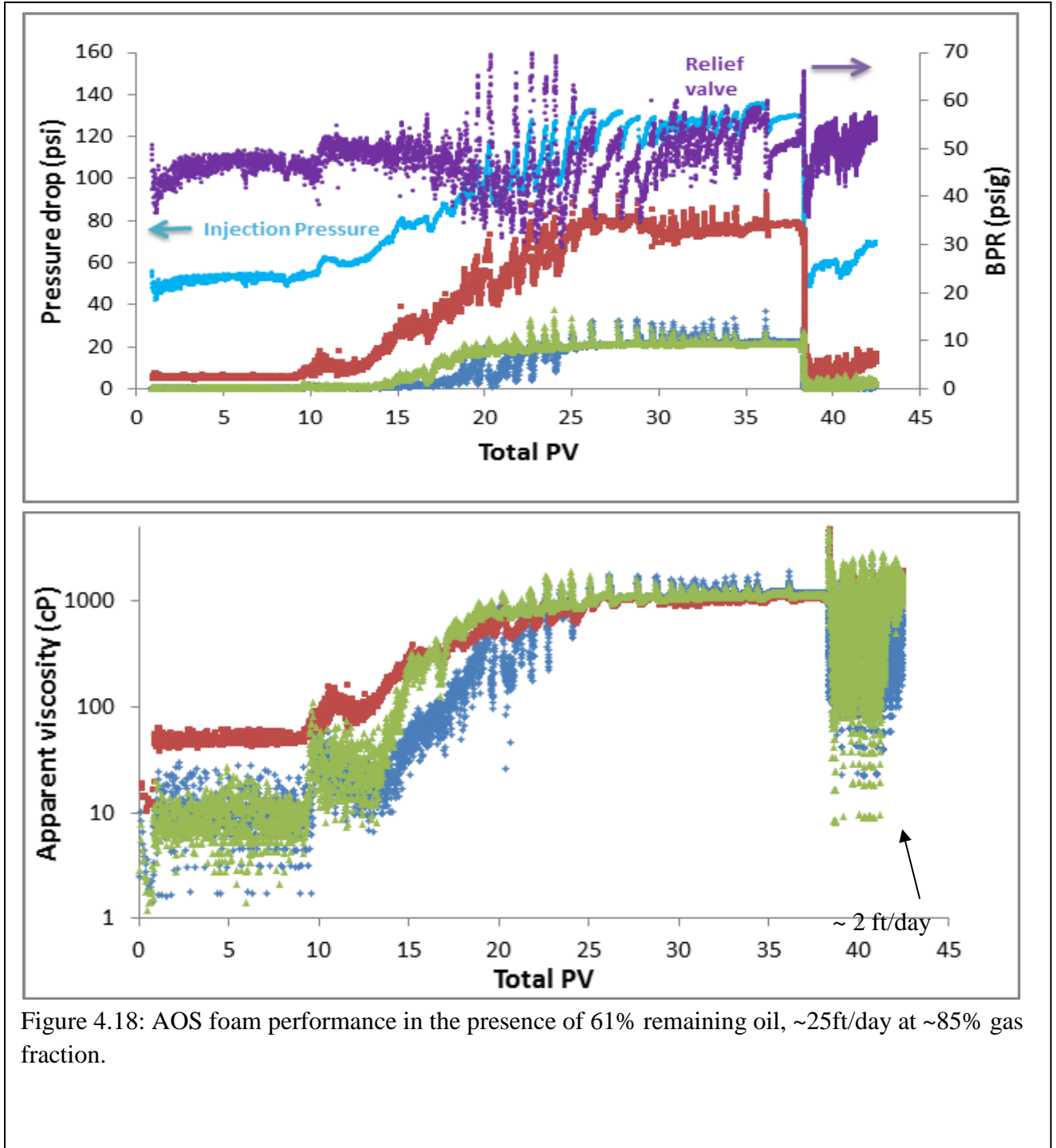
Figure 4.18: AOS foam performance in the presence of 61% remaining oil, ~25ft/day at ~85% gas fraction.
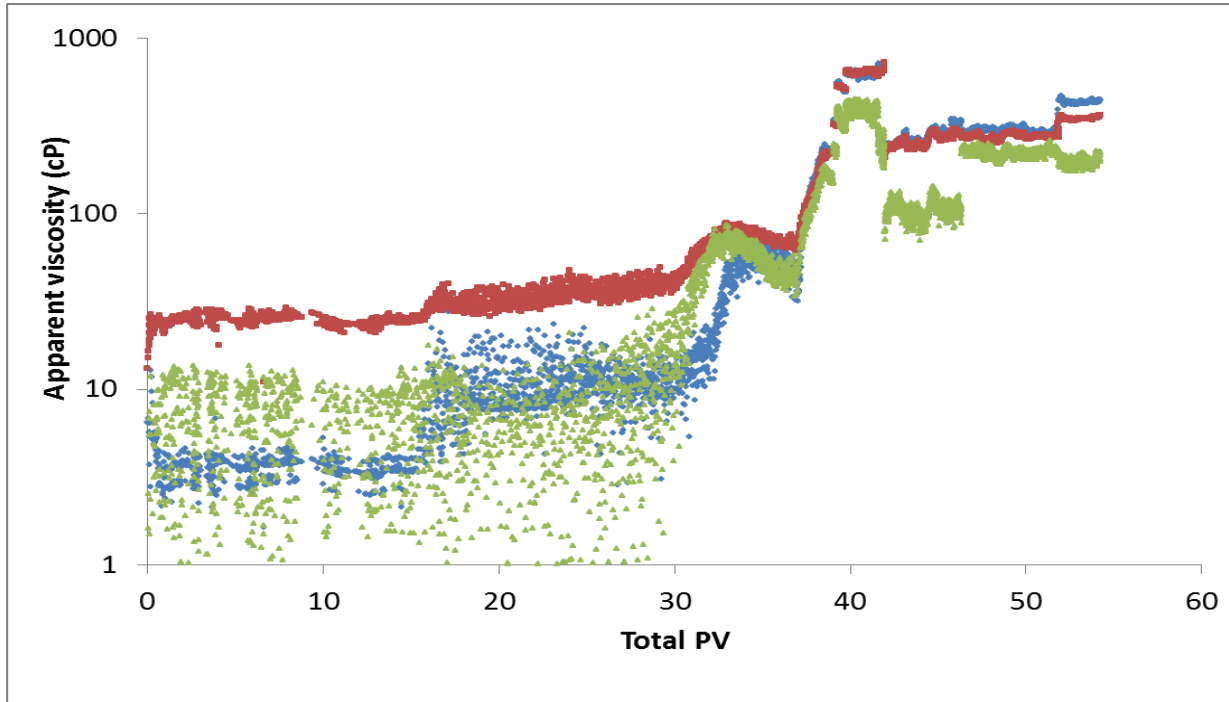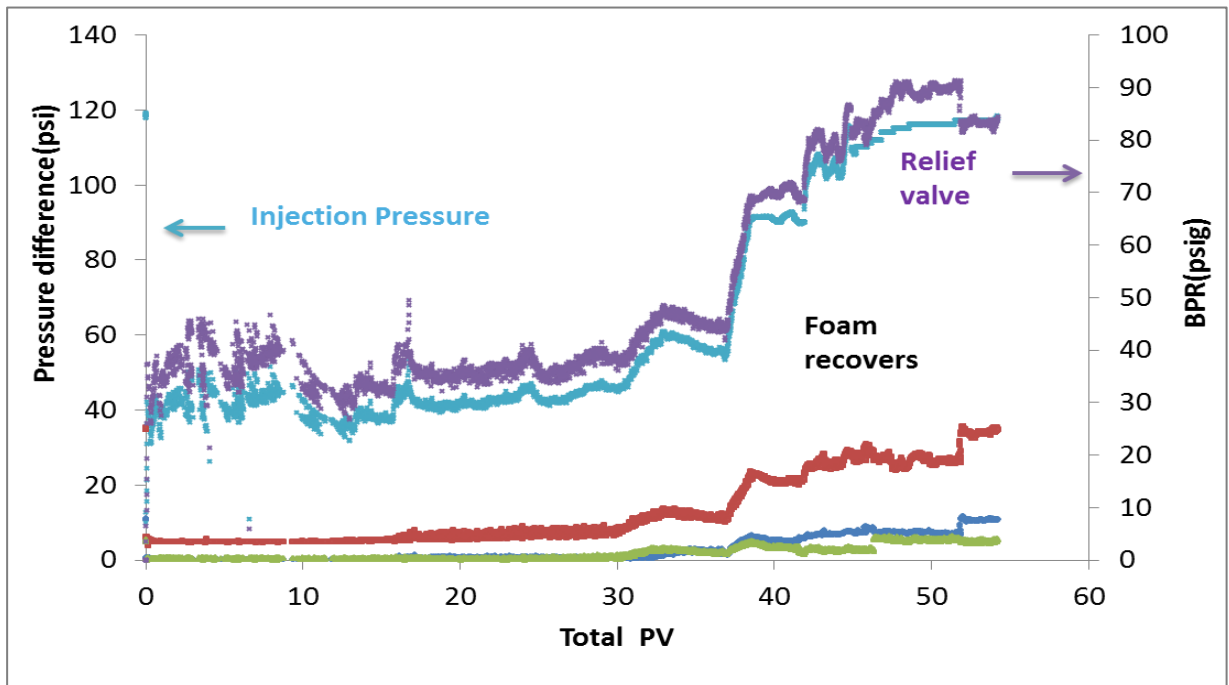
Figure 4.19: Rhodia B foam performance in the presence of 40% remaining oil, ~30-40 ft/day at ~85-90% gas fraction.

Sand after foam displaces oil

Rhodia A (Betaine)

A:AOS(9:1)

A:AOS (1:9)

AOS

Rhodia B (Sultaine)

Figure 4.20: The picture at top is of sand for Rhodia A after a foam flood with no oil present. Bottom picture qualitatively demonstrates the appearance of sand after the foam flood displacing crude oil. Rhodia A seems to be poorly swept compared to all surfactant solutions. Rhodia B foam has taken many PVs but the sand appeared to be entirely clean. AOS foam which had the best overall performance seemed to have left behind some oil. Both the blends had not swept the sand pack clean, with A:AOS 1:9 being the better among the two..

Surfactant	PV to generate strong	PVs to reach steady state *after strong foam generation*	Apparent viscosity cP	Superficial velocity (ft/day) at foam quality%
A	-	-	~5	~40 ft/day at 80%
A:AOS 9:1	8	27	~649	~30 ft/day at ~80%
A:AOS 1:9	22	16	~740	~30 ft/day at ~90%
AOS	13	12	~1000	~25 ft/day at ~85%
B	37	~10(foam got weaker near inlet section)	~600	~30-40 ft/day at 85-90%

Table 4.4: Summary of the foam experiments displacing crude oil at waterflood oil from a   ~ 100 Darcy sand pack.

4.3.4 Phase behavior of Rhodia A, Rhodia B, AOS and A-AOS blends

Winsor developed the well-known phase behavior interpretation to predict the intermolecular attraction between two solvent phases when they are mixed[89]. According to Winsor, Type I phase is obtained when the amphiphilic molecule is preferentially soluble in the water phase. Type II is obtained when the amphiphilic molecule is preferentially soluble in the oleic phase and Type III when the amphiphilic rich phase co exists with the excess oil and excess water phase. Classical phase behavior transition from Type I → Type III → Type II is observed when parameters like salinity, temperature, hydrocarbon chain length, addition of co-solvent etc. are varied. A lot of work can be found in literature and just a few examples are referenced[90–93].

Phase behavior studies were done to understand if the surfactant had partitioned into the oleic phase, which might cause foam to take several PVs to become strong. However, all the surfactants are injected well above the CMC to compensate for these losses. The oil scan was

performed following some studies in literature[94–97]. On examining the phase behavior of the surfactants as an oil scan with varying octane and toluene ratio (two oleic phases used) it was found that all surfactants exhibited Winsor Type I phase behavior where the surfactant actually preferred the aqueous phase. Toluene is known to have an Equivalent alkane carbon number (EACN) of 1. It was anticipated that with toluene the surfactants would exhibit Type II behavior, but the surfactant systems studied are extremely hydrophilic. Figure 4.21 - Figure 4.24 show the oil scans. All the surfactant formed viscous macro emulsions with increasing toluene content. AOS surfactant formed viscous emulsions at all oleic ratios. Some surfactants like Rhodia B seemed to have swept the sand pack clean. One thought was perhaps low IFT was a contributing factor. However it seems like none of the surfactants had low tension, not even the surfactant solutions containing wormlike micelles which actually have a very low cmc.

Octane(ml)										
1	0.9	0.8	0.7	0.6	0.5	0.4	0.3	0.2	0.1	0
Toluene (ml)										
0	0.1	0.2	0.3	0.4	0.5	0.6	0.7	0.8	0.9	1

Figure 4.21: Oil scan for Rhodia A (0.5 wt%). Brine- Sea water, Temperature – Room temperature. Winsor Type I phase behavior is observed.

Octane(ml)										
1	0.9	0.8	0.7	0.6	0.5	0.4	0.3	0.2	0.1	0
Toluene (ml)										
0	0.1	0.2	0.3	0.4	0.5	0.6	0.7	0.8	0.9	1

Figure 4.22: Oil scan for A:AOS 9:1 (0.5 wt%). Brine- Sea water, Temperature – Room temperature. Winsor Type I phase behavior is observed.

Octane(ml)										
1	0.9	0.8	0.7	0.6	0.5	0.4	0.3	0.2	0.1	0
Toluene (ml)										
0	0.1	0.2	0.3	0.4	0.5	0.6	0.7	0.8	0.9	1

Figure 4.23: Oil scan for AOS (0.5 wt%). Brine- Sea water, Temperature – Room temperature. Winsor Type I phase behavior is observed.

Octane(ml)										
1	0.9	0.8	0.7	0.6	0.5	0.4	0.3	0.2	0.1	0
Toluene (ml)										
0	0.1	0.2	0.3	0.4	0.5	0.6	0.7	0.8	0.9	1

Figure 4.24: Oil scan for Rhodia B (0.5 wt%). Brine- Sea water, Temperature – Room temperature. Winsor Type I phase behavior is observed.

4.4 Foam rheology in Bentheimer cores for Lauryl Betaine and AOS $_{14\text{-}16}$ blends, Lauryl Sultaine and AOS $_{14\text{-}16}$ blends

4.4.1 Foam Rheology

Figure 4.25 is the quality scan of LB and AOS blends. The low and high quality regimes are marked and also an arrow mark indicates where the transition is likely taking place. One of the observations from the plot is that AOS foam has the highest foam strength compared to the other surfactant foams. It has been pointed out in Table 4.3 that the cores used in the case of LB:AOS 7:3 and 1:9 had lower permeabilities than the cores used in the case of pure AOS and pure LB. Due to this permeability difference it is rather hard to compare the foam strength on a same scale and hence they are compared at a fixed shear rate rather than fixed velocity. The procedure to do that can be found in literature[2]. Even at fixed shear rate the comparison shows

the blends to be significantly lower in foam strength than AOS, but this may be mainly due to permeability differences as seen in some experiments and simulations[64,98]. Nevertheless LB and AOS have been done on cores having similar permeabilities and it shows that the apparent viscosity of LB is significantly lower in magnitude than AOS. Another key observation is that the foam transition qualities for the blends and pure AOS are at ~85-90%, whereas pure LB has foam transition quality at ~ 60%. The question that can be raised with this observation is the LB:AOS 7:3 blend which has a richer mole fraction of LB , exhibited a foam rheology very similar to pure AOS rather than somewhere in between pure LB and pure AOS. One hypothesis might be that there are some synergistic interactions between LB and AOS where the interface tends to prefer a higher amount of AOS from the mixture thereby causing the foam to behave similar to pure AOS.
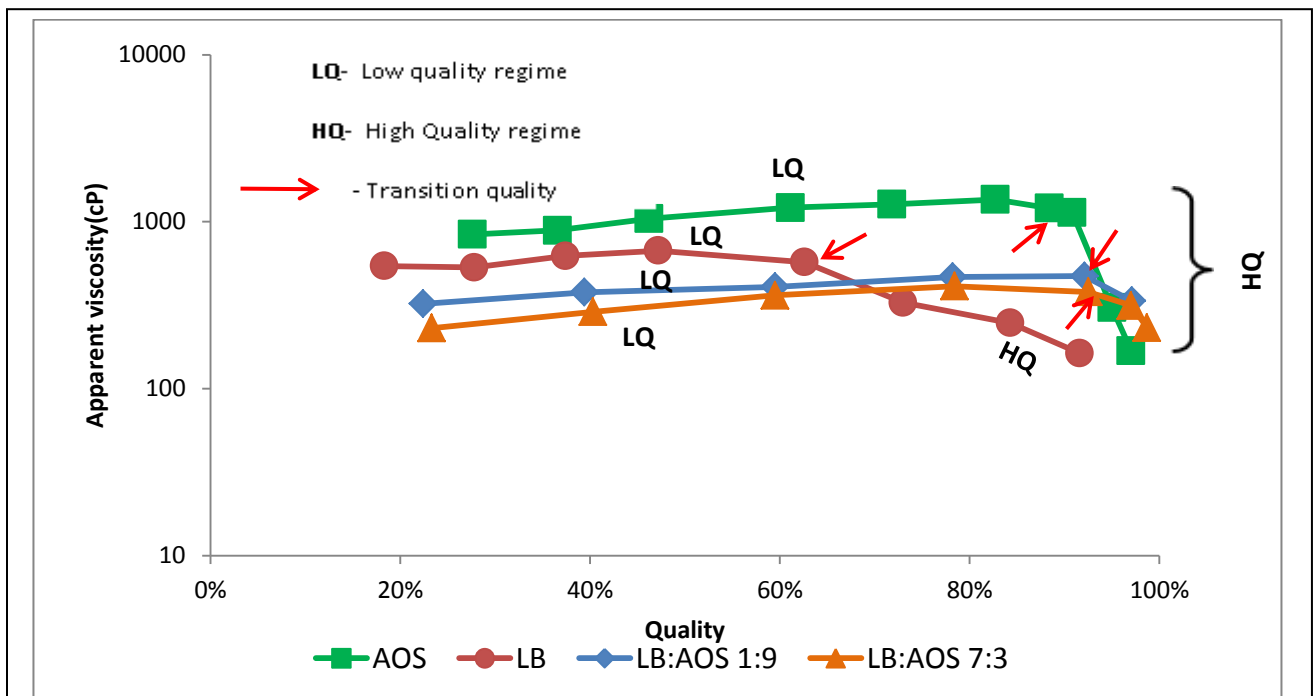
Figure 4.25: Foam quality scan for LB, AOS and their blends at a fixed shear rate of 28.3 s^{-1} and temperature of 45 °C. The plot shows the high quality and low quality regimes.

The LB:AOS 1:9 blend also showed a foam rheology close to pure AOS , part of the reason might be that it is richer in mole fraction of AOS in bulk solution. An analysis done using the regular solution theory is discussed in the next chapter to test the hypothesis. From Figure 4.25 another observation is that the AOS_{14-16} by itself is a strong foamer at the studied test conditions and perhaps the betaine did not enhance the foam strength to any better value, contrary to that which has been observed with AOS_{16-18} and cocoamido propyl betaine [20]. Perhaps the poorly foaming betaine got boosted by the presence of AOS.

Figure 4.26 shows the foam quality scan of the Lauryl Sultaine (LS) and AOS. In these set of experiments all the cores had similar permeabilities. Hence it can be clearly observed that there is no significant effect of the zwitterionic sultaine boosting the foam strength to any better value than pure AOS itself. The foam transition quality for pure LS is ~ 20% and for pure AOS and their blends it is ~85-90% similar to that observed with LB-AOS blends.

4.4.2 Effect of crude oil on shear thinning foam

Shear thinning behavior of foam was studied in the case of LB and AOS blends as well as LS and AOS blends. The flow rates were varied along the transition quality. Figure 4.27 and Figure 4.28 show the shear thinning behavior both in the absence and presence of crude oil. The experimental protocol followed in saturating crude oil is described in section 4.2.2. The blue diamonds in the figure show the shear thinning behavior of foam in the absence of oil. For the experiments in the presence of crude oil, Table 4.5 summarises oil saturations in the core before and after foam flood . Oil was reduced to waterflood residual oil saturation, which was followed by ~ 1-2 PV surfactant injection after which foam was injected. All the cores had a oil saturation of ~ 30-35% before foam injection, except in the case of the cores used for LS and LS:AOS 8:2 surfactant systems, which had a higher oil saturation in 44-47% range.

121

Figure 4.26: Foam quality scan for LS, AOS and their blends at a fixed interstitial velocity of ~20 ft/day and temperature 45 °C. The plot shows the high quality and low quality regimes.
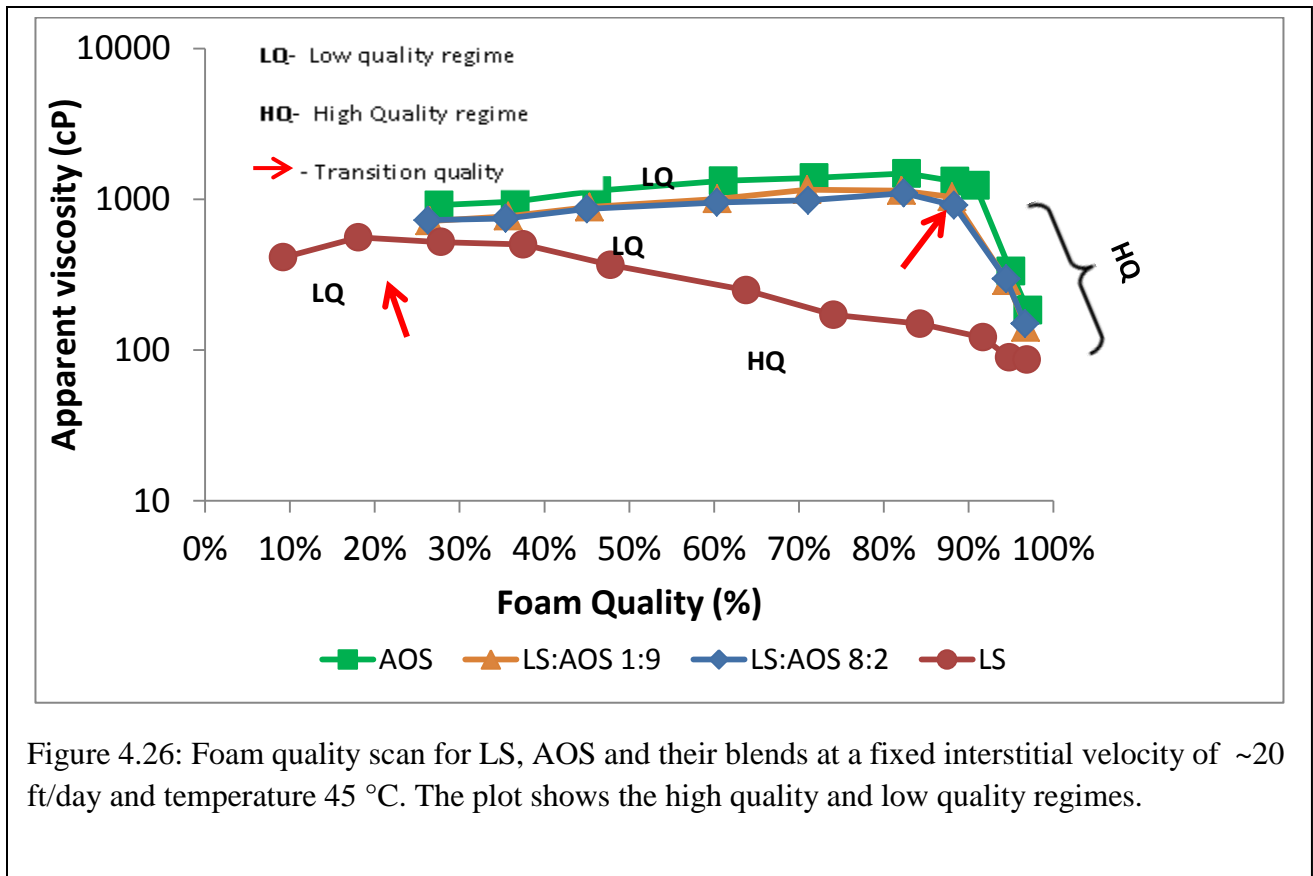
When foam was injected to displace crude oil the flow rate was varied starting from the lowest interstitial velocity ~ 1-5 ft/day. However only in the case of LB:AOS 1:9 surfactant blend foam was injected at ~ 34 ft/day interstitial velocity and then injected at ~ 1 ft/day interstitial velocity due to experimental time limitations. During foam injection in all the experiments oil was produced. We anticipated oil to be immovable so the foam stability could be studied, however since the oil was ~ 60 cP oil at 45° C and foam apparent viscosity was ~ 100cP, there was favorable mobility control and oil was displaced. In Figure 4.27 for example taking the case of AOS foam, the following sequence was followed in terms of velocities for foam injection 1.63 ft/day→ 5.68 ft/day→ 9.42 ft/day→13.26ft/day→ 20.23ft/day→ 0.8 ft/day→ 1.63 ft/day→ 5.6 ft/day→ 13.26 ft/day. This sequence was followed to ensure that true steady state was reached, in the sense that no more oil was produced and just foam steady state in the

presence of minimal oil was studied. One can observe from the plots in Figure 4.27 and Figure 4.28 that foam is initially very weak due to the presence of ~ 30% oil saturation. But as oil gets displaced foam starts gaining strength. This shows that foam is a good mobility control agent and can be injected for an enhanced oil recovery process.

Surfacant	Initial oil saturation (Soi)	Oil saturation after ~1-2 PV surfactant flood	Oil left after foam flood
LB	~90%	~30%	~24%
LB:AOS 7:3	~89%	~28%	~20%
LB:AOS 1:9	~89%	~30%	~<1%
AOS $_{14-16}$	~89%	34.9%	<1%
LS	91.8%	~47±1%	~ 5%
LS:AOS 8:2	~91%	~44%	~ not measured (effluent spilt)
LS:AOS 1:9	~91.1	34.7%	< 0.5%

Table 4.5: Oil saturations in the different cores used for the above mentioned formulations before and after foam flood.

Figure 4.27 shows Lauryl Betaine (LB) and AOS blends. LB was the first experiment to be conducted and hence was started at room temperature(20° C). It can be noticed that the LB foam gets weak when the velocity is below 12 ft/day interstitial velocity, in the absence of oil. Just like Rhodia A betaine, LB also demonstrates a minimum velocity effect which is a reproduceable phenomena. Secondly LB foam is very weak in the presence of oil. This has been observed in literature as well [2,19]. The shear thinning slope of the foams of AOS and LB:AOS 1:9

are very similar both in the absence of oil and also in the presence of mobile crude oil. It seems like the blend LB:AOS 1:9 has a foam rheology very close to AOS even in the presence of oil. The reader should note that the magnitude of foam apparent viscosities for LB:AOS blends should not be compared due to different permeabilities of the cores(Table 4.3). The LB:AOS 7:3 foam seems to get very strong with continuous foam injection.

Since the velocities were varied, it is hard to compare the effect of oil on each surfactant. One way to look at it is AOS, LB:AOS 7:3 both foam with an apparent viscosity of ~ 100 cP at ~ 4 ft/day interstitial velocities in the presence of 28-35% residual oil. Right now nothing can be commented on LB:AOS 1:9 since it was started a higher velocity at residual oil. One conclusion that can be drawn is AOS itself is a good foamer in the presence of residual oil that a blend may not be needed.

Observing Figure 4.28 sultaine may not be of value in the interests of EOR since the foam is conducted at ~ 30% gas fraction. The blend S:AOS 8:2 has an order of magnitude lesser foam apparent viscosity in the presence of oil compared to its own strength in the absence of oil. Both AOS and LS:AOS 1:9 have a foam apparent viscosity of ~ 100 cP at ~ 1 ft/day, in the presence of ~35- 44% residual oil saturation. Again AOS by itself had managed to bring the residual oil saturation to <1 % ,which implies it is a good foamer by itself. Addition of a zwitterionic surfactant did not function as a booster.

Additionally the phase behavior was conducted for all the studied surfactant solutions and all exhibited a Winsor Type I system with the Stat crude oil.
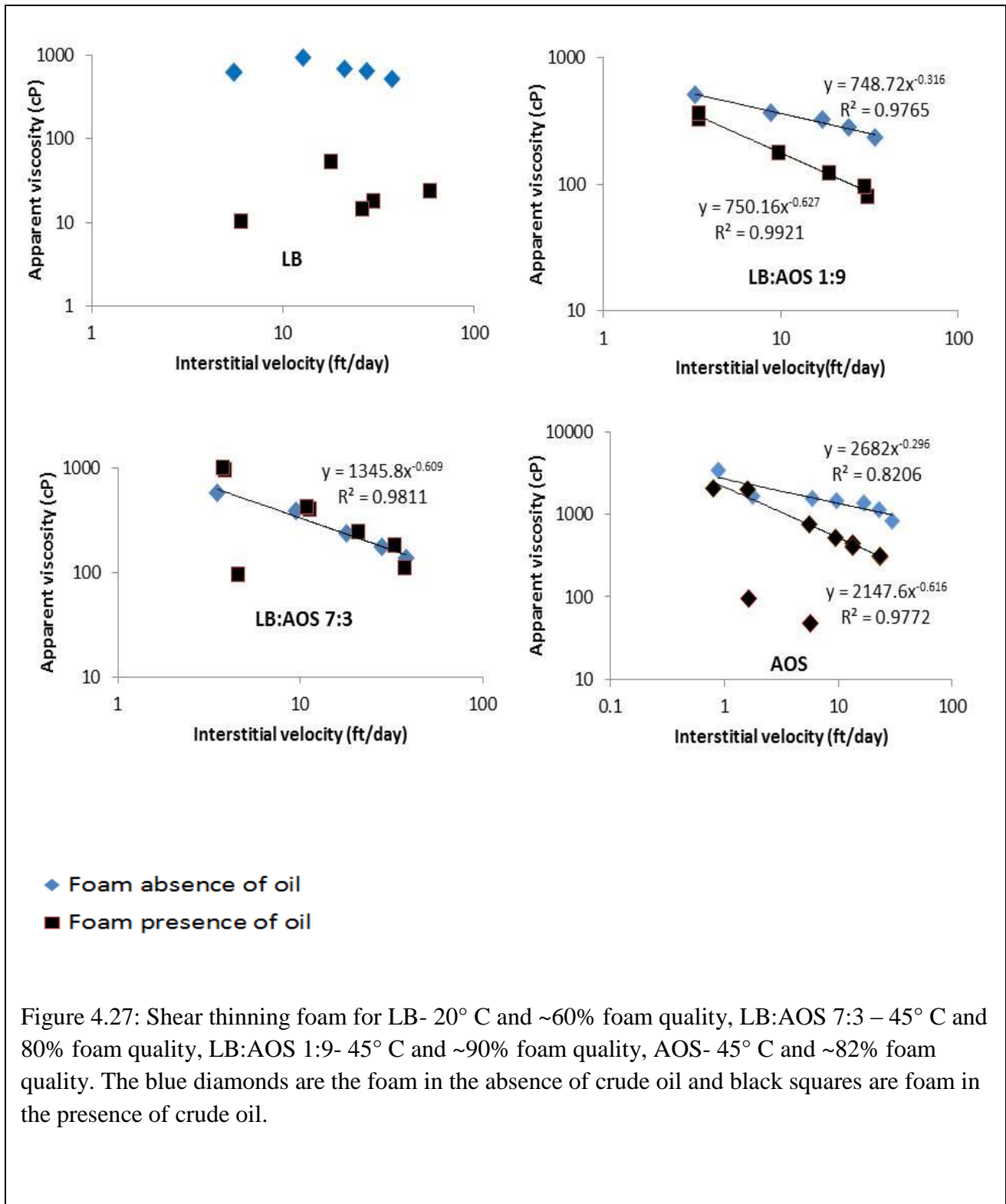
Figure 4.27: Shear thinning foam for LB- 20° C and ~60% foam quality, LB:AOS 7:3 – 45° C and 80% foam quality, LB:AOS 1:9- 45° C and ~90% foam quality, AOS- 45° C and ~82% foam quality. The blue diamonds are the foam in the absence of crude oil and black squares are foam in the presence of crude oil.
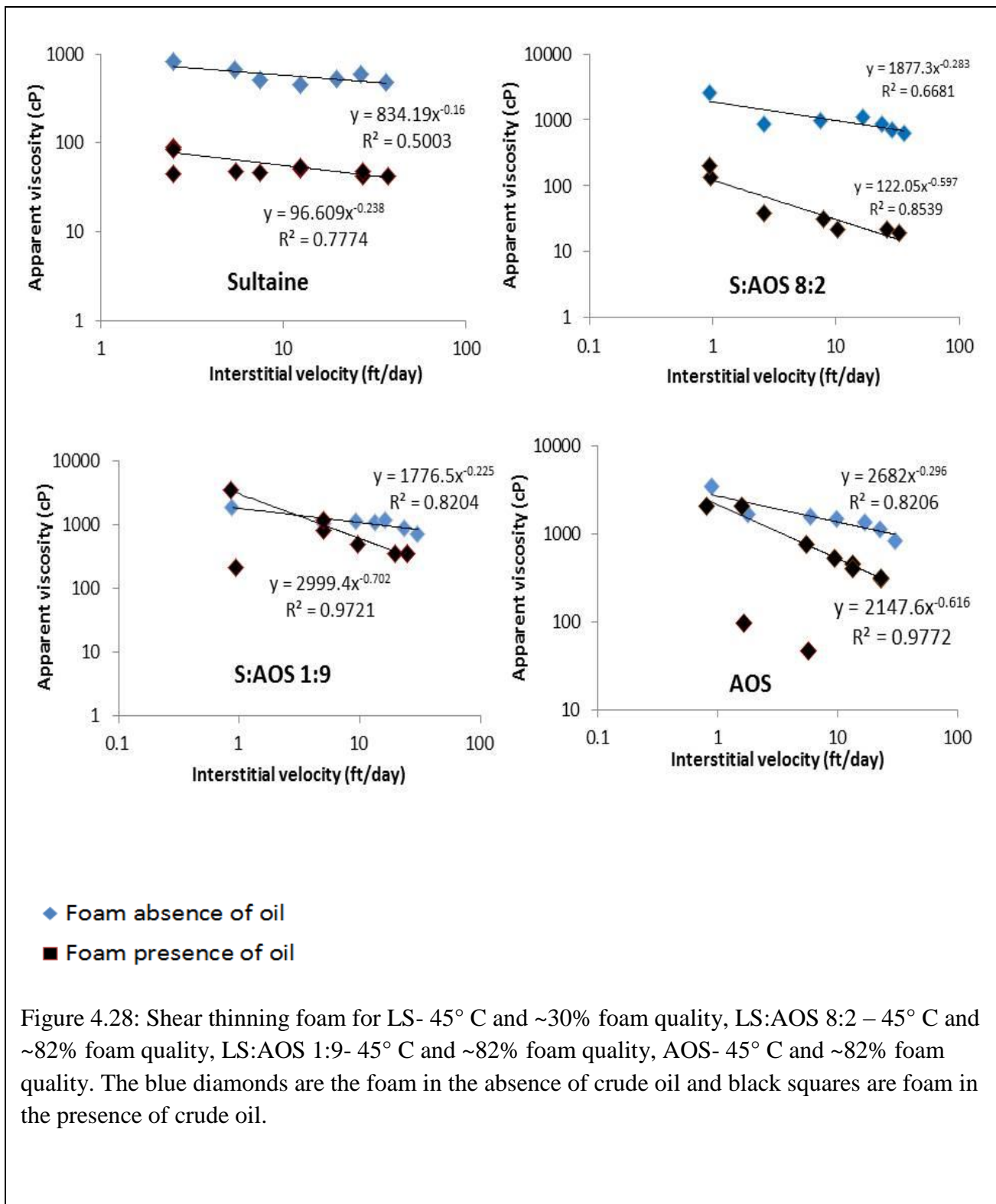
Figure 4.28: Shear thinning foam for LS- 45° C and ~30% foam quality, LS:AOS 8:2 – 45° C and ~82% foam quality, LS:AOS 1:9- 45° C and ~82% foam quality, AOS- 45° C and ~82% foam quality. The blue diamonds are the foam in the absence of crude oil and black squares are foam in the presence of crude oil.

4.5 Observations and conclusions from foam injection in porous media.

In conclusion the following observations are drawn

- Absence of oil: In the case of Rhodia A (C_{18} amido betaine) adding 9 parts of it to AOS $_{14-16}$ (A:AOS 9:1) helped produce very viscoelastic solutions and generate strong foam for a wide range of qualities studied. Whereas straight chain Lauryl betaine and Lauryl sultaine did not help in boosting the foam strength of AOS $_{14-16}$ to any better value than that of pure AOS $_{14-16}$ itself. On the other hand the weakly foaming betaine and sultaine, at higher gas fractions, got boosted by the presence of small amounts of AOS $_{14-16}$.

- Presence of oil: Addition of Rhodia A betaine, Lauryl betaine or Lauryl sultaine did not boost AOS $_{14-16}$ foam strength in the presence of waterflood residual oil. AOS $_{14-16}$ by itself is a very good foamer both in the presence and absence of oil.

- Use of the viscoelastic surfactant blend A:AOS 9:1 helped to generate strong foam in fewer PVs than AOS alone at ~25-30 ft/day and ~ 85% foam quality.However, the overall performance was better in the case of AOS $_{14-16}$ in terms of the number of PVs taken to reach steady state value. Hence one injection strategy that can be considered is to inject a small slug of the viscoelastic blend followed by a larger slug of AOS $_{14-16}$. In this way the viscoelastic surfactant can help generate foam faster and continued injection of AOS would continue to generate equally strong foam without the expensive betaine.

- Systematic coreflood experiments both in silica sand packs and Bentheimer sandstone demonstrated that AOS $_{14-16}$ by itself is a very good foamer and a favorable mobility control agent for enhanced oil recovery.

In the next chapter some bulk surfactant measurements will qualitatively explain foam rheology in porous media. Additionally a hypothesis on the interfacial viscosity giving rise to better foam stability will be discussed.

References:

(1)   Lawson, J. B.; Reisberg, J. **1980,** Alternate Slugs Of Gas And Dilute Surfactant For Mobility Control During Chemical Flooding. Society of Petroleum Engineers, SPE/DOE Enhanced Oil Recovery Symposium, 20-23 April, Tulsa, Oklahoma, SPE-8839-MS,.

(2)   Lopez-Salinas, J. L. Transport of Components and Phases in a Surfactant/Foam EOR Process for a Giant Carbonate Reservoir; Rice University, PhD Dissertation **2012**.

(3)   Andrianov, A.; Farajzadeh, R.; Mahmoodi Nick, M.; Talanana, M.; Zitha, P. L. J. Immiscible Foam for Enhancing Oil Recovery: Bulk and Porous Media Experiments. *Ind. Eng. Chem. Res.* **2012**, *51* (5), 2214–2226.

(4)   Farajzadeh, R.; Andrianov, A.; Zitha, P. L. J. Investigation of Immiscible and Miscible Foam for Enhancing Oil Recovery. *Ind. Eng. Chem. Res.* **2010**, *49* (4), 1910–1919.

(5)   Li, R. F.; Yan, W.; Liu, S.; Hirasaki, G.; Miller, C. A. Foam Mobility Control for Surfactant Enhanced Oil Recovery. *SPE J.* **2010**, *15* (04), 928–942.

(6)   Simjoo, M.; Dong, Y.; Andrianov, A.; Talanana, M.; Zitha, P. L. J. **2012,** A CT Scan Study of Immiscible Foam Flow in Porous Media for EOR. Society of Petroleum Engineers, SPE EOR Conference at Oil and Gas West Asia, 16-18 April, Muscat, SPE-155633-MS.

(7)   Li, R. F.; Hirasaki, G.; Miller, C. A.; Masalmeh, S. K. Wettability Alteration and Foam Mobility Control in a Layered, 2D Heterogeneous Sandpack. *SPE J.* **2012**, *17* (04), 1207–1220.

(8)   Hirasaki, G. J.; Miller, C. A.; Szafranski, R.; Tanzil, D.; Lawson, J. B.; Meinardus, H.; Jin, M.; Londergan, J. T.; Jackson, R. E.; Pope, G. A.; et al. **1997,** Field Demonstration of the Surfactant/Foam Process for Aquifer Remediation; Society of Petroleum Engineers, SPE Annual Technical Conference and Exhibition, 5-8 October, San Antonio, Texas, SPE-39292-MS.

(9)   Patzek, T. W. Field Applications of Steam Foam for Mobility Improvement and Profile Control. *SPE Reserv. Eng.* **1996**, *11* (02), 79–86.

(10)   Turta, A. T.; Singhal, A. K. Field Foam Applications in Enhanced Oil Recovery Projects: Screening and Design Aspects. *J. Can. Pet. Technol.* **2002**, *41* (10).

(11)   Blaker, T.; Aarra, M. G.; Skauge, A.; Rasmussen, L.; Celius, H. K.; Martinsen, H. A.; Vassenden, F. Foam for Gas Mobility Control in the Snorre Field: The FAWAG Project. *SPE Reserv. Eval. Eng.* **2002**, *5* (04), 317–323.

(12)   Schramm, L. L.; Turta, A. T.; Novosad, J. J. Microvisual and Coreflood Studies of Foam Interactions With a Light Crude Oil. *SPE Reserv. Eng.* **1993**, *8* (03), 201–206.

(13)   Lee, J.; Nikolov, A.; Wasan, D. Stability of Aqueous Foams in the Presence of Oil: On the Importance of Dispersed vs Solubilized Oil. *Ind. Eng. Chem. Res.* **2013**, *52* (1), 66–72.

(14)   Verdicchio, R. J.; Walts, J. M. High-Lathering Non-Irritating Detergent Compositions. US3950417 A, April 13, **1976**.

(15) Kinney, J. Thickened Alpha-Olefin Sulfonate Containing Formulations. US 4450090 A, May 22, 1984.

(16) Lomax, E. G. *Amphoteric Surfactants, Second Edition*; CRC Press, **1996**.

(17) Basheva, E. S.; Ganchev, D.; Denkov, N. D.; Kasuga, K.; Satoh, N.; Tsujii, K. Role of Betaine as Foam Booster in the Presence of Silicone Oil Drops. *Langmuir* **2000**, *16* (3), 1000–1013.

(18) Basheva, E. S.; Stoyanov, S.; Denkov, N. D.; Kasuga, K.; Satoh, N.; Tsujii, K. Foam Boosting by Amphiphilic Molecules in the Presence of Silicone Oil. *Langmuir* **2001**, *17* (4), 969–979.

(19) Li, R. F. Study of Foam Mobility Control in Surfactant Enhanced Oil Recovery Processes in One-Dimensional, Heterogeneous Two-Dimensional, and Micro Model Systems. Rice University, PhD Dissertation **2011**.

(20) Cui, L. Application of Foam for Mobility Control in Enhanced Oil Recovery (EOR) Process. Rice University, PhD Dissertation **2014**.

(21) Farajzadeh, R.; Andrianov, A.; Krastev, R.; Hirasaki, G. J.; Rossen, W. R. Foam–oil Interaction in Porous Media: Implications for Foam Assisted Enhanced Oil Recovery. *Adv. Colloid Interface Sci.* **2012**, *183–184*, 1–13.

(22) Joye, J.-L.; Hirasaki, G. J.; Miller, C. A. Asymmetric Drainage in Foam Films. *Langmuir* **1994**, *10* (9), 3174–3179.

(23) Danov, K. D.; Kralchevska, S. D.; Kralchevsky, P. A.; Ananthapadmanabhan, K. P.; Lips, A. Mixed Solutions of Anionic and Zwitterionic Surfactant (Betaine): Surface-Tension Isotherms, Adsorption, and Relaxation Kinetics. *Langmuir* **2004**, *20* (13), 5445–5453.

(24) López-Díaz, D.; García-Mateos, I.; Velázquez, M. M. Synergism in Mixtures of Zwitterionic and Ionic Surfactants. *Colloids Surf. Physicochem. Eng. Asp.* **2005**, *270–271*, 153–162.

(25) Rosen, M. J. Synergism in Mixtures Containing Zwitterionic Surfactants. *Langmuir* **1991**, *7* (5), 885–888.

(26) Rosen, M. J.; Zhu, Z. H.; Gao, T. Synergism in Binary Mixture of Surfactants: 11. Mixtures Containing Mono- and Disulfonated Alkyl- and Dialkyldiphenylethers. *J. Colloid Interface Sci.* **1993**, *157* (1), 254–259.

(27) Rosen, M. J.; Zhu, B. Y. Synergism in Binary Mixtures of Surfactants. *J. Colloid Interface Sci.* **1984**, *99* (2), 427–434.

(28) Rosen, M. J.; Murphy, D. S. Synergism in Binary Mixtures of Surfactants: VIII. Effect of the Hydrocarbon in Hydrocarbon/water Systems. *J. Colloid Interface Sci.* **1989**, *129* (1), 208–216.

(29) Rosen, M. J.; Murphy, D. S. Synergism in Binary Mixtures of Surfactants: V. Two-Phase Liquid—liquid Systems at Low Surfactant Concentrations. *J. Colloid Interface Sci.* **1986**, *110* (1), 224–236.

(30) Zhou, Q.; Rosen, M. J. Molecular Interactions of Surfactants in Mixed Monolayers at the Air/Aqueous Solution Interface and in Mixed Micelles in Aqueous Media: The Regular Solution Approach. *Langmuir* **2003**, *19* (11), 4555–4562.

(31) López-Díaz, D.; García-Mateos, I.; Velázquez, M. M. Surface Properties of Mixed Monolayers of Sulfobetaines and Ionic Surfactants. *J. Colloid Interface Sci.* **2006**, *299* (2), 858–866.

(32) Reif, I.; Somasundaran, P. Asymmetric Excess Free Energies and Variable Interaction Parameters in Mixed Micellization. *Langmuir* **1999**, *15* (10), 3411–3417.

(33) Georgiev, D. G. S. Markov Chain Model of Mixed Surfactant Systems. *Colloid Polym. Sci.* **1996**, *274* (1), 49–58.

(34) Misselyn-Bauduin, A. M.; Thibaut, A.; Grandjean, J.; Broze, G.; Jérôme, R. Mixed Micelles of Anionic−Nonionic and Anionic−Zwitterionic Surfactants Analyzed by Pulsed Field Gradient NMR. *Langmuir* **2000**, *16* (10), 4430–4435.

(35) Nagarajan, R. Molecular Theory for Mixed Micelles. *Langmuir* **1985**, *1* (3), 331–341.

(36) Mulqueen, M.; Blankschtein, D. Prediction of Equilibrium Surface Tension and Surface Adsorption of Aqueous Surfactant Mixtures Containing Zwitterionic Surfactants. *Langmuir* **2000**, *16* (20), 7640–7654.

(37) Hoffmann, H.; Poessnecker, G. The Mixing Behavior of Surfactants. *Langmuir* **1994**, *10* (2), 381–389.

(38) Huang, L.; Somasundaran, P. Theoretical Model and Phase Behavior for Binary Surfactant Mixtures. *Langmuir* **1997**, *13* (25), 6683–6688.

(39) Haque, M. E.; Das, A. R.; Rakshit, A. K.; Moulik, S. P. Properties of Mixed Micelles of Binary Surfactant Combinations. *Langmuir* **1996**, *12* (17), 4084–4089.

(40) Eads, C. D.; Robosky, L. C. NMR Studies of Binary Surfactant Mixture Thermodynamics: Molecular Size Model for Asymmetric Activity Coefficients. *Langmuir* **1999**, *15* (8), 2661–2668.

(41) Abe, M. *Mixed Surfactant Systems, Second Edition*; CRC Press, **2004**.

(42) Tsujii, K.; Okahashi, K.; Takeuchi, T. Addition-Compound Formation between Anionic and Zwitter-Ionic Surfactants in Water. *J. Phys. Chem.* **1982**, *86* (8), 1437–1441.

(43) Carreau, P. J.; Kee, D. D.; Chhabra, R. P. *Rheology of Polymeric Systems: Principles and Applications*; Hanser Publishers, **1997**.

(44) Chang, F.; Qu, Q.; Frenier, W. A Novel Self-Diverting-Acid Developed for Matrix Stimulation of Carbonate Reservoirs; **2001,** Society of Petroleum Engineers, SPE International Symposium on Oilfield Chemistry, 13-16 February, Houston, Texas, MS-65033-MS.

(45) Nasr-El-Din, H. A.; Samuel, E.; Samuel, M. **2003,** Application of a New Class of Surfactants in Stimulation Treatments; Society of Petroleum Engineers, SPE International Improved Oil Recovery Conference in Asia Pacific, 20-21 October, Kuala Lumpur, SPE-84898.

(46) Lungwitz, B.; Fredd, C.; Brady, M.; Miller, M.; Ali, S.; Hughes, K. **2004,** Diversion and Cleanup Studies of Viscoelastic Surfactant-Based Self-Diverting Acid; Society of Petroleum Engineers, SPE International Symposium and Exhibition on Formation Damage Control, 18-20 February, Lafayette, Louisiana, SPE- 86504.

(47) Taylor, D.; Kumar, P. S.; Fu, D.; Jemmali, M.; Helou, H.; Chang, F.; Davies, S.; Al-Mutawa, M. **2003,** Viscoelastic Surfactant Based Self-Diverting Acid for Enhanced Stimulation in Carbonate Reservoirs; Society of Petroleum Engineers, SPE European Formation Damage Conference, 13-14 May, The Hague, Netherlands, SPE- 82263.

(48) Chase, B.; Chmilowski, W.; Marcinew, R.; Mitchell, C.; Dang, Y.; Krauss, K.; Nelson, E.; Lantz, T.; Parham, C.; Plummer, J. Clear Fracturing Fluids for Increased Well Productivity. *Oilfield Rev.* **1997**, *9* (3), 20–33.

(49) Samuel, M.; Polson, D.; Graham, D.; Kordziel, W.; Waite, T.; Waters, G.; Vinod, P. S.; Fu, D.; Downey, R. **2000,** Viscoelastic Surfactant Fracturing Fluids: Applications in Low Permeability Reservoirs; Society of Petroleum Engineers, SPE Rocky Mountain

Regional/Low-Permeability Reservoirs Symposium and Exhibition, 12-15 March, Denver, Colorado, SPE-60322-MS.

(50) Dahayanake, M. S.; Yang, J.; Niu, J. H. Y.; Derian, P.-J.; Li, R.; Dino, D. Viscoelastic Surfactant Fluids and Related Methods of Use. US 6258859 B1, July 10, **2001**.

(51) Christov, N. C.; Denkov, N. D.; Kralchevsky, P. A.; Ananthapadmanabhan, K. P.; Lips, A. Synergistic Sphere-to-Rod Micelle Transition in Mixed Solutions of Sodium Dodecyl Sulfate and Cocoamidopropyl Betaine. *Langmuir* **2004**, *20* (3), 565–571.

(52) Qiao, Y.; Lin, Y.; Wang, Y.; Li, Z.; Huang, J. Metal-Driven Viscoelastic Wormlike Micelle in Anionic/Zwitterionic Surfactant Systems and Template-Directed Synthesis of Dendritic Silver Nanostructures. *Langmuir* **2011**, *27* (5), 1718–1723.

(53) Ghosh, S.; Khatua, D.; Dey, J. Interaction Between Zwitterionic and Anionic Surfactants: Spontaneous Formation of Zwitanionic Vesicles. *Langmuir* **2011**, *27* (9), 5184–5192.

(54) Hirasaki, G. J.; Pope, G. A. Analysis of Factors Influencing Mobility and Adsorption in the Flow of Polymer Solution Through Porous Media. *Soc. Pet. Eng. J.* **1974**, *14* (04), 337–346.

(55) Flew, S.; Sellin, R. H. J. Non-Newtonian Flow in Porous Media-a Laboratory Study of Polyacrylamide Solutions. *J. Non-Newton. Fluid Mech.* **1993**, *47*, 169–210.

(56) Farajzadeh, R.; Andrianov, A.; Bruining, H.; Zitha, P. L. J. Comparative Study of CO2 and N2 Foams in Porous Media at Low and High Pressure−Temperatures. *Ind. Eng. Chem. Res.* **2009**, *48* (9), 4542–4552.

(57) Simjoo, M.; Dong, Y.; Andrianov, A.; Talanana, M.; Zitha, P. L. J. Novel Insight Into Foam Mobility Control. *SPE J.* **2013**, *18* (03), 416–427.

(58) Myers, T. J.; Radke, C. J. Transient Foam Displacement in the Presence of Residual Oil: Experiment and Simulation Using a Population-Balance Model. *Ind. Eng. Chem. Res.* **2000**, *39* (8), 2725–2741.

(59) Alvarez, J. M.; Rivas, H. J.; Rossen, W. R. Unified Model for Steady-State Foam Behavior at High and Low Foam Qualities. *SPE J.* **2001**, *6* (03), 325–333.

(60) Osterloh, W. T.; Jante, M. J. **1992,** Effects of Gas and Liquid Velocity on Steady-State Foam Flow at High Temperature;, Society of Petroleum Engineers, SPE/DOE Enhanced Oil Recovery Symposium, 22-24 April, Tulsa, Oklahoma, SPE-24179-MS.

(61) Khatib, Z. I.; Hirasaki, G. J.; Falls, A. H. Effects of Capillary Pressure on Coalescence and Phase Mobilities in Foams Flowing Through Porous Media. *SPE Reserv. Eng.* **1988**, *3* (03), 919–926.

(62) Rossen, W. R.; Wang, M. W. Modeling Foams for Acid Diversion. *SPE J.* **1999**, *4* (02), 92–100.

(63) Vincent-Bonnieu, S.; Jones, S. A.; others. Comparative Study of Foam Stability in Bulk and Porous Media, TU Delft, Delft University of Technology, Masters Thesis, **2014**.

(64) Kapetas, L.; Vincent-Bonnieu, S.; Farajzadeh, R.; Eftekhari, A. A.; Mohd-Shafian, S. R.; Bahrim, R. K.; Rossen, W. R. **2015,** Effect of Permeability on Foam-Model Parameters-An Integrated Approach from Coreflood Experiments through to Foam Diversion Calculations. *IOR 2015-18th European Symposium on Improved Oil Recovery*.

(65) Aronson, A. S.; Bergeron, V.; Fagan, M. E.; Radke, C. J. The Influence of Disjoining Pressure on Foam Stability and Flow in Porous Media. *Colloids Surf. Physicochem. Eng. Asp.* **1994**, *83* (2), 109–120.

(66) Weers, J. G.; Rathman, J. F.; Axe, F. U.; Crichlow, C. A.; Foland, L. D.; Scheuing, D. R.; Wiersema, R. J.; Zielske, A. G. Effect of the Intramolecular Charge Separation Distance on the Solution Properties of Betaines and Sulfobetaines. *Langmuir* **1991**, *7* (5), 854–867.

(67) Ransohoff, T. C.; Radke, C. J. Mechanisms of Foam Generation in Glass-Bead Packs. *SPE Reserv. Eng.* **1988**, *3* (02), 573–585.

(68) Friedmann, F.; Jensen, J. A. Some Parameters Influencing the Formation and Propagation of Foams in Porous Media; **1986,** Society of Petroleum Engineers, SPE California Regional Meeting, 2-4 April, Oakland, California , SPE- 15087.

(69) Rossen, W. R.; Gauglitz, P. A. Percolation Theory of Creation and Mobilization of Foams in Porous Media. *AIChE J.* **1990**, *36* (8), 1176–1188.

(70) A. Gauglitz, P.; Friedmann, F.; I. Kam, S.; R. Rossen, W. Foam Generation in Homogeneous Porous Media. *Chem. Eng. Sci.* **2002**, *57* (19), 4037–4052.

(71) Rossen, W. R. Theory of Mobilization Pressure Gradient of Flowing Foams in Porous Media. *J. Colloid Interface Sci.* **1990**, *136* (1), 1–16.

(72) Dicksen, T.; Hirasaki, G. J.; Miller, C. A. **2002,** Conditions for Foam Generation in Homogeneous Porous Media**.**Society of Petroleum Engineers, SPE/DOE Improved Oil Recovery Symposium, 13-17 April, Tulsa, Oklahoma, SPE- 75176-MS.

(73) Kam, S. I.; Rossen, W. R. A Model for Foam Generation in Homogeneous Media. *SPE J.* **2003**, *8* (04), 417–425.

(74) Boud, D. C.; Holbrook, O. C. Gas Drive Oil Recovery Process. US2866507 A, December 30, **1958**.

(75) Simjoo, M. *Immiscible Foam for Enhancing Oil Recovery.*;Technical University Delft, PhD thesis, **2012**.

(76) Denkov, N. D. Mechanisms of Foam Destruction by Oil-Based Antifoams. *Langmuir* **2004**, *20* (22), 9463–9505.

(77) Manlowe, D. J.; Radke, C. J. A Pore-Level Investigation of Foam/Oil Interactions in Porous Media. *SPE Reserv. Eng.* **1990**, *5* (04), 495–502.

(78) Bergeron, V.; Fagan, M. E.; Radke, C. J. Generalized Entering Coefficients: A Criterion for Foam Stability against Oil in Porous Media. *Langmuir* **1993**, *9* (7), 1704–1713.

(79) Nikolov, A. D.; Wasan, D. T.; Huang, D. W.; Edwards, D. A. **1986,** The Effect of Oil on Foam Stability: Mechanisms and Implications for Oil Displacement by Foam in Porous Media; Society of Petroleum Engineers, SPE Annual Technical Conference and Exhibition, 5-8 October, New Orleans, Louisiana, SPE- 15443-MS.

(80) Jensen, J. A.; Friedmann, F. **1987,** Physical and Chemical Effects of an Oil Phase on the Propagation of Foam in Porous Media; Society of Petroleum Engineers, SPE California Regional Meeting, 8-10 April, Ventura, California,MS-16375.

(81) Lobo, L.; Wasan, D. T. Mechanisms of Aqueous Foam Stability in the Presence of Emulsified Non-Aqueous-Phase Liquids: Structure and Stability of the Pseudoemulsion Film. *Langmuir* **1993**, *9* (7), 1668–1677.

(82) Schramm, L. L.; Novosad, J. J. Micro-Visualization of Foam Interactions with a Crude Oil. *Colloids Surf.* **1990**, *46* (1), 21–43.

(83) Mannhardt, K.; Novosad, J. J.; Schramm, L. L. **1998,** Foam/Oil Interations at Reservoir Conditions; Society of Petroleum Engineers, SPE/DOE Improved Oil Recovery Symposium, 19-22 April, Tulsa, Oklahoma, SPE-39681.

(84) Vikingstad, A. K.; Aarra, M. G. Comparing the Static and Dynamic Foam Properties of a Fluorinated and an Alpha Olefin Sulfonate Surfactant. *J. Pet. Sci. Eng.* **2009**, *65* (1–2), 105–111.

(85) Schramm, L. L.; Turta, A. T.; Novosad, J. J. Microvisual and Coreflood Studies of Foam Interactions With a Light Crude Oil. *SPE Reserv. Eng.* **1993**, *8* (03), 201–206.

(86) Monteux, C.; Fuller, G. G.; Bergeron, V. Shear and Dilational Surface Rheology of Oppositely Charged Polyelectrolyte/Surfactant Microgels Adsorbed at the Air−Water Interface. Influence on Foam Stability. *J. Phys. Chem. B* **2004**, *108* (42), 16473–16482.

(87) Langevin, D. Influence of Interfacial Rheology on Foam and Emulsion Properties. *Adv. Colloid Interface Sci.* **2000**, *88* (1–2), 209–222.

(88) Stubenrauch, C.; Miller, R. Stability of Foam Films and Surface Rheology: An Oscillating Bubble Study at Low Frequencies. *J. Phys. Chem. B* **2004**, *108* (20), 6412–6421.

(89) Winsor, P. A. Hydrotropy, Solubilisation and Related Emulsification Processes. *Trans. Faraday Soc.* **1948**, *44*, 376–398.

(90) Bellocq, A. M.; Biais, J.; Bothorel, P.; Clin, B.; Fourche, G.; Lalanne, P.; Lemaire, B.; Lemanceau, B.; Roux, D. Microemulsions. *Adv. Colloid Interface Sci.* **1984**, *20* (3–4), 167–272.

(91) Salager, J. L.; Morgan, J. C.; Schechter, R. S.; Wade, W. H.; Vasquez, E. Optimum Formulation of Surfactant/Water/Oil Systems for Minimum Interfacial Tension or Phase Behavior. *Soc. Pet. Eng. J.* **1979**, *19* (02), 107–115.

(92) Healy, R. N.; Reed, R. L.; Stenmark, D. G. Multiphase Microemulsion Systems. *Soc. Pet. Eng. J.* **1976**, *16* (03), 147–160.

(93) Bourrel, M.; Schechter, R. S. *Microemulsions and Related Systems: Formulation, Solvency, and Physical Properties*; Editions TECHNIP, **2010**.

(94) Ysambertt, F.; Anton, R.; Salager, J.-L. Retrograde Transition in the Phase Behaviour of Surfactant-Oil-Water Systems Produced by an Oil Equivalent Alkane Carbon Number Scan. *Colloids Surf. Physicochem. Eng. Asp.* **1997**, *125* (2–3), 131–136.

(95) Kahlweit, M.; Strey, R.; Haase, D. Phase Behavior of Multicomponent Systems Water-Oil-Amphiphile-Electrolyte. 3. *J. Phys. Chem.* **1985**, *89* (1), 163–171.

(96) Queste, S.; Salager, J. L.; Strey, R.; Aubry, J. M. The EACN Scale for Oil Classification Revisited Thanks to Fish Diagrams. *J. Colloid Interface Sci.* **2007**, *312* (1), 98–107.

(97) Cash, L.; Cayias, J. L.; Fournier, G.; Macallister, D.; Schares, T.; Schechter, R. S.; Wade, W. H. The Application of Low Interfacial Tension Scaling Rules to Binary Hydrocarbon Mixtures. *J. Colloid Interface Sci.* **1977**, *59* (1), 39–44.

(98) Farajzadeh, R.; Lotfollahi, M.; Eftekhari, A. A.; Rossen, W. R.; Hirasaki, G. J. H. Effect of Permeability on Implicit-Texture Foam Model Parameters and the Limiting Capillary Pressure. *Energy Fuels* **2015**, *29* (5), 3011–3018.

Chapter 5

Synergism in Binary Surfactant Systems

Introduction:

In Chapter 4, we learnt that the porous media foam rheology of LB and AOS blends and LS and AOS blends followed the behavior of AOS, even the ones which had a low AOS content, but not the LB and LS themselves. This observation gave rise to a question, as to why the blends especially the ones with low AOS content did not behave rheologically in a way somewhere in between the zwitterionic surfactant and AOS foam rheology. The regular solution theory approach of Rubingh, combined with Rosen's application to water-air film interfaces and its adaption to oil-water interfaces is applied in this chapter to understand this behavior, especially the high foam strength observed when the poor-foaming zwitterionics were added to the strong foamer AOS. It was found that the zwitterionic-anionic blends exhibited synergistic interactions with a calculated interfacial mole fraction of AOS of ~50% for the blends which have a low AOS bulk mole fraction. Interaction between anionic and zwitterionic molecules apparently promoted the nearly equimolar composition and strengthened the gas-water interfaces of the foam. For the blends with a high AOS bulk mole fraction, synergism along with the hydrophobicity of AOS tends to enrich the monolayer with AOS. However, the synergism did not lead to improvement in foam performance in porous media beyond that seen for AOS alone.

Additionally foam strength in the presence of water flood residual oil was weak for the pure zwitterionic surfactants, but the blends and pure AOS had comparable foam strength. Interfacial rheological measurements were conducted to observe if AOS was superior as a foamer based on its surface shear viscosity compared to those of the other surfactants. However none of the soluble surfactants possessed any measureable surface shear viscosity.

134

Additional qualitative film drainage studies were conducted, and it was observed that addition of 1 part of betaine to 9 parts of AOS seemed to significantly reduce the rate of film drainage and caused a delayed rupture. The trend that was observed with regard to longevity of the black film(very thin film) was LB:AOS 1:9>LS:AOS 8:2> AOS~= LS:AOS 1:9>LB=LS=LB:AOS 7:3. These bulk film drainage experiments offered no explanation to the foam porous media rheology.

5.1 Surface/Interfacial tension measurements

Surface tensions of aqueous surfactant solution were measured using Kibron –EZ Pi plus, which utilizes the Du-Nuoy Padday principle for measurements. It operates on the similar principle as the Du-Nuoy ring method, instead of a circular ring, a rod is used in Du-Nuoy Padday. The maximum force required to detach the rod from a liquid interface is measured and used to calculate the tension values. A butanol flame was used to burn off impurities from the rod each time before any measurement was made. In order to verify the cleaning procedure, measurements were made with DI water several times, and the value obtained was 72.6±0.2 mN/m. Each surface tension value reported in this study is after a wait time of 10 minutes. All measurements were made at room temperature (21°C ±2).

For interfacial tension (IFT) measurements, octane (Sigma Aldrich >99% purity) was purified by passing through a column of activated alumina and silica gel mixture. The measured value of interfacial tension (IFT) of octane with respect to DI water was 50.08 mN/m, which is close to value in literature[1]. This confirmed that the octane was free of surface active impurities. If this step was not followed values of IFT obtained were ~ 39-41 mN/m. After making measurements with octane the rod was cleaned with an industrial solvent (ZEP Dyna Blue 400) and then rinsed with a flush of DI water. Following this the butanol flame was used to burn off

any remaining impurities. To make sure the rod was indeed clean, DI water surface tension was

measured in between each measurement, and each time the value obtained was 72.6± 0.2 mN/m.

The cleanliness of the rod was very important for each measurement made in this study. Each

IFT value was made after a wait time of 10 minutes to assure that equilibrium between surface

and bulk solution was reached before rod withdrawal began. Each measurement was made three

times and an average of the measurements is reported.

5.2 Regular solution theory(RST)

Regular solution theory is the most simplistic model applied to non ideal binary mixtures

of surfactants. The assumption in the derivation of the model is that entropy of mixing is ideal.

The change in the Gibbs free energy is accounted for using the activity coefficient in the

chemical potential. The activity coeeficient can be characterised using the molecular interaction

parameter β which quantifies if the interaction between two unlike surfactant molecules is more

synergistic or more antagonistic than interactions between like surfactant molecules. Rubingh[2]

used the theory to characterize binary mixed micelles, Holland et.al [3] used it to characterize

multicomponent micellar systems and Rosen extended it to quantify interactions in monolayers[4].

The theory helps in calculating the fraction of one surfactant x_1 in a mixed micelle or mixed

monolayer of a binary system, with known or measured quantities is given as below

$$\frac{x_1^2 \ln(\frac{\alpha_1 C_{12}}{x_1 C_1^0})}{(1-x_1)^2 \ln(\frac{(1-\alpha_1)C_{12}}{(1-x_1)C_2^0})} = 1 \qquad \textbf{Equation 5.1}$$

$$\beta^\sigma = \frac{\ln(\frac{\alpha_1 C_{12}}{x_1 C_1^0})}{(1-x_1^2)} \qquad \textbf{Equation 5.2}$$

$$\frac{x_{M1}^2 \ln\left(\frac{\alpha_1 C_{M12}}{x_{M1} C_{M1}^0}\right)}{(1-x_{M1})^2 \ln\left(\frac{(1-\alpha_1) C_{M12}}{(1-x_{M1}) C_{M2}^0}\right)} = 1 \qquad \textbf{Equation 5.3}$$

$$\beta^M = \frac{\ln\left(\frac{\alpha_1 C_{M12}}{x_{M1} C_{M1}^0}\right)}{(1-x_{M1}^2)} \qquad \textbf{Equation 5.4}$$

α1- mole fraction of surfactant 1 in the prepared bulk solution (the zwitterionic for zwitterionic/AOS mixtures considered here)

x_1- mole fraction of surfactant 1 in the mixed monolayer

x_{M1}- mole fraction of surfactant 1 the mixed micelle

C_{12}, $C_1{}^0$, $C_2{}^0$ are the molar concentrations of zwitterionic: AOS mixture, zwitterionic, AOS respectively chosen to give a particular surface tension value

C_{M12}, $C_{M1}{}^0$, $C_{M2}{}^0$ are the CMCs of the mixture and individual surfactants respectively

β^σ, β^M – molecular interaction parameter in the monolayer or micelle respectively

In Equation 5.2 and Equation 5.4, we note that only x an unknown quantity, and it can be solved. Once x is obtained, β can be easily calculated. A detailed procedure on how to go about the calculation is found in a very good reference[4].

One of the major drawbacks of using the regular solution theory is that it assumes entropy of mixing is zero. Secondly the β parameter quantifies the surfactant interactions only. It does not account for the specific interactions of the surfactants with the counterions in the stern layer. A good molecular theoretical model was developed by Blankschtein and co- workers which models the electrostatic interactions giving consideration to the counterions present [5–8]. Nevertheless the RST helps to calculate the monolayer composition of the surfactant blends and qualitatively gives an explanation for the foam rheological

137

behavior of the blends without any tedious calculations. Many experimental works have found good agreement using this method[4,9–14].
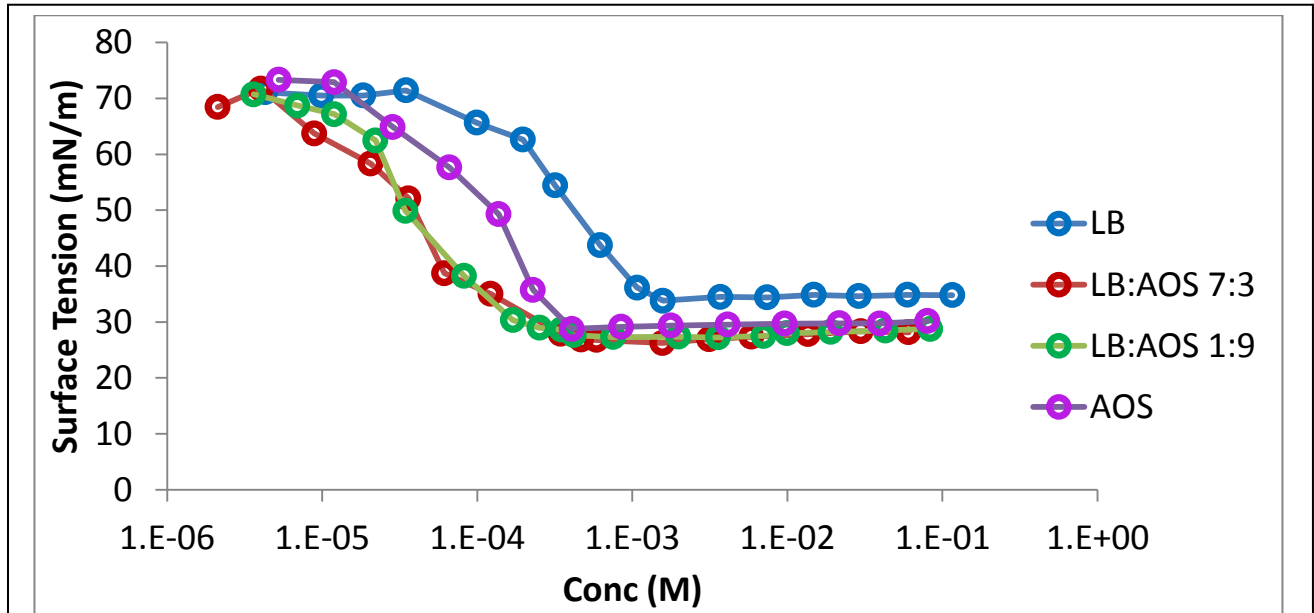
Figure 5.1: Surface tension measurements for (LB) and AOS_{14-16} (AOS) surfactant blends at temperature 20 °C.
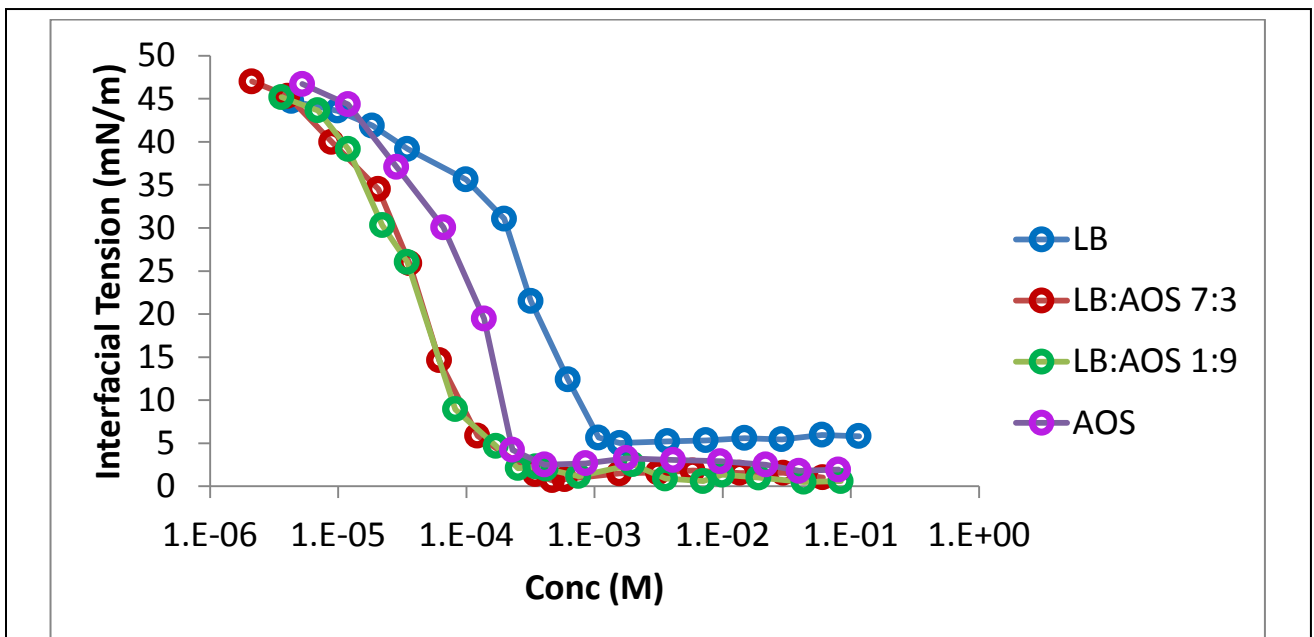
Figure 5.2 : Interfacial tension measurements for (LB) and AOS_{14-16} (AOS) surfactant blends at temperature 20 °C. The oleic phase used was purified octane.

Surfactant	CMC (wt%)	CMC (M)	Surface tension (mN/m)
LB	0.0136	0.00157	33.79
7LB+3AOS	0.0057	0.00034	27.9
1LB+9AOS	0.00415	0.000348	28.65
AOS	0.00508	0.000407	28.76

Table 5.1: CMC values of LB, AOS and their blends

Surfactant	α_{LB}	X_{LB}	$X_{M(LB)}$	β^{σ}	β^{M}
LB:AOS 7:3	0.77	0.49	0.48	-7.08	-2.84
LB:AOS 1:9	0.14	0.31	0.26	-2.72	-1.40

Table 5.2: Estimation of parameter using regular solution theory for LB and AOS blends at air liquid interface.

Surfactant	α_{LB}	X_{LB}	$X_{M(LB)}$	β^{σ}	β^{M}
LB:AOS 7:3	0.77	0.37		-3.24	
LB:AOS 1:9	0.14	0.30	0.27	-2.19	-0.77

Table 5.3: Estimation of parameter using regular solution theory for LB and AOS blends at octane-aqueous interface.

Figure 5.1 shows the surface tension curves of pure LB , pure AOS and two of their blends at the air water interface, and Figure 5.2 show the interfacial tension curves at the octane-water interface for the LB-AOS systems. Table 5.1 tabulates the cmc values which show that LB has close to an order of magnitude higher cmc. The blends have a CMC value comparable to that of pure AOS. However below the cmc the blends do show a lower tension value than the

139

individual surfactants at the same overall concentration. The regular solution theory approach was used to calculate the mole fraction of LB in the mixture for the air water interface and the octane water interface.

The fraction of LB at the air water interface is found to be ~ 50% and 31% for the LB:AOS 7:3 and 1:9 blend respectively (refer to Table 5.2). In the LB:AOS 7:3 mixture, we see that the bulk molar composition contains 77% LB, however the interface has 49%, which means the other 51% is AOS. AOS $_{14-16}$, being the more lipophilic molecule among the zwitterionic and anionic surfactants, tends to have a preference at the interface in spite of being lesser in the bulk. The β^σ value is -7.08, which indicates that there are attractive interactions and the blend is synergistic. The surfactants try to pair as many unlike molecules as possible. It may be hard to say if 51% occupation of the air-water interface with AOS molecules, marks the boundary where the foam starts behaving more like AOS. Nevertheless it is a good estimation from the regular solution theory that the interface has almost equimolar quantity of AOS and LB, and perhaps also a well packed interface, definitely better than for pure LB alone. One of the reason for LB to reach the limiting capillary zone or the high foam quality regime where bubble coalescense takes place at ~ 60% (Chapter 4 , Figure 4.25) , might be the bigger head group of the molecule. It does not pack well at the interfaces.

Table 5.2 shows that LB:AOS 7:3 mixed micelle is again composed of ~50% LB molecules. However the β^M value is -2.84 which shows that interactions in the mixed micelles are less stronger than the interactions at the interface. One reason could be the solubility of surfactants at room temperature (Discussed in Chapter 4 Aqueous stabiliy tests). The surface tension measurements for the LB:AOS 7:3 blend were made immeadiately after sample preparation, as they would not stay clear after few hours. It is possible that due to limited

solubility at room temperature, a solid phase was just beginning to precipitate. Visually when the samples were observed they appeared clear while making the measurements.

The regular solution theory predicts that there should be only one β value to characterise all solution compositions of a particular surfactant blend. However due to limitations in the assumptions, there are many cases where β value is composition dependent[15–21]. The same has been observed in the case of LB/AOS mixtures in this study. The studies used in Rosen's work[22] emphasize on the high purity of the surfactants and also the ionic enviroment. In this study commercial surfactants have been used, and hence it is possible to get a different β values for diffferent solution compositions. Apart from the purity of the surfactants, several authors have pointed out that the weakness of the theory resides on the fact that it imposes a symmetry on the excess free enrgy dependence on the micelle composition. Huang et.al have introduced a packing parameter P* which accounts for non random packing in binary systems. Their method shows that the excess free energy is not symmetric about composition.[23] Similarly conisderation was given by Eads and Robosky to the asymmetry of the activity coefficients[19].

The next case is LB:AOS 1:9 blend (Table 5.2) where β^{σ} becomes less negative(-2.72) at the air-aqueous interface. This could be due to larger number of AOS molecules at the interface causing slight amount of repulsion between the headgroups. The value of β is still negative showing that there is synergism but to a lesser extent than LB:AOS 7:3. The mole fraction of LB at the interface is 31% which means the mole fraction of AOS is 69%. The interfaces being dominated by AOS molecules is good enough to cause the surfactant foam rheology to behave similar to pure AOS. The mixed micelle has a composition of 26% LB and the remaining part AOS. One must also take into consideration, that the reduced β values for the LB:AOS 1:9 blend

for the mixed monolayer could be due to the presence of more like molecules (more negative AOS molecules).

Table 5.3 shows the interaction parameters for the LB:AOS blends at the octane aqueous interface.The LB:AOS 7:3 blend defintiely has a significantly reduced interfacial composition of LB (only 37 %) in the presence of the alkane. The monolayer thus contains 63% AOS. Still the negative β parameter of -3.24 shows that the LB and AOS have significant interactions in the monolayer. The theory could not be solved for the mixed micelle as the solution did not converge. This shows that the more hydrophobic AOS is definitely dominating the octane-aqueous interface. In fact it seems like AOS_{14-16} definitely helps the poorly foaming betaine to perform better in the presence of oil when they are mixed. In this case the AOS acts as the foam booster to the poorly foaming betaine as observed in results in Chapter 4.

At the octane –aqueous interface LB:AOS 1:9 behavior is similar to the interactions at the air-aqueous interface both at the monolayer and in the mixed micelle. The monolayer being composed of 70% AOS molecules might have been causing the foam of LB:AOS 1:9 to behave similar to pure AOS in the presence of oil.

Figure 5.3and Figure 5.4 show the surface and interfacial tension measurements of Lauryl sultaine (LS) and its blends. LS has the higher cmc and the blends and AOS all have comparable cmc's and also tension values(Table 5.4). Table 5.5 shows the regular solution theory parameters for LS and AOS blends. Again in the case of LS:AOS 8:2 blend, the mole fraction of the two surfactants are approximately equimolar at the interface and also in the mixed micelle. The $β^σ$ parameter is negative -1.56 and $β^M$ is -1.92 signifying synergism in the blend. The LS:AOS 1:9 blend has a mole fraction of ~18% LS and ~82% AOS for both the monolayer

and mixed micelle. β^σ and β^M have small positive values , indicating minimal interactions. The work of Zhou et al. [4] point out that the value of x must lie between 0.2-0.8, for the solution to converge. A small content of protonated betaine makes the interactions more attractive as seen in the case of LB and AOS blends.

Table 5.6 shows the molecular interaction parameter for the LS and AOS blends at the octane and surfactant solution interface. The solution converged only in the case of LS:AOS 8:2 mixed monolayer. For the mixed monolayer the composition of LS and AOS is equimolar which is same as at the air aqueous interface.

When comparing the LB/LS interaction with AOS, the betaine had a more attractive interaction with the anionic surfactant than the sultaine. One of the reasons is that the COO^- is capable of being protanated by the H^+ ions in water thereby leaving the positive quaternary ammonium to take part in the interaction with the anionic AOS molecule. The SO_3^- group of the sultaine cannot be readily protonated. This might cause reduced interactions since the SO_3^- group interacts with the negative anionic AOS as well.
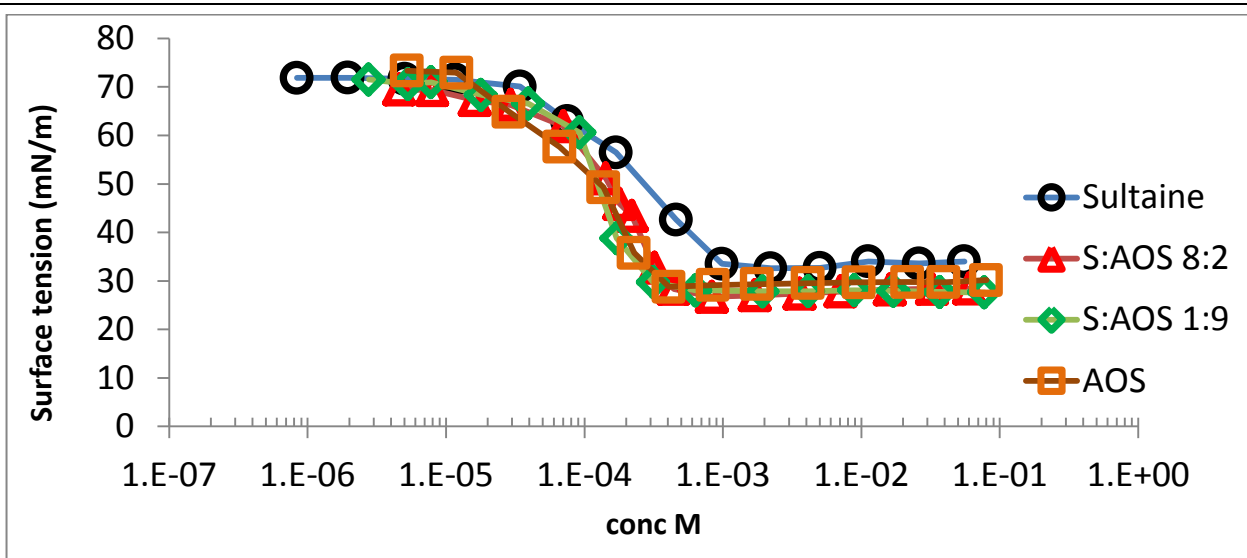
Figure 5.3: Surface tension measurements for (LS) and AOS_{14-16} (AOS) surfactant blends at temperature 20 °C.
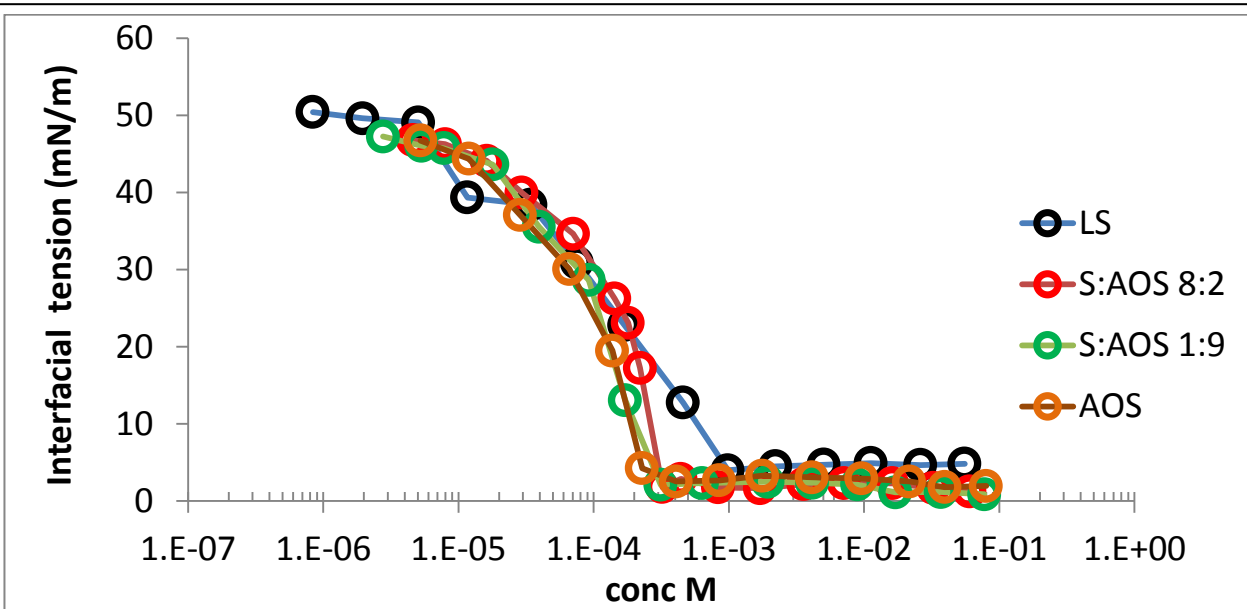
Figure 5.4 : Interfacial tension measurements for (LS) and AOS_{14-16} (AOS) surfactant blends at temperature 20 °C. The oleic phase used was octane.

Surfactant	CMC (wt%)	CMC (M)	Surface tension (mN/m)
LS	0.017	0.000983	33.52
8LS+2AOS	0.0073	0.00044	28.35
1LS+9AOS	0.00404	0.000313	29.74
AOS	0.00508	0.000407	28.76

Table 5.4: CMC values for LS,AOS and their blends

Surfactant	α_{LB}	X_{LS}	$X_{M(LS)}$	β^{σ}	β^{M}
LS:AOS 8:2	0.73	0.50	0.52	-1.56	-1.92
LS:AOS 1:9	0.073	0.18	0.19	+0.24	+0.29

Table 5.5:Estimation of parameter using regular solution theory for LS and AOS blends for the aqueous air interface.

Surfactant	α_{LB}	X_{LS}	$X_{M(LS)}$	β^{σ}	β^{M}
LS:AOS 8:2	0.73	0.50		-1.01	
LS:AOS 1:9	0.072	Cannot solve	Cannot solve	-	-

Table 5.6:Estimation of parameter using regular solution theory for LS and AOS blends for the octane- aqueous interface.

The key message from the above studies is that even though synergism between the surfactants may exist as determined from the regular solution theory approach, the results of Chapter 4 demonstrate that there is no significant enhancement of foam strength using a blended surfactant as compared to pure AOS (absence of oil). But the RST has provided a convenient way to estimate the monolayer composition, which gives some insight on the foam rheological behavior in porous media for the surfactant blends. The message is that there is significant domination of AOS molecues at the interface even in the case of the blends which have a low

composition of AOS in the bulk solution. The reason being that AOS is the more hydrophobic surfactant among the two. The difference in hydrophobicity between the two surfactants and the synergistic interactions between the surfactants promote increased adsorption of AOS molecules on to the interface causing the foam rheology of the blends to behave similar to AOS foam in porous media.

It is quite possible that the monolayer composition has more AOS composition than predicted by the regular solution theory. Neutron reflection studies for other surfactant systems, have shown that the RST predicted compositions don't match the predicted composition measured using the neutron reflection experimental technique[18]. A good literature review on neutron reflection studies performed on binary mixtures and their comparison with the regular solution theory has been described elsewhere[24].

5.2.1 Gibbs surface excess

It is hard to quantify the monolayer concentration of the surfactant molecules. Hence Gibbs developed a thermodynamic relationship between the bulk solution concentration and surface concentration Γ^S at constant temperature as

$$\Gamma^s = \frac{1}{RT}\frac{d\sigma}{d\ln(c)}$$ **Equation 5.5**

Equation 5.5 is applied to a single surfactant with activity equal to concentration. In this specific system, we have a binary mixture of surfactant. According to Chattoraj and Birdie[25] if the surface tension σ measurements are made such that the two components of the mixture are in a constant proportion (say for example LB:AOS 7:3 is at a constant mass ratio of 7:3 for every concentration measured) then the following thermodynamic procedure can be followed

$$-d\sigma = \Gamma_1 d\mu_1 + \Gamma_2 d\mu_2 \qquad \textbf{Equation 5.6}$$

$$-d\sigma = RT(\Gamma_1 dlnc_1 + \Gamma_2 dlnc_2) \textbf{ Equation 5.7}$$

If $c_1 = kc_2$ (since the two components /surfactants are in a constant proportion say k)

$$dlnc_1 = dlnc_2 \qquad \textbf{Equation 5.8}$$

Further if the total concentration c_T of the mixture can be expressed as

$$c_T = c_1 + c_2 \qquad \textbf{Equation 5.9}$$

$$dlnc_T = dlnc_1 = dlnc_2 \qquad \textbf{Equation 5.10}$$

Equation 5.7 in combination with Equation 5.10 yields

$$-d\sigma = RT(\Gamma_1 dlnc_T + \Gamma_2 dlnc_T) \textbf{ Equation 5.11}$$

$$-d\sigma = RT[\Sigma(\Gamma_1 + \Gamma_2)]dlnc_T) \qquad \textbf{Equation 5.12}$$

The total surface Gibbs adsorption Γ_T

$$\Sigma\Gamma_T = -\frac{1}{RT}\frac{d\sigma}{d\ln(c_T)} \qquad \textbf{Equation 5.13}$$

Where σ = surface/interfacial tension

Γ_i = surface excess adsorption of ith species

c_i = bulk surfactant concentrations of ith species

μ_i = chemical potential of ith species

R= Universal gas constant

T= temperature at which surface tension measurement is made

147

In order to account for the effect of the inorganic salts a thermodynamic approach as followed by Gurkov et.al[26] was applied to this study. Accordingly a suitable Gibbs isotherm form was used as follows

$$\Gamma^s = \frac{1}{RT} \frac{d\sigma}{d \ln(aa_t)} \qquad \textbf{Equation 5.14}$$

Activity of surfactant $a = (\gamma_\pm^{NaCl}) c_{surf}$

Total activity $a_t = a + \gamma_\pm^{NaCl} c_{NaCl}$

For consistency sake mean ionic activity is given as $c^* = (a \, a_t)^{1/2}$

R= universal gas constant , σ = surface tension, $\gamma_{\pm} =$ mean ionic activity coefficient

Gurkov et al[26]. proposed that the σ versus ln $(a \, a_t)$ isotherm can be fitted using

$$\sigma = z_0 + z_1 \ln(aa_t) + z_2 (\ln(aa_t))^2 + z_3 (\ln(aa_t))^3 + \cdots \textbf{Equation 5.15}$$

Where z_i are the coefficients of the fitted equations using Equation 5.15

Since the brine used in this study is sea water and it consists of monovalent and divalent salts, the Pitzer model is used to get the activity coefficients for this system. Details of derivations and the interaction parameters used to calculate the activity coefficient can be found in Pitzer's work[27]. The activity coefficients are found in Table 5.7. However to simplify the calculation only the effect of NaCl salt is taken into account as the sea water contains NaCl in the largest proportion.

Salts	Molality(moles/kg water)-C	Activity coefficient $\gamma_\pm$	γC
NaCl	0.461	0.616	0.284
$MgCl_2$	0.0548	0.323	0.017
$CaCl_2$	0.0119	0.295	0.0035
Na_2SO_4	0.0337	0.296	0.01002

Table 5.7: Composition of sea water. All salts were added to deionized water. The ionic strength of sea water = 0.71 M

The method followed in this study was used to calculate the AOS_{14-16} surfactant molecule adsorption at air-water interface in literature[28]. A second order polynomial of form Equation 5.15 was fit to the portion of the surface/interfacial tension curve before the cmc. Using the above method described we obtained the results for LB:AOS betaine at the different interfaces as shown in Figure 5.5, Figure 5.6, Figure 5.7, Figure 5.8.

Figure 5.5 for the betaine and AOS blends at the air water interface, the Gibbs surface excess adsorption is more or less equal for AOS and the blends. Whereas LB has the lowest adsorption. If an analogy of this result is drawn to the foam rheology in porous media in the absence of oil, it is consistent with the fact that both the blends and AOS have a comparable foam rheology (foam transition ~ 85-90% gas fraction), whereas LB foam weakens after 60%. The message from the figure is that AOS and the blends have a tighter packing at the monolayers when compared to pure betaine.

Figure 5.5 LB:AOS 7:3 blend and 1:9 blend have surface excess adsorption that lie on top of each other stating that both the blends have an equal packing (of course with different

compositions as seen in the regular solution analysis) and very slightly higher than the anionic AOS.

Figure 5.5: Gibbs surface excess adsorption for LB, AOS and their blends at the air-aqueous interface
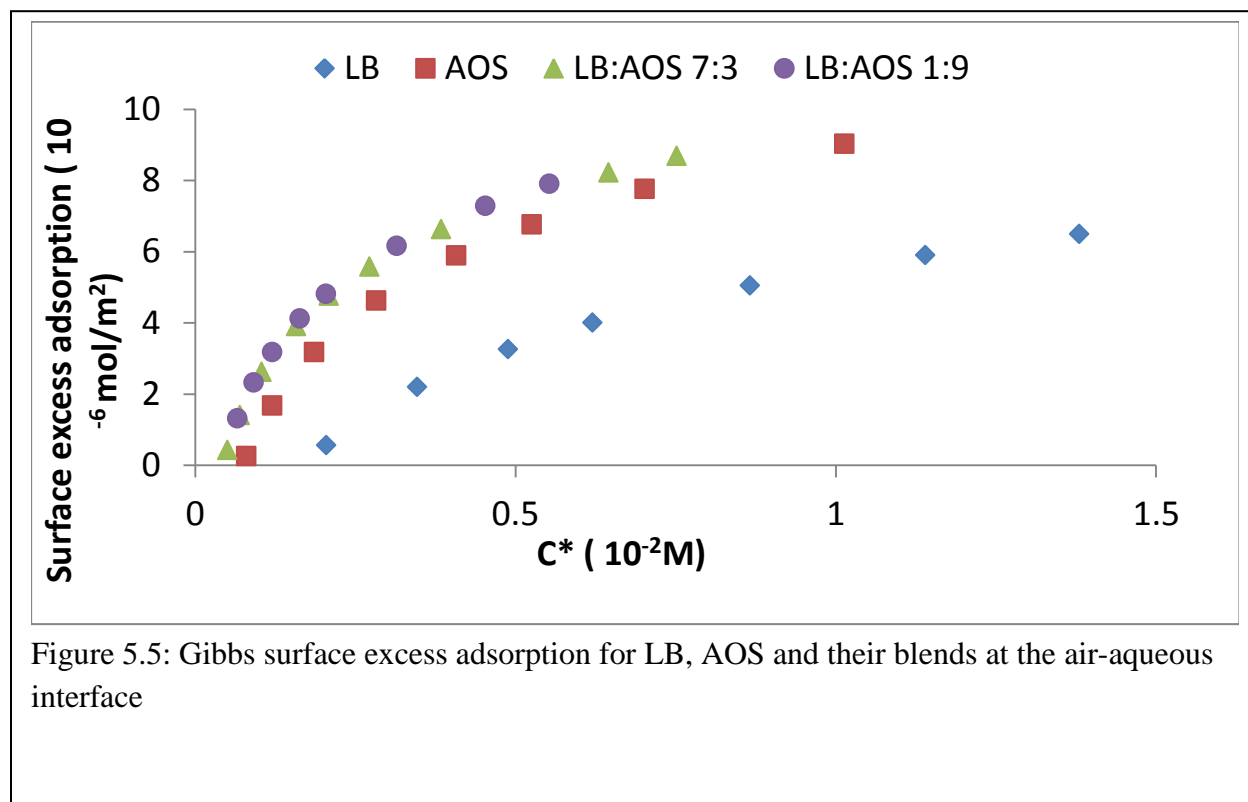
Figure 5.6 shows the Gibbs surface excess adsorption for LB, AOS and their blends at the octane water interface. It turns out that LB:AOS 1:9 has the highest adsorption, followed by AOS and LB:AOS 7:3. LB had the lowest excess surface adsorption. Indeed the foam of LB was the weakest against crude oil. The rest of the surfactant solutions (AOS, LB:AOS 1:9, LB:AOS 7:3) were all able to foam with a strength comparable to their performance in the absence of oil, after certain amount of oil was displaced.
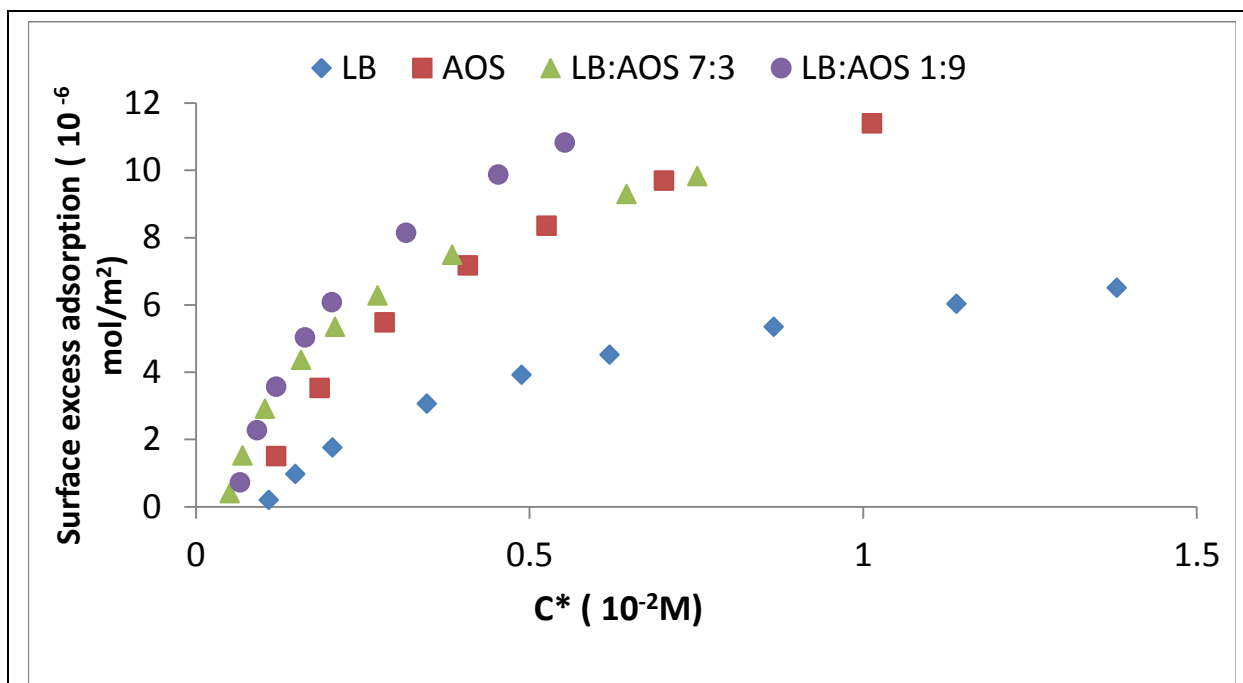
Figure 5.6: Gibbs surface excess adsorption for LB, AOS and their blends at the octane-aqueous interface

Figure 5.7 shows the Gibbs surface excess adsorption for LS (sultaine), AOS and their blends at the air water interface. Strangely both LS:AOS 8:2 and pure LS have low and almost equal surface adsorption. Whereas AOS and LS:AOS 1:9 have a higher and more or less same adsorption. The foam rheology in porous media in the absence of oil was comparable for AOS, LS:AOS 1:9 and 8:2. But the Gibbs adsorption shows a lower value for LS:AOS 8:2. Regular solution theory predicted more synergism (negative value) for LS:AOS 8:2 blend than the LS:AOS 1:9(positive value) blend, has given a different message with regard to the Gibbs excess adsorption. LS:AOS 1:9 indicates that the packing is tighter and hence more adsorption. The Gibbs surface excess adsorption for LS- AOS blends requires additional research with respect to the interpretation of foam rheology in porous media.

151
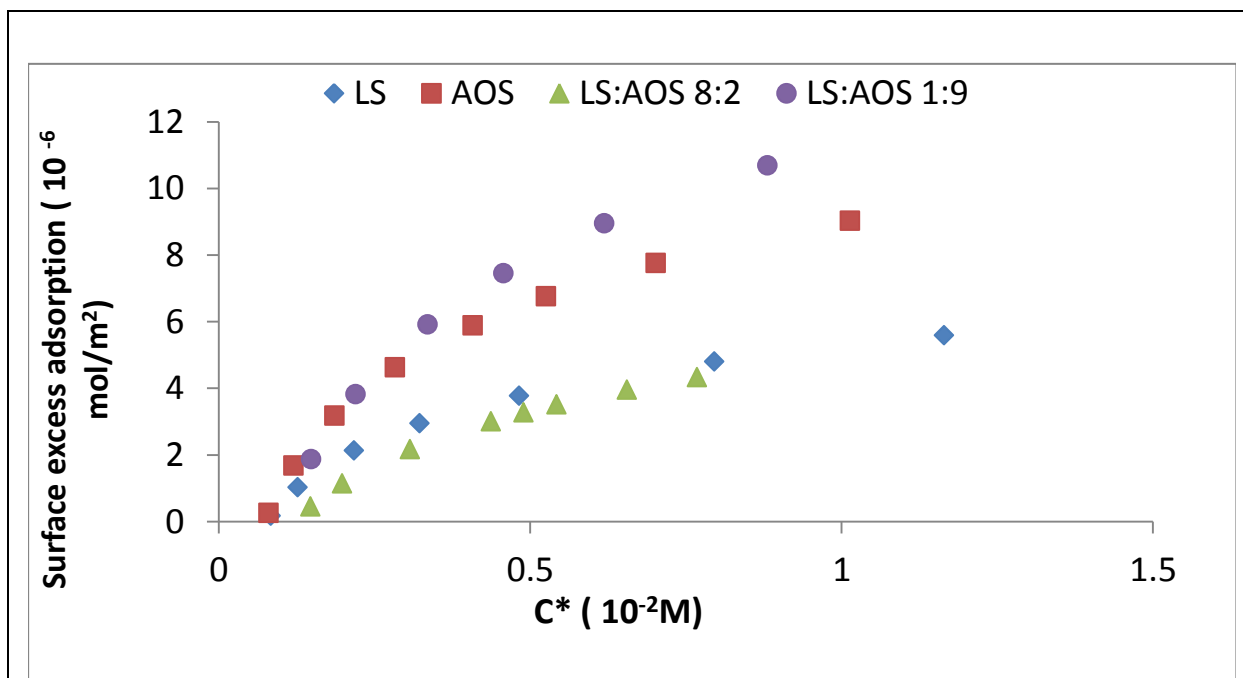
Figure 5.7: Gibbs surface excess adsorption for LS, AOS and their blends at the air-aqueous interface

Figure 5.8 shows the surface adsorption for LS, AOS and their blends at the octane-water interface. The surface adsorption shows that AOS and the blend LS:AOS 1:9 have the highest value which is consistent with the foam rheology observed in the presence of oil (Chapter 4, Figure 4.28). LS had the weakest foam performance and blend LS:AOS 8:2 was slightly better than the pure sultaine solution. Similarly the Gibbs adsorption for the blend LS: AOS 8:2 is in between sultaine and AOS, LS:AOS 1:9 blend.

Hence the Gibbs surface excess adsorption shows some correlation with the porous media foam rheology both in the presence and absence of oil. There is a slight discrepancy observed with the LS:AOS 8:2 blend in the air liquid interface. However in the case of the LB and AOS blends correlation with foam porous media rheology is acceptable. Even the LS and AOS blends

with respect to octane-aqueous interface shows correlation with foam behavior in porous media

in the presence of crude oil.
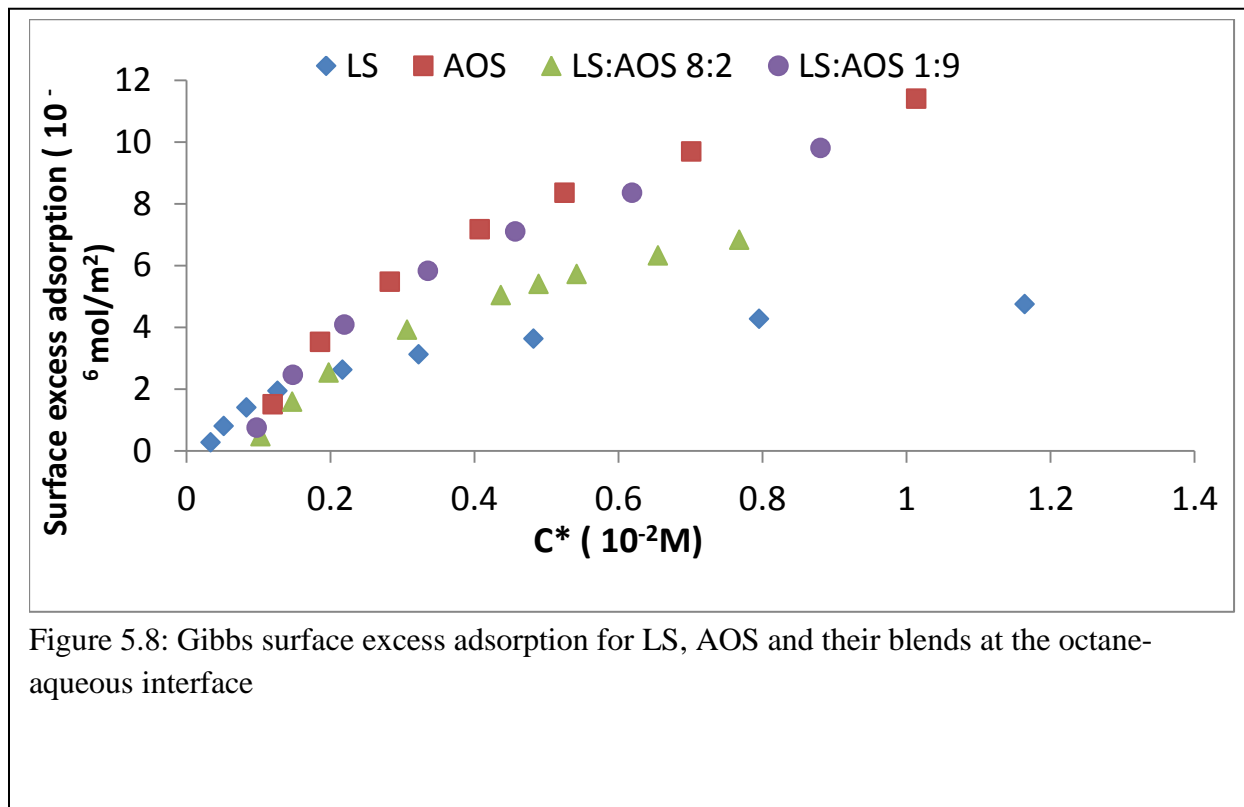
Figure 5.8: Gibbs surface excess adsorption for LS, AOS and their blends at the octane-aqueous interface

Figure 5.9 and **Error! Reference source not found.** compare the Gibbs surface excess

dsorption at the asymmetric interfaces (air-water and octane-water) for LB/AOS blends and

LS/AOS blends respectively. In all the cases the surface excess adsorption is slightly higher for

the octane water interface than the air water interface with the exception being LS. In the case of

LS the surface excess adsorption is slightly higher for the air-water interface close to the CMC.

There is no correlation between the interfaces to give enough understanding with respect to film

stability and surfactant behavior. For AOS, LB:AOS 1:9 and LS:AOS 8:2, the packing seems to

be tighter at the octane water interface than air water interface. However, the porous media

rheology showed that LS:AOS 8:2 was not a strong foamer in the presence of crude oil. This

work needs further research.
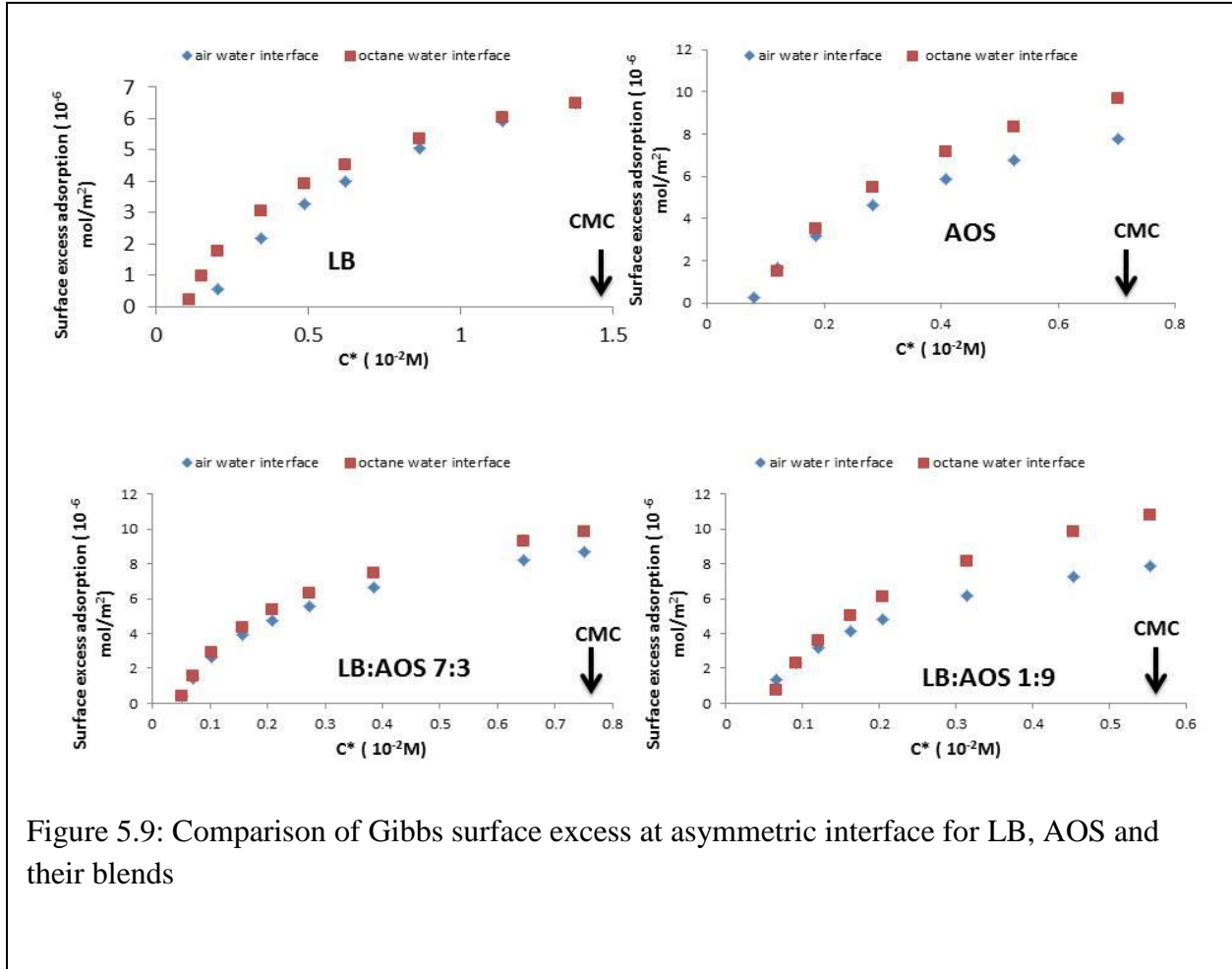
Figure 5.9: Comparison of Gibbs surface excess at asymmetric interface for LB, AOS and their blends

The area occupied per molecule can be calculated from the Gibbs surface excess by the

following Equation 5.16

$$a_s = \frac{10^{\wedge}16}{N\Gamma} \left(\mathring{A}^2 \right) \qquad \text{Equation 5.16}$$

Where a_s = area occupied per molecule in $\mathring{A}^2$

Γ = Gibbs surface excess (mol/cm^2)

N= Avagadro's number
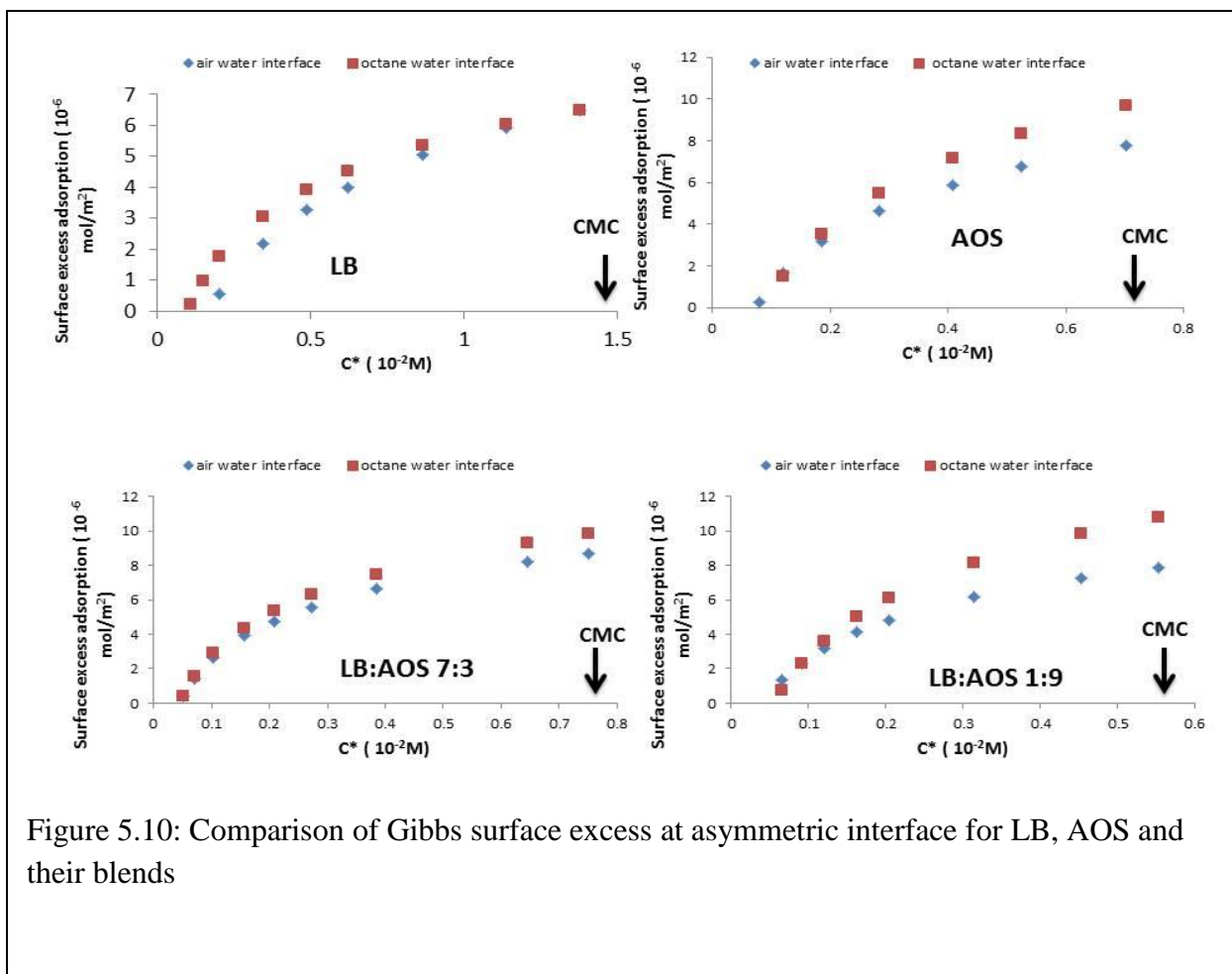
Figure 5.10: Comparison of Gibbs surface excess at asymmetric interface for LB, AOS and their blends

Table 5.8 shows the area occupied per molecule at the air-water and octane-water interface at the CMC, for the different surfactants. At the air water interface AOS, LB:AOS 7:3 and 1:9 blends and LS:AOS 1:9 show values close to that of a single straight hydrocarbon chain (~ 20 Å^2). This indicates the surfactant molecules are well packed. The LB and LS have a higher value of area occupied per molecule. This is consistent with the fact both LB and LS are not good foamers in porous media. LS:AOS 8:2 shows a value higher than LS and LB. This may be due to experimental error. At the octane water interface LB, LS and LS:AOS 8:2 occupy a higher area per molecule, indicating weaker packing. This is consistent with the porous media observation that foam for LB, LS and LS:AOS 8:2 were weak in the presence of crude oil. AOS,

LB:AOS 7:3 and 1:9 and LS:AOS 1:9 have area occupied per molecule close to ~ 15-20 $Å^2$ indicating tight packing (values lower than 20 $Å^2$may be due to slight experimental error). In porous media foam for AOS, LB:AOS 7:3, 1:9 and LS:AOS 1:9 recovered after a certain amount of oil was displaced.

Name of Surfactant	Area per molecule ($Å^2$) air water interface	Area per molecule ($Å^2$) octane water interface
LB	28.13	27.53
AOS	21.39	17.12
LB:AOS 7:3	20.18	17.85
LB:AOS 1:9	21.00	15.34
LS	29.69	34.93
LS:AOS 8:2	38.32	24.31
LS:AOS 1:9	18.54	19.88

Table 5.8: Area occupied per molecule at the air-water and octane-water interface at the CMC

5.3 Surface rheology

Amphiphilic molecules are capable of spontaneously adsorbing at the air water interface or even the oil water interface thereby causing a decrease in the surface/interfacial tension. Surfactant foam stability is governed by the thin liquid film enclosed between the gaseous phases on either side. The stability of the thin film in turn depends on the nature of the surfactant, its structure, concentration, electrolyte environment, temperature etc.

The three main mechanisms for foam collapse are a) liquid drainage, b) Oswald ripening or coarsening which occurs due to the difference in Laplace pressures of different bubble sizes causing gas to diffuse from small bubbles to large bubbles and c) coalescence when two bubbles come together and foam a large bubble.

When surfactant foams films are formed, capillary suction can cause the liquid in the thin film to flow into the Plateau border which in turn locally increases the surface tension. However

in the surface or interface a surface tension gradient is established which causes surfactant molecules to flow in the opposite direction. This fundamental and well known mechanism is called Gibbs-Marangoni flow and is the essence behind stabilizing foam films[29]. This phenomenon also occurs when a film is dilated or stretched. This resistance to deformation can be measured as elasticity and is known to be an important contribution to foam film stability.

Some measurements have provided an insight that a high dilational and compressional elasticity value correlates to bulk foam stability[30–34] and some others show dilational viscosity has some correlation with lamella stability[35]. A wide number of studies have also shown that surface shear viscosity is related to bulk foam stability[36–39] with special emphasis on a mixture of anionic SDS and cationic CTAB/CTAC which showed that when both surfactants had same chain length there was maximum packing at the interfaces thereby giving the maximum film stability[40,41]. Mixtures of zwitterionic cocoamidopropyl betaine (CAPB) and anionic sodium lauryl-dioxyethylene sulfate (SLES) in the presence of fatty acid showed that the addition of betaine solubilized the fatty acid in wider concentration ranges and showed an increased surface modulus , causing immobile surfaces[42]. Studies on SDS in presence of dodecanol have shown that surface shear viscosity can slow down liquid drainage and cause a symmetric drainage in foam films[43]. Hence the viscoelastic properties of a surfactant film have gained importance.

It has been studied using a model that blending of (CAPB) and SDS gives rise to Gibbs elasticity which is thought to be a possible factor for foam stability[44]. Here CAPB is the more surface active among the two. Following these observations there was interest in understanding the surface rheological properties of AOS and the zwitterionic (LB/LS) blends. These surfactant solutions showed comparable foam rheology in porous media and hence it was thought perhaps the surface rheological properties might be more pronounced for AOS and the blends than the

zwitterionics alone. Gibbs surface excess calculation as well supported tighter packing in the blends and AOS monolayers.

It has to be pointed out that surface intrinsic viscosity is different from surface apparent viscosity. In surface intrinsic viscosity, typically for an insoluble monolayer, the measurement is made on a two dimensional surface which has no interaction with the subphase (layer below the monolayer). Whereas in the case of soluble surfactants like the ones used in this study, there is interaction between the monolayer and the subphase which actually makes the measurement in some sense three dimensional. Hence making measurements for soluble surfactants should be considered as a surface excess quantity as it depends on the subphase environment in giving the necessary stress strain relationship. A brief review is found in literature and references therein[45].

Shear interfacial rheological studies have been done for a number of soluble monolayer surfactant systems and have concluded that these solutions don't possess any surface viscosity except Sodium Lauryl sulfate in the presence of lauric acid and lauryl alcohol[46]. Another recent study also performed measurements on many soluble surfactant systems and concluded that there is no surface shear viscosity that can be measured and hence no correlation between foam stability and surface shear viscosity[47]. Based on some conjectures proposed in literature on betaine being a foam booster [48] it was decided to measure the surface shear viscosity as a possible explanation of the tightly packed monolayer of the LB/LS- AOS blended surfactant solutions.

Experimental technique:

The instrument used to measure the interfacial rheology was the magnetic rod interfacial stress rheometer. It was set up at Stanford University. A description with a detailed schematic

diagram can be found in reference done in the same laboratory[49]. The magnetic probe that was used in this study had a length of 37.9 mm, diameter of 0.4 mm and weight of 17.5 mg. The width between the probe and the channel wall was 3.3 mm. The magnetic probe was placed inside a channel made of Teflon. All the surfactant solutions were at a total concentration of 0.5wt% made in sea water. Figure 5.11 are the results obtained for the individual surfactants LB, LS, AOS and the blends LB:AOS 1:9, LS:AOS 1:9. The results show that none of the surfactants had any measureable surface shear viscosity and hence there can be no correlation deduced between the surface shear viscosity and foam rheology in porous media. The results agree with observations in literature[47].

Figure 5.11: Surface viscosity of the surfactant samples in a frequency dependence mode. The solutions were made in sea water. DI water is used as a reference[37] for comparison and the value is very close to ~0.01 mPa.s.m. This shows that the surfactant solutions do not possess any measureable surface viscosity.
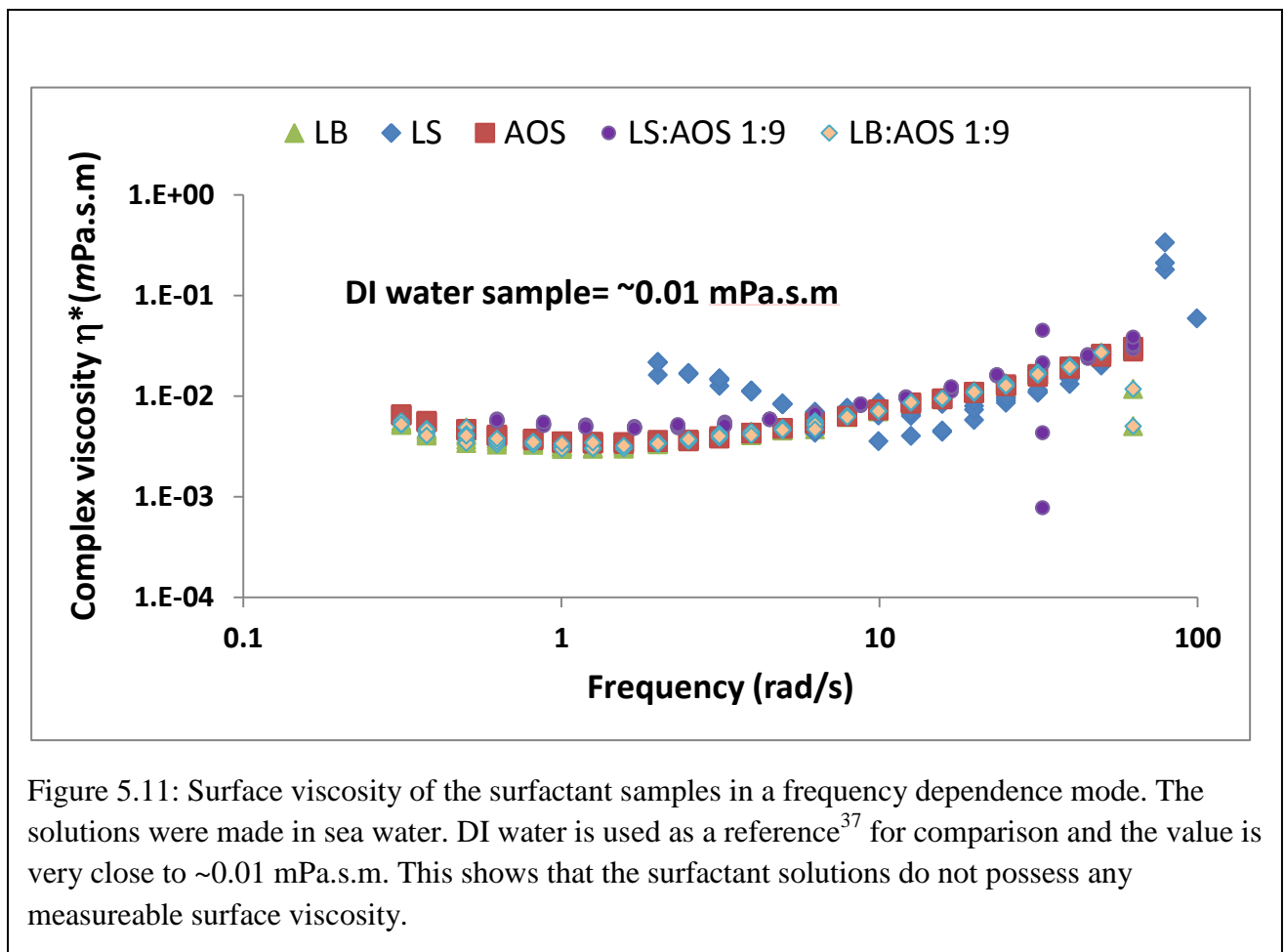
5.3 Film drainage experiments

The set up used to study the film drainage was a patented product called i-DDrOP Interfacial Dewetting and Drainage Optical Platform [50,51] set up at Stanford University. A picture of the apparatus is found in Figure 5.12. The set up consists of a Teflon reservoir which contains the desired surfactant solution. A capillary tube of inner diameter 0.066 inch and outer diameter 0.078 inch is fitted inside the reservoir such that the open end is filled with surfactant solution. The capillary tube is connected to a syringe pump. The syringe pump is used to inject an air bubble which helps to generate a surfactant bubble in the shape of an inverted pendant drop. The reservoir is set on a stage, the speed of which is controlled by a computer software. The stage is lifted slightly to fill the capillary tube with solution. Then at a constant flow rate of 0.6 ml/s an air bubble is introduced inside the capillary. Following this the reservoir stage is lowered down at a set speed for all experiment to aid in the formation of an inverted pendant shape soap bubble. The image of film drainage is monitored through a CCD camera. To ensure all the bubbles formed were of same size, the speed of lowering the stage, air bubble injection and the distance up to which the stage is lowered were all maintained constant for all the experiments. These experiments helped to observe the following images which give us some qualitative understanding of the surfactant solutions with respect to thin film dynamics. The surfactant systems that were studied were LB, LS, AOS, LB: AOS 7:3, LB: AOS 1:9, LS: AOS 8:2 and LS: AOS 1:9. All experiments were repeated for a minimum of three times. The time taken for the film to thin was more or less the same in each attempt.

5.3.1 Discussion of film thinning process

Pictures of film thinning process are shown for AOS (0.5wt% prepared in sea water) in Figure 5.13, and for LB:AOS 1:9 blend (0.5wt% prepared in sea water) in Figure 5.14. Following which a summary of the drainage experiments is tabulated.

In the case of all surfactant films the colored zones in the figure show the thick film region which is greater than 100 nm. Those colored patterns that are present are due to the interference of the reflected rays of white light from both the interfaces of the thin liquid film. The pattern appears due to Maragoni flow. As time progress the film thins and black holes start to form. This type of behavior has been observed in literature and called as stratification or step wise film thinning which occurs due to the micellar structuring in the thin film [52,53]. As time progresses the black holes gradually grow and occupy the frame. The films formed in this study thin down due to flow of liquid downward as a result of gravity and also due to evaporation.

Figure 5.13 shows the step by step thinning with the time taken to come to each stage. Three to four trials for each surfactant solution were made. For this particular trial AOS film ruptured in 24 seconds. Step 1-4 show Maragoni flow patterns as the film continues to thin. Step 5 shows the formation of black holes. Step 6 shows that the black holes start to cover up the frame of observation. This leads to the formation of Newton black film. As time progresses, step 7 shows that the film ruptures.
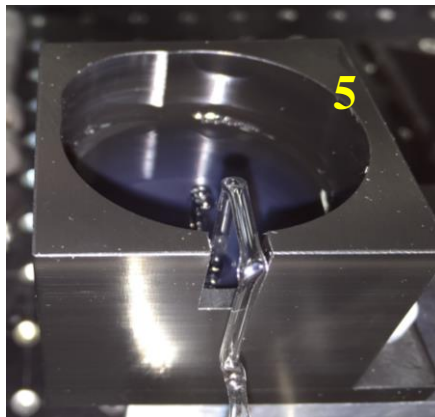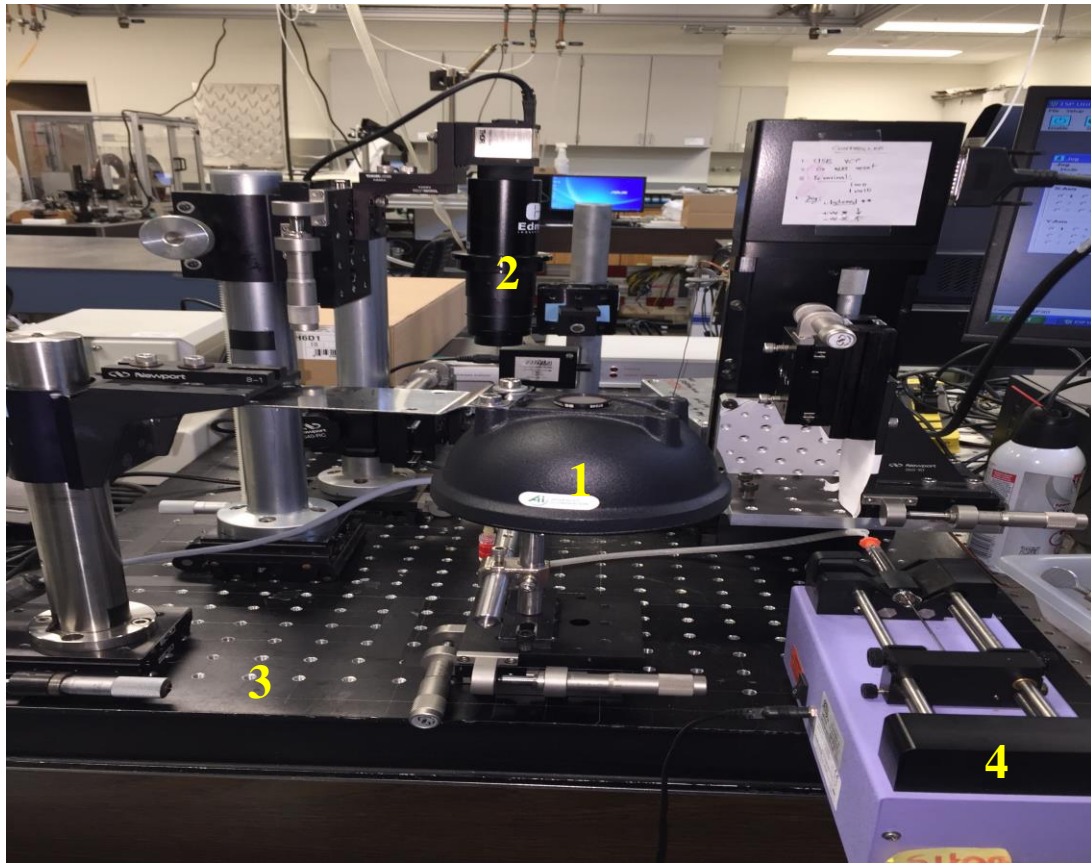
Figure 5.12: Film drainage set up used. The parts numbered are 1- white LED illumination dome , 2- CCD camera, 3- vibration free platform on which set up is built, 4- syringe pump to incorporate an air bubble, 5- the Teflon reservoir filled with surfactant solution and open end of capillary tube is immersed into the reservoir. The capillary tube is connected to the syringe pump. The reservoir is placed underneath the dome as an inverted pendant surfactant bubble is created by air injection into the capillary. The stage on which the reservoir is mounted is computer controlled. The camera is connected to a computer to record the dynamic process of film thinning and eventual rupture.

Figure 5.14 is the film thinning process for LB:AOS 1:9 solution. This film thinning process showed remarkable stages. Steps 1-3 show the drainage of film and the patterns are due to Gibbs-Marangoni flow. The film drainage was significantly slow as the colored film is almost visible for ~ 42 seconds as compared to AOS film which lasted for ~ 13 seconds. In steps 4-5 black holes start to appear. Step 6 shows that these black holes grow to occupy the frame of observation. This is indicative of a thin Newton black film. Step 7 show some interesting features appears. On a black film tiny green colored spots seem to move around for ~ 2 minutes. The whole film of LB:AOS 1:9 takes about ~ 7 minute to rupture. It should be noted that for all the cases evaporation is a contributing factor for film thinning.

When two surfaces of a film come close together the force exerted by them over unit area is called the disjoining pressure. This value is governed by the surfactant structure, the aqueous environment like salt among other reasons. The LB:AOS 1:9 might have a high value of positive disjoining pressure mostly due to the electrostatic repulsion between the interfaces which can keep the film of a certain thickness stable. This has to do with the monolayer composition of the surfactants. It seems like when AOS content is higher (in a LB and AOS mixed monolayer) at either side of the thin liquid film there might be enough repulsion to keep the film from closing. Indeed the zwitterionic molecule might contribute to shielding the repulsions within the monolayer which can cause a tighter packing and resists rupture.

Table 5.9 summarises the film drainage experiments. In terms of longevity of the black film both the zwitterionic surfactants LB, LS have ruptured almost instantaneously. Even LB:AOS 7:3 film ruptured instantaneously. The most stable film obtained in terms of longevity was that of LB:AOS 1:9. Surfactant films of AOS, LS:AOS 8:2 , LS:AOS 1:9 were intermediate

between these two cases. In case of the transition from thick film to thin film LB, LS:AOS 1:9 were the fastest. The rest more or less had the same time ~ 30 seconds.

Following these studies we see there is no correlation with foam rheology of these surfactants in porous media and film drainage experiments. In porous media in the absence of oil, AOS and all the blends seemed to have comparable foam rheology and also foam strength. However none of the surfactants had any measureable interfacial shear rheology. The one thing in common with all is that LB, and LS the zwitterionic surfactant foam were neither strong in terms of porous media rheology and the film drainage studies showed their rupture almost instantaneously. These studies show that there is a more complex phenomenon occurring for foam flow in porous media since there are interactions with the geo chemistries of the rock surface and the surfactant molecules, as well as the intermolecular and intramolecular surfactant interactions along with the brine. Those dynamics cannot be captured by bulk measurements, though some qualitative understanding can be developed. One consistency with observations in literature[43] is that all the surfactant solutions had asymmetric drainage and had no measureable interfacial rheology.
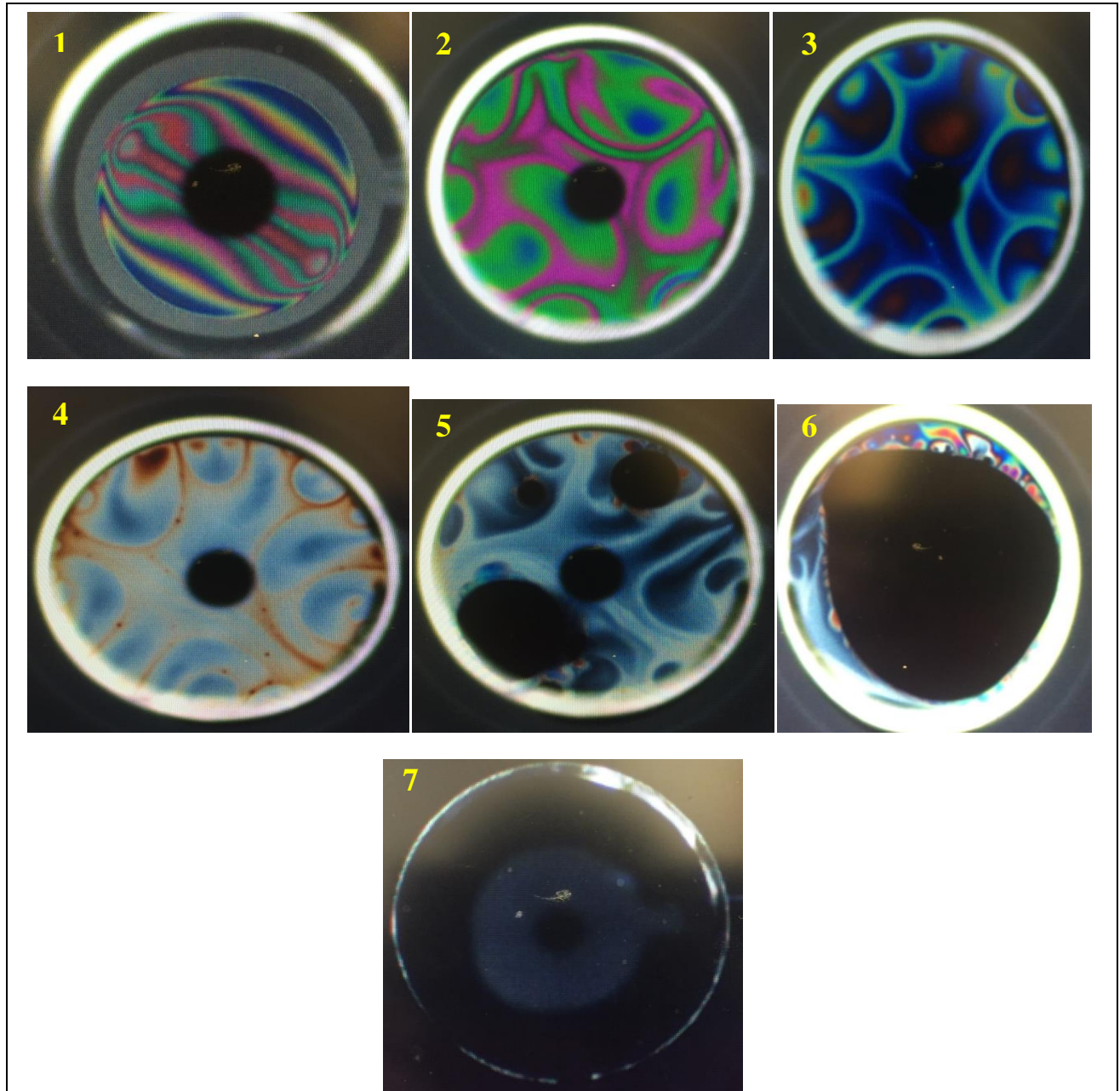
Figure 5.13: : Film thinning process for AOS (0.5 wt% made in sea water). Steps 1-4 indicate the drainage of a thick film as indicated by the colored patterns seen. One can observe the Maragoni flow during the asymmetric drainage . Step 5 shows the formation of holes or called black film. Foam stability is goverened by the stability of this black film. Step 6 shows the holes all join together and form Newton black film that has considerably thinned down. Step 7 the film ruptures. Time of the screen shot 1-1s, 2- 5s, 3- 10s, 4-13s, 5-18s, 6-19s, 7- 24s
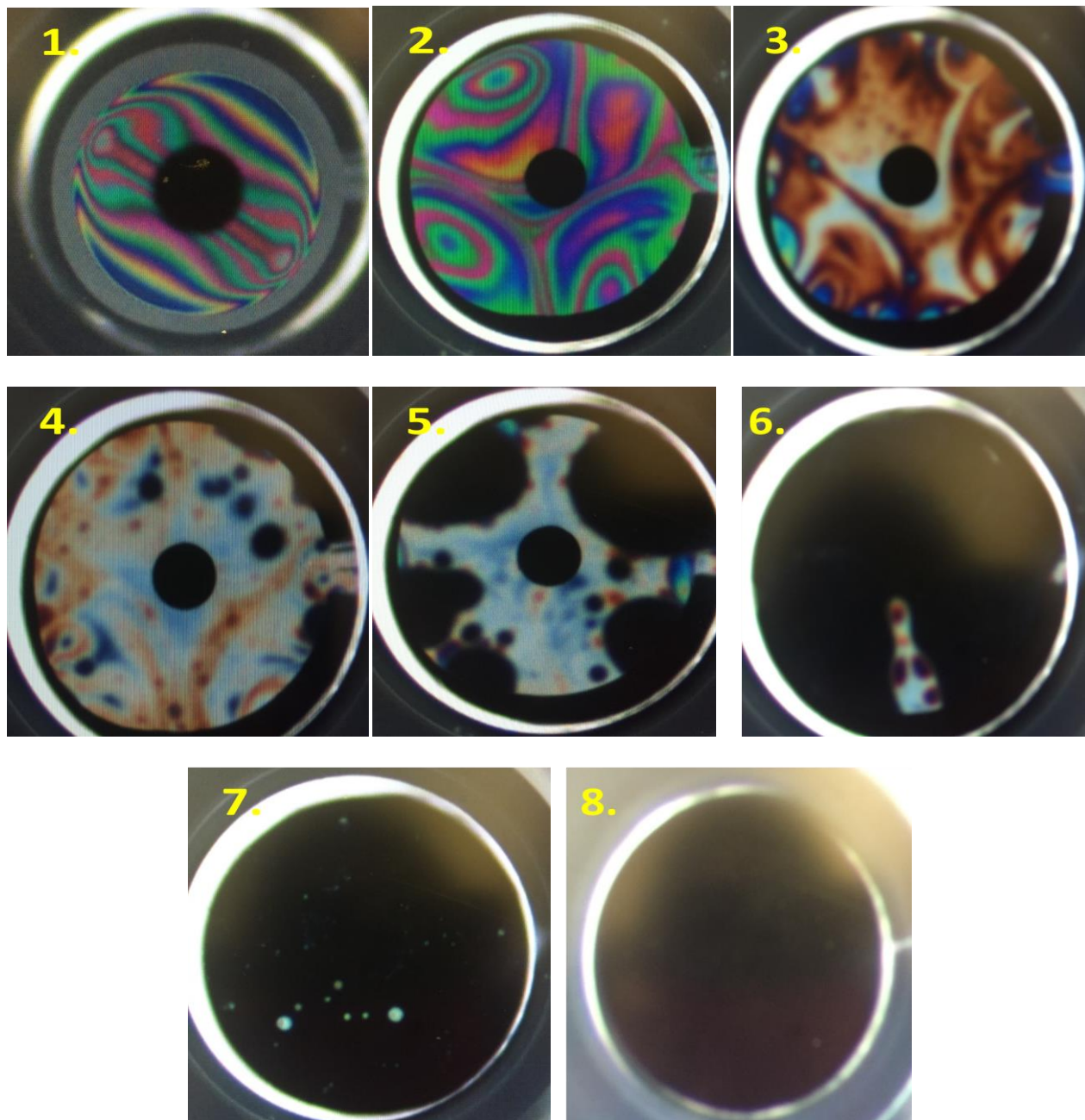
Figure 5.14 Film thinning process for LB:AOS 1:9 (0.5 wt% made in sea water). Steps 1-3 indicate the drainage of a thick film as indicated by the colored patterns seen. Step 4-5 shows the formation of holes or called black film. This is a metastable state. Step 6 shows the holes all join together and form Newton black the film has considerably thinned down. Step 7 is unique to this surfactant blend. Step 8- Film ruptures. Time of the screen shot 1-1s, 2- 16s, 3- 31s, 4-42s, 5-52s, 6-59s, 7- 2min 26 s, 8- 6min 58s.

Surfactant	Time taken for drainage (Thick film)	Time taken by black holes to cover the frame of observation(Formation of thin film)	Longevity of the black film
LB	~10 seconds	Ruptures immediately	N/A
LS	~37 seconds	~6 seconds	Less than 1 second
AOS	~21-30 seconds	~2-6 seconds	~10-20 seconds
LB:AOS 7:3	~33 seconds	~5 seconds	Ruptures immediately
LB:AOS 1:9	~35 seconds	~27 seconds	~5- 6 mintues
LS:AOS 8:2	~30 seconds	~8 seconds	~49 seconds
LS:AOS 1:9	~16-19 seconds	~ 3 seconds	~0-2.5 minutes(two different trials gave different values)

Table 5.9: Summary of film drainage experiments. LB:AOS 1:9 seemed to have the most stable black film as judged by the longevity of the film. In terms of longevity of black film LB:AOS 1:9>LS:AOS 8:2> AOS~= LS:AOS 1:9> LS=LB:AOS 7:3 >LB

5.4 Conclusions

The following conclusions can be drawn from the studies on surfactant synergism

- Regular solution theory: The LB and AOS blends exhibit a more pronouced synergism both in the air-water and octane-water inteface when compared to the LS and AOS blends. The reason most likely is because the carboxylate group in the betaine is capable of getting protonated which leaves the positive quartenary ammonium interacting with the anionic AOS. The sultaine SO_3^- cannot be easily protonated and hence there is some repulsion between the negative anionic and negative SO_3^- group. However the presence of synergistic interactions did not boost foam apparent viscosity to any better value than pure AOS.

167

- Gibbs surface excess adsorption:

    - In th case of LB and AOS blends the surface adsorption is highest for AOS and the blends and lowest for LB at the air-water. This is consistent with studies in porous media in the absence of oil. In the case of octane-water interface the surface adsorption is highest for the LB:AOS 1:9 blend but the blend LB:AOS 7:3 and AOS are very close and just slightly lower than 1:9 blend. This is also consistent with porous media foam rheology in the presence of oil ,where AOS, LB:AOS 1:9 and LB:AOS 7:3 all had comparable foam strength ,to their own performance in the absence of oil, once some amount of oil was recovered. The message being that the foam was capable of generation even in the presence of waterflood oil , had mobility to recover oil and build up its strength. Whereas the LB foam was so weak that it could barely regain any apparent viscosity.

    - In the case of LS and AOS blends, the surface excess adsorption in the air-water interface correlate well for the AOS, LS:AOS 1:9 blend foam rheology in porous media in the absence of oil. However there is some slight discrepancy for the LS:AOS 8:2 blends signifying that the packing is not tight enough. In the case of octane-water interface the surface adsorption show a trend very similar to the trend observed in porous media in the presence of oil.

- Surface rheology: None of the surfactant systems studied had any measurable shear rheology. This is consistent with literature that most soluble surfactant (small molecules like C_{12} chain) monolayers have negligible shear viscosity.

- Film drainage: The LB:AOS 1:9 blend shows the best film stability as assessed by the longevity of the black film. In terms of longevity of black film LB:AOS 1:9>LS:AOS 8:2> AOS~= LS:AOS 1:9> LS=LB:AOS 7:3 >LB. There seemed no correlation of these measurements with the foam rheology in porous media. However all the films drained asymmetrically and possessed no measurable shear rheology. This was consistent with literature[43]. Additionally the betaine film ruptured the fastest which is consistent with all porous media observation(absence of oil). The LS film ruptured in a very short time as well and the foam performance was not the strongest in porous media (absence of oil).

References:

(1) Goebel, A.; Lunkenheimer, K. Interfacial Tension of the Water/n-Alkane Interface. *Langmuir* **1997**, *13*, 369–372.
(2) Rubingh, D. N. Mixed Micelle Solutions. In *Solution Chemistry of Surfactants*; Mittal, K. L., Ed.; Springer New York, **1979**; pp. 337–354.
(3) Holland, P. M.; Rubingh, D. N. Nonideal Multicomponent Mixed Micelle Model. *J. Phys. Chem.* **1983**, *87*, 1984–1990.
(4) Zhou, Q.; Rosen, M. J. Molecular Interactions of Surfactants in Mixed Monolayers at the Air/Aqueous Solution Interface and in Mixed Micelles in Aqueous Media: The Regular Solution Approach. *Langmuir* **2003**, *19*, 4555–4562.
(5) Shiloach, A.; Blankschtein, D. Predicting Micellar Solution Properties of Binary Surfactant Mixtures. *Langmuir* **1998**, *14*, 1618–1636.
(6) Shiloach, A.; Blankschtein, D. Prediction of Critical Micelle Concentrations and Synergism of Binary Surfactant Mixtures Containing Zwitterionic Surfactants. *Langmuir* **1997**, *13*, 3968–3981.
(7) Mulqueen, M.; Blankschtein, D. Prediction of Equilibrium Surface Tension and Surface Adsorption of Aqueous Surfactant Mixtures Containing Zwitterionic Surfactants. *Langmuir* **2000**, *16*, 7640–7654.
(8) Puvvada, S.; Blankschtein, D. Theoretical and Experimental Investigations of Micellar Properties of Aqueous Solutions Containing Binary Mixtures of Nonionic Surfactants. *J. Phys. Chem.* **1992**, *96*, 5579–5592.
(9) Rosen, M. J.; Wang, H.; Shen, P.; Zhu, Y. Ultralow Interfacial Tension for Enhanced Oil Recovery at Very Low Surfactant Concentrations. *Langmuir* **2005**, *21*, 3749–3756.
(10) Rosen, M. J.; Murphy, D. S. Synergism in Binary Mixtures of Surfactants: VIII. Effect of the Hydrocarbon in Hydrocarbon/water Systems. *J. Colloid Interface Sci.* **1989**, *129*, 208–216.

(11) Rosen, M. J.; Murphy, D. S. Synergism in Binary Mixtures of Surfactants: V. Two-Phase Liquid—liquid Systems at Low Surfactant Concentrations. *J. Colloid Interface Sci.* **1986**, *110*, 224–236.

(12) Rosen, M. J.; Zhu, B. Y. Synergism in Binary Mixtures of Surfactants. *J. Colloid Interface Sci.* **1984**, *99*, 427–434.

(13) Rosen, M. J.; Zhu, Z. H.; Gao, T. Synergism in Binary Mixture of Surfactants: 11. Mixtures Containing Mono- and Disulfonated Alkyl- and Dialkyldiphenylethers. *J. Colloid Interface Sci.* **1993**, *157*, 254–259.

(14) Zhu, B. Y.; Rosen, M. J. Synergism in Binary Mixtures of Surfactants: IV. Effectiveness of Surface Tension Reduction. *J. Colloid Interface Sci.* **1984**, *99*, 435–442.

(15) Desai, T. R.; Dixit, S. G. Interaction and Viscous Properties of Aqueous Solutions of Mixed Cationic and Nonionic Surfactants. *J. Colloid Interface Sci.* **1996**, *177*, 471–477.

(16) Ghosh, S.; Khatua, D.; Dey, J. Interaction Between Zwitterionic and Anionic Surfactants: Spontaneous Formation of Zwitanionic Vesicles. *Langmuir* **2011**, *27*, 5184–5192.

(17) Cui, Z.-G.; Canselier, J. P. Interfacial and Micellar Properties of Some Anionic/cationic Binary Surfactant Systems. 1. Surface Properties and Prediction of Surface Tension. *Colloid Polym. Sci.* **2000**, *278*, 22–29.

(18) Hines, J. D.; Thomas, R. K.; Garrett, P. R.; Rennie, G. K.; Penfold, J. Investigation of Mixing in Binary Surfactant Solutions by Surface Tension and Neutron Reflection: Strongly Interacting Anionic/Zwitterionic Mixtures. *J. Phys. Chem. B* **1998**, *102*, 8834–8846.

(19) Eads, C. D.; Robosky, L. C. NMR Studies of Binary Surfactant Mixture Thermodynamics: Molecular Size Model for Asymmetric Activity Coefficients. *Langmuir* **1999**, *15*, 2661–2668.

(20) Misselyn-Bauduin, A. M.; Thibaut, A.; Grandjean, J.; Broze, G.; Jérôme, R. Mixed Micelles of Anionic−Nonionic and Anionic−Zwitterionic Surfactants Analyzed by Pulsed Field Gradient NMR. *Langmuir* **2000**, *16*, 4430–4435.

(21) Hoffmann, H.; Poessnecker, G. The Mixing Behavior of Surfactants. *Langmuir* **1994**, *10*, 381–389.

(22) Rosen, M. J. *Surfactants and Interfacial Phenomena*; Wiley-Interscience: Hoboken, N.J., **2004**.

(23) Huang, L.; Somasundaran, P. Theoretical Model and Phase Behavior for Binary Surfactant Mixtures. *Langmuir* **1997**, *13*, 6683–6688.

(24) Lu, J. R.; Thomas, R. K.; Penfold, J. Surfactant Layers at the Air/water Interface: Structure and Composition. *Adv. Colloid Interface Sci.* **2000**, *84*, 143–304.

(25) Chattoraj, D; Birdie,K.S. *Adsorption and the Gibbs Surface Excess*; Springer Science & Business Media, **2012**.

(26) Gurkov, T. D.; Dimitrova, D. T.; Marinova, K. G.; Bilke-Crause, C.; Gerber, C.; Ivanov, I. B. Ionic Surfactants on Fluid Interfaces: Determination of the Adsorption; Role of the Salt and the Type of the Hydrophobic Phase. *Colloids Surf. Physicochem. Eng. Asp.* **2005**, *261*, 29–38.

(27) Pitzer, K. S.; Mayorga, G. Thermodynamics of Electrolytes. II. Activity and Osmotic Coefficients for Strong Electrolytes with One or Both Ions Univalent. *J. Phys. Chem.* **1973**, *77*, 2300–2308.

(28) Farajzadeh, R.; Krastev, R.; Zitha, P. L. J. Foam Films Stabilized with Alpha Olefin Sulfonate (AOS). *Colloids Surf. Physicochem. Eng. Asp.* **2008**, *324*, 35–40.

(29) D. T. Wasan; K. Koczo; A. D. Nikolov. Mechanisms of Aqueous Foam Stability and Antifoaming Action with and without Oil. In *Foams: Fundamentals and Applications in the Petroleum Industry*; Advances in Chemistry; American Chemical Society, **1994**; Vol. 242, pp. 47–114.

(30) Georgieva, D.; Cagna, A.; Langevin, D. Link between Surface Elasticity and Foam Stability. *Soft Matter* **2009**, *5*, 2063.

(31) Langevin, D. Influence of Interfacial Rheology on Foam and Emulsion Properties. *Adv. Colloid Interface Sci.* **2000**, *88*, 209–222.

(32) Wantke, K.; Małysa, K.; Lunkenheimer, K. A Relation between Dynamic Foam Stability and Surface Elasticity. *Colloids Surf. Physicochem. Eng. Asp.* **1994**, *82*, 183–191.

(33) Sonin, A. A.; Bonfillon, A.; Langevin, D. Thinning of Soap Films: The Role of Surface Viscoelasticity. *J. Colloid Interface Sci.* **1994**, *162*, 323–330.

(34) Bergeron, V. Disjoining Pressures and Film Stability of Alkyltrimethylammonium Bromide Foam Films. *Langmuir* **1997**, *13*, 3474–3482.

(35) Fruhner, H.; Wantke, K.-D.; Lunkenheimer, K. Relationship between Surface Dilational Properties and Foam Stability. *Colloids Surf. Physicochem. Eng. Asp.* **2000**, *162*, 193–202.

(36) Brown, A. G.; Thuman, W. C.; McBain, J. W. The Surface Viscosity of Detergent Solutions as a Factor in Foam Stability. *J. Colloid Sci.* **1953**, *8*, 491–507.

(37) Shah, D. O.; Djabbarah, N. F.; Wasan, D. T. A Correlation of Foam Stability with Surface Shear Viscosity and Area per Molecule in Mixed Surfactant Systems. *Colloid Polym. Sci.* **1978**, *256*, 1002–1008.

(38) Kanicky, J. R.; Poniatowski, A. F.; Mehta, N. R.; Shah, D. O. Cooperativity among Molecules at Interfaces in Relation to Various Technological Processes: Effect of Chain Length on the pKa of Fatty Acid Salt Solutions†. *Langmuir* **2000**, *16*, 172–177.

(39) Chattopadhyay, A. K.; Ghaicha, L.; Oh, S. G.; Shah, D. O. Salt Effects on Monolayers and Their Contribution to Surface Viscosity. *J. Phys. Chem.* **1992**, *96*, 6509–6513.

(40) Patist, A.; Chhabra, V.; Pagidipati, R.; Shah, R.; Shah, D. O. Effect of Chain Length Compatibility on Micellar Stability in Sodium Dodecyl Sulfate/Alkyltrimethylammonium Bromide Solutions. *Langmuir* **1997**, *13*, 432–434.

(41) Patist, A.; Huibers, P. D. T.; Deneka, B.; Shah, D. O. Effect of Tetraalkylammonium Chlorides on Foaming Properties of Sodium Dodecyl Sulfate Solutions. *Langmuir* **1998**, *14*, 4471–4474.

(42) Golemanov, K.; Denkov, N. D.; Tcholakova, S.; Vethamuthu, M.; Lips, A. Surfactant Mixtures for Control of Bubble Surface Mobility in Foam Studies. *Langmuir* **2008**, *24*, 9956–9961.

(43) Joye, J.-L.; Hirasaki, G. J.; Miller, C. A. Asymmetric Drainage in Foam Films. *Langmuir* **1994**, *10*, 3174–3179.

(44) Danov, K. D.; Kralchevska, S. D.; Kralchevsky, P. A.; Ananthapadmanabhan, K. P.; Lips, A. Mixed Solutions of Anionic and Zwitterionic Surfactant (Betaine): Surface-Tension Isotherms, Adsorption, and Relaxation Kinetics. *Langmuir* **2004**, *20*, 5445–5453.

(45) Stevenson, P. Remarks on the Shear Viscosity of Surfaces Stabilised with Soluble Surfactants. *J. Colloid Interface Sci.* **2005**, *290*, 603–606.

(46) Gupta, L.; Wasan, D. T. Surface Shear Viscosity and Related Properties of Adsorbed Surfactant Films. *Ind. Eng. Chem. Fundam.* **1974**, *13*, 26–33.

(47)   Zell, Z. A.; Nowbahar, A.; Mansard, V.; Leal, L. G.; Deshmukh, S. S.; Mecca, J. M.; Tucker, C. J.; Squires, T. M. Surface Shear Inviscidity of Soluble Surfactants. *Proc. Natl. Acad. Sci.* **2014**, *111*, 3677–3682.

(48)   Farajzadeh, R.; Andrianov, A.; Krastev, R.; Hirasaki, G. J.; Rossen, W. R. Foam–oil Interaction in Porous Media: Implications for Foam Assisted Enhanced Oil Recovery. *Adv. Colloid Interface Sci.* **2012**, *183–184*, 1–13.

(49)   Brooks, C. F.; Fuller, G. G.; Frank, C. W.; Robertson, C. R. An Interfacial Stress Rheometer To Study Rheological Transitions in Monolayers at the Air−Water Interface. *Langmuir* **1999**, *15*, 2450–2459.

(50)   Bhamla, M. S.; Fuller, G. G. United States Patent Application: 0150103315 - I-DDrOP: Interfacial Dewetting and Drainage Optical Platform.

(51)   Bhamla, M. S.; Balemans, C.; Fuller, G. G. Dewetting and Deposition of Thin Films with Insoluble Surfactants from Curved Silicone Hydrogel Substrates. *J. Colloid Interface Sci.* **2015**, *449*, 428–435.

(52)   Nikolov, A. D.; Wasan, D. T. Ordered Micelle Structuring in Thin Films Formed from Anionic Surfactant Solutions. *J. Colloid Interface Sci.* **1989**, *133*, 1–12.

(53)   Bergeron, V.; Radke, C. J. Equilibrium Measurements of Oscillatory Disjoining Pressures in Aqueous Foam Films. *Langmuir* **1992**, *8*, 3020–3026.

Chapter 6

Conclusion and Future Work

Foam injection is a well-established method for achieving mobility control in an EOR process. However the effect of oil is detrimental to the foam films and hence finding a suitable formulation is essential. Earlier work has shown betaine to behave as booster when blended with anionic surfactants both in bulk and porous media studies. Systematic core flood studies were conducted to study the effect on foam of mixing short-chain betaine/sultaine and long-chain betaine/sultaine with anionic AOS $_{14-16}$. AOS $_{14-16}$ is a popularly studied foamer in porous media and also performed well in the pilot tests in Snorre field in North Sea. This thesis helped to bring about some fundamental understanding on the behavior of foam rheology when using the zwitterionic /anionic blended surfactants in porous media both in the presence and absence of oil. The following discussion will highlight some of the important conclusions from the study.

6.1 Rheology of viscoelastic surfactant

This thesis evaluated C_{18} chain amido betaine and C_{18-22} amido betaine/sultaine surfactants for their viscoelastic properties. These zwitterionic surfactants formed wormlike micelles at very low concentrations of 0.5 wt% based on surface-active content. The purpose of using a viscoelastic surfactant was to achieve mobility control without using polymer. Also since these surfactants have very low cmcs, it was believed that they may give low interfacial tension and be suitable for an EOR process. Following are the highlights from the rheological measurements.

It was observed that increase in salinity had no effect on the C_{18-22} chain surfactant but had a prominent effect on the C_{18} chain surfactant. A similar behavior was shown in literature where a C_{22} chain betaine was unaffected in the presence of inorganic salt. However, it was

173

affected by aromatic salts[1]. Most of the surfactant studies were in sea water, which contained divalent salts. When these viscoelastic surfactants were studied in porous media, they showed shear thinning behavior very close to that obtained in the shear bulk rheology measurements. Interestingly there were no elongational effects observed in porous media mainly because wormlike micelles have the unique property where they can relax stress by breaking and reforming. One of the surfactants Rhodia C, which had a higher proportion of the C_{22} chain in its formulation, showed yield stress during flow and hence cannot be considered as a suitable candidate for injection in porous media.

In the presence of ~ 25% crude oil the C_{18} betaine lost its viscoelasticity possibly due to shortening of the wormlike micelles which led to reducing its viscosity by an order of magnitude. The other surfactants (except Rhodia C) also lost some amount of viscoelasticity in the presence of oil, however the viscoelastic nature was still maintained. Literature studies have observed that when oil enters the core of the micellar structure, it leads to loss of viscoelasticity. Whereas if oil molecules remain in the palisade layer of the micelle, the solutions tend to retain viscoelasticity or to experience increased viscoelasticity[2].

Further studies were focused on Rhodia A (C_{18} betaine) since it was less viscous and easily injectable in porous media. Rhodia A, which was weakly viscoelastic- when blended with one part of AOS $_{14-16}$, showed a phenomenal increase in viscoelasticity. This is possibly due to the synergistic effect between the positive quaternary ammonium group on the betaine and the negative AOS molecule which aids in much closer packing in the micelle.

6.2 Foam studies of zwitterionic and anionic blended surfactant in porous media

The brine used for preparing all the surfactant solutions was sea water. It had an ionic strength of 0.71 M and contained monovalent and divalent salts. When the zwitterionic surfactants Lauryl betaine (LB), Lauryl sultaine (LS) and Rhodia A were blended with AOS_{14-16}, they gave clear solutions in a very limited window of the mixing ratio. In fact LB:AOS (LB>AOS) blends at room temperature get cloudy over time and hence plug the media. But when the temperature is raised to above 40°C, they appear clear. Systematic aqueous stability tests were done with the other zwitterionic and anionic blends as well, ensuring that two compositions with clear solutions could be picked, in each case for which zwitterionic content was higher in one and lower in the other. This way the effect of blend ratio could be studied.

Systematic foam studies in the absence of oil were conducted in a 100 Darcy silica sand pack for Rhodia A and AOS blends (25°C) and in Bentheimer sandstone core for LB and AOS blends and LS and AOS blends (45°C). Foam rheology was studied as a function of gas fraction (foam quality scan) and as a function of velocity (shears thinning behavior).

The foam quality scan for both the betaines Rhodia A and LB reached the transition foam quality at ~ 60% gas fraction and for LS at 20% gas fraction. Whereas the blends with AOS especially Rhodia A:AOS 9:1 ratio has strong foam at a wide range of qualities studied. In the case of LB:AOS and LS:AOS blends the foam rheology was the same as AOS itself.

The shear thinning foam for the betaines Rhodia A and LB showed a minimum velocity effect where foam got weaker below a certain velocity. However the blends and the individual AOS exhibited strong shear thinning behavior of comparable magnitude.

Although betaines/sultaines are known to behave as foam boosters when blended with anionic surfactants, in this study we demonstrated that the blends did not perform any better than pure AOS itself. Hence AOS $_{14\text{-}16}$ did not need a zwitterionic surfactant as booster to help generate strong foam in porous media.

Additional experiments in the presence of waterflood residual oil were performed. In the case of zwitterionic Rhodia A it was a poor foamer in the presence of crude oil. Rhodia A:AOS 9:1 viscoelastic blend was able to generate strong foam in fewer PVs than AOS. However, the overall propagation was not as good as for AOS. Hence even in the presence of crude oil, the performance of AOS was better based on assessing the overall PVs taken to reach state pressure drop value. In the case of LB:AOS blends (both the 7:3 and 1:9) and AOS by itself were able to generate a foam strength of ~ 100cP apparent viscosity at ~1 ft/day interstitial velocity. The apparent viscosity of foam for the fixed quality and varying flow rate experiment showed that AOS was able to foam at ~ 2 ft/day after some amount of oil was recovered. In fact AOS surfactants recovered close to 99% of the oil. The LB: AOS 7:3 recovered 76% oil, whereas LB:AOS 1:9 recovered close to 99% oil. The foam apparent viscosity of the blends and AOS were comparable in the presence of oil. This states that AOS did not need a booster even in the presence of crude oil.

In the case of LS: AOS blends, LS: AOS 1:9 performed well as gauging by the foam strength at various velocities. It was equivalent to AOS foam performance. However the LS:AOS 8:2 blend was an order of magnitude lower in apparent viscosity compared to its own foam in the absence of oil. Both the zwitterionics LB and LS were weak foamers in the presence of oil. These observations show that $AOS_{14\text{-}16}$ did not need any foam booster in porous media both in the presence and absence of oil.

176

6.3 Interfacial studies and Film Drainage

Surface tension and interfacial tension measurements were made at the air-water and octane-water interface for all LB, LS, AOS and LB-AOS blends and LS-AOS blends. The very first observation was that the blends and AOS in both the cases had comparable cmc values. Whereas, the pure zwitterionic surfactants had an order of magnitude higher cmcs.

Synergistic interactions were studied using the regular solution theory (RST) developed by Rubingh and Rosen's adaption of it to the surfactant monolayer. These studies showed that there were synergistic interactions which promoted an equimolar composition of the zwitterionic and anionic in both the mixed monolayer and in the mixed micelle for LB:AOS 7:3 and LS:AOS 8:2 blends. The blends LB:AOS 1:9 and LS:AOS 1:9 had a higher fraction of AOS in the bulk to begin with and hence the monolayers were predominant in AOS. This synergistic interaction that promoted an equimolar composition was estimated using the regular solution theory which has its own limitations. Neutron reflection studies have shown that direct measurement of certain surfactant blends yielded a different composition than the estimated one from the RST. It is possible that even the LB:AOS 7:3 and LS:AOS 8:2 monolayer composition must have a higher AOS composition at the mixed monolayer than that predicted by RST thereby causing the foam rheology to be very similar to AOS foam. Another possibility is that even a small amount of AOS present along with the zwitterionic surfactant molecules aids in tighter packing of surfactant molecules at the interface.

Synergistic interactions were predicted even at the octane-water interface for the surfactant mixtures. However these synergistic interactions were of lower magnitude as measured by a β parameter and did not lead to foam boosting both in the presence and absence of oil.

Gibbs surface excess calculations were done in this study for the LB, LS, AOS and the surfactant mixtures as well. It showed that AOS and the LB:AOS blends had higher surface excess adsorption indicating tighter packing. The trends found by the Gibbs excess adsorption had good correlation with foam rheology in porous media for the LB-AOS blends both at the air-water interface as well as octane-water interface. There was slight discrepancy for the LS-AOS blends at the air water interface perhaps owing to some experimental error. However, for the octane-water interface there was very good correlation. These studies helped to develop a fundamental understanding of the mixed micelle and mixed monolayer which help explain observed behavior in porous media.

Interfacial shear rheology was performed for LB-AOS and LS-AOS systems and none of the surfactants had any measurable interfacial viscosity. Hence interfacial shear viscosity is not a good means to judge formulations for their foam film stability. Film drainage studies showed asymmetric drainage. LB: AOS 1:9 blend has the highest film stability, higher than AOS as measured by the longevity of the black film. In terms of longevity of black film the following trend was observed LB:AOS 1:9>LS:AOS 8:2> AOS~= LS:AOS 1:9> LS=LB:AOS 7:3 >LB. There seemed no correlation of these measurements with the foam rheology in porous media.

Future work

In order to make use of the viscoelastic blend A:AOS 9:1 foam for good mobility control, one can study the injection of say a 0.2 PV slug of the viscoelastic blend followed by slugs of AOS. In this way the viscoelastic blend can generate foam faster, and continued injection of AOS might improve its foaming propagation better in the sense it does not need to spend more time in generating strong foam.

These viscoelastic surfactants can be evaluated at high temperature. Literature has shown that even on increasing the temperature the C_{22} chain betaine still maintains its viscoelastic nature[1]. Foam studies can be performed at reservoir conditions and in higher salinity brines since the rheology shows that salinity does not affect a $C_{18\text{-}22}$ zwitterionic surfactant.

Literature has shown that the dilation interfacial viscosity and elasticity correlates with foam film stability[3–6]. The viscoelastic surfactant might possess an interfacial viscosity and elasticity. This would be an interesting study to correlate foam behavior with dilational rheological studies.

In this study the regular solution theory was used to estimate monolayer composition to predict foam rheology in porous media. However neutron reflection techniques can give an accurate composition[7–9]. This will help develop a better understanding on the interfacial properties of surfactant mixtures.

The above betaines have high adsorption in porous media especially in the presence of divalents[10]. Even if viscoelastic betaine/anionic blend can indeed generate foam in fewer PVs, for an economical EOR process adsorption must be low. This area of research needs more work especially in terms of finding sacrificial agents to reduce adsorption.

Another interesting study is the effect of wettability. Usually foam is not strong in oil-wet reservoirs. Studies of using a blend of LB and AOS have been shown to alter wettability and generate strong foam in porous media[11]. It would be interesting to understand if using a viscoelastic betaine in combination with AOS is any better than using LB with AOS in oil-wet media as a foam agent.

References

(1) Kumar, R.; Kalur, G. C.; Ziserman, L.; Danino, D.; Raghavan, S. R. Wormlike Micelles of a C22-Tailed Zwitterionic Betaine Surfactant: From Viscoelastic Solutions to Elastic Gels. *Langmuir* **2007**, *23*, 12849–12856.

(2) Sato, T.; Acharya, D. P.; Kaneko, M.; Aramaki, K.; Singh, Y.; Ishitobi, M.; Kunieda, H. Oil-Induced Structural Change of Wormlike Micelles in Sugar Surfactant Systems. *J. Dispers. Sci. Technol.* **2006**, *27*, 611–616.

(3) Langevin, D. Influence of Interfacial Rheology on Foam and Emulsion Properties. *Adv. Colloid Interface Sci.* **2000**, *88*, 209–222.

(4) Langevin, D.; Monroy, F. Interfacial Rheology of Polyelectrolytes and Polymer Monolayers at the Air–water Interface. *Curr. Opin. Colloid Interface Sci.* **2010**, *15*, 283–293.

(5) Oldroyd, J. G. The Effect of Interfacial Stabilizing Films on the Elastic and Viscous Properties of Emulsions. *Proc. R. Soc. Lond. Math. Phys. Eng. Sci.* **1955**, *232*, 567–577.

(6) Wantke, K.; Małysa, K.; Lunkenheimer, K. A Relation between Dynamic Foam Stability and Surface Elasticity. *Colloids Surf. Physicochem. Eng. Asp.* **1994**, *82*, 183–191.

(7) Hines, J. D.; Thomas, R. K.; Garrett, P. R.; Rennie, G. K.; Penfold, J. Investigation of Mixing in Binary Surfactant Solutions by Surface Tension and Neutron Reflection: Anionic/Nonionic and Zwitterionic/Nonionic Mixtures. *J. Phys. Chem. B* **1997**, *101*, 9215–9223.

(8) Hines, J. D.; Garrett, P. R.; Rennie, G. K.; Thomas, R. K.; Penfold, J. Structure of an Adsorbed Layer of N-Dodecyl-N,N-Dimethylamino Acetate at the Air/Solution Interface As Determined by Neutron Reflection. *J. Phys. Chem. B* **1997**, *101*, 7121–7126.

(9) Naumann, C.; Dietrich, C.; Lu, J. R.; Thomas, R. K.; Rennie, A. R.; Penfold, J.; Bayerl, T. M. Structure of Mixed Monolayers of Dipalmitoylglycerophosphocholine and Polyethylene Glycol Monododecyl Ether at the Air/Water Interface Determined by Neutron Reflection and Film Balance Techniques. *Langmuir* **1994**, *10*, 1919–1925.

(10) Mannhardt, K.; Schramm, L. L.; Novosad, J. J. Adsorption of Anionic and Amphoteric Foam-Forming Surfactants on Different Rock Types. *Colloids Surf.* **1992**, *68*, 37–53.

(11) Singh, R.; Mohanty, K. K. Foams With Wettability-Altering Capabilities for Oil-Wet Carbonates: A Synergistic Approach. *SPE J.* **2016**, SPE-175027-PA.